FILTRATION AND TRANSPORT OF COLLOIDS AND NANOPATICLES IN DENSE EMERGENT VEGETATION: THEORY, EXPERIMENT AND MODELING

By

LEI WU

A DISSERTATION PRESENTED TO THE GRADUATE SCHOOL
OF THE UNIVERSITY OF FLORIDA IN PARTIAL FULFILLMENT
OF THE REQUIREMENTS FOR THE DEGREE OF
DOCTOR OF PHILOSOPHY

UNIVERSITY OF FLORIDA

2013

To my family

ACKNOWLEDGMENTS

I express my sincerest gratitude to my advisor, Dr. Rafael Muñoz Carpena, and co-Chair, Dr. Bin Gao, for their support, guidance, patience, and inspiration throughout my graduate study at the University of Florida. Their genuine interest and enthusiasm for this field are very contagious and I always left their office very optimistic and eager to tackle the next problems at hand. I also thank the other members of my committee, Dr. Kirk J. Ziegler, Dr. Jean-Claude Bonzongo, and Dr. Garey A. Fox for their valuable advice, help and support in the past three years.

Special thanks go to Dr. L-C Shen (University of Florida), Dr. Chongyang Shen (China Agricultural University), Dr. Xiqing Li (Peking Univeristy), Dr. Huilian Ma (University of Utah), Dr. Shihong Lin (Yale University), Dr. Gregory V. Lowry (Carnegie Mellon University), Dr. Alexey N. Volkov (University of Virginia), Dr. Y. A. Pachepsky (UDSA), and Dr. David Kaplan (University of Florida), for their thoughtful suggestions and their insight to my research problems.

My colleagues also friends in the hydrologic modeling lab and nanotechnology lab deserve special acknowledgement. They not only gave me help and support to my research, but also helped me remember that there is more to life than research. I would also like to thank the entire office staff, technicians, each of whom has helped me deal with at least crises. Above all others, I wish to thank my parents for their constant love, encouragement, wisdom and unconditional support. I can’t make this far without them.

TABLE OF CONTENTS

page

ACKNOWLEDGMENTS 4

LIST OF TABLES 8

LIST OF FIGURES 12

LIST OF ABBREVIATIONS 15

CHAPTER

1 INTRODUCTION 19

Scientific Questions 19
Literature Review on Question 1 20
Colloidal Particles and Significance 20
Fate and Transport of Colloidal Particles in Subsurface Environment 21
Fate and Transport of Colloidal Particles in Surface Environment 22
Knowledge Gap on Question 1 and Research Scope 24
Research Objectives of Question 1 25
Literature Review on Question 2 27
Carbon Nanotubes and Significance 27
CNTs Releases to the Environment 28
Environmental Fate and transport of CNTs 29
Specific Knowledge Gap 2 and Research Scope 31
Research Objectives 2 32
Organization of the Dissertation 32

2 EXPERIMENTAL ANALYSIS OF COLLOID CAPTURE BY A CYLINDRICAL COLLECTOR IN LAMINAR OVERLAND FLOW 34

Introductory Remarks 34
Theory 37
Materials and Methods 39
Colloids and Collectors 39
Experimental Apparatus 40
Experimental Methods 40
Results and Discussion 41
Effects of Flow Velocity and Colloid and Collector Sizes 41
Comparison of Experimental Data and Theoretical Predictions 43
A Regression Equation 45
Environmental Implication 46

3 SINGLE COLLECTOR ATTACHMENT EFFICIENCY OF COLLOID CAPTURE BY A CYLINDRICAL COLLECTOR 54

Introductory Remarks 54
Theory 57
Materials and Methods 60
Materials 60
Experimental Methods 61
Results and Discussion 63
Effect of Ionic Strength 63
Effect of Flow Velocity 64
Comparison of Experimental Data and Theoretical Predictions 66
A Dimensionless Equation 68
Environmental Implications 70

4 EXTENDED SINGLE STEM EFFICIENCY THEORY FOR COLLOID FILTRATION THROUGH SURFACE DENSE VEGETATION 80

Introductory Remarks 80
Theoretical Background and New Dimensionless Number (N_{STE}) 83
Materials and Methods 87
Materials 87
Vegetation Chamber Experiments 88
Characterize biopolymer brush layer (trichome) on vegetation stem 89
Determine kinetic deposition rate (k_d) 90
Results and Discussion 90
Effect of ionic strength on colloid filtration in dense vegetation 90
Coupled effect of flow velocity and stem density on colloid filtration in dense vegetation 92
Extended single-stem efficiency theory 94
Deposition Mechanisms and Other Potential Effects 96
Environmental Implications 97

5 DLVO INTERACTIONS OF CARBON NANOTUBES WITH ISOTROPIC PLANAR SURFACE 108

Introductory Remarks 108
Theory 113
Results and Discussion 116
DLVO Interactions between a Pristine SWNT and an Isotropic Planar Surface 116
DLVO Interactions between a Surface Modified SWNT and a Charged Isotropic Planar Surface 119
DLVO Forces and Torques of SWNTs with Planar Surfaces 123
DLVO Interactions of MWNTs and Planar Surfaces 124
Environmental Implications 125

6 CONCLUSIONS AND RECOMMENDATIONS 133

Conclusions 133

Recommendations for Further Study 136
Plant filtration theory in overland flow 136
Interactions between CNTs and interfaces 137

APPENDIX

A SUPPORTING INFORMATION FOR CHAPTER 2 139

B SUPPORTING INFORMATION FOR CHAPTER 3 141

C SUPPORTING INFORMATION FOR CHAPTER 4 172

D SUPPORTING INFORMATION FOR CHAPTER 5 197

LIST OF REFERENCES 204

BIOGRAPHICAL SKETCH 229

LIST OF TABLES

Table page

2-1. Summary of experimental conditions and results 48

3-1. Summary of experimental conditions and results 72

3-2. Calculated Maximum energy barriers (Φmax) and primary (Φpri) and secondary minimum (Φsec) under different experimental conditions 73

3-3. Summary of dimensionless parameters governing attachment efficiency 74

4-1. Summary of experimental conditions, biopolymer brush properties and best-fit value of parameters in transport model 99

A-1. Experimental data of single-stem contact efficiency (η_0) under different flow velocity conditions for a given colloid (d_p =1.05μm) and collector (d_c=2cm) 139

A-2. Experimental data of single-stem contact efficiency (η_0) under different sizes of colloid and collector at a given flow velocity (u=0.02cm/s) 140

B-1. Definition of Dimensionless parameters 145

B-2. Summary of stepwise-least square regression results 146

B-3 Experimental data of attachment efficiency (α) under different ionic strength conditions (IS=0.001M) for a given colloid (dp=1.05μm) 150

B-4 Experimental data of attachment efficiency (α) under different ionic strength conditions (IS=0.005M) for a given colloid (dp=1.05μm) 151

B-5 Experimental data of attachment efficiency (α) under different ionic strength conditions (IS=0.01M) for a given colloid (dp=1.05μm) 152

B-6. Experimental data of attachment efficiency (α) under different ionic strength conditions (IS=0.05M) for a given colloid (dp=1.05μm) 153

B-7. Experimental data of attachment efficiency (α) under different ionic strength conditions (IS=0.1M) for a given colloid (dp=1.05μm) 154

B-8. Experimental data of attachment efficiency (α) under different ionic strength conditions (IS=0.001M) for a given colloid (dp=0.1μm) 155

B-9. Experimental data of attachment efficiency (α) under different ionic strength conditions (IS=0.005M) for a given colloid (dp=0.1μm) 156

B-10. Experimental data of attachment efficiency (α) under different ionic strength conditions (IS=0.01M) for a given colloid (dp=0.1μm) 157

B-11. Experimental data of attachment efficiency (α) under different ionic strength conditions (IS=0.05M) for a given colloid (dp=0.1μm) 158

B-12. Experimental data of attachment efficiency (α) under different ionic strength conditions (IS=0.1M) for a given colloid (dp=0.1μm) 159

B-13. Experimental data of attachment efficiency (α) under different flow velocities and ionic strength conditions (u=0.0002cm/s and IS=0.01M) for a given colloid (dp=1.05μm) 160

B-14. Experimental data of attachment efficiency (α) under different flow velocities and ionic strength conditions (u=0.002cm/s and IS=0.01M) for a given colloid (dp=1.05μm) 161

B-15. Experimental data of attachment efficiency (α) under different flow velocities and ionic strength conditions (u=0.2cm/s and IS=0.01M) for a given colloid (dp=1.05μm) 162

B-16. Experimental data of attachment efficiency (α) under different flow velocities and ionic strength conditions (u=0.0002cm/s and IS=0.1M) for a given colloid (dp=1.05μm) 163

B-17. Experimental data of attachment efficiency (α) under different flow velocities and ionic strength conditions (u=0.002cm/s and IS=0.1M) for a given colloid (dp=1.05μm) 164

B-18. Experimental data of attachment efficiency (α) under different flow velocities and ionic strength conditions (u=0.2cm/s and IS=0.1M) for a given colloid (dp=1.05μm) 165

B-19. Experimental data of attachment efficiency (α) under different flow velocities and ionic strength conditions (u=0.0002cm/s and IS=0.01M) for a given colloid (dp=0.1μm) 166

B-20. Experimental data of attachment efficiency (α) under different flow velocities and ionic strength conditions (u=0.002cm/s and IS=0.01M) for a given colloid (dp=0.1μm) 167

B-21. Experimental data of attachment efficiency (α) under different flow velocities and ionic strength conditions (u=0.2cm/s and IS=0.01M) for a given colloid (dp=0.1μm) 168

B-22. Experimental data of attachment efficiency (α) under different flow velocities and ionic strength conditions (u=0.0002cm/s and IS=0.1M) for a given colloid (dp=0.1μm) 169

B-23. Experimental data of attachment efficiency (α) under different flow velocities and ionic strength conditions (u=0.002cm/s and IS=0.1M) for a given colloid (dp=0.1μm) 170

B-24. Experimental data of attachment efficiency (α) under different flow velocities and ionic strength conditions (u=0.2cm/s and IS=0.1M) for a given colloid (dp=0.1μm) 171

C-1. Relevant parameters and constants for interaction between colloid and plant stem surface 172

C-2. Experimental data of breakthrough curve under DI water conditions 178

C-3. Experimental data of breakthrough curve under medium IS conditions (IS=0.01M) 179

C-4. Experimental data of breakthrough curve under high IS conditions (IS=0.1M) . 180

C-5. Experimental data of breakthrough curve under high IS conditions (IS=0.2M) . 181

C-6. Experimental data of breakthrough curve under plant high density conditions (u=0.002 cm/s) 182

C-7. Experimental data of breakthrough curve under plant high density conditions (u=0.01cm/s) 183

C-8. Experimental data of breakthrough curve under plant high density conditions (u=0.05 cm/s) 184

C-9. Experimental data of breakthrough curve under plant high density conditions (u=0.1 cm/s) 185

C-10. Experimental data of breakthrough curve under plant medium density conditions (u=0.002 cm/s) 186

C-11. Experimental data of breakthrough curve under plant medium density conditions (u=0.01 cm/s) 187

C-12. Experimental data of breakthrough curve under plant medium density conditions (u=0.05 cm/s) 188

C-13. Experimental data of breakthrough curve under plant medium density conditions (u=0.1 cm/s) 189

C-14. Experimental data of breakthrough curve under plant low density conditions (u=0.002 cm/s) 190

C-15. Experimental data of breakthrough curve under plant low density conditions (u=0.01 cm/s) 191

C-16. Experimental data of breakthrough curve under plant low density conditions (u=0.05 cm/s) 192

C-17. Experimental data of breakthrough curve under plant low density conditions (u=0.1 cm/s) 193

C-18. Experimental data of breakthrough curve under different sizes of colloid conditions (dp=0.1μm) 194

C-19. Experimental data of breakthrough curve under different sizes of colloid conditions (dp=1.05μm) 195

C-20. Experimental data of breakthrough curve under different sizes of colloid conditions (dp=2.0μm) 196

LIST OF FIGURES

Figure page

1-1. Fate and transport of colloids and nanoparticles in aquatic and terrestrial environments 19

1-2. Illustration of colloid sizes and categories. 21

1-3. Illustration of vegetative filter strips (VFS). 24

1-4. Research scope of development of colloid filtration theory in dense vegetation in overland flow. 25

1-5. Illustration of SWNT and MWNT..... 28

1-6. Illustration of CNTs releases to environment. 29

1-7. CNTs challenges to traditional DLVO theory. 30

1-8. Research scope of interactions between CNTs and planar surface. 32

2-1. Graphical content of chapter 2..... 34

2-2. Schematic of experimental setup for measuring single-collector contact efficiency. 49

2-3. Effect of flow velocity on single-collector contact efficiency. 50

2-4. Effect of colloid and collector sizes on single-collector contact efficiency..... 51

2-5. Comparison of experimental data of single-collector contact efficiency with predictions of (a) equations 1-3, (b) the YAO model, (c) the RT model, and (d) the TE model..... 52

2-6. Comparison of experimental data of single-collector contact efficiency with predictions of the new dimensionless equation (equation 2-6). 53

3-2. Experimental attachment efficiency (α) as a function of ionic strength (IS) for colloid capture by the cylinder in the flow chamber. 75

3-3. DLVO interaction energy between the collector and the colloids: (a) 0.1 μm colloids and (b) 1.05 μm colloids. 76

3-4. Experimental attachment efficiency (α) as a function of flow velocity (u) for colloids captured by the cylinder in the flow chamber..... 77

3-5. Comparison of experimental attachment efficiency (α) with predictions of the Maxwell, modified Maxwell, and Bai-Tien models for colloids captured by the cylinder in the flow chamber at ionic strength of 0.01M. 78

3-6. Comparison of experimental attachment efficiency (α) with predictions of the new dimensionless equation..... 79

4-1. Graphical content of chapter 4..... 80

4-2. (A) Schematic of adsorbed polymer layer; (B) Schematic of grafted polymer brush layer; (C) Schematic of a model for a spherical colloid with diameter of dp impinging upon a biopolymer brush in a solution..... 101

4-3. (A) Morphology of trichomes on the plant stem and (B) air bubbles attached on the surface of trichomes under water. 102

4-4. Schematic and photos of experimental set up for vegetation chamber experiment..... 103

4-5. Effect of ionic strength on the colloid deposition onto the plant stem. 104

4-6. Effect of coupled flow velocity and grass density on the colloid deposition onto the plant stem..... 105

4-7. Goodness-of-fit evaluation of the extended model. 106

4-8. Schematic illustration of three basic mechanisms of colloidal particles deposition on the plant stems..... 107

5-1. Graphical content of chapter 5..... 108

5-2. Schematic illustration of interaction of a SWNT with an infinite isotropic planar surface..... 127

5-3. The van der Waals interaction energy between a pristine SWNT and an isotropic planar surface. 128

5-4. The electrostatic double layer interaction energy ($\Phi EDL/kT$) between a surface modified SWNT and a charged isotropic planar surface..... 129

5-5. Total interaction energy ($\Phi Total/kT$) between a surface modified SWNT and a charged isotropic planar surface..... 130

5-6. DLVO force and torque acting on a surface modified SWNT and a charged isotropic planar surface. 131

5-7. Normalized total interaction energy between a surface modified SWNT or MWNT and a charged isotropic planar surface..... 132

B-1. Comparison of experimental attachment efficiency with predictions of the new dimensionless equation for development dataset. 149

C-1. Breakthrough curves with and without plaster. 174

C-2. Morris sensitivity analysis result chart 175

C-3. Sobol sensitivity analysis indices chart 176

C-4. Comparison of experimental deposition rate with predictions of the new dimensionless equation for development dataset 177

LIST OF ABBREVIATIONS

ADE	Advection-dispersion equation
CNTs	Carbon nanotubes
CFT	Colloid filtration theory
DA	Derjaguin Approximation
DI	Deionized
DLVO	Derjaguin-Landau-Verwey-Overbeek
EDL	Electrical double layer
ENPs	Engineered nanoparticles
EPM	Electrophoretic mobility
HA	Humic acid
IFBL	Interaction force boundary layer
MWNTs	Multi-walled nanotubes
NOM	Natural Organic Matter
PV	Pore volume
PVC	polyvinyl chloride
SDBS	Sodium dodecylbenzene sulfonate
SEI	Surface element integration
SWNTs	Single-walled nanotubes
VDW	Van der Waals

Abstract of Dissertation Presented to the Graduate School
of the University of Florida in Partial Fulfillment of the
Requirements for the Degree of Doctor of Philosophy

FILTRATION AND TRANSPORT OF COLLOIDS AND NANOPARTICLES IN DENSE EMERGENT VEGETATION: THEORY, EXPERIMENT, AND MODELING

By

LEI WU

May 2013

Chair: Rafael Muñoz-Carpena
Co-Chair: Bin Gao
Major: Agricultural and Biological Engineering

A thorough understanding of filtration and transport of colloidal contaminants in the aquatic environment is of great importance to many environmental and biological problems (e.g., contaminant transport in flow, water quality, life cycles of microorganisms, and wetland geomorphology). However, little research has been conducted to investigate the overland flow transport of colloidal particles through emergent vegetation. Understanding this process is critical since, compared to subsurface paths, overland flow constitutes a quick path for environmental transport of pollutants with immediate effects to surface water bodies, that dense vegetation (natural or planted) could help to ameliorate. In this work, first a series of laboratory experiments were conducted to measure the single-stem contact efficiency (η_0) and attachment efficiency (α) of colloid capture by a simulated plant stem in laminar lateral flow. The results showed that existing theoretical and empirical models of colloid contact and attachment efficiency developed originally for porous media fall short in describing the colloid filtration by dense vegetation system in overland flow. For the first time, new single-stem efficiency theory (SSET) was developed to predict colloid filtration by dense

vegetation with reasonable accuracy. In order to upscale SSET from clean single-stem to real dense vegetation, a new dimensionless number was developed to account for the effect of plant stem surface properties on the colloid deposition in overland flow. Laboratory scale dense vegetation chamber experiments and model simulations were conducted to obtain the effective values of colloid kinetic deposition rate (k_d) in the vegetation system under different experimental conditions. The results showed that in addition to flow hydrodynamics (e.g., flow velocity) and solution chemistry (e.g., ionic strength), steric repulsion afforded by the biopolymer brush layer formed by trichomes on the plant stem surface also plays a significant role in the plant stem colloid deposition during overland flow. An extended model including the steric repulsion effect was developed that matched the experimental data well. This extended model can be used to not only help construct and refine dynamic models of colloid transport and filtration through dense vegetation in overland flow, but also is applicable to prediction of colloid deposition on various polymer brush surfaces in natural, engineered and biomedical systems.

In addition to colloidal particles, the ever-increasing use of engineered nanomaterials (e.g., carbon nanotubes, CNTs) will likely lead to heightened levels of these materials in the environment. CNTs aggregation and deposition behavior will dictate their transport potential and thus their environmental fate and potential ecotoxicological impacts of these materials. However, the unique properties of CNTs pose challenges to experimentally and theoretically quantifying their deposition and aggregation in the environment. The surface element integration (SEI) technique was coupled with the Derjaguin-Landau-Verwey-Overbeak (DLVO) theory to determine the

orientation-dependent interaction energy between CNTs and an infinite isotropic planar surface. For the first time, analytical formulas were developed to accurately describe the interactions between not only pristine, but also surface charged CNTs and planar surfaces with arbitrary rotation angles. The new analytical expressions presented in this work can be used as a robust tool to describe the DLVO interaction between CNTs and planar surfaces under various conditions and thus to assist not only the development of effective strategies to reduce the environmental impact of CNTs but also the design and application of CNT-based products.

CHAPTER 1
INTRODUCTION

Scientific Questions

Over the last decade, colloids and nanoparticles have been used more frequently in agricultural, industrial applications and in consumer and medical products. [1] [2, 3] And these applications will likely continue to increase. Concerns about their environmental fate, transport and ultimate environmental impacts have stimulated studies to predict environmental concentrations in aquatic systems. These particles may enter the aquatic system either directly through wastewater treatment effluents or indirectly through surface runoff through dense vegetation systems (Figure 1-1).

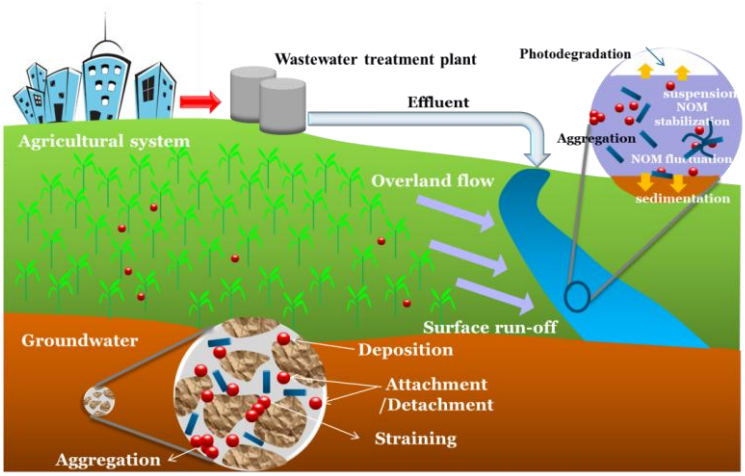

Figure 1-1. Fate and transport of colloids and nanoparticles in aquatic and terrestrial environments

The former has received a lot of attentions in the past few decades; however, much less effort has been dedicated to the fate and transport of colloidal particles in surface runoff, especially through dense vegetation that might help to reduce transport through deposition in the soil-vegetation system. In addition, unique properties of nanoparticles and their suspensions (e.g., shape, size, structure, and chemical composition) challenge the ability of colloid science to understand nanoparticles

aggregation behavior and the subsequent effects on environmental fate and transport of nanoparticles. Therefore, this dissertation focuses on two main questions: (1) are the current colloid filtration theories developed for porous media applicable to a vegetation system in surface water? And (2) are the current approaches and models used in quantifying colloidal interactions and transport applicable to nanoparticles?

Literature Review on Question 1

Colloidal Particles and Significance

A thorough understanding of deposition of colloidal particles in surface water flow is of great importance to many environmental and biological processes [4-7] (e.g., transport and fate of contaminants, deterioration of water quality, life cycles of microorganisms and changes in wetland geomorphology). Colloidal particles with effective diameters of around 10 nm to 10 μm (Figure 1-2) can be categorized into two categories: abiotic colloids (e.g., amorphous iron, and manganese oxides, engineered nanomaterial) and biotic colloids (e.g., viruses, bacteria, and protozoa) [8, 9]. Having relatively high specific surface areas and charge densities, colloids serve as efficient carrier of various pollutants and enhance their mobility along hydrologic pathways [10-12]. Furthermore, many of biotic colloids pose a risk to public health and are therefore contaminants of concern in surface water and drinking water supplies and on agricultural produce [13-16]. Hence, effective treatment processes for many colloidal particles and contaminants rely on the optimization of colloid transport and retention in surface water flow.

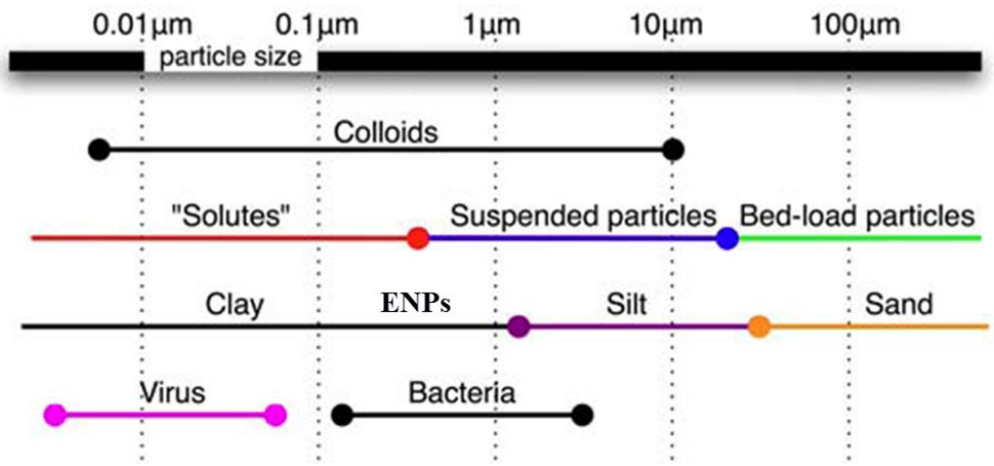

Figure 1-2. Illustration of colloid sizes and categories.

Fate and Transport of Colloidal Particles in Subsurface Environment

Considerable research has been devoted to study the fate and transport of colloidal particles in the subsurface environment (vadose zone and groundwater). Reviews have been given by Ryan and Elimelech, 1996 [17]; Schijven and Hassanizadeh, 2000 [18]; Harvey and Harms, 2007 [19]; Jin and Flury, 2002 [20]; Ginn et al., 2002 [21]; de Jonge et al., 2004 [22]; DeNovio et al., 2004 [23]; Rockhold et al., 2004 [24]; Sen and Khilar, 2006 [25]; Tufenkji et al., 2006 [26]. Briefly, with the exception of a few field-scale studies that examined the effect of infiltration on colloid mobilization [27-29], undisturbed soil columns have been used to mimic the subsurface in laboratory research [30-34]. Bench-scale soil-packed column experiments have been conducted to examine the transport behaviors of different types of colloids including viruses, bacteria, clay particles, and synthetic microspheres, and engineered nanoparticles [35-38]. Relationships between system physicochemical properties (e.g., flow velocity, solution chemistry, and surface properties) and colloid mobility in porous media were evaluated [39-42]. In addition, the influences of biological factors (e.g., cell size and shape, cell motility, and micro-molecular length and composition) on bio-colloid

fate and transport in porous media have been assessed [43, 44]. Findings from these experimental investigations have revealed some of the fundamental transport mechanisms and enhanced current ability to predict colloid fate and transport in subsurface environments [25, 45-47].

Fate and Transport of Colloidal Particles in Surface Environment

Considerably less attention has been dedicated to the fate and transport of colloidal particles in surface flow, particularly with respect to colloid transport through vegetation in overland flow [48-50].

Dense submerged vegetation in aquatic systems have been shown to reduce the flow velocity in open channels to promote the deposition of sediments [51-53], suppress turbulence to favorably influence growth and distribution of aquatic organisms such as phytoplankton [54-56], and alter the resident time to affect water quality [57-59]. Plant surrogates (e.g., vertical cylinders) have often been used in the laboratory for exploring the key determinants of flow dynamics and governing mechanisms of contaminant transport through submerged vegetation [60-62]. Findings from the laboratory experiments with simulated systems have greatly enhanced the understanding of flow and transport processes in rivers, estuaries, and natural and constructed wetlands [63-67]. In addition to flow and sediment transport, the influence of submerged aquatic vegetation on the fate and transport of suspended fine particles has also been investigated in laboratory and field environments. Leonard et al [53] observed that the capture of suspended particles on the stems and leaves of *Juncus roemerianus* marsh contributed up to 10% of the total sediment deposition to a tidal marsh. Similarly, Pluntke and Kozerski [58] suggested that sedimentation onto plant structures should be considered when quantifying particle retention in submerged macrophyte stands.

Particle retention in a sea grass meadow (*Posidonia oceanica*) was found to be up to 15 times greater than the equivalent non-vegetated bed [68]. In a wetland field site in the Florida Everglades, Huang et al. [69] found that submerged aquatic vegetation could also remove colloidal particles from surface flow. These evidences strongly suggest that filtration by plant structures, such as stems, has a significant effect on the fate and transport of colloidal particles in surface flow. Unfortunately, current understanding of the capture of colloidal particles by emergent terrestrial vegetation in overland flow is still very limited.

Dense emergent vegetation in terrestrial systems has been proven to be effective in removal the non-point source pollutants (including sediment, plant nutrients, and pesticides) from agricultural field and urban areas [70-72]. Vegetative filter strips (VFS) (Figure 1-3), a common runoff pollution control practice, have been promoted to help control the movement of pollutants from cropland and urban runoff. Many laboratory and field studies have been conducted to determine the efficiency of VFS in protecting water resources from non-point source pollution [73-75]. For instance, it was reported that a well-installed VFS can remove suspended sediments (up to 90%), phosphorus (75%), nitrogen (up to 87%), and pesticides (40%) [76-79].

Recently, a growing research effort is aimed at reducing the transport of biocolloids (particularly pathogens) in overland flow [80-83]. Emergent terrestrial vegetation (e.g., VFS) has been suggested as being effective in attenuating the loading of manure-borne microorganisms from farms and other agricultural and urban lands to runoff [84-86]. For instance, Fox, et al. [87] recently determined vegetative filter strips (VFS) effectiveness in removing *E.coli* from runoff relative to inflow rate, infiltration

capacity, and flow concentration in a laboratory- scale VFS soil box. Field experiments conducted by Ferguson et al. [88] also showed that colloid size played an important role in controlling the mobility of microorganisms (biocolloids) in dense vegetation. Results from those studies have informed the optimization of the design and maintenance of the emergent terrestrial vegetation filters to remove sediments and agricultural chemicals [89-92].

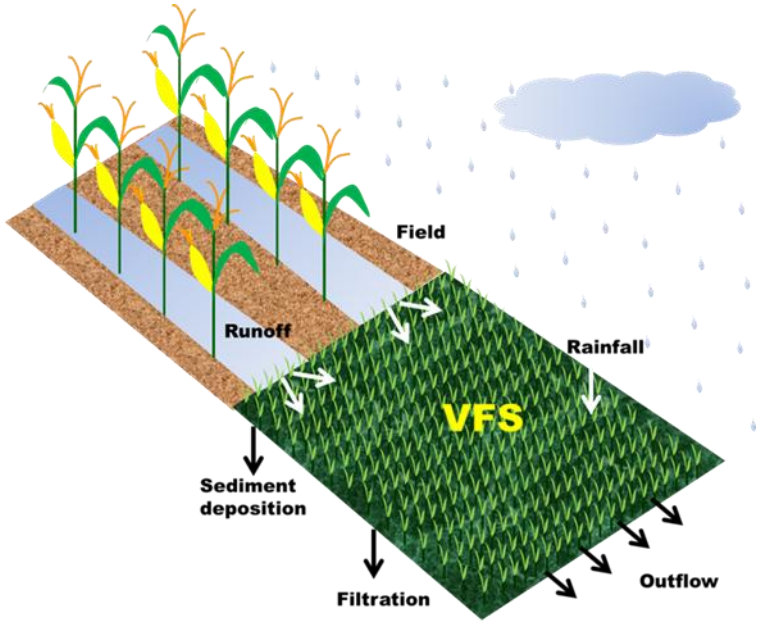

Figure 1-3. Illustration of vegetative filter strips (VFS).

Knowledge Gap on Question 1 and Research Scope

From the evidence presented above, it can be concluded that although colloid and colloid-facilitated transport in water flow is a well-known contamination process, little research has been conducted to investigate the transport of colloidal particles through emergent vegetation in overland flow. There exists a knowledge gap regarding theories and mechanisms that govern colloid fate and transport in terrestrial dense vegetation in overland flow. Therefore, systemic studies to identify the fundamental

processes of colloid transport through dense emergent terrestrial vegetation are needed.

In overland flow, the depth of water is usually below the top of the sheaths of dense vegetation and thus plant stems may control flow and transport processes [93, 94]. Under these conditions, plant stems can be modeled as rigid, cylindrical collectors for colloid deposition [95]. Therefore, establishing a single-stem efficiency theory of colloids filtration by dense emergent vegetation will advance the understanding the fate and transport of colloids in surface flow. The scope of this research is shown in Figure 1-4.

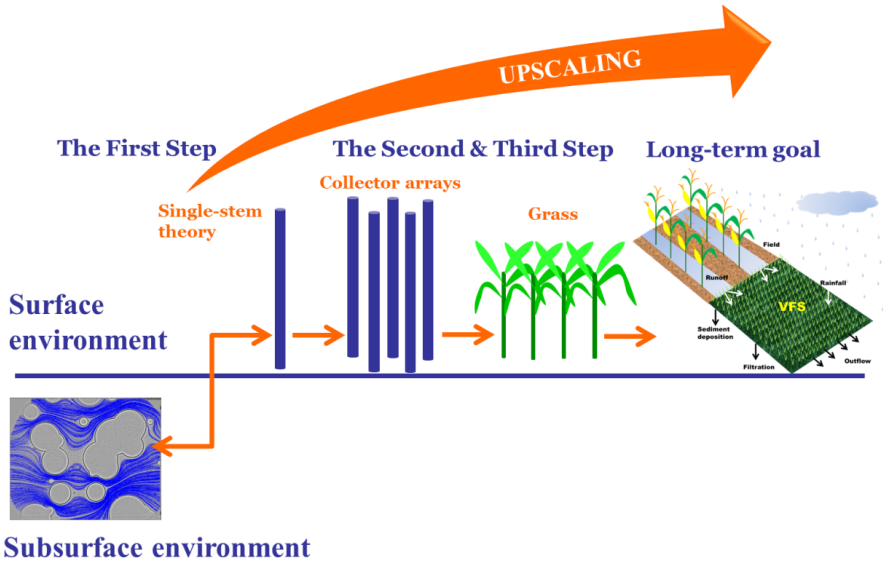

Figure 1-4. Research scope of development of colloid filtration theory in dense vegetation in overland flow.

Research Objectives of Question 1

The overall (long-term) research goal is to develop a single-stem efficiency theory for plant filtration of colloids through dense vegetation in overland flow. *It is our central hypothesis that the stems of the surface vegetation can be modeled as rigid*

filtration collectors for colloids in shallow overland flow. Specific hypothesis and objectives are as follows:

Hypothesis 1: System physical factors will affect colloid capture by vegetation stem in shallow overland flow, and colloid filtration theory in porous media can be used to predict the colloid capture by dense vegetation in laminar overland flow.

Objective 1: develop a theory for predicting the single-stem contact efficiency (η_0) of colloid filtration by emergent dense vegetation in shallow overland flow.

The specific objectives are to (1) determine how flow velocity, colloid size, and collector size affect the single-stem efficiency of colloid capture by a cylindrical collector in laminar overland flow through flow chamber experiment, (2) test whether existing single-collector contact efficiency models can be used to predict colloid capture by a cylinder in laminar overland flow, and (3) develop a dimensionless equation to describe the single-stem efficiency of colloid transport through emergent vegetation in laminar overland flow.

Hypothesis 2: System physicochemical properties and flow velocity will affect colloids attachment onto the surface of stem, and DLVO theory coupled with torque balance approach can be used to interpret the colloid attachment onto the surface of collector in overland flow.

Objective 2: develop a theory for predicting the single-stem attachment efficiency (α) of colloid filtration by emergent vegetation in shallow overland flow.

The specific objectives are to: (1) determine how ionic strength, colloid size and flow velocity affect the attachment efficiency of colloid capture by a cylindrical collector in laminar overland flow through flow chamber experiment; (2) test whether existing

attachment efficiency models can be used to predict colloidal particles attachment onto vegetation stems in laminar overland flow; (3) if existing theories prove limited, develop a new equation to describe the attachment process of colloidal particles onto vegetation stems in laminar overland flow; and (4) if it is necessary to develop a new equation, test the performance of attachment efficiency through column experiments.

Hypothesis 3: surface properties of plant stem will affect colloid kinetic deposition rate, and these can be used to improve the prediction of colloid filtration by dense vegetation in shallow overland flow.

Objective 3: to apply and modify the single-stem efficiency theory to dense vegetation system in overland flow.

The hypothesis and objectives will be tested and developed through the following experimental tasks: (1) determine the effect of flow velocity, vegetation density, colloid size and ionic strength on the colloid kinetic deposition rate; (2) determine whether existing single-stem efficiency theory ("for clean rigid stem") can be used to predict kinetic deposition rate of colloid in dense vegetation system in overland flow; (3) develop a new theory (extended model) to predict the deposition of colloidal particles on plant stem in laminar overland flow.

Literature Review on Question 2

Carbon Nanotubes and Significance

Nanoparticles (NPs), defined as particles with at least one dimension smaller than 100 nm, have received much recent attention because of their potential toxic effects and the rapid development of nanotechnology [96-103]. Carbon nanotubes (CNTs) are among the top NPs of concern in the environment [104-106]. Entirely composed of carbon with a significantly large length-to-diameter ratio and unique physicochemical

properties, CNTs are rolled-up graphene sheets with exceptional mechanical, electrical, optical, and thermal properties [107-110]. There are mainly two types of CNTs: single- and multi-walled. Single-walled carbon nanotubes (SWNTs) are one-layered graphitic cylinders having diameters on the order of a few nanometers, while multi-walled carbon nanotubes (MWNTs) comprise of 2 to 30 concentric cylinders having outer diameters often between 2-25 nm (Figure 1-5). They are largely used in many novel applications in nanotechnology, electronics, optics, thermal conductors, and other fields in material science and engineering [111-114].

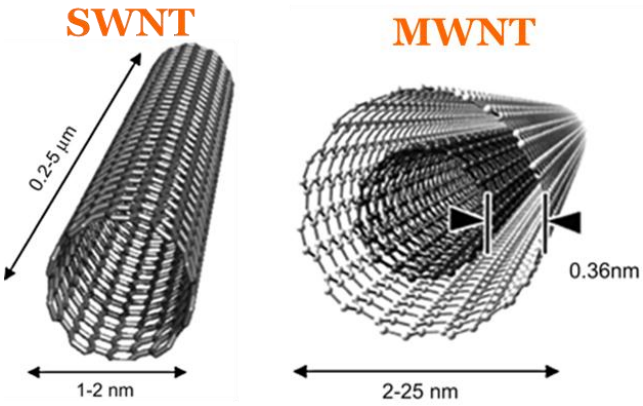

Figure 1-5. Illustration of SWNT and MWNT.

CNTs Releases to the Environment

The exponential growth in production of CNTs and their widespread applications in consumer products will inevitably result in their release into the environment (e.g., air, water, soil, and sediment, Figure 1-6). [115, 116]. Release may come from point sources (e.g., manufacturing and wastewater effluent) or from non-point sources (e.g., attrition from CNTs products). Biochemical cycling of CNTs may involve photochemical reactions in the air; aggregation and filtration in the soil; suspension, flocculation, sedimentation, deposition and aggregation in the water and uptake, accumulation and

degradation in organisms. Human exposure to CNTs is most likely during manufacturing, nut inhalation of CNTs released to the atmosphere and ingestion of drinking water or food. Dermal exposure from sunscreens and cosmetics is also likely.[1]

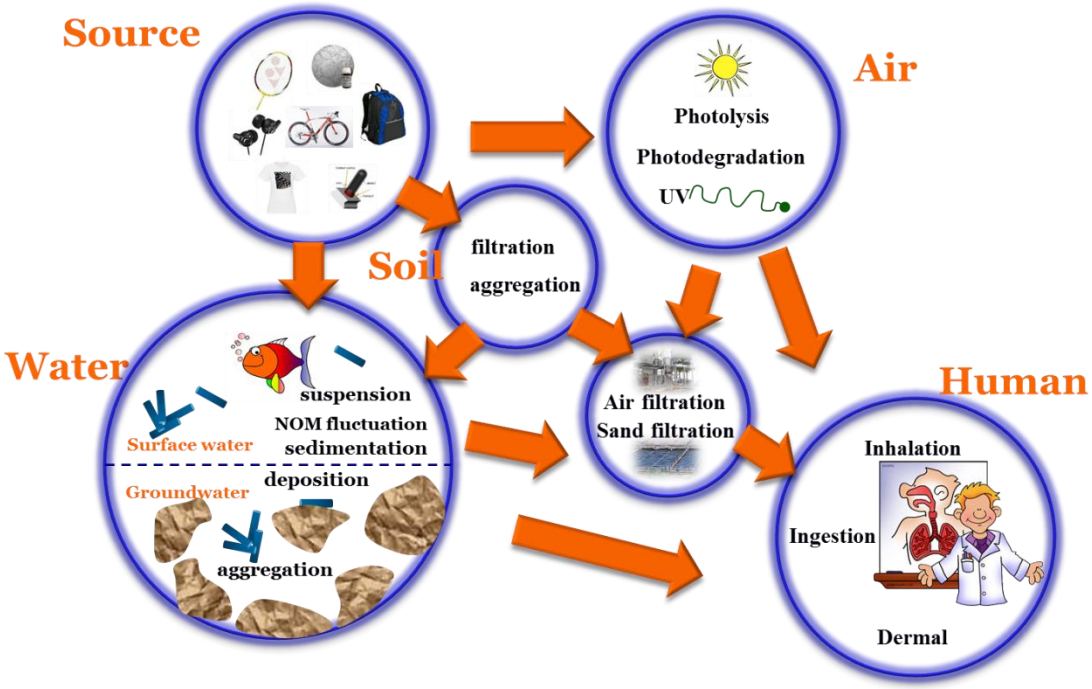

Figure 1-6. Illustration of CNTs releases to environment.

Environmental Fate and transport of CNTs

Once CNTs are released into the environment through any of the release pathways, their mobility and colloidal stability are expected to control their bioavailability and impact on the environment. While CNTs release occurs within all of these environments, this dissertation focuses on CNTs deposition behavior in aquatic systems. When released into aquatic environments, CNTs deposition is controlled by CNTs specific properties (e.g., shape, size, chemical composition, surface structure and coating), the surrounding solution chemistry (e.g., pH, ionic strength, and natural organic matter), and hydrodynamic conditions. [117] In recent years, several studies have been conducted to investigate CNTs deposition on solid surface in aquatic system

either by experimental approach or by theoretical approach.[118-121] Traditionally, the interactions between CNTs and other solid surfaces have been investigated through column filtration experiments. [118-123] However, the theoretical interpretation of results from such systems is still far from satisfaction because most of the theoretical studies are based on colloid science principles- Derjaguin-Landau-Verwey-Overbeak (DLVO) theory which can't be applicable to CNTs directly.[117, 120]

CNTs challenge the limits of colloid science due to their small size, tubular shape, structure, surface coating (Figure 1-7). Among these challenges, shape effect was reported to play an significant role in the DLVO framework.[2]

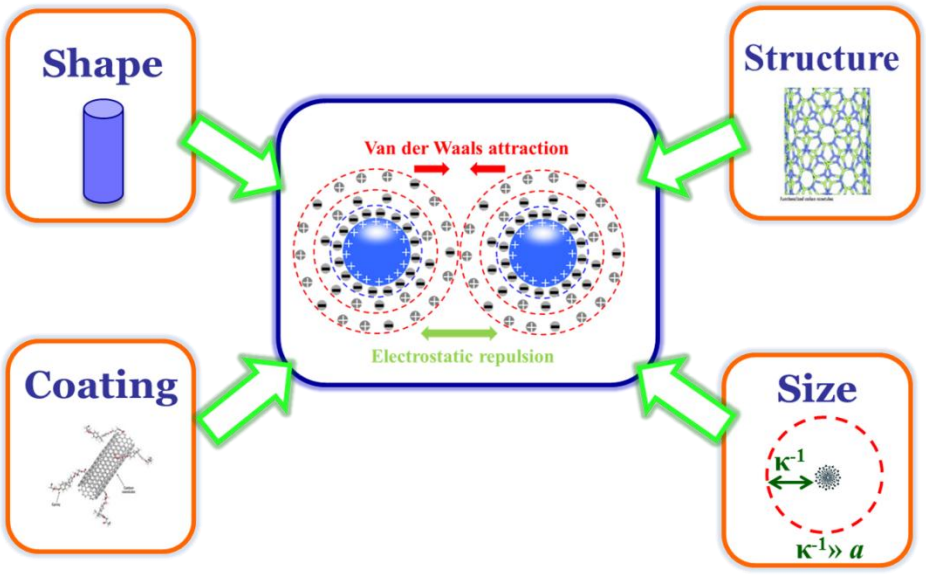

Figure 1-7. CNTs challenges to traditional DLVO theory.

In DLVO theory (modeling), one of the primary assumptions is that particles are spherical. The assumption is reasonable for ideal latex particles and some ideal colloidal contaminants. However, CNTs come in tube shapes, thereby, complicating traditional DLVO theory. Both van der Waals and electrostatic double layer forces are affected by the changes in shape. Several researchers have investigated these

changes.[124-126] And these results imply that shape can theoretically control interactions between particles and different interfaces. Several techniques have been developed to calculate the interaction force/energy between curved surfaces/bodies, including the Derjaguin Approximation (DA) and surface element integration (SEI).[124] The DA method estimates the interaction energy between two finite size bodies by relating it to that between two infinite parallel flat plates.[125] It can only be applied to surfaces that are separated by a small distance and to circumstances when the interaction range is substantially smaller than the radii of curvature of the surfaces. For very small non-spherical particles, such as SWNTs, the DA method may lead to inaccuracies in calculating their interaction with planar surfaces. [127] The SEI technique takes into account curvature effects over the whole object, by integrating the interaction energy between a surface element of the object and the plane surface using the exact surface geometry of the object. It can precisely determine the interaction forces between a planar surface and a curved body with any defined shape, including CNTs.[117]

Specific Knowledge Gap 2 and Research Scope

From the evidence presented above, it can be concluded that the traditional DLVO theory often failed to provide an accurate estimation of the interaction forces between CNTs and planar surfaces. Furthermore, the interaction of CNTs and planar surfaces is orientation dependent, which gives rise to a torque orienting the CNTs in an energetically favorable configuration to approach/depart the planar surfaces. Such a dynamic behavior cannot be explained merely on the basis of spherically symmetric interaction potentials of the traditional DLVO theory. A theory/model that can accurately

describe the interaction between a CNT and a planar surface therefore is in critical need. The scope of this research is shown in the Figure 1-8.

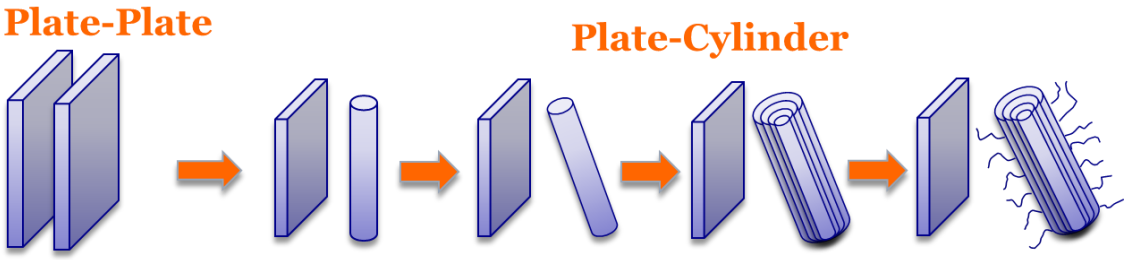

Figure 1-8. Research scope of interactions between CNTs and planar surface.

Research Objectives 2

The overarching objective of this work was to develop analytical formulas that can precisely describe the orientation-dependent interaction energy/forces between a CNT and an isotropic planar surface. *It was hypothesized that the interaction of CNTs with planar surfaces is mainly controlled by the van der Waals and electrical double layer (EDL) forces, which are the same as the classic DLVO forces.* Specific objectives are as follows:

Objective 1: develop an analytical formula of the orientation-dependent interaction energy between a pristine SWNT and an isotropic planar surface.

Objective 2: develop an analytical formula of the orientation-dependent interaction energy between a surface charged SWNT and an isotropic charged planar surface.

Objective 3: evaluate DLVO forces and torques of SWNTs with planar surfaces

Organization of the Dissertation

This Ph.D. dissertation has six chapters, including the present introductory chapter (Chapter 1). In Chapter 2, laboratory experiments were conducted to measure the single-stem contact efficiency (η_0) of colloid capture by a cylindrical collector in

laminar overland flow. A dimensionless equation of η_0 as a function of collector Reynolds number (Re_c) and Peclet number (N_{Pe}) was developed and matched the experimental data very well. In Chapter 3, the single stem attachment efficiency (α) of colloid capture by a simulated plant stem (i.e. cylindrical collector) in laminar overland flow was measured directly in laboratory flow chamber experiments. A new dimensionless equation was proposed that predicts the α of colloid capture by a cylindrical collector in laminar overland flow with reasonable accuracy. In addition, the equation was also effective in predicting the attachment efficiency of colloid deposition in porous media. In Chapter 4, in order to upscale single-stem efficiency theory to real dense vegetation, a new dimensionless number was developed to account for the effect of plant stem surface properties on the colloid deposition onto the plant stem in overland flow. An extended model including steric repulsion effect was developed that fit the experimental data with acceptable accuracy. This extended single-stem efficiency theory can be used to help construct and refine mathematical models of colloid transport and filtration in laminar overland flow on vegetated surfaces. In Chapter 5, the surface element integration (SEI) technique was coupled with the DLVO theory to determine the orientation-dependent interaction energy between a single-walled carbon nanotube (SWNT) and an infinite isotropic planar surface. For the first time, an analytical formula was developed to accurately describe the interaction between CNTs and planar surfaces with arbitrary rotation angles, which can be used to predict CNTs deposition on plant stem surface. Chapter 6 summarizes the results of all the previous chapters and makes recommendations on future work. References are included at the end of this document.

CHAPTER 2
EXPERIMENTAL ANALYSIS OF COLLOID CAPTURE BY A CYLINDRICAL COLLECTOR IN LAMINAR OVERLAND FLOW [1]

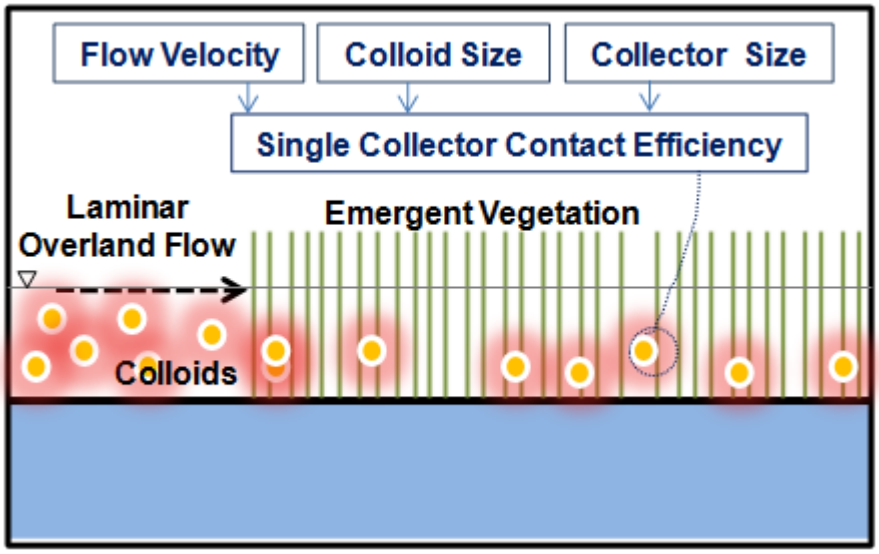

Figure 2-1. Graphical content of chapter 2

Introductory Remarks

Transport of colloidal particles in water flow is an important contamination process that can deteriorate both surface and groundwater quality. Suspended colloids are capable of carrying a variety of contaminants and enhance their mobility in aquatic systems [4]. In addition, movement of colloidal particles in soils may also affect their primary productivity, nutrient cycling, and species composition [128].

A substantial research effort has been made to understand colloid and colloidal-facilitated transport in porous media including the soil vadose zone and groundwater. Bench-scale packed column experiments have been conducted to examine the transport behaviors of different types of colloids including viruses, bacteria, clay

[1]. Reprinted with permission from ***Wu, L.,*** B. Gao, and R. Munoz-Carpena (2011), Experimental Analysis of Colloid Capture by a Cylindrical Collector in Laminar Overland Flow, ***Environmental Science & Technology***, *45*(18), 7777-7784.doi: 10.1021/es201578n.

particles, and synthetic microspheres, and engineered nanoparticles [35-38]. Relationships between system physicochemical properties (e.g., flow velocity, solution chemistry, and surface properties) and colloid mobility in porous media were evaluated [39-42]. In addition, the influences of biological factors (e.g., cell size and shape, cell motility, and micro-molecular length and composition) on bio-colloid fate and transport in porous media have been assessed [43, 44]. Finding from these investigations have enhanced current ability to predict and monitor the fate and transport of colloidal particles in subsurface flow.

Considerably less attention has been dedicated to the fate and transport of colloidal particles in surface flow, particularly with respect to colloid transport through vegetation in overland flow [48-50]. Several studies have shown that vegetation structures (submerged or emergent) can remove suspended particles including colloidal particles from surface flow [50, 52, 69]. Leonard et al [53] observed that the capture of suspended particles on the stems and leaves of *Juncus roemerianus* marsh contributed up to 10% of the total sediment deposition to a tidal marsh. Similarly, Pluntke and Kozerski [58] suggested that sedimentation onto plant structures should be considered when quantifying particle retention in submerged macrophyte stands. Particle retention in a sea grass meadow (*Posidonia oceanica*) was found to be up to 15 times greater than the equivalent non-vegetated bed [68]. In a wetland field site in the Florida Everglades, Huang et al. [69] found that aquatic vegetation could also remove colloidal particles from surface flow. These evidences strongly suggest that filtration by plant structures, such as stems, has a significant effect on the fate and transport of colloidal

particles in surface flow. Unfortunately, current understanding of the capture of colloidal particles by plant structures in surface water is still very limited.

In laminar overland flow, the depth of water is usually below the top of the sheaths of grassy vegetation and thus plan stems may dominant flow and transport processes [93, 94]. Under many circumstances, plant stems can be modeled as rigid, cylindrical collectors for colloid deposition [95]. Therefore, establishing a single-collector efficiency theory of colloids captured by a cylinder will advance the understanding the fate and transport of colloids in surface flow. The single-collector concept has not only been widely used in colloid filtration in porous media [129, 130], but also been successfully applied to sediment removal by aquatic plants [131]. However, only few studies have directly measured particle capture by a single collector, particularly with respect to a spherical or cylindrical collector [131, 132]. Their measurements validated the mathematical models of single-collector contact efficiency of colloids and suspended sediments. Nevertheless, it is unclear whether existing models can be used to describe the capture of colloids by a cylindrical collector in overland flow.

In this study, laboratory experiments were conducted to measure the single-collector contact efficiency of colloid capture by a cylindrical collector in laminar overland flow. A glass cylinder installed in a small size flow chamber was used as the collector. Silicone grease was applied to the collector surface to facilitate colloid deposition. Florescent microsphere suspension was used in the experiment as colloid flux. The amount of colloids deposition onto the cylinder surface was measured to determine the single-collector contact efficiency under various experimental conditions. Our objectives are to: 1) determine how perturbations in flow velocity, colloid size, and

collector size affect the single-collector efficiency of colloid capture by a cylindrical collector in laminar overland flow, 2) test whether existing single-collector contact efficiency models can be used to predict colloid capture by a cylinder in laminar overland flow, and 3) develop a dimensionless equation to describe the single-collector efficiency of colloid transport through emergent vegetation in laminar overland flow.

Theory

The contact efficiency of a single collector (η_0) is a ratio of the rate at which colloids strike the collector divided by the rate at which colloids flow toward the collector [129]. The magnitude of η_0 is assumed to be controlled by three transport mechanisms: interception, sedimentation, and diffusion. Interception takes place when a suspended colloid moving along flow streamlines come into contact with the collector by virtue of its size. Sedimentation occurs when a suspended colloid has a density greater than the fluid density, and the particle can then collide with a collector. Diffusion reflects the Brownian motion of the suspended colloid in fluid that leads to diffusive transport of the particle to the collector surface. The interception and sedimentation processes contribute significantly to the single-collector contact efficiency for colloids with diameters greater than 1 μm; while the diffusion mechanism becomes significant when colloids are smaller than 1 μm [129, 130, 133]. Because the sedimentation process is gravity driven, it affects the single-collector contact efficiency only when the collectors are assembled along the gravity line. In case of laminar overland flow on a flat surface or a moderate slope, we can assume the contribution from the sedimentation processes to η_0 is trivial. If only interception and diffusion transport mechanisms are considered, the single-collector contact efficiency of colloids in laminar overland flow captured by a cylinder can be expressed as:

$$\eta_0 = \eta_I + \eta_D \tag{2-1}$$

where η_I and η_D are the contributions from interception and diffusion, respectively. Usually the contact efficiency of each mechanism is first determined separately and then the overall single-collector contact efficiency can be obtained by summing the individual contributions [129, 130, 133].

Several models have been developed to calculate the single-collector contact efficiency of colloids, but almost all of them are for spherical collectors. For example, the Yao [129], RT [130], and TE [133] models have been widely used to determine the single-collector contact efficiency of colloid filtration in porous media. It is unclear whether these models can be applied to describe the single-collector contact efficiency of colloids to a cylinder collector.

Recently, Palmer et al. [131] established a theory to calculate the single-collector contact efficiency of suspended sediments for cylindrical collectors in aquatic systems. Based on their approach, each component of the single-collector contact efficiency of the cylindrical collector can then be determined analytically as functions of the particle/collector size ratio ($R=d_p/d_c$, where d_p is particle diameter and d_c is cylinder diameter in this case), and the collector Reynolds number, $R_{ec}.=ud_c/v$, where u is flow velocity, and v is the kinematic viscosity [131]. For instance, under creeping flow conditions (i.e. $Rec<1$), particle contact efficiency due to direct interception (η_I) to a cylinder can be expressed as [134]:

$$\eta_I = \frac{1}{(2-\ln \mathrm{Re}_c)}\left[(1+R)\ln(1+R) - \frac{R(2+R)}{2(1+R)}\right] \tag{2-2}$$

The contact efficiency due to colloid diffusion (η_D) for creeping flow can be written as [135]:

$$\eta_D = \frac{1.17\pi D^{2/3}}{u d_c}\left[\frac{\mathrm{Re}_c \nu}{2(2-\ln \mathrm{Re}_c)}\right] \quad (2\text{-}3)$$

where D is the particle diffusion coefficient, which can be obtained from the Einstein's diffusion equation [136]. Equations 2-2 and 2-3 are based on the aerosol filtration theory of mass transfer to a cylinder, which could be very similar to transport and deposition of colloids in overland flow through emergent dense vegetation. Therefore, we conducted a range of experiments to test whether the single-collector contact efficiency equations can be used to describe the capture of colloids by the cylindrical collector in laminar overland flow.

Materials and Methods

Colloids and Collectors

Fluorescent, carboxylated, polystyrene latex microspheres (Magsphere, Inc) of four different sizes (0.1, 1.05, 2.0 and 10.5 *μm*) were used in the experiment as model colloids. The density of the colloids, as reported by the manufacture, was 1.05 g/cm^3. Colloid suspensions for testing were made by diluting the stock solution (1.05g/mL, corresponding to 1.0×10^{15}, 8.6×10^{11}, 1.2×10^{11}, and 8.6×10^{8} no./mL for 0.1, 1.05, 2.0, and 10.5 *μm* colloids) to the target concentrations (10 mg/L, corresponding to 1.0×10^{10}, 8.6×10^{6}, 1.2×10^{6}, and 8.6×10^{3} no./mL for 0.1, 1.05, 2.0, and 10.5 *μm* colloids) with deionized (DI) water. The pH of the colloid suspensions were around 5.3.

Two glass cylinders of diameters 1.0 and 2.0 cm were used in the experiment as the collectors to simulate plant stems. Clear silicone grease (Baysilone, GE Bayer) was applied to the collector to mark off a 1 cm test section at the bottom end (Figure 2-2) to

simulate “sticky” plant surfaces, which would ensure deposition of colloids on the collector area and make the attachment efficiency (α) equal to one [131]. The final grease thickness (« 0.5 mm) was regarded not thick enough to significant change the diameter of the cylinder. This process was repeatable such that the grease layer thickness was constant every test.

Experimental Apparatus

The experimental apparatus used in this study was similar to that of Palmer et al. [131] but at a much smaller scale (Figure 2-2). The main component was an open flow channel flow chamber made of Plexiglas of 20 cm long, 10 cm wide, and 10 cm high. A recirculating peristaltic pump (Masterflex L/S, Cole Parmer) was used to provide the desired system flow velocities. An aluminum screen (holes diameter 3.0 mm, 55% open area) was installed in the flow chamber to straighten the flow. A flat velocity profile could be obtained near the center part of the flow channel as long as low velocities (< 0.3 cm/s) were used. Therefore, the longitudinal location 10 cm downstream of the inlet was chosen for the cylinder test position. The water depth in the flow chamber was controlled to be slightly above 1cm to ensure that the collector area was under water surface.

Experimental Methods

Before each test, the flow channel, the pipe and collector were cleaned thoroughly with DI water. The colloid suspension was then poured into the flume, and then stirred until the colloids spread out over the whole channel. A peristaltic pump was then used to circulate the flow in the chamber system for about 2 minutes. After the flow system properties (i.e., flow rate, water table, colloid distribution) stabilized, the cylinder collector was then carefully positioned into the chamber for durations ranging from 5 to

120 minutes (i.e., 5, 10, 30, 60, 120 minutes). Nine different flow velocities (0.02-0.2 cm/s), two collector sizes (1 and 2 cm), and four colloid sizes (0.1-10.5 μm) were tested in the experiment. At the end of each run, the flow was stopped and the collector was gently pulled out to measure the amount of colloids attached. Pre-experimental tests showed that the colloids attached to the silicon grease on the collector surface can be fully recovered with a 4% surfactant (sodium dodecylbenzene sulfonate, 10 mL) solution. A fluorescent spectrophotometer (PerkinElmer LS 45) was used to determine the amount of colloids recovered. Each experiment was repeated at least three times. The colloid capture rate (r_c) by the collector was determined by measuring the increases in number of colloids on the collector over different time intervals.

$$r_c = \frac{dN}{dt} \tag{2-4}$$

where *dN* the number of colloids increased on the collector surface over a time interval (*dt*). Thus, the single-collector contact efficiency (η_0) of colloids captured by a cylindrical collector in laminar flow can be written as:

$$\eta_0 = \frac{r_c}{N_0 u\ d_c l_c} \tag{2-5}$$

where N_0 is the number of colloids in the suspension, u is the flow approach velocity, d_c is the diameter of collector, and l_c is the height of coated area of collector.

Results and Discussion

Effects of Flow Velocity and Colloid and Collector Sizes

For all the experimental conditions tested, the number of colloids increased on the collector surface (*dN*) and the experimental time intervals (*dt*) showed good linear relationships with almost all R^2 larger than 0.9 except one (Table 1-1). Therefore, the

slopes of the linear regressions were used as the colloid capture rates (r_c) to determine the experimental single-collector contact efficiencies (η_0). Standard errors were computed for three replicate trials to estimate the uncertainties. These results demonstrate the dependence of η_0 on flow velocity (u), colloid particle diameter (d_p), and collector diameter (d_c).

Increases in u reduced η_0 when d_p and d_c were 1.05 μm and 2 cm, respectively (Figure 2-3). For example, η_0 decreased by 2 orders of magnitude when the u increased from 0.002 to 0.2 cm/s, indicating a negative correlation between the single-collector contact efficiency and the colloid approach velocity. This trend is consistent with the findings of previous studies on colloid transport in porous media (spherical collectors). A number of experimental and modeling studies have demonstrated that the filtration/removal rate of colloids through a porous medium filter decreases when the flow rate increases [137-139]. Compere et al. [139] observed that deposition rate of clay colloids decreases with flow velocity whereas the collector efficiency increases by a factor of 5.1 as flow velocity decreases by a factor of 0.11. Similarly, Camesano and Logan [138] observed that, for passive colloids, the fractional retention would increase by more than 800% as the pore velocity was decreased from 120 to 0.56 m/day. For suspended sediments captured by a cylinder collector, however, Palmer et al [131] observed an opposite result showing the increases of contact efficiency with higher flow rates. This divergence might be attributed to the high settling/sedimentation rate of suspended sediments in the overland flow, which is much higher than that of colloids (negligible in this study). In the study of Palmer et al [131], increasing in flow rate could

offset the sedimentation processes and increase the capture rate of sediments by the cylinder collector, and thus increase the single-collector contact efficiency.

For collectors of different sizes (i.e., d_c = 1 or 2 cm), the single-collector efficiency (η_0) varied with colloid diameters (d_p), suggesting that a minimum value of η_0 might exist at a critical colloid size (Figure 2-4). This is consistent with the classic single-collector efficiency theory of colloid filtration in porous media [129]. For colloid transport in porous media under unfavorable conditions, Elimelech [140] found that particles with diameter of 1.15 μm had a lower collector efficiency than particles with diameters of 0.08, 0.17, or 2.52 μm. In a test of colloids with a wide range of particle sizes, Zhuang et al. [141] found that dependence of colloid retention on particle size was nonlinear and there existed a fraction of colloids with greater mobility (i.e., minimum value of η_0) than other fractions. On the other hand, however, several studies have also observed the independence of collector efficiency on particle size [115, 142]. Further investigations are still needed to quantify the relationship between colloid size and collector efficiency.

Comparisons of the η_0 values between the two collectors of different sizes also revealed that, for the same u and d_p, the smaller collector (i.e., 1 cm) had higher values of η_0 than the larger collector (i.e., 2 cm). Similar relationship between η_0 and d_c was observed for the removal of suspended sediments by cylinder collectors in overland flow [131].

Comparison of Experimental Data and Theoretical Predictions

The experimental data discussed above were compared with their corresponding values of η_0 based on the theoretical predications of suspended particles captured by a cylinder collector in creeping flow (i.e., equations 2-1-2-3). Under shallow overland flow conditions, average overland flow velocity is often used to determine the single-collector

contact efficiency at a cross section of the cylinder (two dimensional) [131]. As a result, mathematical formualtions of the single-collector contact efficiency on colloid transport in porous media, such as the Yao model [129], RT model [130], and TE model [133], can be also used to calculate the theoretical predications of colloids captured by a cylinder collector.

For all conditions tested, the experimental single-collector contact efficiencies were larger than the corresponding theoretical values of equations 2-1-2-3 (Figure 2-5a). This discrepancy is probably due to the relatively high collector Reynolds numbers in the experiments. Although the experimental flow velocities was controlled to be low, the Rec was between 0.4 and 40 (Laminar flow), still larger than the limitation of the equations 2-1-2-3 (Rec<1, creeping flow). Under creeping flow conditions, it is reasonable to assume that only interception and diffusion processes are the main contributors to the single-collector contact efficiency. When the R_{ec} is higher, however, other processes, such as mechanical dispersion, could also alter the contact of colloids to the collector. A number of studies of the transport of colloids and other suspended particles in aquatic systems have emphasized the importance of longitudinal and vertical dispersion on their removal by vegetation [69, 143, 144]. Similarly, the sphere collector models also underestimated the experimental η_0 for all the experimental conditions (Figure 2-5b-d). The failures of the theoretical predictions suggested that none of the existing equations/models of single collator efficiency could be applied directly to determine the filtration rate of colloidal particles by dense, non-submerged vegetation in laminar overland flow.

A Regression Equation

Our experimental data indicated that the actual single-collector contact efficiency should be a function of the flow velocity, collector size, and colloid size. Therefore, a dimensionless equation in the form of $\eta_0 \approx$ a $(R_{ec})^{b}$ $(N_{Pe})^{c}$ can be formulated, where N_{pe} is the Peclet number ($N_{pe}=ud_c/D$). Based on the experimental data obtained (R_{ec} =0.42-42 and N_{Pe} =4.5×10^5-9.7×10^7), the best-fit (R^2 > 0.98, Figure 2-6) dimensionless equation can be written as:

$$\eta_0 = 0.0044\, R_{ec}^{-0.94}\, N_{Pe}^{-0.03} \qquad (2\text{-}6)$$

Although this dimensionless equation can be applied to a wide range of Peclet numbers (two orders), it is only valid for predicting the single-collector contact efficiency of colloids approaching cylindrical collectors (plan stems) under laminar flow conditions. It was impossible to further validate the dimensionless equation for field conditions because only few/no studies have been conducted to measure the removal of colloidal particles by plant stems in laminar overland flow. In a recent study, Huang et al. [69] measured the filtration of 1μm latex microspheres within emergent vegetation at a wetland field site located in the Florida Everglades. They found that plant stems could effectively remove the colloids (microspheres) from flow and the average single collector removal efficiency was 0.002. Unfortunately, the Rec value of Huang et al. [69] was above the limitation of the dimensionless equation, as a result, the dimensionless equation could not be applied to their experiment. Additional investigations, particularly experimental studies, are in critical need to measure the removal of colloids by plant stems in laminar overland flow.

Environmental Implication

Laboratory experiments were conducted to measure the single-collector contact efficiency of colloids by cylindrical collectors in a flow chamber under laminar flow conditions. Our results indicated that η_0 decreased with flow velocity (u) and collector diameter (d_c), and a minimum value of η_0 might exist at a critical colloid size (d_p). We also found that existing single-collector contact efficiency models underestimated the η_0 of colloid capture by the cylinders in laminar overland flow. A new dimensionless equation was thus developed to determine η_0 as a function of Reynolds and Peclet numbers (R_{ec} and N_{Pe}) that matched the experimental data very well. Although additional investigations of its generality are still needed, this dimensionless equation can be used to determine the colloid filtration/deposition rate in dense, non-submerged vegetation (e.g., vegetative filter strips) in laminar overland flow, and to enhance current capacity to predict the fate and transport of colloidal contaminants in surface runoff.

For colloid removal by emergent vegetation in laminar overland flow, the single-collector removal efficiency (η) is often lower than the single-collector contact efficiency (η_0) because the contacts between colloids and plant stems may not guarantee 100% removal. Therefore, single collector removal efficiency is often expressed as a product of an empirical attachment (collision) efficiency (α) and the single-collector contact efficiency [129]:

$$\eta=\alpha\eta_0 \qquad (2\text{-}7)$$

The attachment efficiency is defined as the fraction of contacts between colloids and the collector that result in attachment, which reflects the chemistry of the system [129]. Several theoretically formulations have been established to calculate α based on

the Derjaguin-Landau-Verwey-Overbeek (DLVO) interaction energy profiles between colloids and the collector upon close separation [145-147].

For colloids in overland flow, convection-dispersion equations coupled with deposition kinetics are commonly used to predict their fate and transport in dense vegetation [148]. The kinetic deposition rate is often represented by the particle deposition rate coefficient, k_d [129, 133]. For a vegetation system of a spacing density (f), which is defined as the ratio of the empty area among the plant stems divided by the total vegetated area, the relationship between k_d and η can be written as:

$$k_d = \frac{4(1-f)}{\pi d_c}\frac{u}{f}\eta \tag{2-8}$$

where the ratio of the approach velocity to the spacing density (u/f) is the interstitial fluid velocity commonly used in modeling colloid transport in filter media.

Table 2-1. Summary of experimental conditions and results

Test No.*	Particle diameter d_p (μm)	Flow velocity u (cm/s)	Collector diameter d_p (cm)	Increased colloids no. as a function of time intervals (r_c=dN/dt)	R^2	Single-collector contact efficiency (η_0) Mean (%)
I.1	1.05	0.002	2	13310±821	0.991	6.4E-03±4.0E-04
I.2	1.05	0.004	2	13764±969	0.994	3.3E-03±2.3E-04
I.3	1.05	0.008	2	14145±899	0.990	1.7E-03±1.0E-04
I.4	1.05	0.01	2	14346±600	0.986	1.4E-03±5.8E-05
I.5	1.05	0.02	2	14477±629	0.991	6.9E-04±3.0E-05
I.6	1.05	0.04	2	14656±629	0.989	3.5E-04±3.0E-05
I.7	1.05	0.08	2	14934±629	0.981	1.8E-04±9.7E-06
I.8	1.05	0.10	2	14895±617	0.992	1.4E-04±6.0E-06
I.9	1.05	0.20	2	15143±566	0.983	7.3E-05±1.8E-06
II.1	0.1	0.02	2	16957±1145	0.942	8.2E-04±5.5E-05
II.2	0.1	0.02	1	14977±876	0.954	1.5E-03±8.5E-05
II.3	1.05	0.02	1	12102±481	0.981	1.1E-03±4.6E-05
II.4	2.0	0.02	2	15421±1194	0.985	7.4E-04±5.7E-05
II.5	2.0	0.02	1	12664±718	0.978	1.2E-03±6.9E-05
II.6	10.5	0.02	2	23612±589	0.886	1.1E-03±1.1E-05
II.7	10.5	0.02	1	22603±402	0.972	2.1E-03±3.8E-05

*No. I.1-I.9 summarize the effect of flow velocity; No. II.1-II.7 summarize the effect of colloid size and collector size

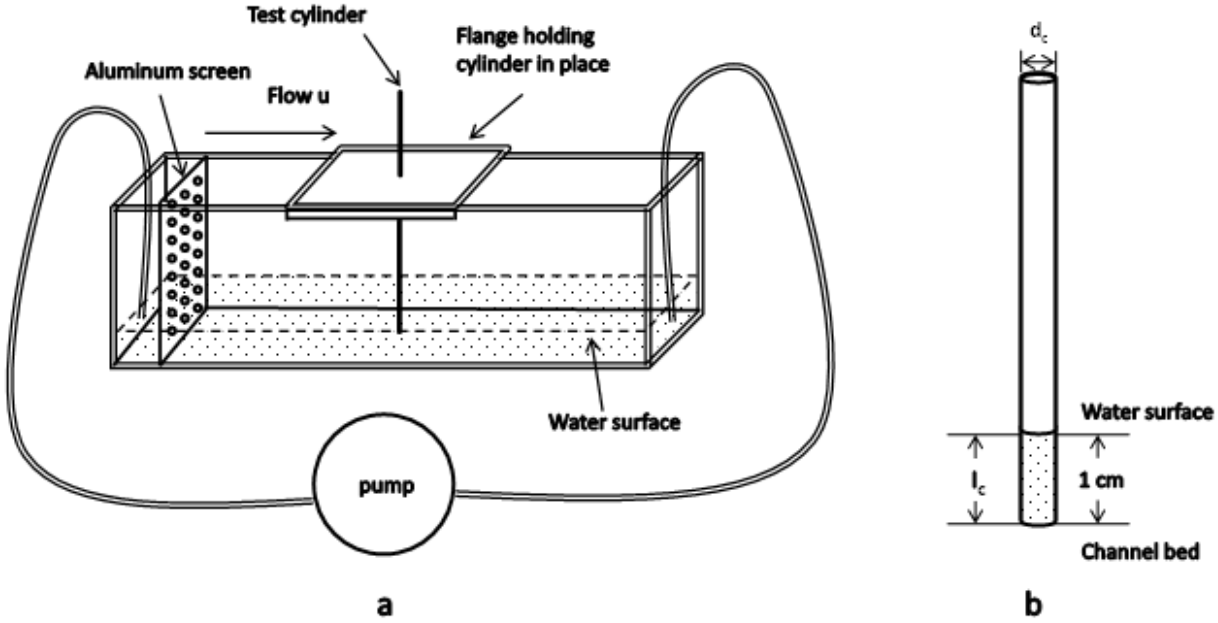

Figure 2-2. Schematic of experimental setup for measuring single-collector contact efficiency.

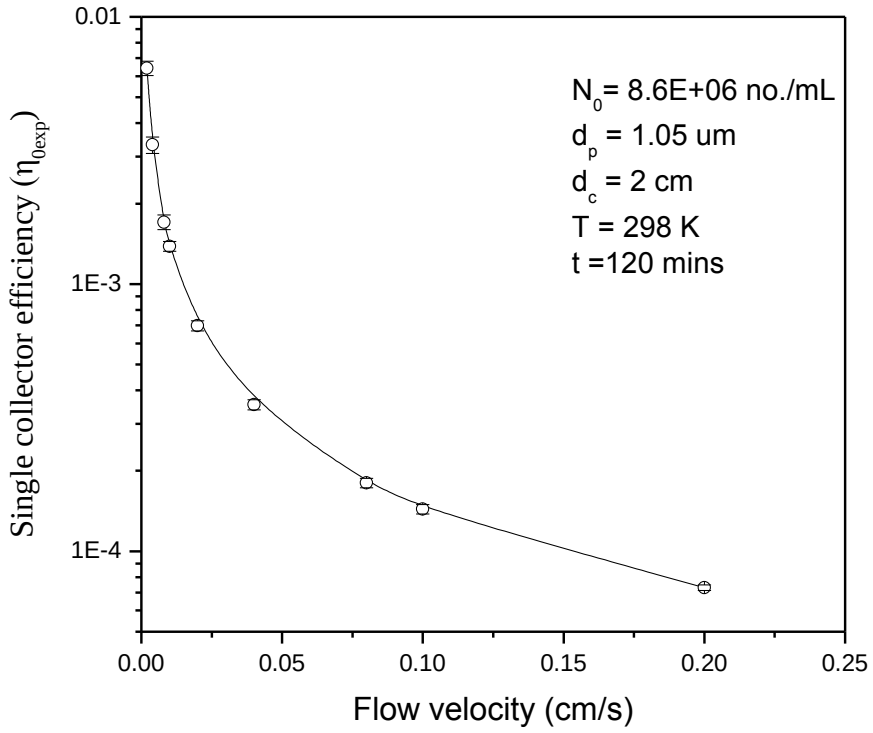

* η_{0exp}—*E*

Figure 2-3. Effect of flow velocity on single-collector contact efficiency.

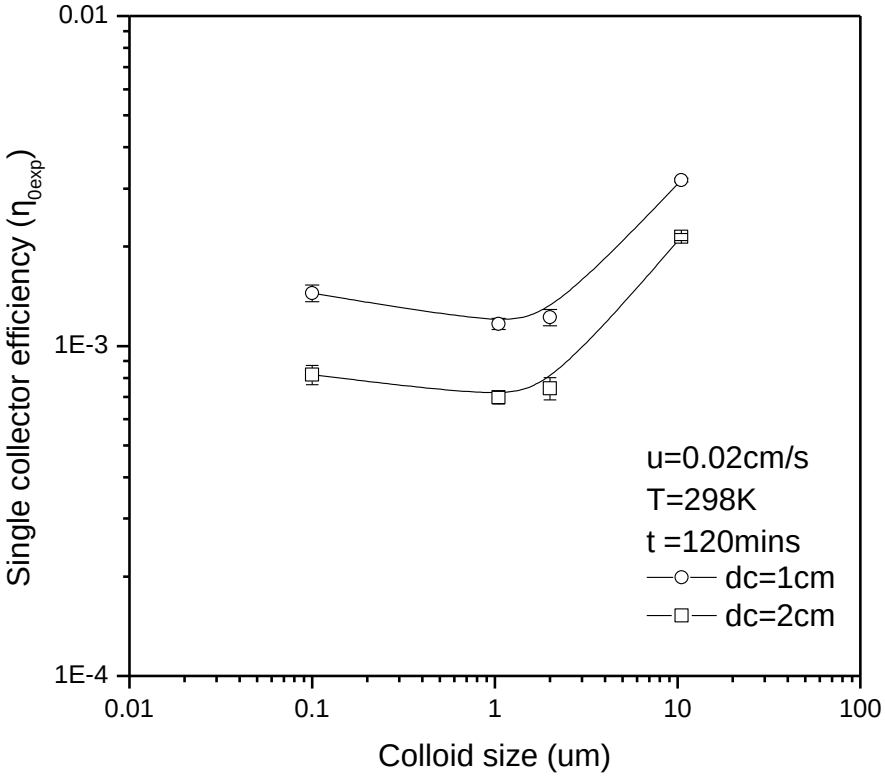

* η_{0exp}—η_0-experimental

Figure 2-4. Effect of colloid and collector sizes on single-collector contact efficiency.

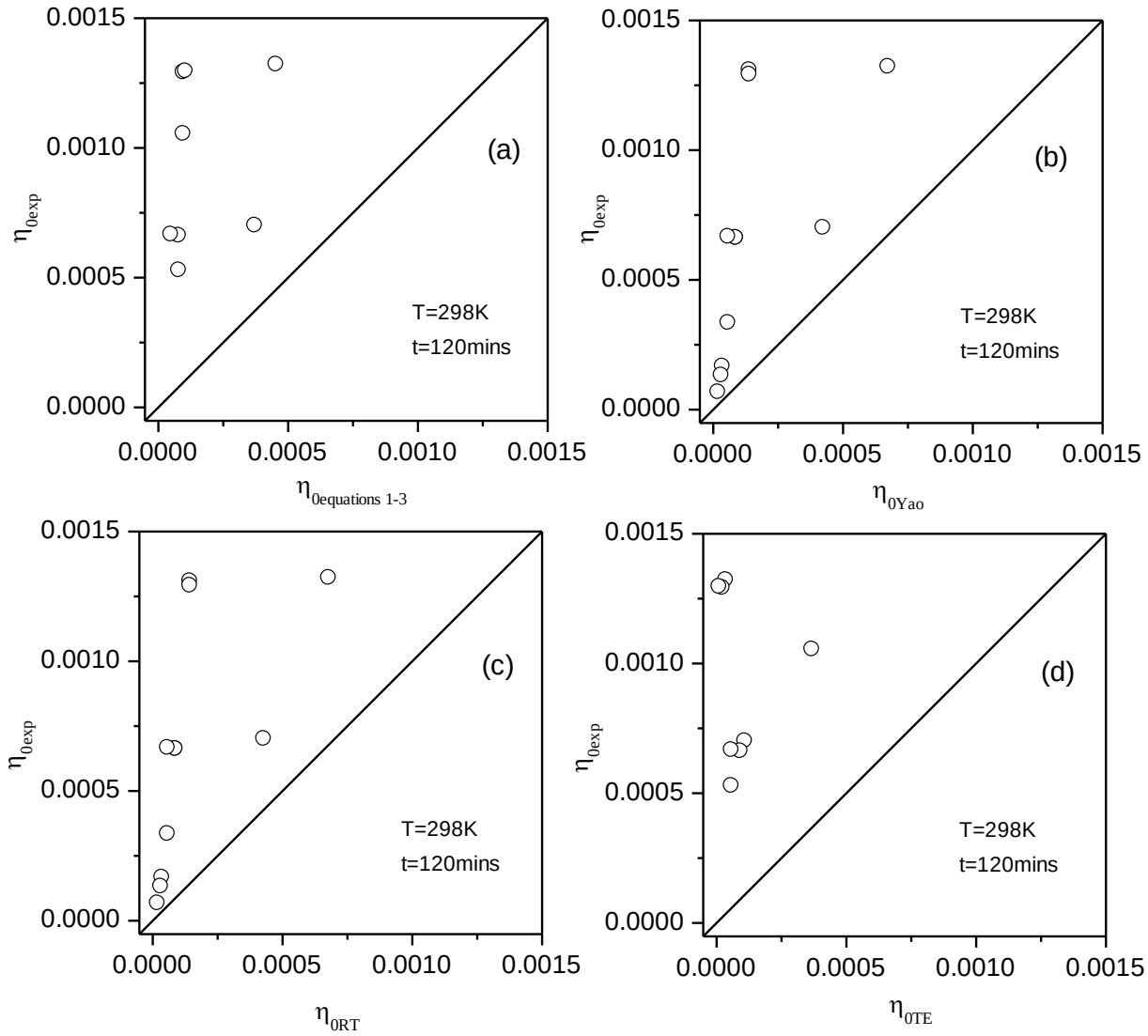

* η_{0exp}—η_0-experimental; $\eta_{0equations1-3}$—η_0-equations 2-1-2-3; η_{0Yao}—η_0-Yao; η_{0RT}—η_0-RT; η_{0TE}—η_{0-TE}

Figure 2-5. Comparison of experimental data of single-collector contact efficiency with predictions of (a) equations 1-3, (b) the YAO model, (c) the RT model, and (d) the TE model.

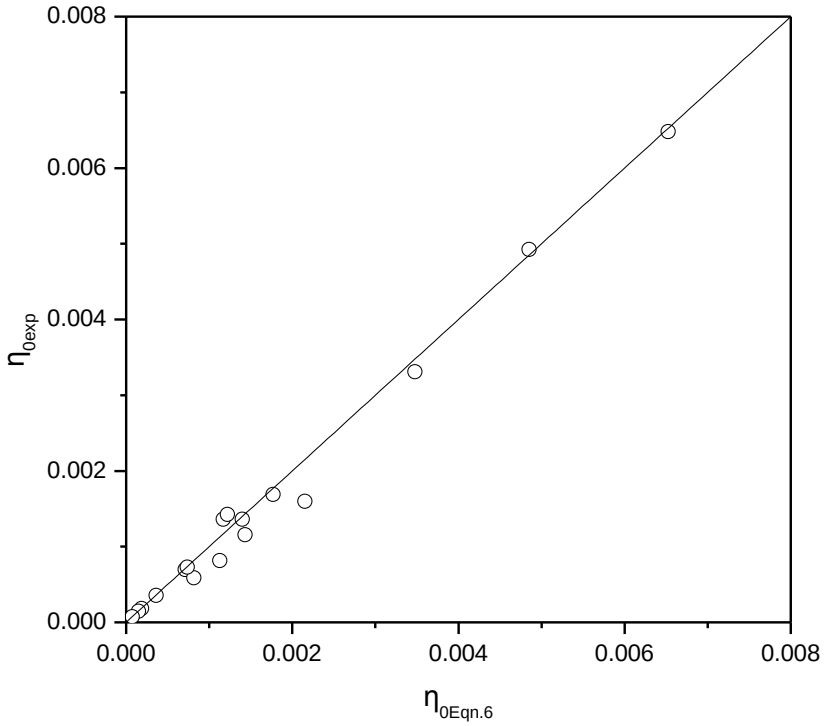

* η_{0exp}—η_0-experimental; $\eta_{0Eqn.6}$—η_0-Equation 6

Figure 2-6. Comparison of experimental data of single-collector contact efficiency with predictions of the new dimensionless equation (equation 2-6).

CHAPTER 3
SINGLE COLLECTOR ATTACHMENT EFFICIENCY OF COLLOID CAPTURE BY A CYLINDRICAL COLLECTOR [1]

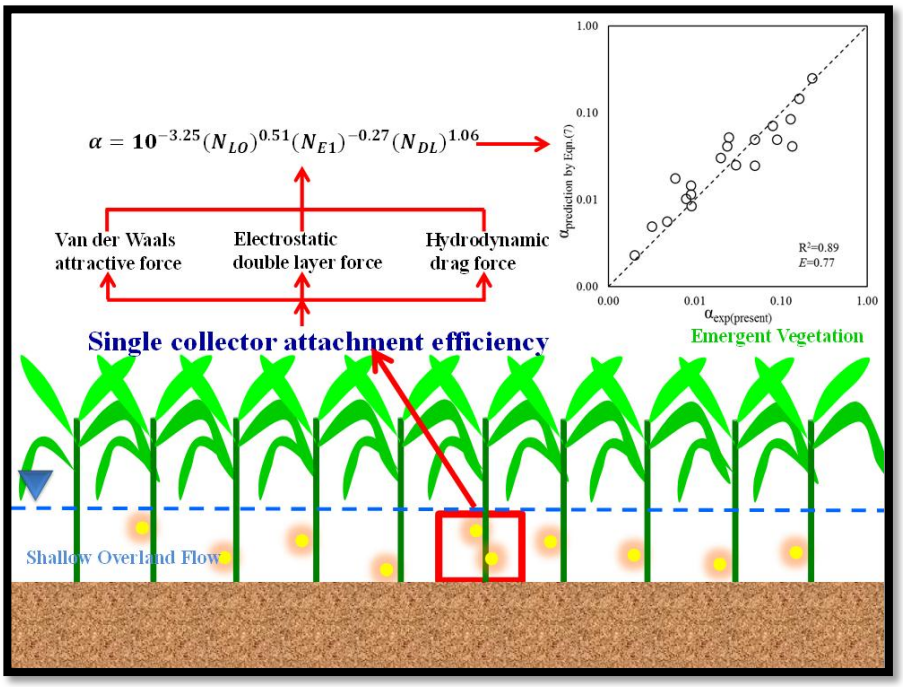

Figure 3-1. Graphical content of chapter 3

Introductory Remarks

Colloidal particles in surface runoff may have adverse effects on many environmental and biological processes, e.g., facilitating contaminant transport in flow, impairing water quality, disturbing life cycles of microorganisms, and altering wetland geomorphology [39, 42, 149, 150]. It has been suggested that vegetation systems in surface flow can act as a filter or as storage to reduce contaminant loading into natural water bodies [72, 151, 152]. Recent studies found both emergent and submergent plants were effective to remove colloids from water flow [153, 154]. However, only

[1] Reprinted with permission from ***Wu, L.***, B. Gao, R. Munoz-Carpena, and Y. A. Pachepsky (2012), Single collector attachment efficiency of colloid capture by a cylindrical collector in laminar overland flow, ***Environmental Science & Technology***, *46*(16), 8878-8886.doi: 10.1021/es301365f

limited research has been conducted to explore the governing mechanisms of colloid filtration by plants in overland flow [155].

Field deposition of colloids in overland flow through dense vegetation is comprised of subsurface soil infiltration and surface filtration by vegetation processes. The surface filtration of colloids by emergent plants can be considered to be governed by two sequential interactions between colloids and plants: physically controlled contact process and chemically controlled attachment process [129, 145, 146, 156]. The transport of colloidal particles from the bulk suspension to make a contact to a plant stem collector is mainly controlled by the interception and Brownian diffusion mechanisms [129, 155]. The single contact efficiency (η_0) theory of colloid filtration by vegetation has been established recently based on the two mechanisms [155]. Under unfavorable chemical conditions (i.e., in the presence of repulsive electric double layer interactions), however, the contact with a collector surface per se does not ensure the capture of colloidal particles by the collector as a result of the repulsive interaction forces between the colloid and collector surfaces [129, 145]. Under most circumstances, the surface water environment is chemically unfavorable for the attachment of colloids on plant collectors because not only do most colloids and plants carry overall negative surface charges [157, 158], but also the ionic strength of surface water is typically low (0.0001-0.01M) [149, 159]. To fully understand the fate and transport of colloids in surface water, it is therefore critical to develop a theory to describe the attachment process of colloids on plant collectors.

Based on the framework of the classic filtration theory (CFT) [129], the concept of single collector attachment efficiency (α) was introduced together with the single

contact efficiency (η_0) theory to predict the removal of colloids by vegetation in laminar overland flow under unfavorable conditions [155]:

$$\eta = \alpha\eta_0 \tag{3-1}$$

where η is the single collector removal efficiency of colloid filtration by plants.

Very limited literature exists on the values of α for colloid filtration by surface vegetation; however, a substantial research effort has been made to understand the attachment process of colloids in porous media under unfavorable conditions. According to the original assumptions in the CFT, α should only depend on chemical properties of the system, such as surface charge and solution chemistry, which exert significant effect on the interaction forces between the colloid and collector surfaces [129, 145, 156]. Derjaguin-Landau-Verwey-Overbeek (DLVO) theory is often used to predict the attachment efficiency of colloids in porous media; however, discrepancies were reported between the theoretical predictions and experimental observations [142, 160, 161]. To account for these discrepancies, various assumptions have been made to modify the DLVO -based α theory , including deposition in the secondary minimum energy well [146, 147], collector charge variability [162], and surface charge heterogeneities [39, 163, 164]. Researchers have also suggested that the discrepancies may also occur as a result of physical effects that are not included in filtration theory. For example, effect of hydrodynamic shear stress on α should not be neglected under unfavorable conditions especially when colloids are weakly deposited in the secondary minimum [165, 166]. In addition, other physical factors, such as surface roughness [41, 167], pore geometry [168, 169], and stagnation zones [170, 171], were also reported to affect the α of colloids in porous media. Findings from investigations studying these effects could be

very useful to the development of single collector attachment efficiency theory for plant filtration of colloids in overland flow.

The overarching goal of this work was to establish the single collector attachment efficiency (α) theory for colloid transport through dense emergent vegetation, such as vegetative filter strips, in laminar overland flow. Under such condition, the water depth is usually below the top of the sheaths of vegetation and only plant stems are submerged to affect flow and transport processes [155]. Laboratory experiments were conducted to measure the colloid attachment efficiency on a cylindrical collector in laminar overland flow under unfavorable chemical conditions. A glass cylinder was installed in a small size flow chamber to simulate plant stem collector under laminar flow conditions. Rigid cylinders, such as glass or plastic rods and nails have been demonstrated to be effective representations of plant stems in surface runoff under various flow conditions [131, 155, 172]. Fluorescent microspheres were applied to the flow system as experimental colloids and the amount of colloids deposited onto the collector surface was measured to determine the attachment efficiency under various conditions. Specific objectives were as follows: (1) quantify the effect of ionic strength, colloid size, and flow velocity on the single collector attachment efficiency of colloid capture by the cylindrical collector in laminar overland flow, (2) determine whether existing single collector attachment efficiency models of porous media can be applied directly to vegetation systems, (3) establish a theory to predict the deposition of colloidal particles on vegetation in laminar overland flow conditions.

Theory

The single collector attachment efficiency (α) is defined as the ratio of the rate at which particles successfully attach to the collector divided by the rate at which colloids

strike the collector [129]. Under unfavorable chemical conditions, the magnitude of α is assumed to be mainly controlled by the interaction forces between the colloidal particle and the collector [129]. The classic and extended DLVO theories, which describe the attractive (Van der Waals) and repulsive (electrostatic double layer) forces between colloid and collector surfaces, are often used to determine the inter-surface interactions. Several models have been developed based on the DLVO theory to predict the α of colloid deposition in porous media under unfavorable conditions using either the interaction force boundary layer (IFBL) approximation or the Maxwell approach [142, 145, 146].

Models based on the IFBL approximation or its extensions determine the *α* of colloid deposition in porous media through analytically or numerically solving the convective-diffusion equation with repulsive colloidal interactions. Previous studies, however, found the predictions from the IFBL models had rather poor agreement with measurements due to several factors [142, 145, 146]. The most important one was that the IFBL models do not consider the contributions of the secondary minimum energy well, which may play an important role in colloid deposition under unfavorable chemical conditions [146]. The Maxwell approach was then developed to determine colloid attachment efficiency through deposition in the secondary minimum [146]. If both primary and secondary energy minimum depositions are considered, the single-collector attachment efficiency (*α*) of colloid deposition in porous media can then be expressed as [146, 173]:

$$\alpha = \alpha_{pri} + \alpha_{sec} \tag{3-2}$$

where α_{pri} and α_{sec} are the fractions of single-collector attachment efficiency of colloid deposition in the primary energy minimum and secondary energy minimum, respectively. In the Maxwell model, the single-collector attachment efficiency is considered to be only influenced by chemical factors, such as solution chemistry and surface properties [129, 142, 145, 146]. Predictions of the Maxwell model were more accurate for column experiments under unfavorable conditions than that of the IFBL models [146, 173]. Some deviations from experimental measurements, however, were also observed for the Maxwell model, particularly with respect to deposition of relatively large size particles in porous media [147, 173].

Experimental measurements have shown that α of colloid deposition in porous media may also be affected by hydrodynamic factors (e.g., flow velocity)[165, 174-176]. The effect of hydrodynamic drag on α was determined through hydrodynamic torques analysis [166, 177]. It is reported that the Maxwell model coupled with the hydrodynamic torques approach can provide an improved prediction of α of colloid deposition in porous media under unfavorable conditions [178]. The attachment efficiency can be expressed as [178]:

$$\alpha = f_{pri}\alpha_{pri} + f_{sec}\alpha_{sec} \quad (3\text{-}3)$$

where f_{pri} and f_{sec} are the fractions of single collector surface area over which the adhesive torques acting on the colloids retained in the primary and secondary minimum are greater than the fluid hydrodynamic drags, respectively.

In addition to the theoretical approach, empirical expressions (e.g., Bai-Tien model) have also been developed to predict the α of colloid deposition in porous media in terms of dimensionless parameters [179-182]. Detailed description of the theoretical

and empirical models of the α of colloid deposition in porous media can be found in the APPENDIX.

Because of the differences in flow and transport processes between surface vegetation and subsurface porous media systems, however, it is unclear whether the existing theoretical and empirical models of α can be applied to describe the attachment processes of colloids on the plant collector under laminar flow conditions.

Materials and Methods

Materials

Fluorescent, carboxylated, polystyrene latex microspheres (Magsphere, Inc) of two sizes (0.1 and 1.05 μm) were used as experimental colloids. As reported by the manufacturer, the density of the colloids is 1.05 g/cm^3 and the surface carboxyl group coverage is 8.28×10^{17} and 1.19×10^{18} /m^2 for 0.1 and 1.05 μm colloids, respectively. Experimental solutions were made by diluting the stock colloid solution (1.05 g/mL, corresponding to 1.0×10^{15} and 8.6×10^{11} no./mL for 0.1 and 1.05 μm colloids, respectively) to the target concentration (10.5 mg/L) with deionized (DI) water.

A circular cylinder glass rod with diameter 0.5 cm was used as the collector to simulate plant stems. The glass rod was cleaned with acetone and then soaked in a 6 M HNO_3 solution for 5 h at 80 °C to remove metal oxides and other impurities on its surface [141, 142, 166]. For each measurement, a new glass rod without any coating was used to measure the α under various experimental conditions.

Analytical reagent grade KCl (Fisher Scientific) and DI water were used to prepare electrolyte solutions at desired ionic strengths. The pH for all the electrolyte solutions was adjusted to 7 with 1 mM $KHCO_3$ solution The experiments were conducted at five ionic strengths (0.001, 0.005, 0.01, 0.05, and 0.1 M) so that different

attachment efficiencies could be measured. While the first three were selected to represent the typically low ionic strengths of overland flow [149, 159], the latter two (i.e., 0.05 and 0.1 M) were used to exam the effect of high ionic strength on attachment efficiency. Because carboxyl group is acidic and has a pKa value of 5 [43], almost all (>99%) of the function groups on the colloids surface would deprotonate ($-COO^-$) and because negative charged for all the tested experimental conditions. Thus, the corresponding ξ potentials (i.e., electrokinetic potential) of the 0.1 and 1.05 μm colloids were -80.4, -70.3, -60.8, -48.1, -38.0 mV and –68.6, -63.9, -59.2, -41.2, -35.4mV, respectively, whereas the corresponding ξ potentials of the glass collector were -57.8, -52.1, -50.5, -32.0, -18.8mV, which were determined with a ZetaPlus (Brookhaven Instrument Co., Holtsville, NY). The ξ potentials of the glass rod were determined with colloidal glass suspensions (obtained from sonicating the glass rod) under various chemical conditions following the method developed by Johnson et al. [183]

Experimental Methods

The experimental apparatus and procedures used in this study were described in detail in our previous work [155]. Briefly, the Plexiglass flow chamber was 20 cm long, 10 cm wide and 10 cm high. For each run, one clean glass cylinder was installed on the chamber bed as the single collector. A recirculating peristaltic pump (Masterflex L/S, Cole Parmer) was used to provide the desired system flow velocities. Once the colloid suspension was stabilized (i.e., flow rate, water table, colloid distribution), the collector was then positioned into the chamber for durations of 5, 10, 30, 60, or 120 minutes to determine the colloid attachment rate on the collector surface over different time intervals [155]. At the end of each run, the flow was stopped and the collector was pulled out to measure the amount of colloids attached. Pre-experiments showed that

colloids attached to the clean collector surface under all experimental conditions could be fully recovered in DI water after 5 minutes of ultra-sonication. A fluorescent spectrophotometer (PerkinElmer LS 45) was used to determine the colloid concentration. Each experiment was repeated at least three times.

Two sets of experiments were conducted in the flow chamber system. The first set of experiments was designed to measure the α under different ionic strength conditions (0.001, 0.005, 0.01, 0.05, and 0.1 M) at an approach flow velocity of 2×10^{-2} cm/s for both 0.1 and 1.05 μm colloids. The second set of experiments was designed to measure the α under different flow velocity conditions (2×10^{-4}, 2×10^{-3}, 2×10^{-2}, 2×10^{-1} and 1 cm/s) at 0.01 and 0.1M ionic strength with both 0.1 and 1.05 μm colloids (Table 3-1).

The colloid capture rate (r_c') by the single collector was determined by measuring the increases in number of colloids on the collector over different time intervals.

$$r_c' = \frac{\Delta N'}{\Delta t} \tag{3-4}$$

where $\Delta N'$ (no.) is the increment in number of colloids on the clean collector surface over a time interval Δt (s).Thus, the single collector removal efficiency (η) of colloids by a cylindrical collector in laminar flow can be written as follows:

$$\eta = \frac{r_c'}{N_0 u d_c l_c} \tag{3-5}$$

where N_0 (no./m^3) is the number concentration of colloids in the suspension, u (m/s) is the flow approach velocity, d_c (m) is the diameter of collector, l_c (m) is the height of test area of collector. The values of the single-collector contact efficiency (η_0) of the microspheres captured by the cylinder in the same flow chamber system had been

determined previously,[155] therefore, the single-collector attachment efficiency (α) of each experiment in this work was calculated using equation (3-1).

Results and Discussion

Effect of Ionic Strength

Measurements from the flow chamber experiments showed that the single collector attachment efficiencies (α) varied by several orders of magnitude depending on experimental conditions (Table 1). When the flow ionic strength increased, α increased for both 0.1 and 1.05 μm colloids (Figure 1), which matched the trend from the DLVO calculations. The DLVO energy profiles between the colloids and the collector surface (Figure 3-3) confirmed the experimental conditions were unfavorable for attachment. When the ionic strength increased from 0.001 to 0.1M, the depth of the secondary minimum energy well (Φ_{sec}) increased from 0.03 to 0.41 kT and from 0.72 to 12.8 kT for 0.1 and 1.05 μm colloids, respectively (Table 3-2). At the same time, however, the height of the energy barrier (Φ_{max}) decreased from 162.1 to 49.1 kT and from 1145.3 to 412.8 kT for particle diameters 0.1 μm and 1.05 μm, respectively. Calculations from the Maxwell theory [146, 173] showed that the α_{pri} was close to zero because the Φ_{max} was too high for all the tested experimental conditions, suggesting that deposition of colloids in the primary minimum energy well was insignificant. Instead, most the colloid attachment was in the secondary minimum and α_{sec} was notable when Φ_{sec} was larger than 0.5 kT. For any given ionic strength, the 1.05 μm colloids had a larger α than the 0.1 μm ones, which is also consistent with both the DLVO and the Maxwell theory predictions that increase in colloid diameter would also increase the Φ_{sec} and thus enhance the deposition in the secondary minimum.

Although no previous investigations examined the effect of perturbations in solution chemistry or variations in particle size on the attachment processes of colloids on vegetation surfaces in overland flow, similar research has been well documented in the literatures of colloid deposition in porous media [17, 141, 142, 184-187]. A number of studies of colloid transport in porous media have demonstrated that a rise in ionic strength can increase the attachment of colloids on grain surfaces by reducing the thickness of the diffuse double layer between colloid and collector surfaces and thus reducing the repulsive forces [17, 188], which is consistent with the observations in this study. Several recent studies have also shown that colloid sizes can significantly affect colloid deposition in porous media [141, 184, 187]. In a column transport study with different sizes latex microspheres, Hahn et al [161] observed that larger colloids had larger α than the smaller ones and emphasized the dominance of secondary minimum deposition on colloid retention in porous media.

In this work, observations from the ionic strength experiments indicated that the secondary minimum may play a dominant role in colloid deposition on the cylindrical collector under all the tested experimental conditions. Hence, the Maxwell theory [146, 173] could be used to determine the α of colloid deposition on stem collectors if the attachment processes were only controlled by chemical factors.

Effect of Flow Velocity

Flow velocity also had a strong effect on the α of the 0.1μm and 1.05 μm colloids in the flow chamber at ionic strengths of 0.01 or 0.1M (Figure 3-4), which suggested physical factors such as hydrodynamics also play an important role in controlling attachment efficiency of colloid deposition on cylindrical collectors in overland flow. Increases in flow velocity reduced the attachment of colloids on the cylinder probably

due to the hydrodynamic shear forces [166]. Similar phenomena were observed in studies of colloid filtration and transport in emergent vegetation in wetland systems. In a field flume in the Everglades (FL), Harvey et al.[150] observed that particle attachment to vegetation stems decreased when flow velocity increased from 0.3 cm/s up to 6 cm/s. Similarly, Huang et al.[154] found that high flow velocity in their field flume in the Everglades significantly reduced the removal of colloids by the emergent vegetation. These findings are consistent with current experimental observations; however, none of the previous studies has quantitatively examined the effect of hydrodynamic shear forces on the attachment efficiency of colloid capture by vegetation surfaces.

Previous studies of colloid transport in porous media have emphasized the hydrodynamic effect on colloid deposition and demonstrated that the α decreased with increasing flow velocity under unfavorable chemical conditions [166, 177, 189]. In a laboratory column experiment, Tong and Johnson [189] found a decrease of attachment efficiency when flow velocity increased from 2.3×10^{-5} to 9.2×10^{-5} m/s for colloids of 0.1-2.0 μm. They attributed the changes in the α to the hydrodynamic drag force, which could shear the colloids off the porous medium surfaces. It is suggested that hydrodynamic drag may indirectly prevent colloid deposition into the primary minimum by reducing the possibility for the “attached” colloids within the secondary minimum to cross the energy barrier [190]. Under certain conditions, the hydrodynamic drag may also reduce the retention of colloidal particles in the secondary minimum via following mechanisms: (1) reduce colloid retention capacity due to reduction of stagnant flow zone volumes [166], (2) enhance hydrodynamic collisions between mobile and surface associated colloids [166], and (3) increased diffusion “out” of the secondary minimum

driven by increased colloid concentration gradients away from zones of accumulation (i.e., rear stagnation points) [146].

Both current experimental results and findings from colloid transport studies in porous media suggest that the original assumption of chemical governing attachment processes in the CFT may need to be revisited. Physical factors such as flow velocity may play an important role in controlling the α of colloid deposition in both vegetation and porous media systems. In the literature, a hydrodynamic torque approach was introduced to improve the Maxwell theory to predict the α of colloid deposition in porous media [178]. Surface vegetation, however, may have very different flow dynamics as compared with porous media. It is anticipated that the modified Maxwell theory may not be applicable to estimate the attachment efficiency of colloid capture by cylindrical collectors even under laminar flow conditions.

Comparison of Experimental Data and Theoretical Predictions

The Maxwell model [146], the modified Maxwell model (i.e., coupled by hydrodynamic torques) [178], and the empirical Bai-Tien model [180] were used to estimate the α of colloid capture by the cylindrical collector under all experimental conditions (Figure 3-5). Detailed information about the three models used in the study can be found in the APPENDIX.

Although it was reported that the Maxwell model works well for describing attachment processes of colloids (particularly small size colloids) in porous media [146, 191], it failed to match the experimental data obtained from the flow chamber (Figure 3-5). The model overestimated the α of colloid deposition on the cylinder up to 1-2 orders of magnitude for almost all experimental measurements. This result further confirmed that physical factors, such as hydrodynamics, should be considered in the theory of

colloid attachment efficiency. The modified Maxwell model, which considers the hydrodynamic factor, did show a better agreement with the experimental measurements than the original Maxwell model (Figure 3-5). However, significant differences between model and experimental results were still observed, especially when flow velocity became high (e.g., 0.2 cm/s and 1cm/s), suggesting that, even after the consideration of hydrodynamic effect, the modified Maxwell model cannot be applied directly to describe the α of colloid deposition on vegetation in laminar overland flow. Similarly, the Bai-Tien model [180] overestimated up to 1 order of magnitude to the corresponding experimental results.

In general, the experimental attachment efficiencies of colloid capture by the cylinder in laminar overland flow were much smaller than the predictions of the porous media models, which could be mainly attributed to the different flow dynamics in surface vegetation and porous media. Other possible causes of the discrepancy between the experimental data and theoretical predictions (i.e., Maxwell approaches) might include (1) the Maxwell models (original and modified) use the deepest point of the secondary minimum well to determine the α, but colloid may be initially attached in other positions with the secondary minimum; and (2) none-DLVO forces, such as short-range hydration and hydrophobic forces are not included in the Maxwell models [146, 192]. Although progresses have been made, current understanding of the governing factors of colloid attachment process in porous media is still quite limited.

Because the surface property and geometry of the stem collector, as well as flow dynamics in vegetation systems could be much more complicated than that in porous media, it may not be feasible to establish a theoretical model to describe the α of colloid

capture by the cylinder under laminar flow conditions at this point. However, the direct experimental measurements obtained in this work provide an opportunity to develop an empirical model to predict the attachment efficiency of colloid filtration by plants in overland flow.

A Dimensionless Equation

Based on the Buckingham- π theorem, the α of colloid deposition on the cylinder could be a function of 8 dimensionless parameters [179, 180] (defined in APPENDIX). The experimental data was divided into a calibration/development subset with 58 data points randomly selected from the original 78 point dataset (Table 3-1) while ensuring a good distribution that covers the experimental conditions, and a verification subset consisting of the remaining 20 data points. The step-wise least-square method was used in this study to fit the development data subset. The coefficients of determination (R^2) and Nash-Sutcliffe efficiency (E) were used as quantitative descriptors of the predictive accuracy of the new dimensionless equation. The Nash-Sutcliffe efficiency coefficient is defined as:

$$E = 1 - \frac{\sum_{i=1}^{m} (\alpha_{\exp i} - \alpha_{prei})^2}{\sum_{i=1}^{m} (\alpha_{\exp i} - \overline{\alpha_{\exp}})^2} \quad (3\text{-}6)$$

where m is the number of observations, α_{exp}, α_{pre}, and $\overline{\alpha_{\exp}}$ are the experimentally observed, model predicted, and mean single collector attachment efficiency, respectively. The R^2 value reflects strength of the linear relationship between observed and simulated data and the E value indicates how well observed and simulated data fit

the 1:1 line. Predictions of the new dimensionless equation are near perfect when both R^2 and E are close to one.

The analysis of the development data subset showed that only three dimensionless parameters (defined in Table 3-3) were strongly correlated with the α (p-value smaller than 0.05). The results of step-wise regression are presented in APPENDIX C-3. A dimensionless/regression equation (R^2=0.92 and E=0.85) can be written as follows:

$$\alpha = 10^{-3.25}(N_{LO})^{0.51}(N_{E1})^{-0.27}(N_{DL})^{1.06} \quad (3\text{-}7)$$

It is worth noting that although α is less sensitive to the electrokinetic parameter (N_{E1}) than to other two dimensionless parameters, the N_{E1} term is a key component of the equation to reflect the effect of surface potential (APPENDIX).

To further validate the new dimensionless equation of the α, it was tested against the rest of the 20 experimental data (Figure 5a, R^2=0.89 and E=0.77), which indicate that the new dimensionless equation is effective in fitting the experimental observations of colloid attachment efficiency on the cylinder with reasonable accuracy. Unfortunately, it was not possible to further validate the dimensionless equation for field conditions because only a few studies have been conducted to measure the removal of colloidal particles by plant stems in laminar overland flow. Hence, additional investigations, particularly experimental studies, are needed to measure the removal of colloids by plant stems in laminar overland flow.

Although its generality still needs to be tested, the dimensionless equation can be used to determine the attachment efficiency of colloid capture by a single vegetation stem in laminar overland flow with stem-diameter-based Reynolds number ($Re_c=ud_c/v$)

smaller than 50. If stems in a vegetation system have similar physicochemical properties, this equation, when coupled with spacing and geometry factors, can be applied to describe the attachment efficiency of colloid capture by stems in the vegetation system [129, 155].

Because most of the flow in porous media is creeping flow with Reynolds number smaller than 1[17], the regression equation could also be applicable to describe the attachment processes of colloid deposition in porous media when the hydrodynamic effect is negligible (i.e., α is dominated by chemical factors). To test this hypothesis, simulations of the new dimensionless equation were tested against measurements of α obtained from well-controlled column experiments of colloid transport in porous media under unfavorable conditions [156, 160, 178, 189, 193] (Figure 3-6b). Results showed that the new dimensionless equation indeed can be used to predict the α of colloid deposition in porous media with an R^2 value of 0.80 and E value of 0.69.

Environmental Implications

Only a very limited number of studies have been made to examine colloid transport in surface runoff, particularly with respect to develop theories or models to predict the filtration processes of colloid capture by vegetation collectors in overland flow. For the first time, laboratory experiments were conducted to directly measure attachment efficiency of colloid capture by a cylindrical collector in surface runoff under laminar flow conditions. Our results showed that both solution chemistry and hydrodynamic shear played important roles in colloid attachment processes. Because existing attachment efficiency models overestimated the α of colloid attachment onto cylinders in laminar overland flow, a dimensionless equation was thus derived from experimental data and was found to predict the colloid attachment onto cylinders in

surface water flow with reasonable accuracy. In addition, this new equation may also be used to predict colloid attachment efficiency in porous media if the attachment processes were mainly controlled by chemical factors.

This attachment efficiency equation, when combined with the contact efficiency equation reported previously [133, 155, 194] , can be used to determine kinetic deposition rate of colloidal particles in both vegetation and porous media systems. Based on this work, for the case of colloid filtration and transport in a vegetation system on a real field under laminar flow conditions, the kinetic deposition rate (k_d) at the field scale can be written as:

$$k_d = 4 \times 10^{-5.6} \frac{(1-f)}{\pi d_c} \frac{u}{f} {Re_c}^{-0.94} {N_{Pe}}^{-0.03} {N_{LO}}^{0.51} {N_{E1}}^{-0.27} {N_{DL}}^{1.1} \quad (3\text{-}8)$$

where f is the ratio of the empty area among the plant stems divided by the total vegetated area, d_c is diameter of the vegetation stem, u is the approaching velocity, Re_c and N_{pe} are Reynolds number ($Re_c = ud_c/v$) and Peclet number ($N_{pe} = ud_c/D$), respectively. Because equation (3-8) is completely untested, additional experiments would need to be designed to test the suitability of this equation to monitor and predict the fate and transport of colloids in vegetation in laminar surface flow, and perhaps inform the design of engineered/natural surface runoff filtration systems, such as vegetative filter strips and constructed wetlands, to remove colloidal contaminants from surface runoff.

Table 3-1. Summary of experimental conditions and results

Test no.[a]	ionic strength IS (M)	flow velocity u (cm/s)	particle diameter $d_{p\ (\mu m)}$	attachment efficiency (α) mean ± std
I.1	0.001	0.02	1.05	$8.0\times10^{-3}\pm6.2\times10^{-4}$
I.2	0.005	0.02	1.05	$9.1\times10^{-3}\pm8.0\times10^{-4}$
I.3	0.010	0.02	1.05	$1.9\times10^{-2}\pm3.6\times10^{-3}$
I.4	0.050	0.02	1.05	$8.3\times10^{-2}\pm1.1\times10^{-2}$
I.5	0.100	0.02	1.05	$1.2\times10^{-1}\pm1.5\times10^{-2}$
I.6	0.001	0.02	0.1	$2.6\times10^{-3}\pm3.5\times10^{-4}$
I.7	0.005	0.02	0.1	$4.4\times10^{-3}\pm6.3\times10^{-4}$
I.8	0.010	0.02	0.1	$1.5\times10^{-2}\pm2.1\times10^{-3}$
I.9	0.050	0.02	0.1	$5.0\times10^{-2}\pm4.3\times10^{-3}$
I.10	0.100	0.02	0.1	$1.0\times10^{-1}\pm9.0\times10^{-3}$
II.1	0.01	0.0002	1.05	$2.5\times10^{-2}\pm2.2\times10^{-3}$
II.2	0.01	0.002	1.05	$2.0\times10^{-2}\pm1.9\times10^{-3}$
II.3	0.01	0.2	1.05	$9.0\times10^{-3}\pm8.1\times10^{-4}$
II.4	0.01	1	1.05	$6.4\times10^{-3}\pm7.0\times10^{-4}$
II.5	0.1	0.0002	1.05	$2.2\times10^{-1}\pm2.3\times10^{-2}$
II.6	0.1	0.002	1.05	$1.5\times10^{-1}\pm2.1\times10^{-2}$
II.7	0.1	0.2	1.05	$5.0\times10^{-2}\pm6.3\times10^{-3}$
II.8	0.1	1	1.05	$3.4\times10^{-2}\pm4.1\times10^{-3}$
II.9	0.01	0.0002	0.1	$2.3\times10^{-2}\pm2.9\times10^{-3}$
II.10	0.01	0.002	0.1	$1.5\times10^{-2}\pm2.0\times10^{-3}$
II.11	0.01	0.2	0.1	$2.0\times10^{-3}\pm3.6\times10^{-4}$
II.12	0.01	1	0.1	$8.9\times10^{-4}\pm1.1\times10^{-4}$
II.13	0.1	0.0002	0.1	$1.3\times10^{-1}\pm2.1\times10^{-2}$
II.14	0.1	0.002	0.1	$8.9\times10^{-2}\pm8.0\times10^{-3}$
II.15	0.1	0.2	0.1	$8.1\times10^{-3}\pm1.1\times10^{-3}$
II.16	0.1	1	0.1	$6.0\times10^{-3}\pm7.3\times10^{-4}$

[a] No.I.1- I.10 summarize the effect of ionic strength; No.II.1- II.16 summarize the coupled effect of flow velocity and ionic strength.

Table 3-2. Calculated Maximum energy barriers ($\Phi_{\max}$) and primary (Φ_{pri}) and secondary minimum (Φ_{sec}) under different experimental conditions

Ionic strength	Φ_{max} (kT[a])		$\boldsymbol{\Phi_{pri}}$				$\boldsymbol{\Phi_{sec}}$			
			Depth (kT)		Distance (nm)		Depth (kT)		Distance (nm)	
I (M)	0.1μm	1.05μm	0.1μm	1.05μm	0.1μm	1.05μm	0.1μm	1.05μm	0.1μm	1.05μm
0.001	162.1	1145.3	NA[b]	NA	NA	NA	0.03	0.72	103	93
0.005	148.9	1077.4	NA	NA	NA	NA	0.07	1.86	43	36
0.01	143.4	1065.5	NA	NA	NA	NA	0.11	2.83	30	25
0.05	85.8	708.8	NA	NA	NA	NA	0.25	7.9	11	9
0.1	49.1	412.8	NA	NA	NA	NA	0.41	12.8	7	6

[a] kT: k is the Boltzmann's constant (1.381×10^{-23} C^2 J K^{-1}), T is the absolute temperature,

[b] NA: Not applicable, no primary minimum existing in the DLVO interaction energy profiles.

Table 3-3. Summary of dimensionless parameters governing attachment efficiency

Parameter	Definition	
$\boldsymbol{N_{LO}}$	$\frac{4A}{9\pi\mu {d_p}^2 u}$	London number
$\boldsymbol{N_{E1}}$	$\frac{\varepsilon\varepsilon_0({\xi_p}^2 + {\xi_c}^2)}{3\pi\mu u d_p}$	First electrokinetic parameter
$\boldsymbol{N_{DL}}$	κd_p	Double-layer force parameter

*A is the Hamaker constant, μ is the fluid viscosity, d_p is the colloidal particle diameter, u is the flow velocity, ε is the relative permittivity of the fluid (78.4 for water), ε_0 is the permittivity in a vacuum (8.854×10^{-12} C^2 N^{-1} m^{-2}), ξ_p and ξ_c are the surface potential of the colloidal particles and collectors respectively, κ is the reciprocal of double layer thickness

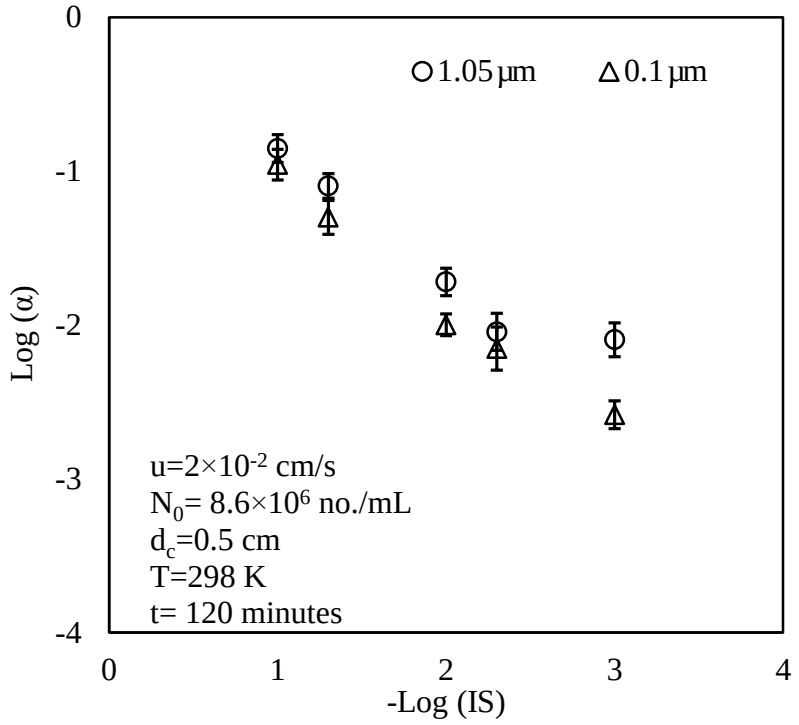

Figure 3-2. Experimental attachment efficiency (α) as a function of ionic strength (IS) for colloid capture by the cylinder in the flow chamber.

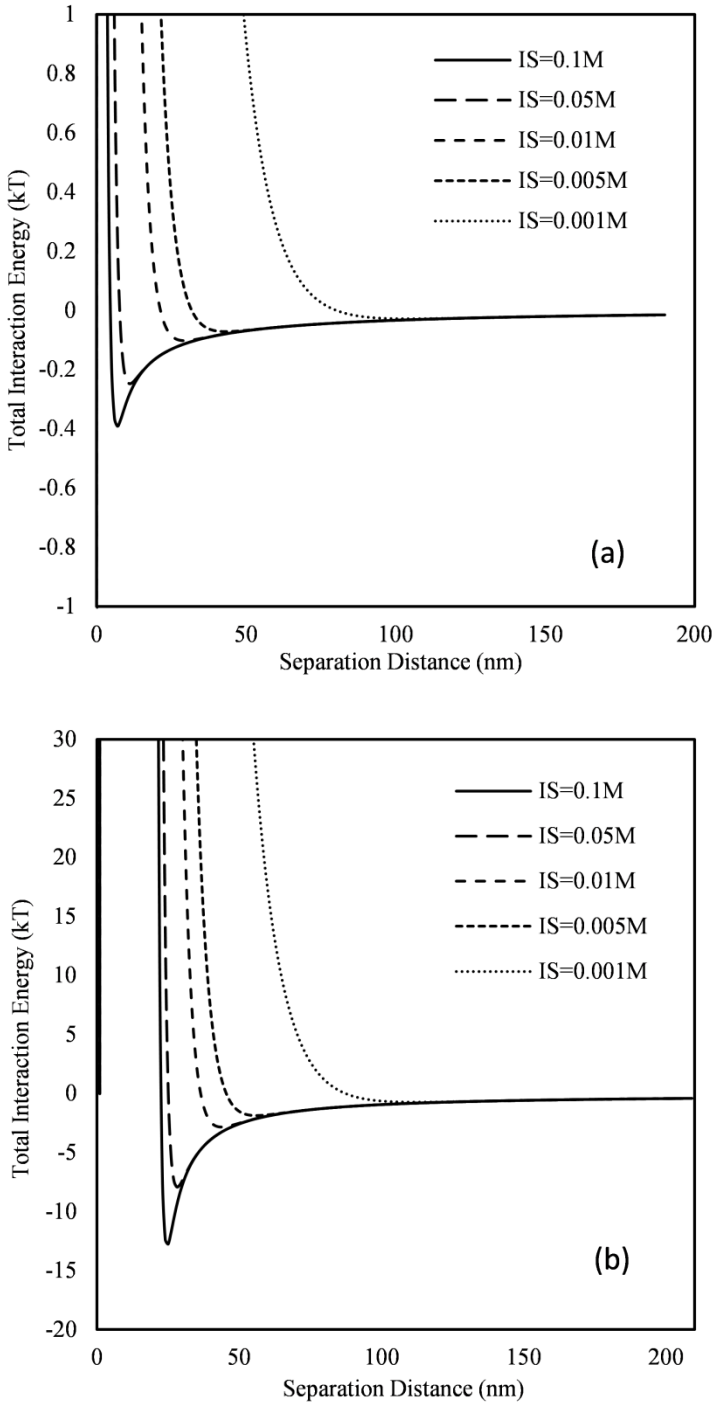

Figure 3-3. DLVO interaction energy between the collector and the colloids: (a) 0.1 µm colloids and (b) 1.05 µm colloids.

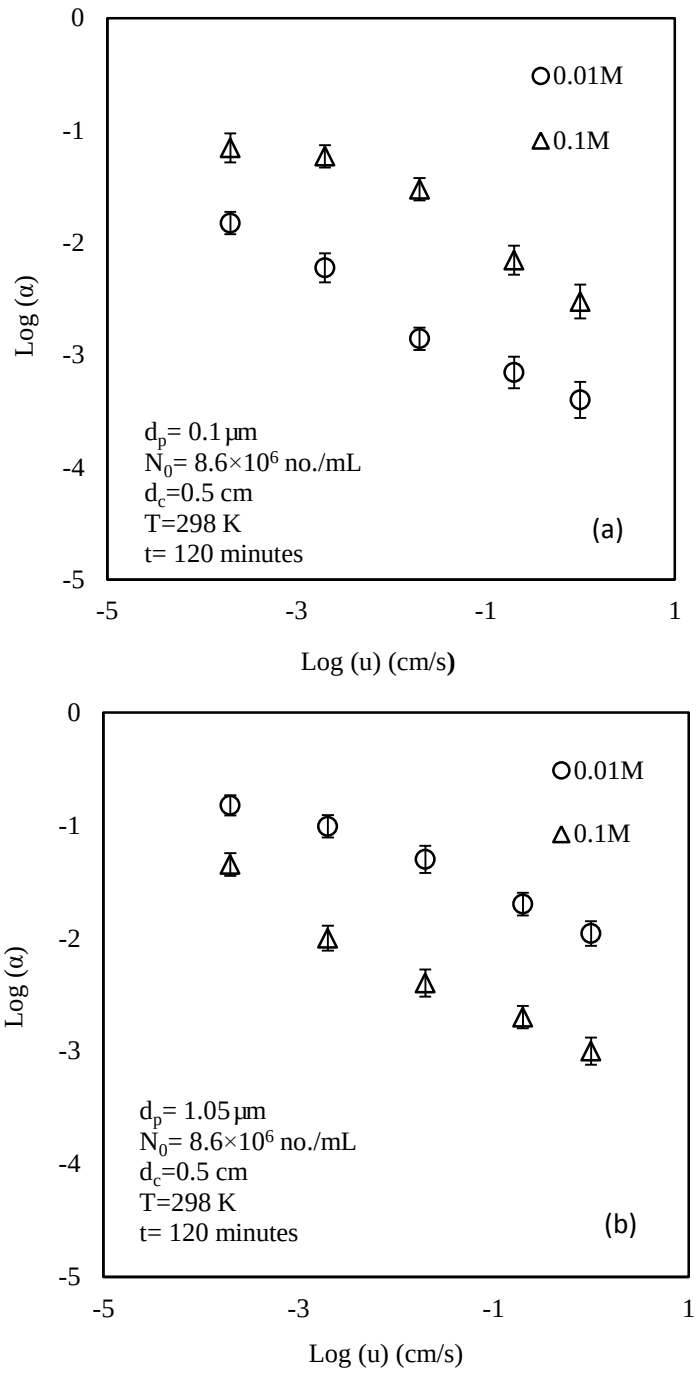

Figure 3-4. Experimental attachment efficiency (α) as a function of flow velocity (u) for colloids captured by the cylinder in the flow chamber.

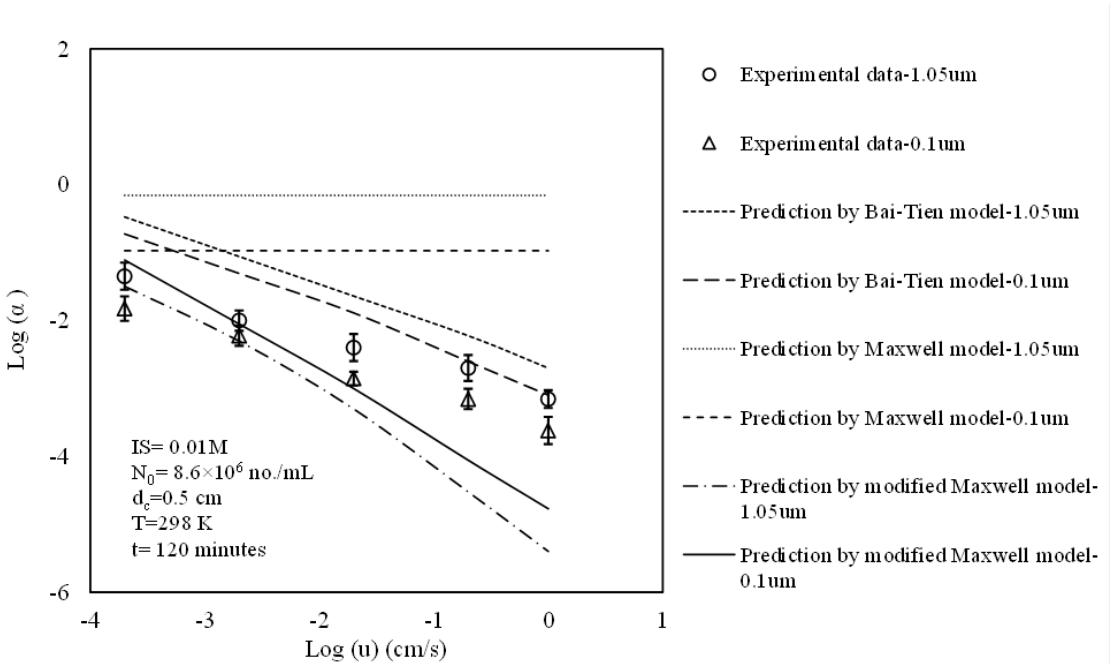

Figure 3-5. Comparison of experimental attachment efficiency (α) with predictions of the Maxwell, modified Maxwell, and Bai-Tien models for colloids captured by the cylinder in the flow chamber at ionic strength of 0.01M.

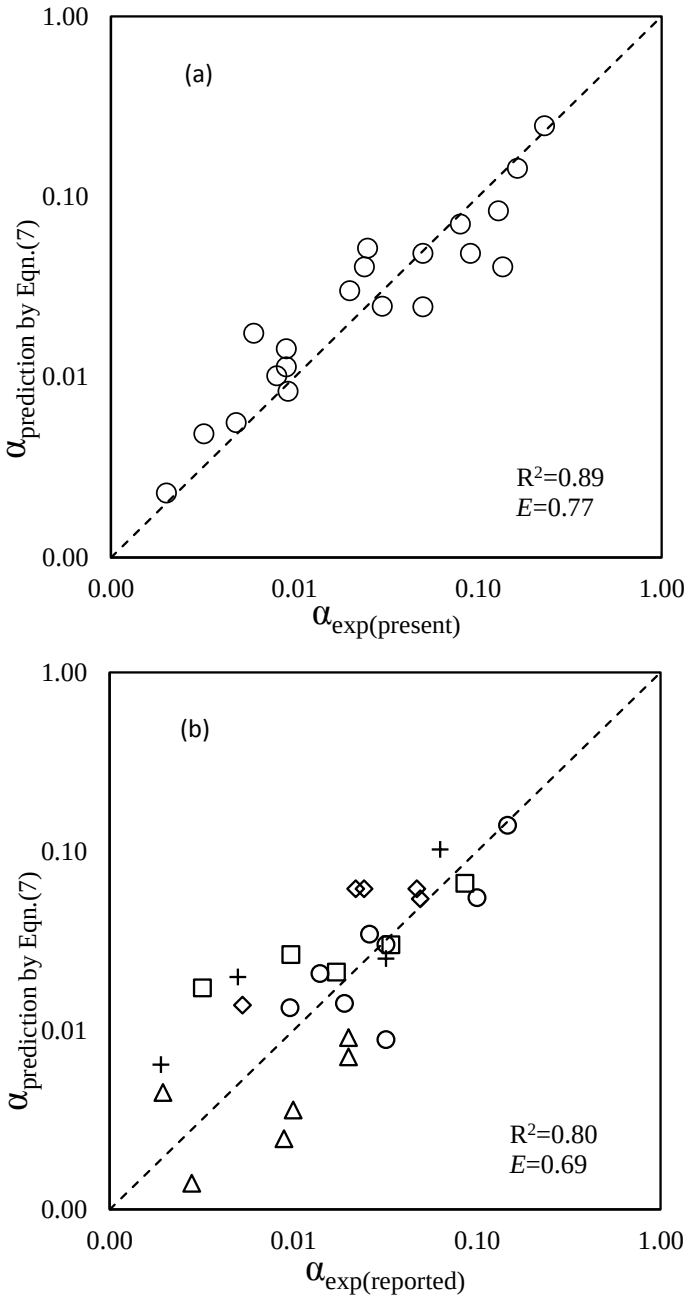

Figure 3-6. Comparison of experimental attachment efficiency (α) with predictions of the new dimensionless equation.

CHAPTER 4
EXTENDED SINGLE STEM EFFICIENCY THEORY FOR COLLOID FILTRATION THROUGH SURFACE DENSE VEGETATION

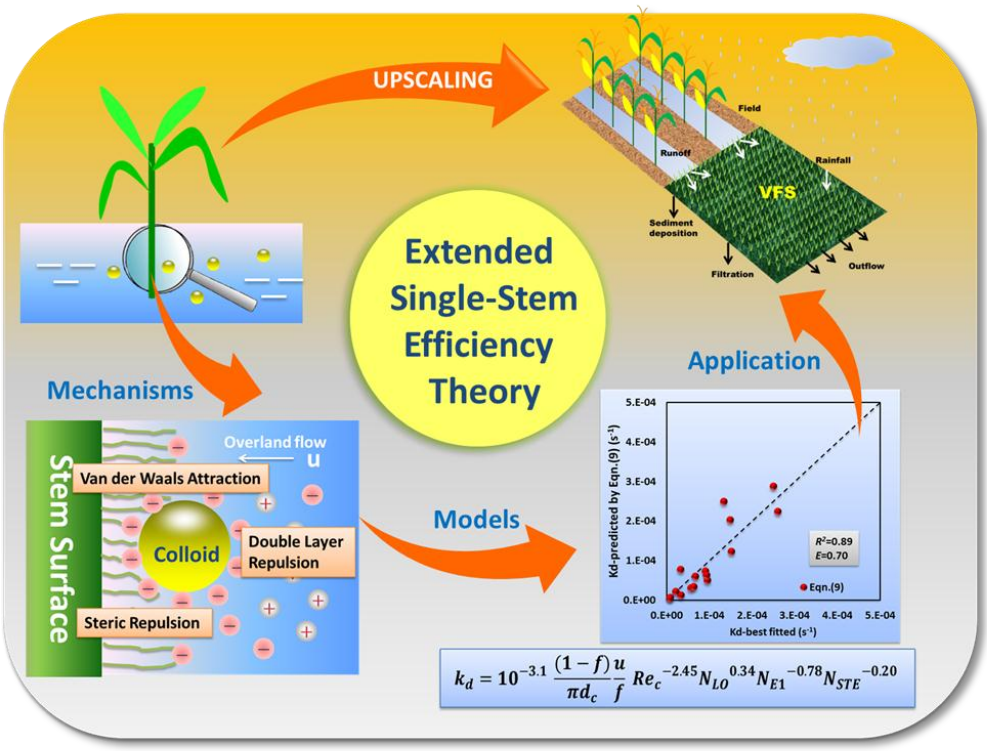

Figure 4-1. Graphical content of chapter 4

Introductory Remarks

The presence of colloidal particles (e.g., pathogen and engineered nanoparticles) in runoffs has raised increasing concerns regarding water quality and public health recently. [150, 155, 195-197]A number of previous investigations showed that both natural and engineered vegetation systems, such as vegetative filter strips and wetland, can act as a filter to remove colloidal contaminants in runoffs from agricultural and urban lands. [72, 87, 151] Lab and field scaled experiments and model simulations thus have been conducted to explore the movements of colloids with water flow in vegetation systems and advanced the understanding of theories and mechanisms that govern these processes. [78, 79, 198-200] Nevertheless, current ability to predict the fate and

transport of colloidal particles in surface runoff through emergent dense vegetation systems is still limited.

To fill the knowledge gap, we recently developed a single-stem efficiency theory to predict the filtration and transport of colloids in in surface runoff through emergent dense vegetation systems.[155, 197] Laboratory flow chamber experiments demonstrated that the theory predicted both the contact efficiency (η_0) and the single-stem attachment efficiency (α) for colloid capture by a simulated plant stem in laminar overland flow very well.[155, 197] Based on the single-stem efficiency theory, a plant colloid filtration theory to quantify the kinetic deposition rate of colloids on plan surfaces in vegetation systems under laminar flow conditions was developed. [197] It is anticipated that this plant colloid filtration theory could be applied directly to determine the filtration rate of colloids by plant stems in vegetative filter strips or wetlands; however, none of the previous studies has experimentally tested the theory against data collected from real vegetation systems.

One of the most important assumptions of the single-stem efficiency theory was that the plant stems could be modeled as rigid rods with homogeneous surfaces. In reality, however, the surfaces of plant stems are commonly covered by non-glandular and glandular trichomes (hair or brush-like protuberances) [201], which, if not considered, may introduce errors in the perditions of the single-stem efficiency theory. For example, previous studies showed that non-glandular trichomes could reduce the attachment of particles, including bio-colloids, on plant surfaces. [202, 203] In addition, glandular trichomes on plant surfaces may secrete lipophilic substances to provide chemical or physicochemical protection against the adhesion of pathogens and other

microorganisms. [201, 204] More importantly, trichomes can also serve as a dense "brush" (biopolymer layer) around plant stem or other organs, [205, 206] which may introduce steric repulsion forces to inhibit particle attachment. To better predict the filtration and transport of colloids in real vegetation systems, it is thus important to consider the effect of steric repulsion on the single-stem efficiency theory.

In the literature of colloid transport in porous media, the importance of steric repulsion to colloid attachment processes has been emphasized by many recent studies and several correlation equations have been successfully developed to include the steric repulsion effect in attachment efficiency of colloids on porous medium surfaces coated with polymers. [207-212] The biopolymer brush layers on the surfaces of plant stems, however, are different from those studied in porous media, which are adsorbed on medium surfaces as clusters (Figure 4-2A).[207] They are attached (grafted) by one end to the stem surfaces at relatively high coverage and stretch away along normal direction to avoid overlapping (Figure 4-2B). These differences may cause the steric repulsion equations developed for porous media to be inappropriate in determining the attachment efficiency of colloids on plant stems.

The steric repulsion between polymer brush layers and colloidal particles has been examined previously. [213-215] de Kerchove and Elimelech experimentally studied the effect of alginate conditioning film on the deposition kinetics of motile and non-motile *Pseudomonas aeruginosa* and confirmed that steric interactions between the alginate brushes and the flagellated bacteria could hindered the deposition [213]. Theoretical models have been also developed to predict the interaction of polymer brush layer with incoming particles. [212, 216, 217] According to Halperin's model,[216]

an incoming particle may penetrate the brush and adsorb in the primary minimum at the substrate surface, or it may be trapped in the secondary minimum at the edge of the brush layer. Findings from these investigations have advanced the knowledge of steric repulsion of polymer brushes and could potentially be applied to determine the interactions between colloidal particles and biopolymer brushes of plant stems. To our knowledge, however, none of the previous studies have attempted to use the polymer brush theories to quantify the effect steric repulsion on attachment efficiency of colloids on plant stems.

The overarching objective of this work was to modify the plant filtration theory so it can accurately predict colloid attachment rate on plant stems for real vegetation systems. Laboratory flow chamber experiments and model simulations were conducted to determine the deposition rates of colloids on stems of real plants under various physicochemical conditions. The results were used to test and refine the single-stem efficiency theory of colloid filtration in dense vegetation systems. Our specific objectives were as follows: (1) measure the filtration of colloids by dense vegetation in laminar flow over impermeable soil under different flow velocity, grass density, colloid size, and ionic strength conditions, (2) determine the kinetic deposition rates of colloids on the plant stems in the vegetation systems, (3) test the current single-stem efficiency theory against the obtained results, and (4) develop an extended single-stem efficiency theory with considerations of the effects of the steric repulsion of biopolymer brushes on natural plant stems.

Theoretical Background and New Dimensionless Number (N_{STE})

Based on the colloid plant filtration theory, the deposition rate (k_d) of colloids on plant stems in dense vegetation in laminar overland flow can be written as:[155, 197]

$$k_d = \frac{4(1-f)}{\pi d_c}\frac{u}{f}\eta_0\alpha \tag{4-1}$$

where *f* is the ratio of the empty area among the plant stems divided by the total vegetated area, d_c is diameter of the vegetation stem, *u* is the approaching flow velocity, and η_0 and α are the single-stem contact efficiency and the single-stem attachment efficiency, respectively. The current single–stem efficiency theory assumes that the η_0 is a function of the interception and diffusion processes (i.e. physical processes), while the α is a function of the van der Waals attraction, electrostatic double layer repulsion, and hydrodynamic shear interactions (i.e. physical and chemical processes) and can be written as: [155, 197]

$$\eta_0 = 0.0044\,\mathrm{Re}_c^{-0.94} N_{Pe}^{-0.03} \tag{4-2}$$

$$\alpha = 10^{-3.25}\left(N_{LO}\right)^{0.51}\left(N_{E1}\right)^{-0.27}\left(N_{DL}\right)^{1.06} \tag{4-3}$$

where Re_c is the Reynolds number ($Re_c = ud_c/v$), N_{pe} is the Peclet number ($N_{pe} = ud_c/D$), and N_{LO}, is the London number ($N_{LO} = 4A/9\pi\mu d_p{}^2 u$), N_{E1} is the first electrokinetic parameter ($N_{E1} = \varepsilon\varepsilon_0(\xi_p{}^2 + \xi_c{}^2)/3\pi\mu u d_p$), N_{DL} is the double-layer force parameter ($N_{DL} = \kappa d_p$), *A* is the Hamaker constant, μ is the fluid viscosity, d_p is the colloidal particle diameter, ε is the relative permittivity of the fluid (78.4 for water), ε_0 is the permittivity in a vacuum (8.854×10^{-12} C^2 N^{-1} m^{-2}), ξ_p and ξ_c are the surface potential of the colloidal particles and collectors respectively, and κ is the reciprocal of double layer thickness.

As discussed previously, the single-stem efficiency theory (equations 4-2-4-3) was developed without considering the effects of biopolymer brushes (trichomes) on plant stem surfaces. Although the biopolymer brush layers might not affect the long

distance transport/contact process much (η_0), they could significantly affect the short distance attachment process, particularly through introducing the steric repulsive forces to reduce the attachment efficiency (α). [207] In addition, the presence of biopolymer brush could also reduce the friction forces and lead to a greater chance of colloid rolling and detachment by hydrodynamic shearing. [218, 219] As a result, the single-stem attachment efficiency model (i.e., equation 3), which only includes terms of the van der Waals attraction, electrostatic double layer repulsion, and hydrodynamic shear interactions, may overestimate the actual attachment rate of colloids on real plant stems with biopolymer layers. To improve the accuracy of the single-stem efficiency theory, we propose to introduce a new term to single-stem attachment efficiency model (i.e., equation 4-3) with a dimensionless number to reflect the biopolymer brush effects.

Figure 1C shows a simple representation of a spherical particle with diameter of d_p impinging upon a biopolymer brush, which has a uniform density of $\sigma = n/A$, where n is the total number of polymer chains and A is the surface area of the substrate. Each polymer chain has a natural end-to –end length of $aN^{1/2}$, where a is the average segment length and N is the number of segments per chain, a dependent of the polymer molecular weight (M_W). Based on the theory of grafted polymer brush, the equilibrium free energy ($F(L;\infty)$) of each polymer chain can be written as:[220, 221]

$$\frac{F(L;\infty)}{nk_BT} = \frac{9\pi^2 L_0^2}{40a^2N} h\left(\frac{L}{L_0}\right) \tag{4-4}$$

where $h(x) = \frac{\left(5x^{-1} + 5x^2 - x^5\right)}{9}$ for $x \le 1$ and $h(x) = 1$ for x >1. L_0 is the height (thickness) of the biopolymer brush and L is the separation distance (Figure 4-2C). The

repulsion energy exerted on a spherical particle by the polymer brush thus can be derived using equation (4-4) coupled with the Derjaguin Approximation:[217]

$$\frac{F(L;d_p)}{k_BT}=\frac{9\pi^3\sigma d_p L_0^3}{40a^2N}H\left(\frac{L}{L_0}\right) \tag{4-5}$$

where $H(x)=\frac{\left(-45-30\ln x+54x-10x^3+x^6\right)}{54}$ for $x\le 1$ and $H(x)=0$ for x >1.

Although there is theoretical evidence that the Derjaguin Approximation may overestimate the steric repulsion energy, especially for small size particles, equations (4-5) still can provide a clear and fundamental estimation of steric interaction.[217]

As shown in equation (4-5), steric repulsion is a function of several parameters related to particle and biopolymer brush properties, including d_p, L_0, σ, and *Mw*. In addition, the enhanced rolling and detachment caused by the biopolymer brush should a function of fluid viscosity (μ) and fluid velocity (*u*). [207] Based on the Buckingham-Π methods, the new dimensionless number (N_{STE}) that should be included as a term in the single-collect attachment efficiency model to reflect the biopolymer brush effect can be expressed as:

$$N_{STE}=\frac{d_p L_0^3\sigma\mu N_a}{(u/f)M_W} \tag{4-6}$$

where N_a is Avogadro's number. Detailed information about the derivation of N_{STE} can be found in the APPENDIX. Thus, in the extended single-collector theory for real plants with biopolymer brushes, the single-collector attachment efficiency equation can be written as:

$$\alpha=10^m\left(N_{LO}\right)^{0.51}\left(N_{E1}\right)^{-0.27}\left(N_{DL}\right)^{1.06}{N_{STE}}^n \tag{4-7}$$

where *m* and *n* are unknown constant that will be experimentally determined.

Materials and Methods

Materials

Fluorescent, carboxylated, polystyrene latex microspheres (Magsphere, Inc) of three sizes (0.3, 1.05 and 2 μm) were used as experimental colloids. As reported by the manufacturer, the density of the colloids is 1.05 g/cm^3 and the surface carboxyl group coverage is 9.28×10^{17}, 1.19×10^{18} and 1.68×10^{18} /m^2 for 0.1, 1.05 and 2 μm colloids, respectively. Experimental solutions were made by diluting the stock colloid solution (1.05 g/mL) to the target concentration (10.5 mg/L, corresponding to 3.7×10^{10}, 8.6×10^{8} and 1.1×10^{8} no./mL for 0.1, 1.05 and 2 μm colloids, respectively) with deionized (DI) water.

Analytical reagent grade KCl (Fisher Scientific) and DI water were used to prepare electrolyte solutions at desired ionic strengths. The pH for all the electrolyte solutions was adjusted to 7 with 1 mM $KHCO_3$ solution. The experiments were conducted at four ionic strengths (DI water, 0.01, 0.1 and 0.2 M) so that different deposition kinetic rates could be tested. The corresponding ξ potentials (i.e., electrokinetic potential) of the 0.1, 1.05 and 2 μm colloids were -80.4, -60.8, -38.0, -29.4 mV, -68.6, -59.2, -35.4, -28.1mV and –56.7, -47.3, -32.1,-26.2 mV, respectively, whereas the corresponding ξ potentials of the grass stem were -57.8, -50.5, -18.8 and -16.9 mV, which were determined with a ZetaPlus (Brookhaven Instrument Co., Holtsville, NY). The ξ potentials of the grass stem were determined with colloidal grass suspensions (obtained from sonicating the grass stem) under various chemical conditions following the method used in the previous study.[197]

Vegetation Chamber Experiments

Small size vegetation chambers were used in the experiments (Figure 4-4). The chambers were made of Plexiglas of 20 cm long, 20 cm wide, and 10 cm high and equipped with a run off outlet. Quartz sand (Standard Sand & Silica Co.) with a size range between 0.5 to 0.6 mm and a density of 1.54 g/cm^3 was added into the chambers (5 cm) as the growth soil. Brown Top Millet seedlings (1-2 weeks) were selected as experimental dense vegetation. The average diameter of fully grown stems (d_c) was around 1.2 mm. High, medium and low stem densities with 2545, 4900 and 8184 stems/m^2, respectively, were used in the experiments. A peristaltic pump (Masterflex L/S, Cole Parmer) was used to apply the inflow, bromide and colloid solutions to the chambers at four different overland flow velocities (0.02-0.2 cm/s). Prior to the runoff experiment, plaster (DAP Products. Inc) was used to seal the top sand surface to prevent infiltration and to eliminate the filtration of colloids by the soil (Figure 4-3A). Pre-experiment with the flow chambers under the same treatments but without of dense vegetation showed that more than 98% bromide and colloids were recovered from the system, indicating no deposition of colloids on the plaster layer. Comparison of the breakthrough curves of colloid with and without plaster layer was shown in APPENDIX.

Colloid transport data were collected in duplicate from 17 vegetation surface flow chamber experiments with different combinations of four flow velocities, three plant stem densities, four ionic strengths, and three colloid sizes (Table 4-1). For each breakthrough study, DI water was first applied to flush the vegetation system for about 60 min until the flow reach steady state. The breakthrough experiment was then initiated by switching from DI water to the colloid suspension for 30 min, and then the column was flushed with DI water again for 90 min. Effluent samples were collected from the

outlet with a fraction collector. Bromide was also applied to the system as a conservative tracer. Colloid and bromide concentrations in the samples were determined with a fluorescent spectrophotometer (PerkinElmer LS 45) and an Ion Chromatograph (Dionex ICS-90), respectively.

Characterize biopolymer brush layer (trichome) on vegetation stem

The structure and composition of the trichome varies largely among plants, organs, and growth stages, but it is mainly composed by esterified fatty acids hydroxylated and epoxy hydroxylated with chain lengths mostly between 16 to 18 atoms of carbon. [222] The 9- or 10, 16-dihydroxyhexadecanoic acid, 16-hydroxyhexadecanoic acid, 18-hydroxy-9,10- epoxyoctadecaonoic acid and 9,10,18-trihydroxyoctadecanoic acid are the major components of C_{16} and C_{18} family. Their reported average of molecular weight (400 *kg*/ mol) was thus used in this study. [223, 224] Five plant stems were sampled from the vegetation chambers to determine the morphology, density, and length of the trichome on their surfaces. Images were obtained using self-referencing system fitted with Navitar Precise Eye optics at 1.20x magnification. Average optical density of trichome was calculated using an image processing software (ImageJ 1.46, NIH). The results (Table 4-1) were found in good agreement with reported data. [225] We assume that the biopolymer brush density is a constant for the vegetation stems used in the experiments. Previous studies reported that the height of the polymer brush layer extends with increasing charge density or decreasing ionic strength (*I*). [226, 227] Several models have been proposed to relate the brush layer height to ionic strength and everyone has a general form of $L \sim (I)^{-m}$, where *m* is a fractional exponent.[228] In this study, the height of biopolymer brush layer was thus determined by assigning *m* as 2/3. [36, 45]

Determine kinetic deposition rate (k_d)

Filtration and transport of colloids in dense vegetation system can be described by the advection-dispersion equation coupled with a first order kinetic deposition.[197] The governing equations can be written as follows:

$$\frac{\partial C}{\partial t} = D\frac{\partial^2 C}{\partial z^2} - \frac{u}{f}\frac{\partial C}{\partial t} - k_d C \qquad (4\text{-}8)$$

where C is the concentration of colloid suspension, z is the travel distance in the direction of flow, and D is the dispersion rate. The equation was run as an inverse problem to obtain the optimized parameters by fitting an analytical solution [229] to experimental breakthrough curves using a nonlinear least-squares method. This inverse optimization method was first applied to bromide breakthrough data to estimate D and assumed that the dispersion coefficient (D) of colloid is the same as that of the bromide tracer in this study. The best-fit values of the kinetic deposition rate (k_d) of colloids on stems of the vegetation systems were determined by fitting the colloid breakthrough curves. Predictions of the single-stem efficiency theory were tested against the best-fit k_d values. In addition, the best-fit values were also used to refine the extended-stem efficiency theory and to determine the m and n value of equation (4-7).

Results and Discussion

Effect of ionic strength on colloid filtration in dense vegetation

The effect of ionic strength on colloid deposition on plant stems is shown in breakthrough curves obtained from the vegetation chamber experiments (Figure. 4-5A). The results showed that the removal of colloids in the dense vegetation system was a dependent of solution ionic strength. When the solution ionic strength increased from DI water to 0.2 M, the mass recovery of colloids from the vegetation system reduced from

90.3% to 72.4%. This trend was also observed in many previous studies of colloid transport in porous media and was attributed to the fact that higher ionic strength could reduce the repulsive electric double layer forces to promote colloid deposition.[188, 197] Simulations of the advection-dispersion model (equation 4-8) matched the colloid breakthrough curves very well for all the ionic strength conditions tested. The best-fit k_d values increased from 6.3×10^{-5} to 3.2×10^{-4} s^{-1} as the ionic strength increased, confirming the importance of ionic strength to colloid deposition on plant stems in the dense vegetation system.

The classical DLVO theory, which includes the van der Waals and the electrostatic double layer interactions, has been often used to describe the deposition of colloidal particles on surfaces under various conditions.[188, 197] In this study, however, predictions of the DLVO theory were inconsistent with the experimental data, probably because this classical theory neglects the steric repulsion afforded by biopolymer brush layer. The DLVO energy profiles showed that deep secondary minimum energy wells (e.g., 12.5 and 58.7 *kT*) exist under both medium and high ionic strength conditions (Figure.4-5C-F, blue line in inset), corresponding to perfect attachment efficiency (i.e., α=1) as predicted by the Maxwell theory. The observed removal of colloids by the dense vegetation under the two ionic strength conditions, however, was much smaller than the predictions by the theory.

Extended DLVO theory that considers the steric repulsion (equation 4-5) thus was applied in this study to determine the effect of ionic strength on the interactions between colloids and plant stems. Recent studies have shown that that ionic strength (salt concentration) could also affect the steric repulsion forces by altering the

dimensions of the biopolymer brush layer (scaling relations, Figure 4-5B). [226] To test this hypothesis, two scenarios of steric repulsion (with and without scaling relations) were evaluated. The results indicated that the steric repulsion without scaling relations (Figure. 4-5C-F, yellow dash line in inset) produced unrealistically high repulsive energy barriers and no secondary minimum existed under all tested conditions, indicating no deposition of colloids in the systems. Removal of colloids by the dense vegetation, however, was observed for all the experimental conditions tested in this work. When the scaling relation was included, the extended DLVO energy profiles (Figure. 4-4C-F, red line in inset) were consistent with the experimental observations of colloid deposition on plant stems (Figure. 4-5A). Shallow secondary minimum wells were identified, indicating that colloids may deposited on the edge of biopolymer brush layer in these shallow secondary minimum wells. In addition, the high repulsive energy barriers at all ionic strength conditions indicated that removal of colloids by the plant stems through primary minimum deposition might not be feasible. These results showed that including steric repulsion with scaling relations into the total energy profile improved the accuracy of the predictions of the DLVO theory. Additional investigations are still needed to refine the extended DLVO theory to accurately predict the interactions between colloids and vegetation surfaces.

Coupled effect of flow velocity and stem density on colloid filtration in dense vegetation

Both flow velocity and stem density affected the filtration and transport of colloids in the vegetation chambers (Figure 4-6). For all the three stem densities, colloid removal decreased with increasing of flow velocity (Table 4-1), which is consistent with findings from our previous flow chamber experiments with glass rods as simulated plant stems.

[155, 197] For example, mass balance calculations showed that at low density condition, the recovery of colloid was 76.7%, 80.8%, 86.5%, and 90.1% for flow velocity of 0.002, 0.01, 0.05, and 0.1 cm/s, respectively. Previous studies have demonstrated that high flow velocity may introduce hydrodynamic drag force to reduce colloid deposition on surfaces,[166, 177, 197, 230] which also applies in this work. Similarly, the advection-dispersion model (equation 4-8) described the colloid breakthrough curves very well for all the combinations of flow velocities and stem densities. The best-fit k_d values are listed in Table 4-1.

Although some theoretical studies[231, 232] showed that weak shear flow may have no effect on the polymer brush density profile and its height, others reported that hydrodynamic thickness (Figure 4-6D) of surface-attached polymer layers decreased with increasing of flow velocity. [233] This may reduce the net friction forces and thus reduce the deposition of colloids on the stem surfaces. It has also been reported that although low flow velocities may not affect the normal force between the polymer brush surface and approaching particles, a sharp onset of additional repulsion force could appear when the velocity is above a certain threshold. [233] [234] [235] The origin of the repulsion could be traced to the swelling of the polymer brushes with the increasing of flow velocity (Figure 4-6E). These findings are also consistent with the observed experimental data that colloid deposition decreased with increasing of flow velocity.

Plant stem density also showed strong effect on the filtration and transport of colloids in the vegetation chambers (Figure 4-6 and Table 4-1). For a given flow velocity, much less colloids were recovered from the system when grass density increased. Results of global sensitivity analysis (APPENDIX) showed that vegetation

density not only have a significant first order effect on the kinetic deposition rate of colloid in dense vegetation but also has a large effect by interactions with other parameters mainly through altering the flow field around the plant stems to affect both the contact and attachment processes.

Extended single-stem efficiency theory

The best-fit k_d data were divided into a calibration/development subset with 18 experimental data, which were randomly selected from the original 34 point dataset while ensuring a good distribution that covers the experimental conditions, and a verification subset consisting of the remaining 16 experimental data. The least-square method was used to fit the development data subset to determine the constant *n* in equation (4-7). A combination of graphical results, absolute value error statistics (e.g., root mean square error, *RMSE*), and normalized goodness- of -fit statistics (e.g., Nash-Sutcliffe efficiency, *NSE*) was used as quantitative statistics of the predictive accuracy of the new extended model. More details of the least-square method and model goodness-of-fit assessment can be found in previous publications. [197, 236].

Based on this method, the best-fit *m* and *n* was -1.74 and -0.45. Thus, the extended single-stem model (*RMSE*=0 and *NSE*=0.97, APPENDIX) including effect of steric repulsion afforded by biopolymer brush layer on the plant stem surface can be written as follows:

$$\alpha = 10^{-1.74}\left(N_{LO}\right)^{0.51}\left(N_{E1}\right)^{-0.27}\left(N_{DL}\right)^{1.1}\left(N_{STE}\right)^{-0.45} \quad (4\text{-}9)$$

The exponent coefficient for N_{STE} is negative (-0.45), indicating that steric repulsion caused by biopolymer brush layer inhibit colloid deposition onto plant stem as expected.

To further validate the extended single-stem efficiency theory, equations (4-1), (4-2), and (4-9) were used to predict the kinetic deposition rate (k_d) under different experimental conditions. The predicted k_d was tested against the rest of the 16 experimental data (Figure 4-6A, *RMSE*=0 and *NSE* =0.88). The results indicated that the extended single-stem efficiency theory is effective in filtration of colloids in real dense vegetation system with the fitted results span from acceptable to very good (Figure 4-7A-D). Furthermore, extended theory validity is significant since there is no probability of the fit being unsatisfactory (*NSE*<0.65). The evolution of observed and predicted values (Figure 4-7C) indicated that the predictions by extended theory are in good agreement with the experimental observations throughout the whole time series, although there is a slight discrepancy between the model predictions and experimental observations in the first period of the time series.

Figure 4-6A also illustrated that the extended single-stem efficiency theory significantly improves the predictions of k_d over the original one (equations 4-1-4-3, *RMSE*=0 and *NSE* =-2.35) which overestimated the k_d in most cases. In addition to neglecting of steric repulsion, the overpredictions of original equation may also be caused by actual velocities within the brush layer which follow the Darcy law and are larger than the approaching velocities. [233]

Furthermore, it is worth noting that especially under either low flow velocity or high ionic strength conditions, the prediction of the original single-stem efficiency theory deteriorated (Figure 4-7A). This could be attributed to follows: (1) low flow velocity might make the effect of hydrodynamic shear force on the attachment process less important relative to interactions between colloid and stem surface especially in the presence of

steric repulsion; (2) under high ionic strength conditions, compared to electrostatic double layer, steric repulsion is less sensitive to the Debye screening effect since the charge on the plant stem surface is governed by the Donnan potential inside the brush layer and not just the compression of EDL alone like bare surface.[207] And this may cause inaccuracy when previous equations were used to describe the steric repulsion dominated interaction. Therefore, the above results clearly illustrated the critical need to include this biopolymer brush effect into the previous equations since the extended theory indeed capture the fundamental mechanisms (including contact process and attachment process) which govern the colloidal particles deposition onto plant stem in overland flow, particularly in the presence of steric repulsions and decrease of the friction promoted by biopolymer brush layer.

Deposition Mechanisms and Other Potential Effects

Based on this new extended single-stem efficiency theory and previous studies of adsorption of particles on grafted polymers, [237] we proposed the deposition of colloidal particles on plant stem in overland flow could through three ways (Figure 4-8): (1) “type I deposition” that happens when the diameter of colloids is smaller than the separation distance between the trichomes; (2) “type II deposition” that occurs when the diameter of colloids is larger than the separation distance between the trichomes and the particles are attached on the edge of trichome layer; and (3) “type III deposition” that takes place when the diameter of colloids is larger than the separation distance between the trichomes and the particles are attached on the tips of the trichome. Although these mechanisms are similar to those of colloid stabilized by grafted polymer, trichomes on plant surfaces in overland flow could behavior different from the grafted

polymer, further theoretical and experimental studies are thus in critical need to better understand the mechanisms governing colloid deposition on stem surfaces.

In this study, air bubbles were found attaching on the plant stem surfaces (Figure 4-3B), which is consistent with recent findings that also that trichomes could keep a long-lasting air (gas) film under water. [201] As a result, other well-documented colloid deposition mechanisms for multiphase media, such as air-water-solid interface capture,[238] water-film straining, [239] storage in immobile water zones,[240] and air-water interface capture [241], could also potentially affect the filtration of colloids in dense vegetation systems. Additional investigations are still needed to incorporate these potential mechanisms to further refine the extended single-stem efficiency theory to better predict the filtration and transport of colloids in dense vegetation in overland flow.

Environmental Implications

An extended single-stem efficiency theory of colloid deposition on plant stem in overland flow was developed. The new theory represents an important step in advancing current understanding of fate and transport of colloidal particles in dense vegetation in overland flow. It also provides several insights into the fundamental mechanisms governing colloid filtration by plant stems. First, steric repulsion afforded by the trichomes (brush like structure) on the plant surface plays an important role in affecting the interaction between colloids and stems. Second, structure of the biopolymer brush layer on stem surface is depending on the solution chemistry and is one of the essential factors controlling colloid deposition process. Third, the extended single-stem efficiency theory predicted the filtration of colloids by real vegetation

reasonable well and thus could be incorporated in large-scale models, such as VFSMOD [72] to predict the fate and transport of colloidal particles in the field.

Although the extended single-stem efficiency theory is developed for colloid deposition on stems, its application is not just limited to vegetation systems. The theory should also be applicable to colloid deposition on various polymer brush surfaces in natural, engineered and biomedical systems.

Table 4-1. Summary of experimental conditions, biopolymer brush properties and best-fit value of parameters in transport model

Test no[a].	u (cm/s)	f	IS (M)	d_p (μm)	σ^b (*no./cm²*) (Mean+SD)	$L_0{}^c$ *(cm)* (Mean+SD)	D^d (cm^2/s)	k_d (S^{-1}) (Mean)	MR *(%)* (Mean)	R^2 (Mean)
I.1-1	0.002 (Re_c=0.2)	0.62	DI water	1.05	$4.5\times10^{3}\pm3.2\times10^{2}$	$3.3\times10^{-3}\pm8.1\times10^{-4}$	9.7×10^{-4}	3.2×10^{-5}	84.8	0.95
I.1-2	0.01 (Re_c=1.0)	0.62	DI water	1.05	$4.5\times10^{3}\pm3.2\times10^{2}$	$3.3\times10^{-3}\pm8.1\times10^{-4}$	4.1×10^{-3}	1.9×10^{-5}	90.9	0.97
I.1-3	0.05 (Re_c=5.0)	0.62	DI water	1.05	$4.5\times10^{3}\pm3.2\times10^{2}$	$3.3\times10^{-3}\pm8.1\times10^{-4}$	6.4×10^{-3}	8.9×10^{-6}	94.1	0.97
I.1-4	0.1 (Re_c=10)	0.62	DI water	1.05	$4.5\times10^{3}\pm3.2\times10^{2}$	$3.3\times10^{-3}\pm8.1\times10^{-4}$	9.6×10^{-3}	7.0×10^{-6}	95.0	0.97
I.2-1	0.002 (Re_c=0.2)	0.33	DI water	1.05	$4.5\times10^{3}\pm3.2\times10^{2}$	$3.3\times10^{-3}\pm8.1\times10^{-4}$	1.2×10^{-3}	1.3×10^{-4}	79.2	0.94
I.2-2	0.01 (Re_c=1.0)	0.33	DI water	1.05	$4.5\times10^{3}\pm3.2\times10^{2}$	$3.3\times10^{-3}\pm8.1\times10^{-4}$	4.8×10^{-3}	6.3×10^{-5}	90.3	0.97
I.2-3	0.05 (Re_c=1.0)	0.33	DI water	1.05	$4.5\times10^{3}\pm3.2\times10^{2}$	$3.3\times10^{-3}\pm8.1\times10^{-4}$	7.0×10^{-3}	1.2×10^{-5}	92.1	0.97
I.2-4	0.1 (Re_c=10)	0.33	DI water	1.05	$4.5\times10^{3}\pm3.2\times10^{2}$	$3.3\times10^{-3}\pm8.1\times10^{-4}$	9.9×10^{-3}	9.2×10^{-6}	93.6	0.97
I.3-1	0.002 (Re_c=0.2)	0.15	DI water	1.05	$4.5\times10^{3}\pm3.2\times10^{2}$	$3.3\times10^{-3}\pm8.1\times10^{-4}$	1.6×10^{-3}	1.9×10^{-4}	76.7	0.94
I.3-2	0.01 (Re_c=1.0)	0.15	DI water	1.05	$4.5\times10^{3}\pm3.2\times10^{2}$	$3.3\times10^{-3}\pm8.1\times10^{-4}$	5.0×10^{-3}	1.8×10^{-4}	80.9	0.96
I.3-3	0.05 (Re_c=5.0)	0.15	DI water	1.05	$4.5\times10^{3}\pm3.2\times10^{2}$	$3.3\times10^{-3}\pm8.1\times10^{-4}$	8.9×10^{-3}	8.3×10^{-5}	86.5	0.97
I.3-4	0.1 (Re_c=10)	0.15	DI water	1.05	$4.5\times10^{3}\pm3.2\times10^{2}$	$3.3\times10^{-3}\pm8.1\times10^{-4}$	1.2×10^{-2}	2.1×10^{-5}	90.1	0.96
II.1	0.01 (Re_c=1.0)	0.33	0.01	1.05	$4.5\times10^{3}\pm3.2\times10^{2}$	$1.4\times10^{-4}\pm3.7\times10^{-5}$	4.8×10^{-3}	8.4×10^{-5}	87.3	0.95
II.2	0.01 (Re_c=1.0)	0.33	0.1	1.05	$4.5\times10^{3}\pm3.2\times10^{2}$	$1.2\times10^{-5}\pm3.2\times10^{-6}$	4.8×10^{-3}	1.4×10^{-4}	79.7	0.95

Table 4-1. Continued

Test no[a].	u (cm/s)	f	IS (M)	d_p (μm)	σ^b (*no./cm^2*) (Mean+SD)	$L_0{}^c$ *(cm)* (Mean+SD)	D^d (cm^2/s)	k_d (S^{-1}) (Mean)	MR *(%)* (Mean)	R^2 (Mean)
II.3	0.01 (Re_c=1.0)	0.33	0.2	1.05	$4.5\times10^{3}\pm3.2\times10^{2}$	$8.7\times10^{-6}\pm2.4\times10^{-6}$	4.8×10^{-3}	3.2×10^{-4}	72.4	0.94
Ш.1	0.01 (Re_c=1.0)	0.33	0.05	2.0	$4.5\times10^{3}\pm3.2\times10^{2}$	$4.8\times10^{-5}\pm1.3\times10^{-5}$	4.8×10^{-3}	7.4×10^{-5}	93.2	0.97
Ш.2	0.01 (Re_c=1.0)	0.33	0.05	0.3	$4.5\times10^{3}\pm3.2\times10^{2}$	$4.8\times10^{-5}\pm1.3\times10^{-5}$	4.8×10^{-3}	2.0×10^{-5}	90.7	0.96

a No.I.1-1- I.3-4 summarize the coupled effect of flow velocity and density; No. I.2 -2 and II.1- II.3 summarize the effect of ionic strength; No. I.2 -2 and Ш.1- Ш.2summarize the effect of colloid size; b data obtained from literature [225]; c for low IS condition data obtained from literature [225], for medium and high ionic IS conditions data estimated from equation (7); d determined from the bromide breakthrough curv

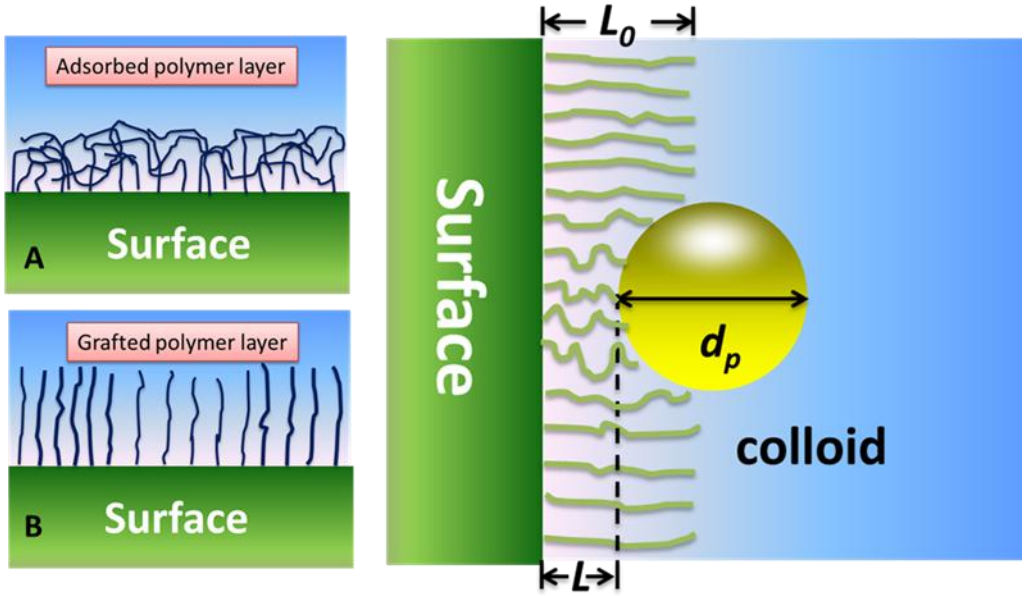

Figure 4-2. (A) Schematic of adsorbed polymer layer; (B) Schematic of grafted polymer brush layer; (C) Schematic of a model for a spherical colloid with diameter of dp impinging upon a biopolymer brush in a solution.

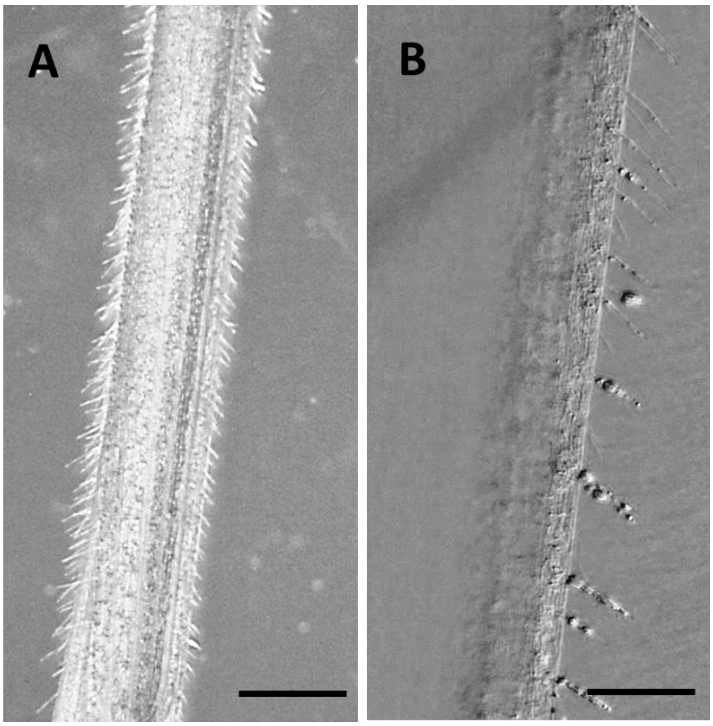

Figure 4-3. (A) Morphology of trichomes on the plant stem and (B) air bubbles attached on the surface of trichomes under water.

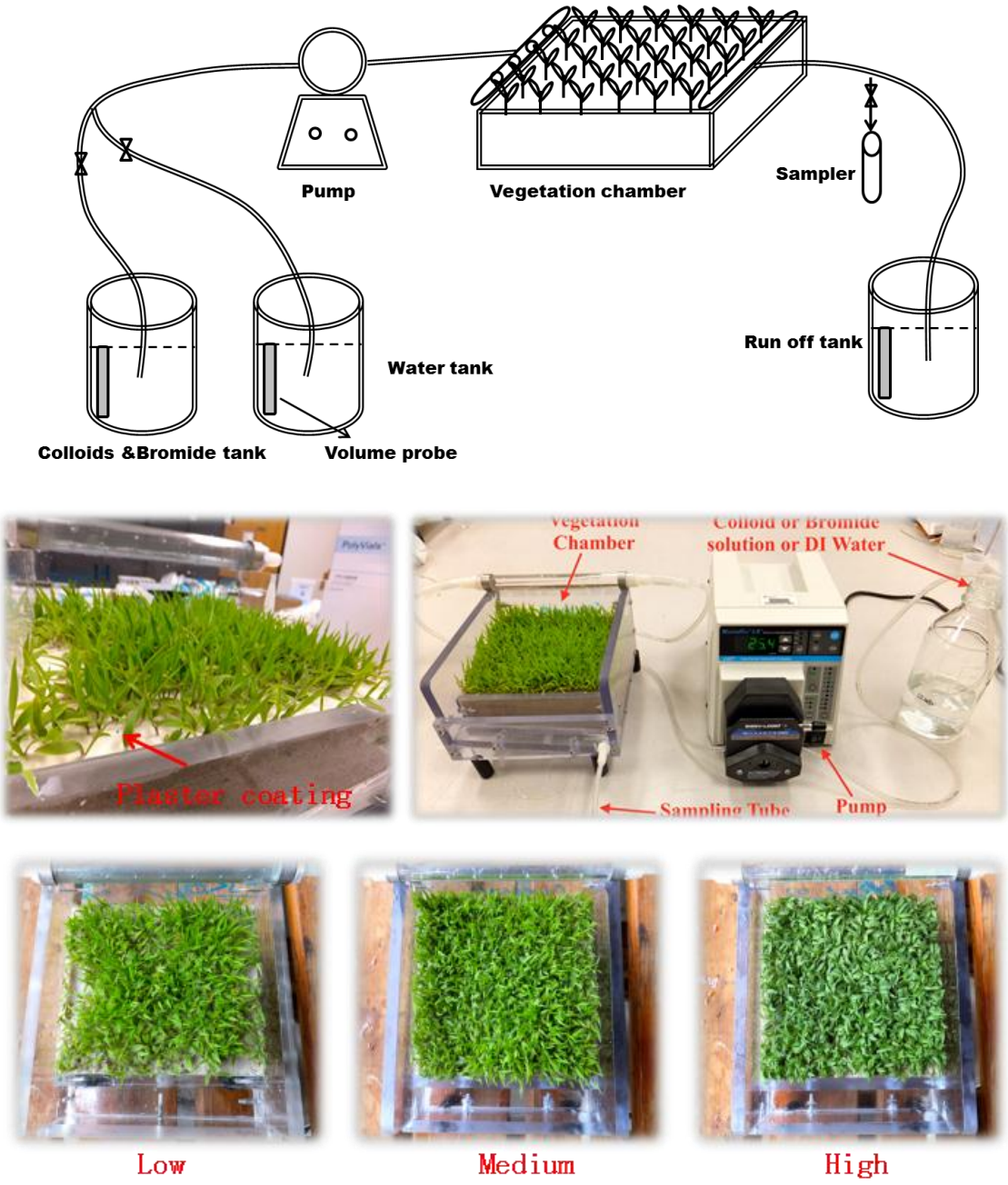

Figure 4-4. Schematic and photos of experimental set up for vegetation chamber experiment.

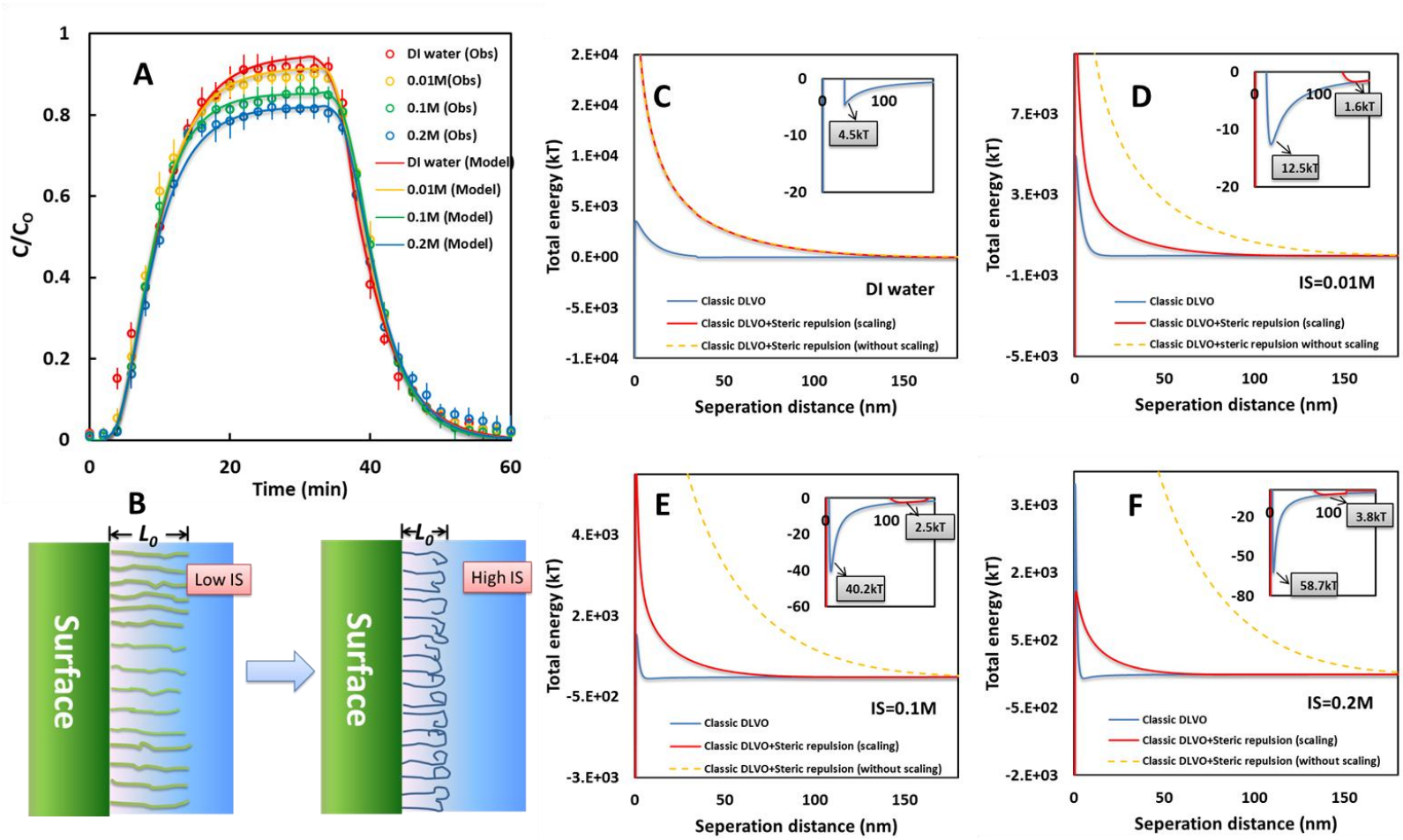

Figure 4-5. Effect of ionic strength on the colloid deposition onto the plant stem.

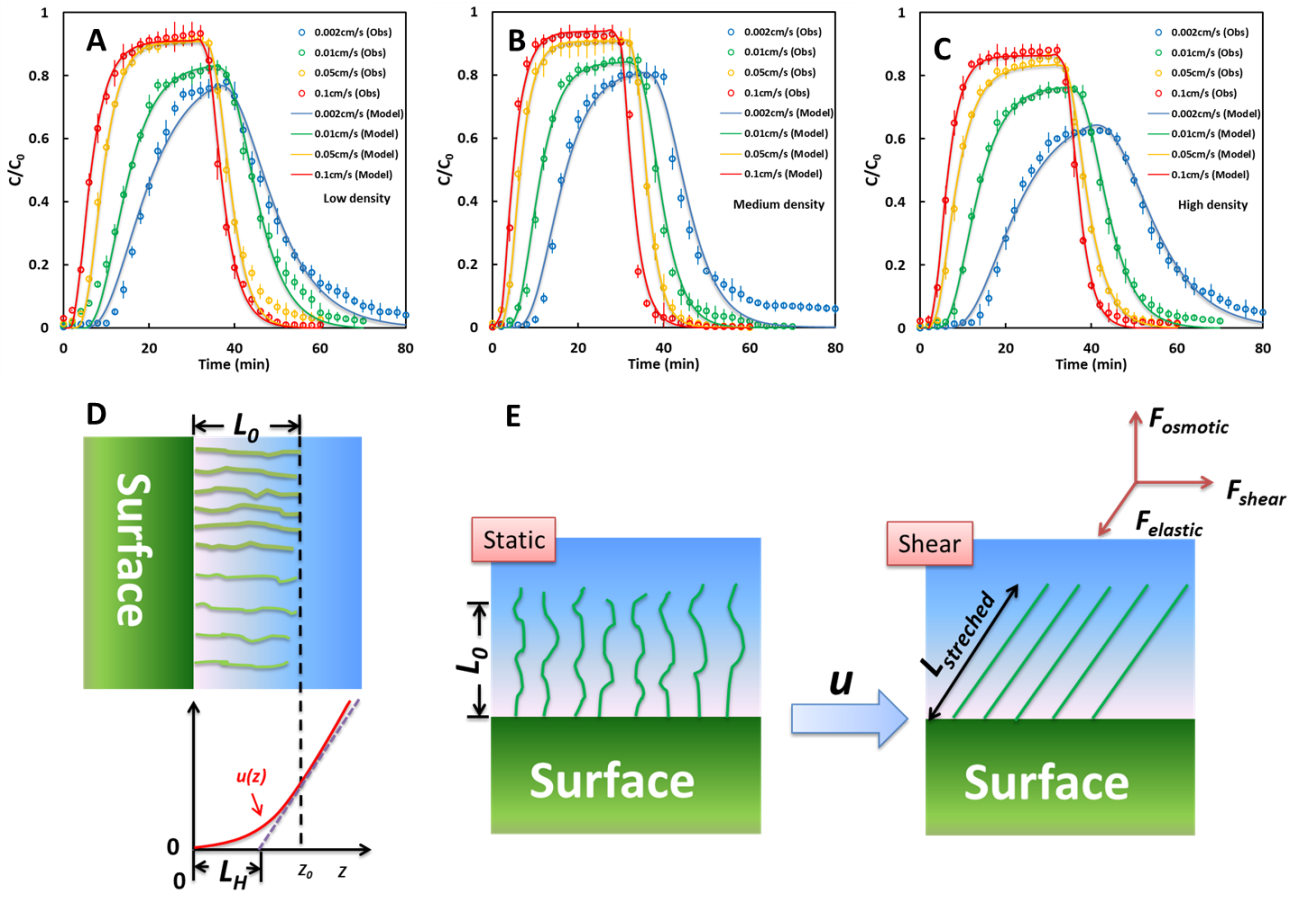

Figure 4-6. Effect of coupled flow velocity and grass density on the colloid deposition onto the plant stem.

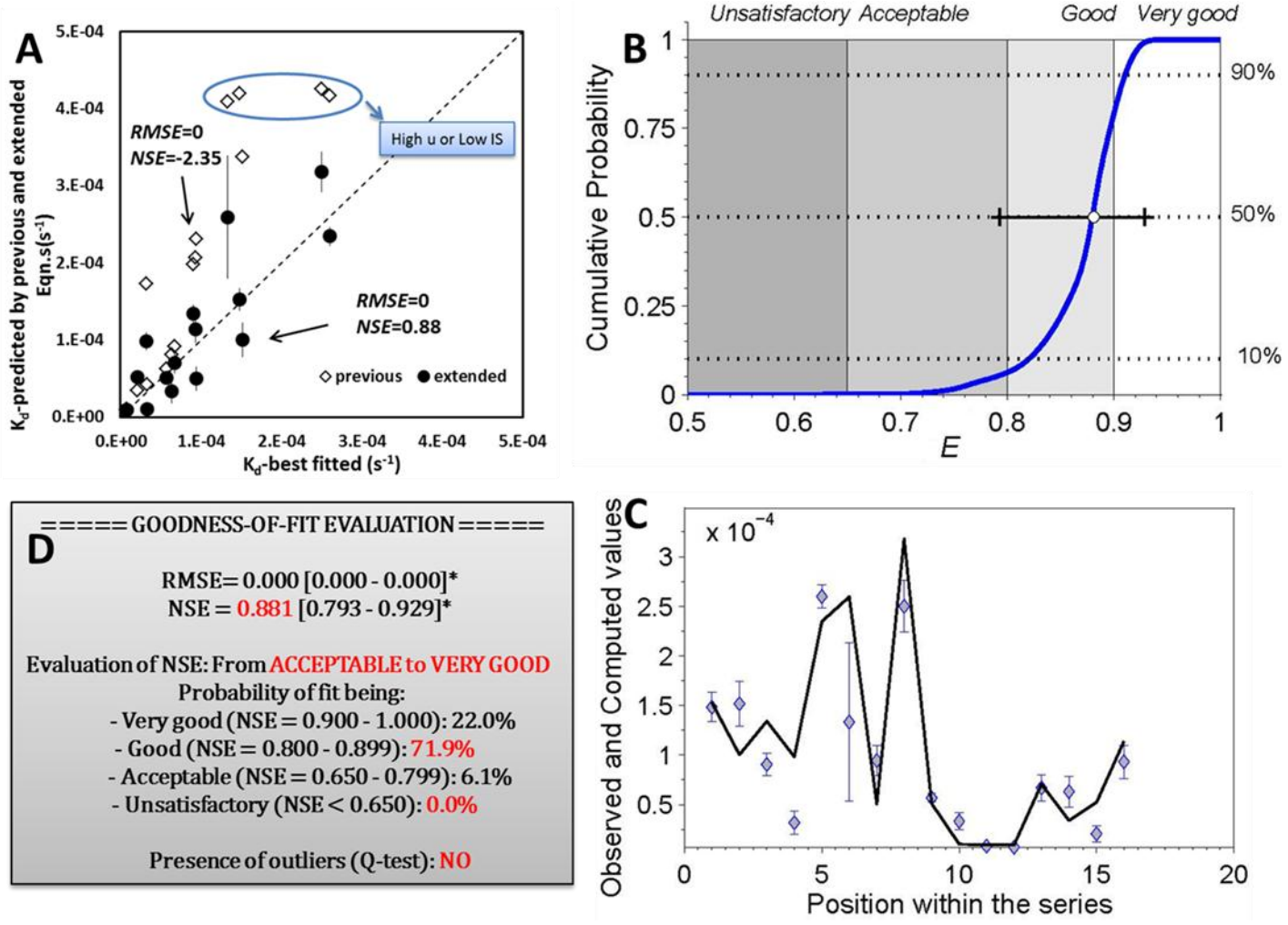

Figure 4-7. Goodness-of-fit evaluation of the extended model.

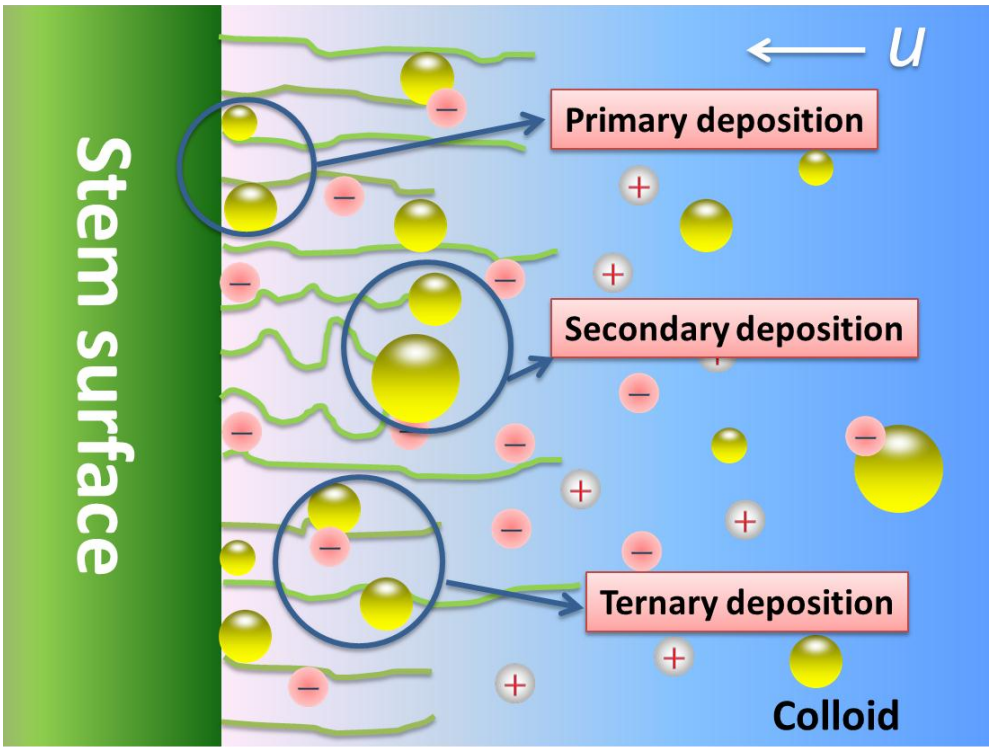

Figure 4-8. Schematic illustration of three basic mechanisms of colloidal particles deposition on the plant stems.

CHAPTER 5
DLVO INTERACTIONS OF CARBON NANOTUBES WITH ISOTROPIC PLANAR SURFACE[1]

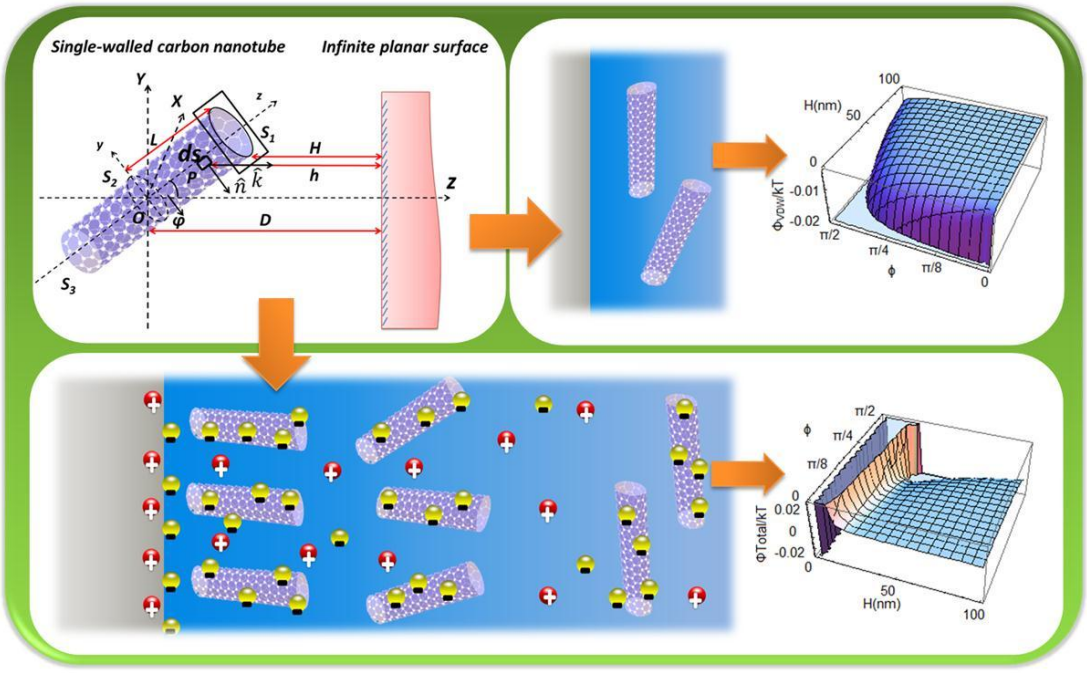

Figure 5-1. Graphical content of chapter 5

Introductory Remarks

Carbon nanotubes (CNTs) are cylinder-shaped nanoparticles with an extremely high length-to-diameter ratio.[107] Single-walled carbon nanotubes (SWNTs) possess the simplest geometry among the CNTs, and have diameters ranging from 0.4 to 3 nm. Multi-walled carbon nanotubes (MWNTs) are composed of a concentric arrangement of many SWNTs, which can reach diameters up to 100 nm. Their novel properties, such as exceptional mechanical strength, and superior electrical and thermal conductivity, prompt their applications in quantum wires,[242] high-resolution scanning probes,[243] transistors,[244] electron field emission sources,[245] chemical and biological

[1] Reprinted with permission from ***Wu, L.***, B. Gao, Y, Tian, R. Munoz-Carpena, and Kirk J. Zigler, (2013) DLVO interactions between a carbon nanotube and an isotropic planar surface. *Langmuir* 2013, *29* (12):3976-3988. doi: 10.1021/la3048328

sensors,[246, 247] reinforced composite materials,[248] nanomedicine,[249] and in many other areas. Some of these applications require assembling or depositing individual CNTs on surfaces of bulk materials with desired parameters, including location, orientation, geometry and density.[250-252] As a result, good understanding of the interaction forces between CNTs and the host surfaces is essential to creation and optimization of CNT-based products. Furthermore, this knowledge may be also used to inform the development of effective strategies to reduce the environmental impacts of the CNTs because surface interaction is one of most important factors governing the fate and transport of manufactured materials in soil and aquatic systems.[117-119, 123] A theory/model that can accurately describe the interaction between a CNT and a planar surface therefore is in critical need.

Pristine CNTs are crystalline graphitic rods and are often considered to have no surface charge. Their interaction with a surface therefore is mainly controlled by van der Waals forces. [253] In the literature, the van der Waals interaction between CNTs and substrate surfaces is determined either by the continuum Lennard-Jones (LJ) model (nanoscopic) with considerations of all pairs of interacting atoms[254-258] or by the Lifshitz theory (microscopic) in terms of the Hamaker coefficients.[253, 259] The shape and range of the attractive van der Waals interaction (potential) varies with different dimensions (nanoscopic and microscopic). The LJ model is successful in describing the short range van der Waals interaction potential in CNT systems. The latter has recently been adapted in a form to describe long-range van der Waals interaction between pristine SWNTs and anisotropic surfaces with good accuracy.[253] However, application

of this method requires ab-initio optical properties, which are not only barely documented in the literature but also difficult to measure.

Because of strong inter-tube attractions, pristine CNTs tend to aggregate and form “bundles” or “ropes”. To optimize their use, considerable research has been conducted to disperse CNTs in aqueous or organic media.[260-262] Surface modification methods, such as chemical functionalization (*e.g.,* acid oxidization) and polymeric coating (*e.g.,* surfactant, dissolved organic matter, and ligand) are often used to improve the stability of CNT suspensions by introducing repulsive electrostatics forces.[262-264] For example, Mamedov *et al.,*[265] used nitric acid oxidization to introduce negative charges on SWNTs, which enable the assemble of a stable SWNT composite film. Thus, for highly charged CNTs, dispersion of CNTs is mainly controlled by electrostatic forces. Unfortunately, there are only limited amount of studies that have been attempted to theoretically determine the interaction, particularly electrostatic interaction, of surface modified CNTs with charged surfaces. For example, Chapot *et al*.,[266] and Lowen [267] proposed frameworks allowing one to compute the interactions between charged rodlike colloidal particles, respectively. However, it is still unknown whether these frameworks can be directly applied to calculate the electrostatic double layer repulsion between charged CNTs and planar interface. The surface charge form an electric double layer at the CNTs surfaces, which is similar to the phenomenon observed with colloidal particles.[268] In addition, previous studies have indicated that, although CNTs are molecular objects with two dimensions in the nanometric range, their dispersion, deposition and aggregation behaviors follow the principles of the classical colloidal system (especially for MWNTs).[269],[11, 13, [270]] The Derjaguin-Landau-Verwey-

Overbeek (DLVO) theory, which was originally developed for spherical colloids, thus has been used to semi-quantitatively describe the stability of surface modified CNTs and their interaction with planar surfaces.[117, 119, 122, 123, 271, 272] Because an oversimplified assumption that tubular CNTs have “equivalent’ spherical diameters was used, the DLVO theory often failed to provide an accurate estimation of the interaction forces under various conditions.[117] Furthermore, the interaction of CNTs and planar surfaces is orientation dependent, which gives rise to a torque orienting the CNTs in an energetically favorable configuration to approach/depart the planar surfaces. Such a dynamic behavior cannot be explained merely on the basis of spherically symmetric interaction potentials of the classic DLVO theory.

Several techniques have been developed to calculate the interaction force/energy between curved surfaces/bodies, including the Derjaguin Approximation (DA) and surface element integration (SEI).[124] The DA method estimates the interaction energy between two finite size bodies by relating it to that between two infinite parallel flat plates. It can only be applied to surfaces that are separated by a small distance and to circumstances when the interaction range is substantially smaller than the radii of curvature of the surfaces. For very small non-spherical particles, such as SWNTs, the DA method may lead to inaccuracies in calculating their interaction with planar surfaces. [127] The SEI technique takes into account curvature effects over the whole object, by integrating the interaction energy between a surface element of the object and the plane surface using the exact surface geometry of the object. It can precisely determine the interaction forces between a planar surface and a curved body with any defined shape, including CNTs.[117] For instance, Stolarczyk *et al*.,[127]

successfully applied the SEI method to numerically evaluate the interaction forces between functionalized MWNTs and ligand-stabilized gold nanoparticles (modeled as cylinder-sphere system). However, the calculation is quite complex and time consuming. Thus, although the SEI has made a remarkable breakthrough in the accurate calculation of interaction energy between a curved body and planar surface or two curved bodies, the difficulty in numerical implement restrict its wide application in describing the interface interactions. Nevertheless, little research effort has been made to apply the SEI to quantify the interaction of CNTs with planar surfaces, particularly with respect to obtaining analytical expressions. Therefore, accurate and efficient analytical calculation of interaction energy between CNTs and planar surface is of great scientific and practical significance.

The overarching objective of this work was to develop analytical formulas that can precisely describe the orientation-dependent interaction energy/forces between a CNT and an isotropic planar surface. It was hypothesized that the interaction of CNTs with planar surfaces is mainly controlled by the van der Waals and electrical double layer (EDL) forces, which are the same as the classic DLVO forces. The SEI method was thus integrated into the DLVO theory framework to obtain the analytical expressions of the orientation-dependent interaction energy between an SWNT and an isotropic planar surface. The interaction energy was evaluated for two different situations: 1) a pristine SWNT and an isotropic planar surface and 2) a surface charged SWNT and an isotropic planar surface. After validations, the analytical expressions were also extended to determine the interaction between a MWNT and the planar surface.

Theory

The general expression representing the interaction between an SWNT and planar surface are presented in Fig. 5-2. For convenience, two coordinate systems were used: a set of body-fixed coordinates (*x,y,z*) to account for the internal geometric properties of the tubular SWNT and a space-fixed coordinate system (*X,Y,Z*) to account for the orientation of the tubular SWNT relative to the planar surface. The SWNT was modeled as a hollow cylinder (*e.g.,* SWNTs can be converted from nearly endless, highly tangled ropes into short, open-ended pipes after acid oxidation).[273] The top, side, and bottom surfaces of the SWNT were defined as S_1, S_2, and S_3, respectively. It is worth noting that the presence of hemispherical caps at the ends of the SWMTs is also important and is currently a topic of ongoing investigation but is beyond the scope of this study.

The SEI method was used in this work to determine the total interaction energy between an SWNT of finite length and an infinite planar surface.[124-126] The governing equation of the SEI method can be written as:

$$\Phi(D,\varphi) = \int_{Si} \hat{n}_{Si} \cdot \hat{k}\ E(h_i) dS \qquad (5\text{-}1)$$

where $\Phi(D,\phi)$ is the total interaction energy when the center of the SWNT with arbitrary angle (ϕ) is located at a distance D from the planar surface, $\hat{\boldsymbol{n}}_{\boldsymbol{Si}}$ is the outer unit normal vector to the SWNT surface element *dS*, (*i*=1,2,3, and represents top, side, and bottom surfaces of the SWNT, respectively), $\hat{\boldsymbol{k}}$ is a unit vector normal to the planar surface, $E(h_i)$ represents the unit interaction energy between the surface element and the planar surface at a distance of h_i.

It is worth noting that the sign of $\hat{\boldsymbol{n}}_{\boldsymbol{Si}} \cdot \hat{\boldsymbol{k}}$ governs the magnitude of the total interaction energy. When the unit normal to the surface at a given point makes an obtuse angle with $\hat{\boldsymbol{k}}$, the sign of $\hat{\boldsymbol{n}}_{\boldsymbol{Si}} \cdot \hat{\boldsymbol{k}}$ is negative, and hence, the energy contribution of the corresponding surface element is also negative. Thus, we need to subtract the interaction energy of those regions of the surface that "face away" from the planar plate. The differential area of the surface element *dS* of the SWNT then can be written as:

$dS = adzd\theta$ for outer S_2, (5-2-1)

$dS = (a - R)dzd\theta$ for inner S_2 (5-2-2)

$dS = \rho d\rho d\theta$ for S_1 and S_3 (5-3)

where *a* is semi axes of the SWNT directed along *x* and *y* axes, *ρ* and *θ* are radial and angular coordinate in a cylindrical coordinate system, respectively, and *R* is diameter of carbon atom (1.54×10^{-10}m).

The expressions of $\hat{\boldsymbol{n}}_{\boldsymbol{Si}} \cdot \hat{\boldsymbol{k}}$ in the equation (5-1) can be written as:

$\hat{n}_{S2} \cdot \hat{k} = \sin\theta \sin\varphi$ for S_2 (5-4)

$\hat{n}_{S1} \cdot \hat{k} = \cos\varphi$ for S_1 (5-5)

$\hat{n}_{S3} \cdot \hat{k} = -\cos\varphi$ for S_3 (5-5)

where *φ* is orientation angle of the tubular SWNT.

The distance between the surface element and the planar surface, h_i, can be written as:

$h_1 = D - L\cos\varphi - \rho\sin\varphi\sin\theta$ for S_1 (5-6)

$h_2 = D - z\cos\varphi - a\sin\varphi\sin\theta$ for outer S_2 (5-7-1)

$h_2 = D - z\cos\varphi - (a - R)\sin\varphi\sin\theta$ for inner S_2 (5-7-2)

$h_3 = D + L\cos\varphi - \rho\sin\varphi\sin\theta$ for S_3 (5-8)

where *D* is separation distance of infinite planar surface from the center of the SWNT and *L* is semi axe of an SWNT directed along *z* axis.

The interaction between the surface element and the planar surface was assumed to be mainly controlled by the DLVO forces,[268, 274, 275] thus the $E(h_i)$ can be written as:

$$E(h_i) = E_{vdw}(h_i) + E_{edl}(h_i) \quad (5\text{-}9)$$

where $E_{vdw}(h_i)$ and $E_{edl}(h_i)$ are the van der Waals and EDL interaction energy per unit area between two infinite flat plates, respectively.

For van der Waals interaction, instead of the Lifshitz approach which is obtained from complex optical properties, the Hamaker approach was used in this study and $E_{vdw}(h_i)$ can be written as:[276]

$$E_{vdw}(h_i) = -\frac{A}{12\pi(h_i)^2} \quad (5\text{-}10)$$

where *A* is the effective Hamaker constant.

For EDL interaction, linear superposition approach is regarded as the most accurate physical description of the EDL interaction for CNTs since it gives intermediate values between those for the constant potential (mobile charges that keep the potential between the two surfaces constant) and constant charge (assuming immobile charges) cases, and $E_{edl}(h_i)$ is given by Gregory: [277]

$$E_{edl}(h_i) = 32\varepsilon_0\varepsilon_r\gamma_1\gamma_2\kappa\left(\frac{kT}{ve}\right)^2 \exp(-\kappa h_i) \quad (5\text{-}11)$$

where $\varepsilon_0$is the permittivity of vacuum, ε_r is the relative permittivity of the solution, $\gamma = tanh(ve\psi/4kT)$, ψ is the surface potential, κ is the Debye-Huckel parameter, *k* is the Boltzmann's constant, *T* is the temperature, ν is the valence of electrolyte, *e* is the electron charge. Ideally, the surface potential must be used in Eqn. (5-11). In recent studies, ψ is often approximated by the zeta potential (ζ), the potential located at the

electrokinetic plane of shear.[184, 278-282] It is worth noting that there is debate of charges distribution on the surface of CNTs: Paillet *et al.,*[283] provided the experimental confirmation that charges are distributed uniformly along the nanotubes while open-ends and defect sites were reported to be preferentially charged areas.[270, 284, 285] By using theoretically an atomic charge-dipole model and experimentally electrostatic force microscopy, Wang *et al.,* [286] demonstrate that the charge enhancement at the end already becomes insignificant for an SWNT with length around 30nm, and will become negligible for micrometer-long CNTs. Hence, in this study, we assume that charge on the SWNTs surface is uniformly distributed on the surface.

Results and Discussion

DLVO Interactions between a Pristine SWNT and an Isotropic Planar Surface

The interaction between a pristine SWNT (without charge) and an isotropic planar surface is mainly controlled by the attractive van der Waals forces. For this case, mathematical analysis of the interaction energy between a pristine SWNT and an isotropic planar surface with arbitrary angle position yields the analytical solution:

$$\Phi_{VDW}(D,\varphi) =$$

$$\begin{cases} -\frac{Asec\varphi}{3\pi}\left[\begin{array}{c}\frac{(D-Lcos\varphi)Arctan\left(\frac{asin\varphi}{M_1}\right)}{M_1}-\frac{(D+Lcos\varphi)Arctan\left(\frac{asin\varphi}{M_2}\right)}{M_2}\\ -\frac{(D-Lcos\varphi)Arctan\left(\frac{(a-R)sin\varphi}{M_3}\right)}{M_3}+\frac{(D+Lcos\varphi)Arctan\left(\frac{(a-R)sin\varphi}{M_4}\right)}{M_4}\end{array}\right] \\ -\frac{Acos\varphi csc\varphi^2}{6}\left[(D-Lcos\varphi)\left(\frac{1}{M_1}-\frac{1}{M_3}\right)+(D+Lcos\varphi)\left(\frac{1}{M_2}-\frac{1}{M_4}\right)\right], & 0<\varphi<\pi/2 \\ -\frac{A\left(2aR-R^2\right)}{12}\left[\frac{1}{(D-L)^2}+\frac{1}{(D+L)^2}\right], & \varphi=0 \\ -\frac{2aAL\left[\sqrt{D^2-a^2}+aArctan\left(\frac{a}{\sqrt{D^2-a^2}}\right)\right]}{3\pi(D^2-a^2)^{\frac{3}{2}}}+\frac{2(a-R)AL\left[\sqrt{D^2-(a-R)^2}+(a-R)Arctan\left(\frac{(a-R)}{\sqrt{D^2-(a-R)^2}}\right)\right]}{3\pi(D^2-(a-R)^2)^{\frac{3}{2}}}, & \varphi=\pi/2 \end{cases}$$

(5-12)

where $M_1=\sqrt{(D-Lcos\varphi)^2-(asin\varphi)^2}$, $M_2=\sqrt{(D+Lcos\varphi)^2-(asin\varphi)^2}$, $M_3=\sqrt{(D-Lcos\varphi)^2-\left((a-R)sin\varphi\right)^2}$, $M_4=\sqrt{(D+Lcos\varphi)^2-\left((a-R)sin\varphi\right)^2}$. Detailed math derivations of Equation (5-12) can be found in the Appendix.

Equation (5-12) was used to determine the interaction energy profiles (scaled to *kT*) between a pristine SWNT and a planar quartz surface in water for arbitrary angle approaching patterns. The interaction energy between the pristine SWNT and the flat surface was attractive, suggesting pristine SWNTs intend to attach to surfaces due to the attractive van der Waals forces. Overall, the magnitude of van der Waals interaction energy depends on the orientation of the SWNT with respect to the planar surface (Figure 5-3A). The attractive interaction energy increases when the arbitrary angle increases from ϕ=0 (“end-on”, attached by tube end) to ϕ=π/2 (“side-on”, attached by tube side). The attractive energy of the side-on pattern was much higher (at least two-orders of magnitude) than that of the end-on pattern, indicating that it is more favorable

for pristine SWNTs to attach on planar surfaces through the side-on approaching pattern (Figure 5-3B). For a randomly positioned pristine SWNT in the system, the difference in attractive energy between the two approaching patterns may generate a torque to drive the SWNT to attach on the planar surface through the side-on pattern.

Because of their nanosized diameter, SWNTs are often modeled as solid cylinders (without open ends) instead of tubes for convenience.[127] This practice, however, may generate errors when used to determine the interaction energy between SWNTs and flat surfaces using the SEI method. When a pristine SWNT of a relatively small diameter (*e.g.,* 0.2 nm) was modeled as a cylinder, the energy profile matched that of the tubular SWNT closely (Figure 5-2C). When a pristine SWNT of a relatively large diameter (*e.g.,* 1.5nm) was modeled as a cylinder, however, the results showed large deviations between the two energy profiles. These results suggest that SWNTs, especially with large diameters, should be modeled as tubes instead of cylinders to accurately describe their interaction with planar surfaces.

Recently, Rajter *et al.,*[253] developed a model to calculate the van der Waals interaction energy between optically anisotropic SWNTs and planar surfaces based on the optical properties of the SWNTs and the Lifshitz theory. This model was applied in this work to determine the energy profile between the pristine SWNT and the planar surface for the side-on pattern. The interaction energy profile obtained from the Rajter model was compared with that of this work and of the widely used DA method (Figure 5-3D). The results demonstrated excellent agreements between the new model and the Rajter model, indicating the SEI approach can be integrated into the DLVO theory to accurately describe the interaction between SWNTs and planar surfaces. In contrast,

the DA method overestimated the interaction of between a SWNT and planar surface up to three-order of magnitude, confirming the method is not suitable for nanosized non-spherical particles[127].

DLVO Interactions between a Surface Modified SWNT and a Charged Isotropic Planar Surface

Both van der Waals and EDL forces are important to the interaction between a surface modified SWNT and a charged isotropic planar surface. While the attractive van der Waals interaction energy is the same as discussed previously (Eqn.(5-12)), analytical expression of the EDL interaction energy between the surface charged SWNT and the planar surface with arbitrary angle can be written as:

$$\Phi_{EDL}(D,\varphi) =$$

$$\begin{Bmatrix} 32\pi\varepsilon_0\varepsilon_r\gamma_1\gamma_2\left(\frac{kT}{ve}\right)^2 e^{-\kappa D}\begin{Bmatrix} 2atan\varphi N_1 N_4 \\ +\kappa cos\varphi N_5[a^2\mathrm{N}_2-(a-R)^2\mathrm{N}_3]\end{Bmatrix}, & 0<\varphi<\pi/2 \\ 32\pi(2aR-R^2)\varepsilon_0\varepsilon_r\gamma_1\gamma_2\kappa\left(\frac{kT}{ve}\right)^2\left[e^{-\kappa(D-L)}+e^{-\kappa(D+L)}\right], & \varphi=0 \\ 128\pi aL\varepsilon_0\varepsilon_r\gamma_1\gamma_2\kappa\left(\frac{kT}{ve}\right)^2 exp(-\kappa D)L_{-1}(\kappa a), & \varphi=\pi/2 \end{Bmatrix} \quad (5\text{-}13)$$

where $\mathrm{N}_1 = L_{-1}(\kappa a sin\varphi)$; $\mathrm{N}_2 = I_0(\kappa a sin\varphi) - I_2(\kappa a sin\varphi)$; $\mathrm{N}_3 = I_0(\kappa(a-R)sin\varphi) - I_2(\kappa(a-R)sin\varphi)$; $N_4 = (e^{\kappa L cos\varphi} - e^{-\kappa L cos\varphi})$; $N_5 = (e^{\kappa L cos\varphi} + e^{-\kappa L cos\varphi})$; $I_0(x)$, $I_0(x)$, and $I_2(x)$ are modified Bessel function of order zero, first, and second, respectively; and $L_{-1}(x)$ is modified Struve function of order -1. Detailed math derivations of Eqn. (5-13) can be found in the appendix. Here, the electrostatic interaction was considered as the only force introduced by the surface modification, which is reasonable for surface charged CNTs. Other interaction forces, such as steric repulsion and hydrophobic interaction, however, may be trigged by other surface modification methods (*e.g.,* coating with surfactants or polymers)[256, 258] which are beyond the scope of this study. Thus,

further investigations are necessary to include these non-DLVO interaction forces to describe the extended DLVO interaction of surfactant or polymer modified SWNTs and planar surfaces in the future.

Eqn. (5-13) was used to determine the scaled EDL energy profiles between a charged SWNT (*i.e.,* humic acid coated SWNT[271]) and a planar quartz surface in water for arbitrary angle approaching patterns (Figure 5-3A). The ξ potential values of the SWNT and the glass beads under two ionic strength conditions were obtained from reported values in the literature.[122, 271] It is worth noting that by measuring the electrophoretic mobility and then relating to the reported ξ potential of SWNTs was calculated from the Smoluchowski approximation for spherical particles, which may overestimate the actual ξ potential of the tubular SWNTs by up to 20%. [264] Several research efforts have been made to modify the Smoluchowski equation to apply to higher aspect-ratio structures (*i.e.,* cylindrical particles).[287] [288, 289] Additional investigations, however, are still needed to determine whether the modified Smoluchowski equations can provide accurate solution to the ξ potential of tubular SWNTs.

The EDL interaction energy between the charged SWNTs and the quartz surface was repulsive and the repulsive energy was four orders of magnitude stronger for the side-on pattern than for the end-on pattern under both ionic strength conditions (Figure 5-4B). Furthermore, the predicted EDL energy was very sensitive to ionic strength and decreased dramatically for arbitrary angle pattern when solution ionic strength increased from 0.001M to 0.1M. This is consistent with the DLVO theory that increases

in ionic strength can compress the double layer to reduce the repulsive electrostatic forces between two charged surfaces in electrolyte solutions.[268, 275]

Based on the equations (5-12) and (5-13), the total interaction energy between the surface modified SWNT and the charged planar surface for arbitrary angle attachment thus can be written as:

$$\Phi_{Total}(D,\varphi) = \Phi_{VDW}(D,\varphi) + \Phi_{EDL}(D,\varphi) \quad (5\text{-}14)$$

Eqn. (9) was used to determine the scaled DLVO energy profiles between a surface modified SWNT and a planar quartz surface (using the physicochemical and surface properties mentioned above) in water for arbitrary angle approaching patterns (Figure 5A).

The coupled effects of orientation and ionic strength on the total interaction energy profile of SWNTs and planar surfaces were also investigated (Figure 5-5 B-E). Both the height of the energy barrier and the depth of the secondary minimum increased with the increase of the approaching angle for the two tested ionic strength conditions. The total interaction energy of the side-on pattern was several orders of magnitude higher than that of end-on pattern over the entire range of separation distances. The energy barrier of the side-on pattern was (0.001M: 173.52 *kT* and 0.1M: 87.64 *kT*) more than three hundred times higher than that of the end-on pattern (0.001M: 0.55 *kT* and 0.1M: 0.47 *kT*). These results indicated that it might be much easier for the SWNT to overcome the energy barrier to attach to the planar surface through the end-on pattern than through the side-on pattern when repulsive EDL forces presence. For all arbitrary angle patterns, the EDL interaction became short ranged with the presence of electrolyte (*i.e.,* 0.1M). As a result, shallow secondary minimum energy

wells were identified in the energy profiles for all approaching patterns. For example, the depth of secondary minimum for side-on pattern is 0.87 *kT*, indicating that the SWNT could also attach to the planar surface through side-on pattern in the secondary minima under high energy barrier conditions although the deposition in secondary minimum is temporary since the depth is close to the average kinetic energy of a particle (1.5 *kT*). No secondary minimum wells were found in the energy profiles for the low ionic strength conditions over the entire range of separation distance shown (0-100nm) for both patterns.

Figure 5-5 F-I show the coupled effects of radii and orientation (approaching angle) on the total interaction energy profile of SWNTs and planar surfaces. For easy comparison, zeta potential and length of SWNTs of different radii were assumed to the same under the tested conditions. Overall, both of the interaction energy barriers and depths of secondary minimum increase when the radii of the SWNTs increase for all the approaching patterns. When the SWNTs radii are fixed, heights of the interaction energy barrier and depths of secondary minimum increased as the rotation angles increase from 0 to π/2, which is consistent with the discussion above. When the orientation angle is fixed, the separation distance at the secondary minimum well is independent of SWNTs radius. For example, the secondary minimum locations (separation distances) of three tested SWNTs with different radii were at 10.1, 7.4, 7.3, and 9.5 nm when the approaching angle is 0, π/6, π/4, and π/2, respectively (dash lines in insets). These results are in agreement with findings from previous studies using the LJ potential approach[255]. Based on the results shown in Figure 5-5 F-I, there may exist a critical rotation angle, at which the secondary minimum well separation distance

reaches the minimum value. Volkov and Zhigilei [257] also reported that the equilibrium distance between two CNTs of finite length depends on their rotation angles.

DLVO Forces and Torques of SWNTs with Planar Surfaces

The analytical expressions of interaction energy of SWNTs with planar surfaces enable a straightforward analysis of force $F(D,\varphi)$ and torque $\tau(D,\varphi)$, which can be written as the derivatives of the energy potential:

$$F(D,\varphi) = -\frac{\partial \Phi_{Total}(D,\varphi)}{\partial D} \quad (5\text{-}15)$$

$$\tau(D,\varphi) = -\frac{\partial \Phi_{Total}(D,\varphi)}{\partial \varphi} \quad (5\text{-}16)$$

Thus, the DLVO force and torque between a charged SWNT and a planar quartz surface (of the same properties as mentioned above) in water for arbitrary angle approaching patterns can be determined using the two equations (Figure 5-6A and Figure 5-6B, respectively). Figures 5-6C shows the DLVO force profiles of SWNTs of different radii interacting with the planar surface under side-on approaching pattern. The results indicated that the distance where the attractive force reaches its maximum is a constant (9.7 nm) for all the tested conditions, which is in consistent with the fact that the corresponding secondary energy minimum wells are located at around 9.5 nm (Figure 5-6D) as discussed above. The inset in Figure 5-6C indicates that the surfaces jumped to a primary minimum from H=0.87 nm. Figure 5-6D shows the dependences of torque on the rotation angle ϕ of the SWNT approaching to the surface. The results suggested that that torque direction is depended on the separation distance. For close separation distance (e.g., 2 nm) between the SWNT and the surface, where repulsion dominates, the torque (negative) acts to misalign the SWNT to be ‘end-on’ (perpendicular) to the planar surface. For intermediate separation distance, in vicinity of

the equilibrium position, the equilibrium angle (when the torque is zero) may not necessary to be 0 or π/2 (e.g., when H=10nm, the equilibrium angle is π/10). For relatively long separation distance, where attraction may dominate, and the torque (positive) acts to align the CNTs to be 'side-on' (parallel) to the planar surface.

DLVO Interactions of MWNTs and Planar Surfaces

The analytical expressions can be extended to describe the interaction of MWNTs and planar surfaces. Because MWNTs are made of several layers of SWNTs, it is reasonable to assume that each layer interacts with the planar surface as one SWNT. Thus, the total van der Waals interaction energy between a MWNT and a planar surface can be obtained by summation over all layers with an assumption that the interlayer spacing is a constant (i.e., 3.39 nm).[290] For the EDL interaction of modified MWNTs, previous studies have shown that all the surface charge may uniformly distributed on their out layer surfaces [291] and thus the EDL expression (i.e., Eqn. (5-13)) can be applied directly.

Figure 5-7 compares normalized interaction energy profiles ($\Phi_{Total}/|\Phi_{sec}|$ vs. $\frac{H}{H_{sec}}$, where Φ_{sec} is the secondary minimum and H_{sec} is the corresponding separation distance) of a modified SWNT and a modified MWNT (same surface charge density and length) interact with the charged planar surface at three different rotation angles. When the rotation angle is fixed, the normalized interaction energy profiles of SWNTs and MWNTs were almost identical regardless of the differences in their radii. This result is consistent with the findings from previous studies based on the continuum LJ potential model [254, 255, 292, 293] and confirmed the analytical expressions are applicable to the MWNT systems. Because the normalized energy profile is independent of the

Hamaker constant, surface charge density, and CNT properties, further research is needed to explore the mathematical connections among the maximum energy barrier, secondary energy minimum, and their corresponding separation distances (equilibrium distance). This will allow the development of new mathematical tools to determine the interaction of CNTs and planar surfaces.

Environmental Implications

Interaction between a tubular SWNT and an isotropic planar surface with arbitrary orientation angles was quantified by integrating the SEI method into the DLVO theory. For the first time, exact analytical solutions of the DLVO interaction energy were developed not only for pristine SWNTs and planar surfaces, but also for surface modified SWNTs and charged planar surfaces with arbitrary orientation angles. Simplified formulas were also given for the case of “end-on” and “side-on” approaching patterns. Compared to the results of other methods, the new solutions were either convenient or more accurate than existing approach to describe the interaction of SWNTs with isotropic surfaces. The analytical formulas derived for SWNTs can also be applied to MWNTs with minor modifications. The analysis of DLVO force and torque showed that in the region close to the planar surface, the repulsive interaction creates preferential alignment of CNTs perpendicular to the planar surface; without this interaction, parallel alignment is favored. The new model presented in this work provides a clear picture of the interaction energy/forces/torques between CNTs and planar surfaces with arbitrary orientation and sheds light on understanding the approaching patterns of CNTs to the planar surfaces under various conditions. It can be used as an effective tool by end-users to predict and optimize the interaction between CNTs and planar surfaces for a wide variety of fields of interests (*e.g.,* bio-devices,

biomedicine, *etc*.). Although in this work the interaction energy is developed for CNTs, it is not limited to CNTs and can be readily applied for various types of nano- and micro-tubular structures for analysis of their interaction with planar surfaces.

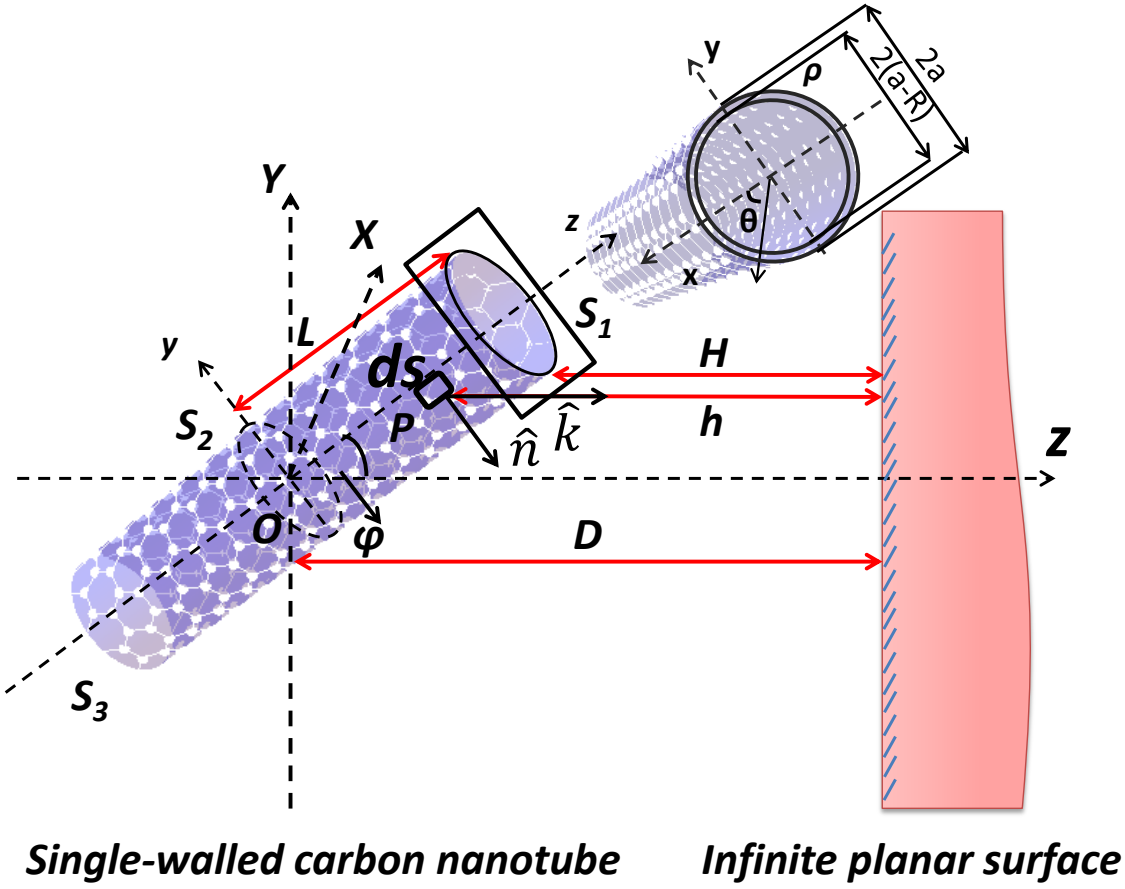

Figure 5-2. Schematic illustration of interaction of a SWNT with an infinite isotropic planar surface.

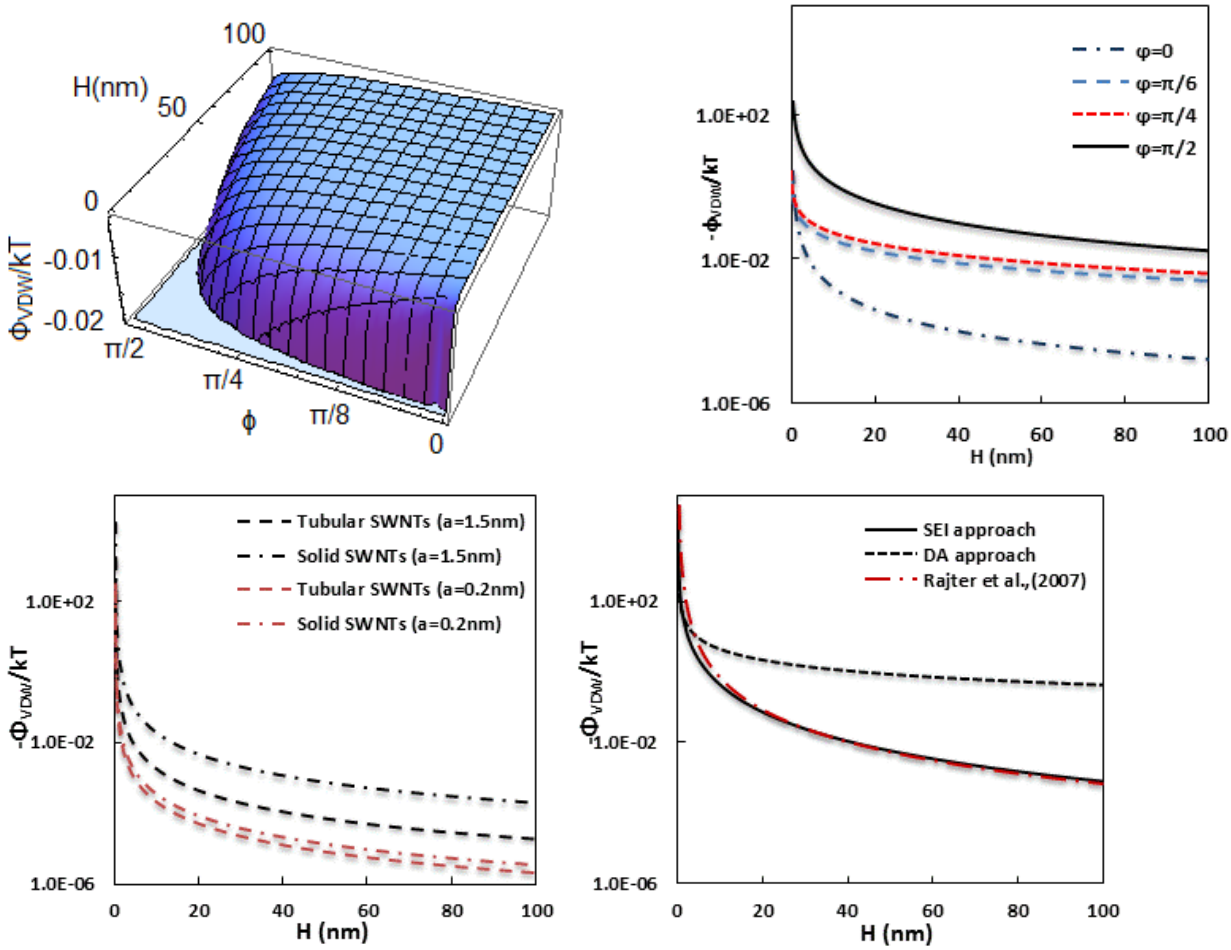

Figure 5-3. The van der Waals interaction energy between a pristine SWNT and an isotropic planar surface.

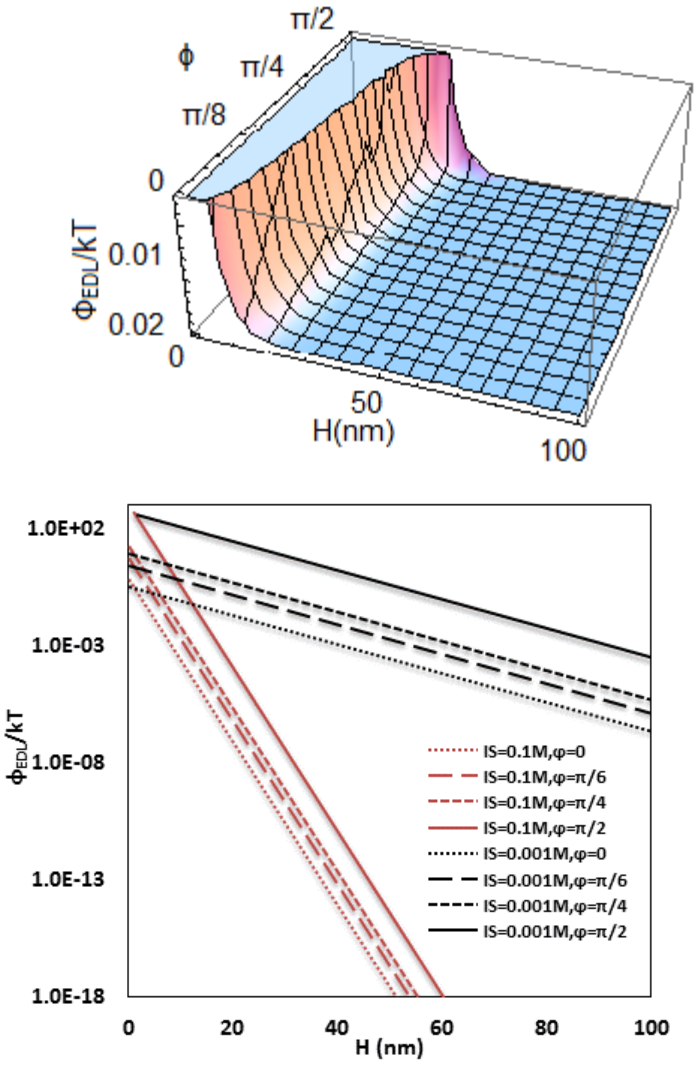

Figure 5-4. The electrostatic double layer interaction energy (Φ_{EDL}/kT) between a surface modified SWNT and a charged isotropic planar surface.

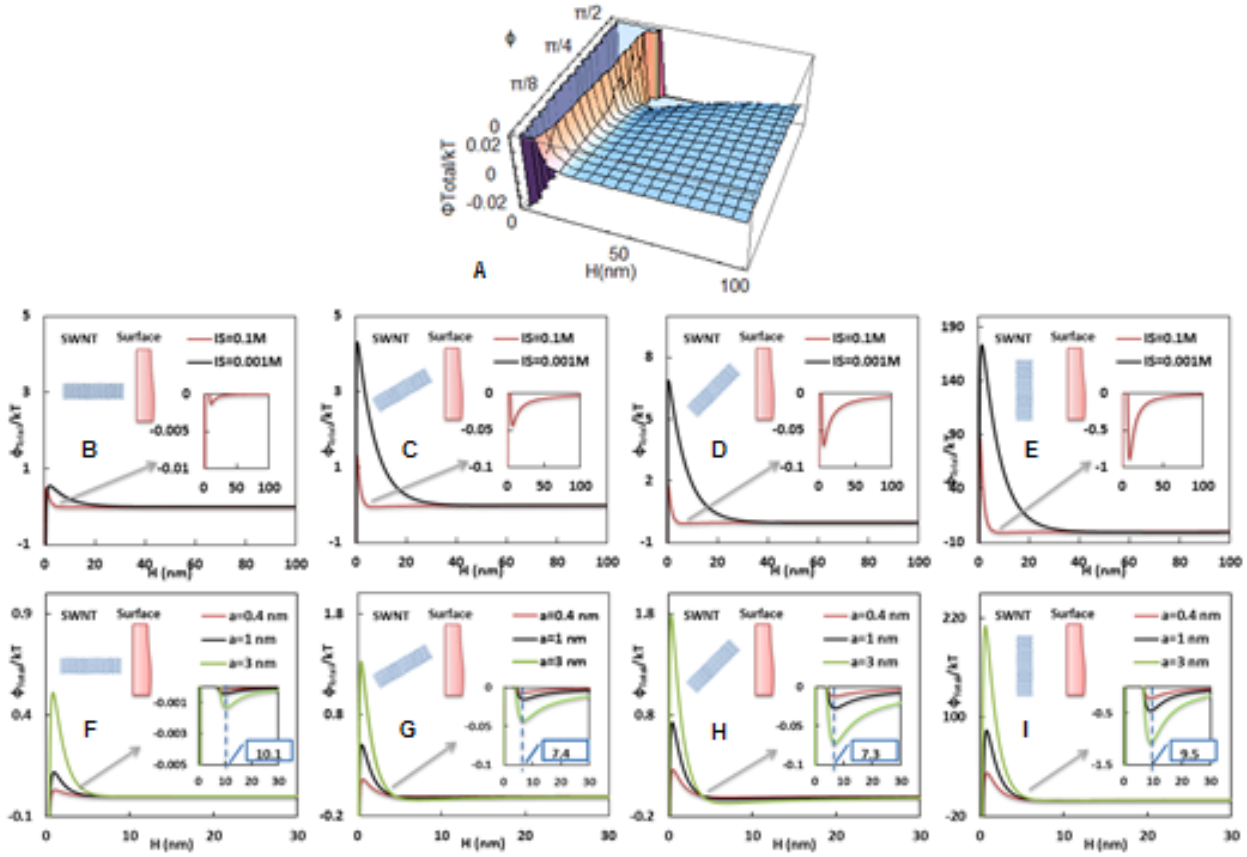

Figure 5-5. Total interaction energy ($\Phi_{\mathrm{Total}}/\mathrm{kT}$) between a surface modified SWNT and a charged isotropic planar surface.

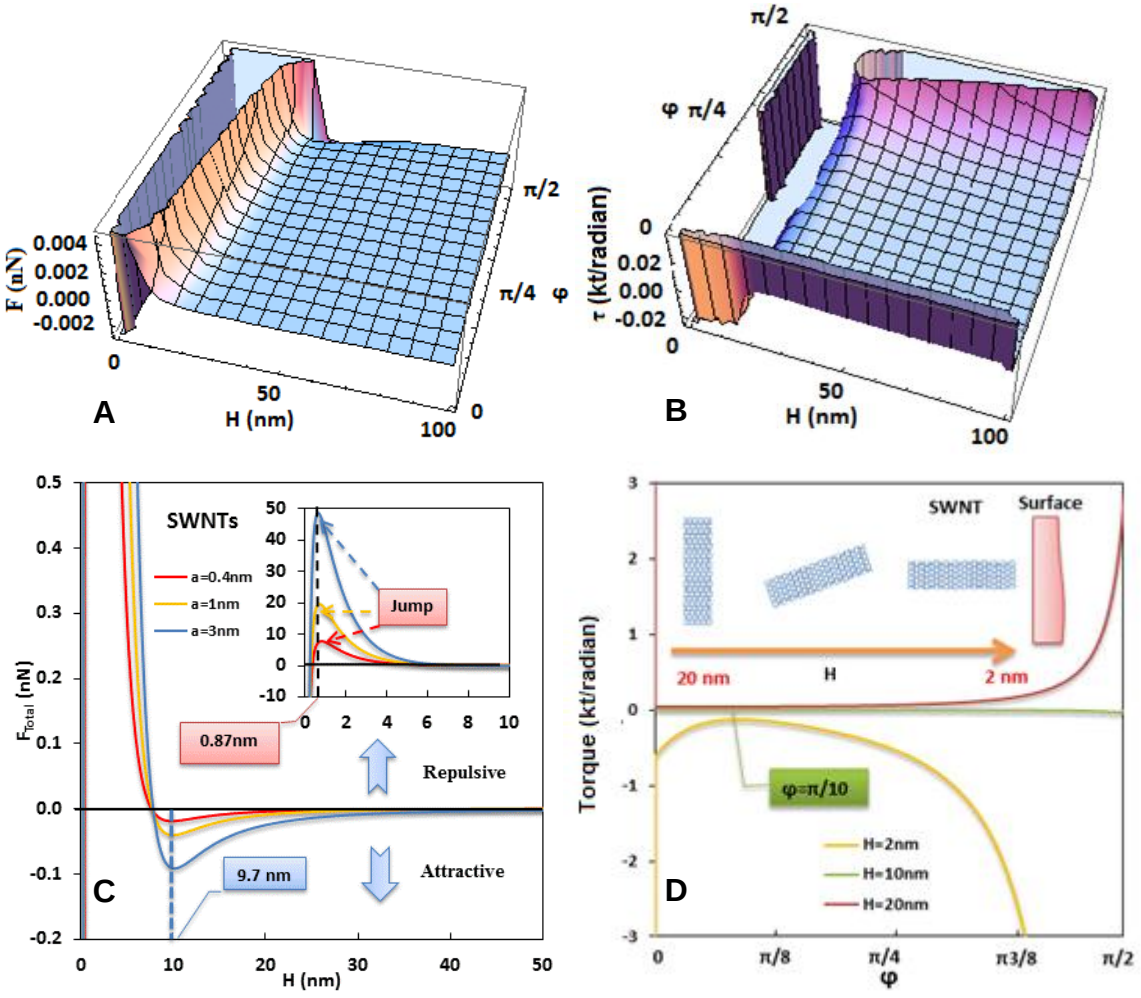

Figure 5-6. DLVO force and torque acting on a surface modified SWNT and a charged isotropic planar surface.

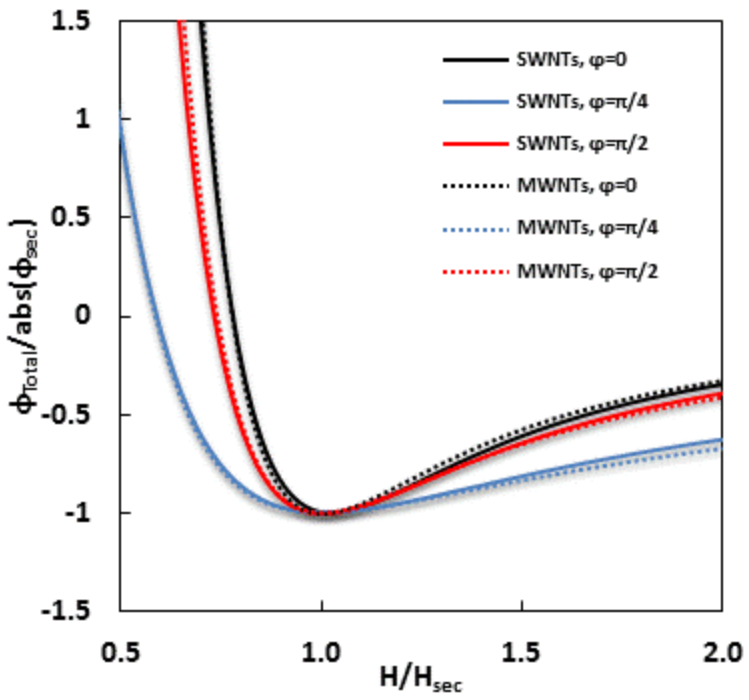

Figure 5-7. Normalized total interaction energy between a surface modified SWNT or MWNT and a charged isotropic planar surface.

CHAPTER 6
CONCLUSIONS AND RECOMMENDATIONS

Conclusions

This PhD dissertation systematically addresses fundamental research on colloid filtration and transport in overland flow through dense emergent vegetation systems and interfacial interactions between nanoparticles (CNTs) and planar surface.

In the first part of the study, a series of laboratory experiments were successfully conducted to measure the single-collector contact efficiency (η_0) and attachment efficiency (α) of colloid capture by a simulated plant stem in laminar overland flow. Florescent microspheres of various sizes were used as experimental colloids. The colloid suspensions were applied to a glass cylinder installed in a small size flow chamber at different flow rates. Silicone grease was applied to the cylinder surface to determine the single-collector contact efficiency (η_0) under favorable conditions. Different solution ionic strengths (*IS*) were used in the experiments to simulate unfavorable attachment conditions. Our results showed that increases in flow rate and collector size reduced the value of η_0 and a minimum value of η_0 might exist at a critical colloid size. α increased with IS and decreased with flow velocity. The experimental observations of η_0 and α were compared to theoretical predictions of different single-collector contact efficiency models and attachment models, respectively. The results indicated that both of existing single-collector contact efficiency models and attachment models fall short in matching the η_0 and α of colloid capture by the simulated plant in laminar overland flow. For the first time, single-stem efficiency theory including dimensionless equations of η_0 and α was developed that matched the experimental data with reasonable accuracy. In addition, for the case of colloid filtration and transport in a

vegetation system under shallow laminar flow conditions, a new equation was also proposed to calculate the colloid kinetic deposition rate at the field scale. In order to upscale single stem efficiency theory to real dense vegetation, a new dimensionless number was developed to account for the effect of plant stem surface properties on the colloid deposition in overland flow. Laboratory scale dense vegetation chamber experiments and model simulations were conducted to obtain the effective value of colloid kinetic deposition rate in vegetation system under different experimental conditions. The results showed that in addition to flow hydrodynamics (e.g., flow velocity) and solution chemistry (e.g., ionic strength), steric repulsion afforded by biopolymer brush player on the pant stem also plays a significant role in colloid deposition onto the plant in overland flow. For the first time, extended single stem efficiency theory including steric repulsion effect was developed that fit the experimental data with acceptable accuracy. Findings from this work filled the existing knowledge gap regarding the fundamental mechanisms that govern overland flow colloid transport through emergent vegetation and are regarded as first steps for accurate quantitative prediction of colloid fate and transport in surface flow through these vegetation systems. They can also inform guidelines for the design, establishment, and maintenance of surface vegetation as filters for colloidal contaminants, such as pathogens. Because establishment of dense vegetated areas in the form of grass filters is a low-cost and potentially effective pollution control practice, optimization of the design and implementation of these filters can produce significant societal and environmental benefits. In addition, although the extended single-stem efficiency theory is developed for prediction of colloid kinetic deposition onto plant stem, its application is not limited to

plant stem and can be also used for various polymer brush surfaces in natural, engineered and biomedical systems.

In the second part of the study, the surface element integration (SEI) technique was coupled with the DLVO theory to determine the orientation-dependent interaction energy between a single-walled carbon nanotube (SWNT) and an infinite isotropic planar surface. For the first time, an analytical formula was successfully developed to accurately describe the interaction between not only pristine but also surface charged CNTs and planar surfaces with arbitrary rotation angles. Simplified formulas were also given for the case of “end-on” and “side-on” approaching patterns. Compared to other methods, the new analytical formulas were either more convenient or more accurate to describe the interaction between CNTs and planar surface especially with respect to arbitrary angles. The results revealed complex dependences of both force and torque between SWNTs and planar surfaces on the separation distances and rotation angles. With minor modifications, the analytical formulas derived for SWNTs can also be applied to multi-walled carbon nanotubes (MWNTs). The findings from this part of my work provide a clear picture of the interaction energy/forces/torques between CNTs and planar surfaces with arbitrary orientation and sheds light on understanding the approaching patterns of CNTs to the planar surfaces under various conditions. They can be used as effective tools by end-users to predict and optimize the interaction between CNTs and planar surfaces for a wide variety of fields of interests (e.g., bio-devices, biomedicine, etc.). Although in this work the interaction energy is developed for CNTs, it is not limited to CNTs and can be readily applied for various types of nano- and micro-tubular structures for analysis of their interaction with planar surfaces.

Recommendations for Further Study

During the course of this study, several unresolved issues that need to be addressed in more detail have been identified. A brief discussion of these issues is presented below. In addition to these unresolved issues, future work resulting from interesting preliminary results is also suggested.

Plant filtration theory in overland flow

One of the primary trends of current and future research is moving from ideal and well-controlled systems to real and more complex systems. For example, investigating natural colloidal contaminants (e.g., bacteria and virus) deposition on plant stem surface under real field conditions is a necessary next step.

The extended single stem efficiency theory is based on a limited set of data including shallow laminar flow conditions, biopolymer brush layer properties, and colloid kinetic deposition rates fitted from breakthrough curves. Additional characterizations of broader range of flow velocities, plant stem surface properties, and measurements of deposition kinetics of colloids under different environmental conditions are needed to further evaluate the robustness of extended model.

Other possible effects controlling the colloid deposition on plant stem further investigations. For example, long-lasting air film (bubbles) due to hair-like structures on the stem surface may also play an important role in colloid deposition. To address this, some of the mechanisms that control the colloid deposition in unsaturated conditions (e.g., air-water-solid interface capture, water film straining, storage in immobile water zones, and air-water interface capture) are worth further investigation.

On the basis of findings from this study, classic colloid filtration theory in porous media and theoretical studies of adsorption of particles on grafted polymers, we

proposed three different mechanisms of colloidal particles deposition on plant stem in overland flow: Type Ⅰ primary deposition, Type Ⅱ secondary deposition and Type Ⅲ ternary deposition. Although these mechanisms are similar to those of colloids stabilized by grafted polymer, plant stem surface properties and dynamic overland flow conditions make these poorly understood mechanisms, so in-depth theoretical and experimental studies are in critical need.

Interactions between CNTs and interfaces

As the capability of CNTs to be modified with various surface functional groups is utilized in consumer products, a related research effort should be to provide models to predict how certain surface functionalization and coatings influence their environmental fate and transport in aquatic system. For example, CNTs are commonly manufactured with surface coatings (e.g., polymers and surfactants and polyelectrolytes) to enhance dispersion stability in solution. In this case, in addition to traditional DLVO interaction (van der Waals attraction and electrostatic double layer repulsion), steric repulsion afforded by an adsorbed polymeric layer also needs to be considered. Therefore, theoretical models to calculate accurately steric interactions between CNTs and different interfaces are in critical need.

Similarly to the future work stated above, another important trend for future research in this second topic is moving from well-defined systems to more complex and environmentally relevant systems. For example, investigating deposition of CNTs on the more complex surfaces such as collectors with different mineralogical compositions and different types of soils, is more challenging but critical for a full understanding of their environmental transport.

For the framework of interactions between CNTs and different interfaces, in addition to modeling interactions between CNTs and planar surface, developments of the theories to quantify the interactions between two CNTs (tube-tube system), as well as CNTs and other nanoparticles (tube-sphere system) are also of great importance and in critical need to fully understand the interactions between CNTs and different interfaces.

APPENDIX A
SUPPORTING INFORMATION FOR CHAPTER 2

Table A-1. Experimental data of single-stem contact efficiency (η_0) under different flow velocity conditions for a given colloid (d_p =1.05μm) and collector (d_c=2cm)

	Replicate 1			Replicate 2			Replicate 3		
u (cm/s)	$r_c=\Delta N/\Delta t$	R^2	η_0	$r_c=\Delta N/\Delta t$	R^2	η_0	$r_c=\Delta N/\Delta t$	R^2	η_0
0.002	1.35E+04	0.96	6.53E-03	1.24E+04	0.95	5.98E-03	1.40E+04	0.97	6.75E-03
0.004	1.44E+04	0.98	3.48E-03	1.27E+04	0.97	3.05E-03	1.42E+04	0.97	3.43E-03
0.008	1.47E+04	0.98	1.77E-03	1.31E+04	0.98	1.58E-03	1.47E+04	0.96	1.77E-03
0.01	1.45E+04	0.98	1.40E-03	1.37E+04	0.96	1.32E-03	1.49E+04	0.96	1.43E-03
0.02	1.47E+04	0.98	7.10E-04	1.38E+04	0.98	6.64E-04	1.49E+04	0.97	7.21E-04
0.04	1.50E+04	0.98	3.62E-04	1.39E+04	0.97	3.36E-04	1.50E+04	0.97	3.62E-04
0.08	1.54E+04	0.97	1.86E-04	1.42E+04	0.96	1.72E-04	1.52E+04	0.97	1.83E-04
0.1	1.54E+04	0.98	1.49E-04	1.42E+04	0.97	1.37E-04	1.51E+04	0.98	1.45E-04
0.2	1.55E+04	0.98	7.47E-05	1.48E+04	0.95	7.12E-05	1.52E+04	0.98	7.33E-05

Table A-2. Experimental data of single-stem contact efficiency (η_0) under different sizes of colloid and collector at a given flow velocity (u=0.02cm/s)

		Replicate 1			Replicate 2			Replicate 3		
d_p (μm)	d_c (cm)	$r_c=\Delta N/\Delta t$	R^2	η_0	$r_c=\Delta N/\Delta t$	R^2	η_0	$r_c=\Delta N/\Delta t$	R^2	η_0
0.1	2	1.69E+04	0.91	4.30E-06	1.58E+04	0.92	4.02E-06	1.81E+04	0.95	4.60E-06
1.05	2	1.47E+04	0.98	3.74E-06	1.38E+04	0.98	3.49E-06	1.49E+04	0.97	3.79E-06
2	2	1.53E+04	0.95	3.88E-06	1.43E+04	0.97	3.63E-06	1.67E+04	0.93	4.23E-06
10.5	2	2.34E+04	0.90	5.95E-06	2.36E+04	0.92	5.99E-06	2.38E+04	0.86	6.04E-06
0.1	1	1.48E+04	0.91	7.54E-06	1.42E+04	0.92	7.20E-06	1.59E+04	0.87	8.08E-06
1.05	1	1.21E+04	0.95	6.15E-06	1.16E+04	0.97	5.90E-06	1.26E+04	0.95	6.38E-06
2	1	1.27E+04	0.91	6.43E-06	1.19E+04	0.93	6.07E-06	1.34E+04	0.92	6.80E-06
10.5	1	2.23E+04	0.92	1.13E-05	2.24E+04	0.92	1.14E-05	2.31E+04	0.93	1.17E-05

APPENDIX B
SUPPORTING INFORMATION FOR CHAPTER 3

DLVO Interaction Energy Profiles.

DLVO theory[294, 295] was used to calculate the total interaction energy (sum of London-van der Waals attraction and electrostatic double-layer repulsion) between colloid and glass cylinder surfaces under different conditions.

The Lifshitz - van der Waals attraction energy (ΔG_{LW}) for a sphere-plate system can be written as [296]:

$$\Delta G_{LW} = -\frac{A}{6}\left[\frac{r}{h} + \frac{r}{h+2r} + ln\left(\frac{h}{h+2r}\right)\right] \quad \text{(B-1)}$$

where A (1×10^{-20} J) is the Hamaker constant for the polystyrene-water-glass system [142, 145], h is the separation distance, and r is the radius of the particle. The EDL repulsion energy (ΔG_{EDL})for a sphere-plate system can be written as [296]:

$$\Delta G_{EDL} = 64\pi r\varepsilon\varepsilon_0\left[\frac{kT}{ze}\right]^2 tanh\left[\frac{ze\psi_1}{4kT}\right] tanh\left[\frac{ze\psi_2}{4kT}\right] exp(-\kappa h) \quad \text{(B-2)}$$

where ε is the dielectric constant of the medium (78.4 for water), ε_0 is the vacuum permittivity (8.854×10^{-12} $C^2\,N^{-1}\,m^{-2}$), k is the Boltzmann's constant (1.381×10^{-23} $C^2\,J\,K^{-1}$), T is the temperature, z is the valence of electrolyte, e is the electron charge (1.602×10^{-19} C), ψ_1 and ψ_2 are the surface potential of the colloid and the collector surface, and κ is the reciprocal of the Debye length. The surface potential of colloids and collector can be determined following van Oss et al. [297]:

$$\psi = \xi\left(1 + \frac{d}{r}\right) exp(\kappa d) \quad \text{(B-3)}$$

where d is the distance between the surface of the charged particle and the slipping plane and usually taken as 5 angstroms (10^{-10} m).

Existing models of estimating attachment efficiency

I. Maxwell model

Detailed description of the Maxwell model can be found in the literature [146, 191]. The model assumes that velocity distribution of a colloid in the secondary minimum follows the Maxwell function:

$$f_{Max}(v) = 4\pi \left(\frac{m}{2\pi kT}\right)^{3/2} v^2 \exp\left(\frac{-\frac{1}{2}mv^2}{kT}\right) \quad \text{(B-4)}$$

$$\int_0^\infty f_{Max}(v)dv = 1 \quad \text{(B-5)}$$

where m is mass of the colloid and v is the velocity.

The fraction of successful collision resulting in the colloid deposition in the secondary minimum, α_{sec} can be written as:

$$\alpha_{sec} = \int_0^{\sqrt{\Phi_{sec}}} \frac{4}{\pi^{1/2}} x^2 \exp(-x^2)\, dx \quad \text{(B-6)}$$

$$x^2 = \frac{mv^2}{2kT} \quad \text{(B-7)}$$

Similarly, the fraction of successful collision resulting in the colloid deposition in the primary minimum, α_{pri} can be written as:

$$\alpha_{pri} = \int_{\sqrt{\Delta\Phi}}^\infty \frac{4}{\pi^{1/2}} x^2 \exp(-x^2)dx \quad \text{(B-8)}$$

The single collector attachment efficiency, *α,* can be written as:

$$\alpha = \int_{\sqrt{\Delta\Phi}}^\infty \frac{4}{\pi^{1/2}} x^2 \exp(-x^2)dx + \int_0^{\sqrt{\Phi_{sec}}} \frac{4}{\pi^{1/2}} x^2 \exp(-x^2)\, dx \quad \text{(B-9)}$$

II. Modified Maxwell model

To account for the influence of fluid hydrodynamic drag on the attachment efficiency, two hydrodynamic factors, f_{pri} and f_{sec}, are introduced to modify the Maxwell model [298]:

$$\alpha = f_{pri}\alpha_{pri} + f_{sec}\alpha_{sec} \quad \text{(B-10)}$$

where f_{pri} and f_{sec}, are the fractions of single collector surface area over which the adhesive torques acting on the colloids retained in the primary and secondary minimum are greater than the fluid hydrodynamic drags, respectively.

The values of adhesive force (F_A) are estimated as the sum of $\frac{\Phi_{pri}}{h}$ and $\frac{\Phi_{sec}}{h}$ for colloids retained in the energy wells[298]:

$$F_A = \frac{\Phi_{pri}}{h} + \frac{\Phi_{sec}}{h} \quad \text{(B-11)}$$

where Φ_{pri} and Φ_{sec} are primary and secondary minimum, respectively; and h is separation distance. The value of lever arm (l_x) of the adhesive torque can be estimated with: [298]

$$l_x = \left(\frac{F_A a_p}{K}\right)^{1/3} \quad \text{(B-12)}$$

where a_p is colloid radius, and K is the composite Young's modulus (4.014 x 10^9 Nm^{-2}). The adhesive torque can then be expressed as:

$$T_A = F_A \times l_x \quad \text{(B-13)}$$

The drag force (F_H) that acts on a colloid attached on the collector interface at a separation distance (h) can be written as [299, 300]:

$$F_H = 6\pi\mu\tau a_p\left(a_p + h\right)C_h \quad \text{(B-14)}$$

where μ is fluid viscosity and τ is hydrodynamic shear, $C_h$is a constant defined as [299, 300]:

$$C_h = \frac{1.7007337 + 1.0221616\left(\frac{h}{a_p}\right)}{1 + 1.0458291\left(\frac{h}{a_p}\right) - 0.0014884708\left(\frac{h}{a_p}\right)^2} \quad \text{(B-15)}$$

On a smooth surface the value of the applied hydrodynamic torque that acts on the colloid at h is given as [299, 300]:

$$T_H = a_p F_H + 4\pi\mu\tau {a_p}^3 C_{2h} \quad \text{(B-16)}$$

In this case, C_{2h} is a second dimensionless function that depends on h is given as [299, 300]:

$$C_{2h} = 0.054651334\left\{18.276952 - exp\left[-1.422943\left(\frac{h}{a_p}\right)\right]\right\} \quad \text{(B-17)}$$

Where a_p is much greater than h, the value of T_H is more simply given as [177, 298]:

$$T_H = 14.287\pi\mu\tau {a_p}^3 \quad \text{(B-18)}$$

III. Bai-Tien model.

An empirical correlation equation developed by Bai and Tien [180] was also used in this work. The equation of the Bai-Tien model can be written as:

$$\alpha = 2.57 \times 10^{-3}(N_{LO})^{0.7031}(N_{E1})^{-0.3121}(N_{E2})^{3.5111}(N_{DL})^{1.352} \quad \text{(B-19)}$$

Definitions of the dimensionless parameters are listed in Table B-1.

Table B-1. Definition of Dimensionless parameters

Parameter	Definition	
$\boldsymbol{N_{LO}}$	$\frac{4A}{9\pi\mu {d_p}^2 u}$	London number
$\boldsymbol{N_{E1}}$	$\frac{\varepsilon\varepsilon_0({\xi_p}^2+{\xi_c}^2)}{3\pi\mu u d_p}$	First electrokinetic parameter
$\boldsymbol{N_{E2}}$	$\frac{2\xi_p\xi_c}{({\xi_p}^2+{\xi_c}^2)}$	Second electrokinetic parameter
$\boldsymbol{N_{E3}}$	$N_A I {d_c}^3$	Third electrokinetic parameter
$\boldsymbol{N_{DL}}$	κd_p	Double-layer force parameter
$\boldsymbol{N_{Re}}$	$\frac{u d_c}{\nu}$	Reynolds number
$\boldsymbol{N_R}$	$\frac{d_p}{d_c}$	Aspect ratio
$\boldsymbol{N_{Pe}}$	$\frac{u d_c}{D_\infty}$	Peclet number

*A is the Hamaker constant, μ is the fluid viscosity, d_p is the colloidal particle diameter, u is the flow velocity, ε is the relative permittivity of the fluid, ε_0 is the permittivity in a vacuum, ξ_p and ξ_c are the surface potential of the colloidal particles and collectors respectively, κ is the reciprocal of double layer thickness, N_A is Avogadro's constant, I is the ionic strength, ν is kinetic viscosity, D_∞ is the bulk diffusion coefficient (described by Stokes-Einstein equation).

Table B-2. Summary of stepwise-least square regression results

Step 1 - Entering variable: log(NE2)

Summary measures

Multiple R	0.7046
R-Square	0.4964
Adj R-Square	0.4850
StErr of Est	0.4167

ANOVA Table

Source	df	SS	MS	F	p-value
Explained	1	7.5325	7.5325	43.3739	0.0000
Unexplained	44	7.6412	0.1737		

Regression coefficients

	Coefficient	Std Err	t-value	p-value	Lower limit	Upper limit
Constant	-2.0256	0.0875	-23.1621	0.0000	-2.2019	-1.8494
log(NE2)	-9.2662	1.4070	-6.5859	0.0000	-12.1018	-6.4306

Step 2 - Entering variable: log(NE1)

Summary measures		Change	% Change
Multiple R	0.7683	0.0638	9.0%
R-Square	0.5903	0.0939	18.9%
Adj R-Square	0.5713	0.0863	17.8%
StErr of Est	0.3802	-0.0365	-8.8%

ANOVA Table

Source	df	SS	MS	F	p-value
Explained	2	8.9575	4.4787	30.9813	0.0000
Unexplained	43	6.2162	0.1446		

Regression coefficients

	Coefficient	Std Err	t-value	p-value	Lower limit	Upper limit
Constant	-2.2197	0.1009	-21.9934	0.0000	-2.4232	-2.0161
log(NE2)	-10.0772	1.3094	-7.6959	0.0000	-12.7179	-7.4365
log(NE1)	0.1588	0.0506	3.1396	0.0031	0.0568	0.2608

Table B-2. Continued

Step 3 - Entering variable: log(NDL)

Summary measures		Change	% Change
Multiple R	0.8894	0.1211	15.8%
R-Square	0.7911	0.2007	34.0%
Adj R-Square	0.7761	0.2049	35.9%
StErr of Est	0.2747	-0.1055	-27.7%

ANOVA Table

Source	df	SS	MS	F	p-value
Explained	3	12.0034	4.0011	53.0086	0.0000
Unexplained	42	3.1702	0.0755		

Regression coefficients

	Coefficient	Std Err	t-value	p-value	Lower limit	Upper limit
Constant	-3.3878	0.1978	-17.1261	0.0000	-3.7870	-2.9886
log(NE2)	-6.4480	1.1053	-5.8339	0.0000	-8.6786	-4.2175
log(NE1)	0.2592	0.0398	6.5100	0.0000	0.1788	0.3396
log(NDL)	0.5649	0.0889	6.3525	0.0000	0.3855	0.7444

Step 4 - Entering variable: log(NLO)

Summary measures		Change	% Change
Multiple R	0.9233	0.0338	3.8%
R-Square	0.8524	0.0613	7.8%
Adj R-Square	0.8380	0.0619	8.0%
StErr of Est	0.2337	-0.0410	-14.9%

ANOVA Table

Source	df	SS	MS	F	p-value
Explained	4	12.9342	3.2335	59.2001	0.0000
Unexplained	41	2.2394	0.0546		

Table B-2. Continued

Regression coefficients

	Coefficient	Std Err	t-value	p-value	Lower limit	Upper limit
Constant	-3.2475	0.1717	-18.9171	0.0000	-3.5942	-2.9008
log(NE2)	-1.1545	1.5901	-0.7260	0.4719	-4.3658	2.0568
log(NE1)	-0.2072	0.1179	-1.7564	0.0865	-0.4453	0.0310
log(NDL)	0.9858	0.1270	7.7647	0.0000	0.7294	1.2422
log(NLO)	0.4453	0.1079	4.1280	0.0002	0.2274	0.6631

Step 5 - Leaving variable: log(NE2)

Summary measures		Change	% Change
Multiple R	0.9222	-0.0010	-0.1%
R-Square	0.8505	-0.0019	-0.2%
Adj R-Square	0.8398	0.0018	0.2%
StErr of Est	0.2324	-0.0013	-0.6%

ANOVA Table

Source	df	SS	MS	F	p-value
Explained	3	12.9054	4.3018	79.6545	0.0000
Unexplained	42	2.2682	0.0540		

Regression coefficients

	Coefficient	Std Err	t-value	p-value	Lower limit	Upper limit
Constant	-3.2470	0.1707	-19.0216	0.0000	-3.5915	-2.9025
log(NE1)	-0.2726	0.0757	-3.6019	0.0008	-0.4253	-0.1199
log(NDL)	1.0623	0.0705	15.0774	0.0000	0.9201	1.2045
log(NLO)	0.5084	0.0634	8.0168	0.0000	0.3804	0.6364

Evaluation of new dimensionless equation on development dataset

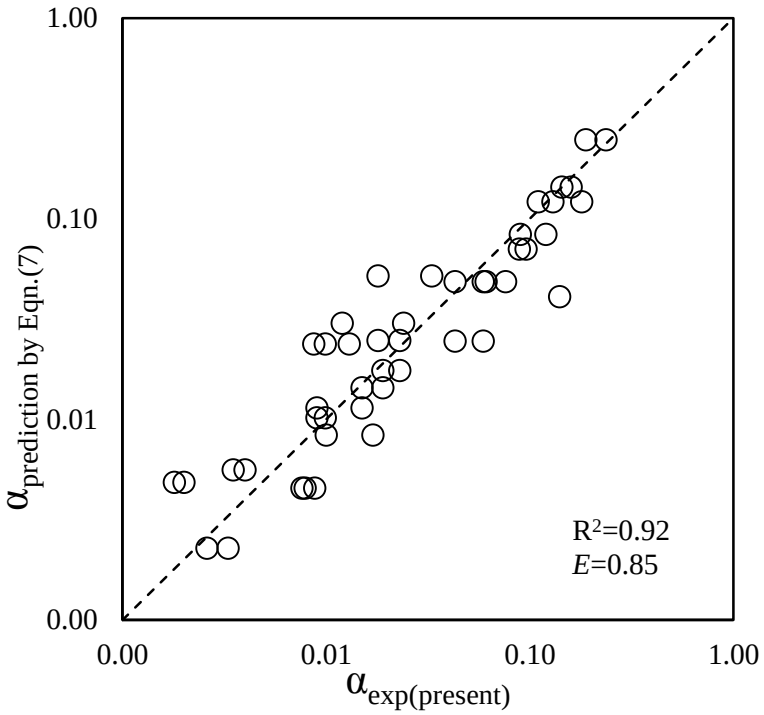

Figure B-1. Comparison of experimental attachment efficiency with predictions of the new dimensionless equation for development dataset.

Table B-3 Experimental data of attachment efficiency (α) under different ionic strength conditions (IS=0.001M) for a given colloid (dp=1.05μm)

IS=0.001M				
Parameters		Replicate 1	Replicate 2	Replicate 3
Approaching velocity	u	2.00E-04	2.00E-04	2.00E-04
Ionic strength	IS	1.00E-03	1.00E-03	1.00E-03
Particle diameter	d_p	1.05E-06	1.05E-06	1.05E-06
Collector diameter	d_c	5.00E-03	5.00E-03	5.00E-03
Hamaker constant	A	1.00E-20	1.00E-20	1.00E-20
Boltzman's constant	K_B	1.38E-23	1.38E-23	1.38E-23
Absolute temperature	T	2.98E+02	2.98E+02	2.98E+02
Reciprocal of double layer thickness	κ	1.04E+08	1.04E+08	1.04E+08
Avogadro's number	N_A	6.02E+23	6.02E+23	6.02E+23
Elementary charge	e	1.60E-19	1.60E-19	1.60E-19
Density of suspension	ρ	1.05E+03	1.05E+03	1.05E+03
Fluid viscosity	μ	1.00E-03	1.00E-03	1.00E-03
Brownian diffusivity	D	4.16E-13	4.16E-13	4.16E-13
Relative permittivity of fluid media	ε	7.85E+01	7.85E+01	7.85E+01
Permittivity in vacuum	ε_0	8.85E-12	8.85E-12	8.85E-12
Zeta potentials of particles	ζ_P	8.00E-02	8.00E-02	8.00E-02
Zeta potentials of collector	ζ_C	5.70E-02	5.70E-02	5.70E-02
Surface potentials of particles	Ψ_P	0.084284	0.084284	0.084284
Surface potentials of collector	Ψ_C	0.060038	0.060038	0.060038
Reynolds number	N_{Re}	1.05E+00	1.05E+00	1.05E+00
Aspect ratio	N_R	2.10E-04	2.10E-04	2.10E-04
Peclet number	N_{pe}	2.41E+06	2.41E+06	2.41E+06
Froude number	N_{Fr}	8.15E-07	8.15E-07	8.15E-07
London number	N_{LO}	6.42E-03	6.42E-03	6.42E-03
First electrokinetic parameter	N_{E1}	3.39E+00	3.39E+00	3.39E+00
Second electrokinetic parameter	N_{E2}	9.45E-01	9.45E-01	9.45E-01
Third electrokinetic parameter	N_{E3}	7.53E+13	7.53E+13	7.53E+13
Double layer force parameter	N_{DL}	1.09E+02	1.09E+02	1.09E+02
Attachment efficiency	α	0.0076	0.0079	0.0088

Table B-4 Experimental data of attachment efficiency (α) under different ionic strength conditions (IS=0.005M) for a given colloid (dp=1.05μm)

IS=0.005M				
Parameters		Replicate 1	Replicate 2	Replicate 3
Approaching velocity	u	2.00E-04	2.00E-04	2.00E-04
Ionic strength	IS	5.00E-03	5.00E-03	5.00E-03
Particle diameter	d_p	1.05E-06	1.05E-06	1.05E-06
Collector diameter	d_c	5.00E-03	5.00E-03	5.00E-03
Hamaker constant	A	1.00E-20	1.00E-20	1.00E-20
Boltzman's constant	K_B	1.38E-23	1.38E-23	1.38E-23
Absolute temperature	T	2.98E+02	2.98E+02	2.98E+02
Reciprocal of double layer thickness	κ	2.32E+08	2.32E+08	2.32E+08
Avogadro's number	N_A	6.02E+23	6.02E+23	6.02E+23
Elementary charge	e	1.60E-19	1.60E-19	1.60E-19
Density of suspension	ρ	1.05E+03	1.05E+03	1.05E+03
Fluid viscosity	μ	1.00E-03	1.00E-03	1.00E-03
Brownian diffusivity	D	4.16E-13	4.16E-13	4.16E-13
Relative permittivity of fluid media	ε	7.85E+01	7.85E+01	7.85E+01
Permittivity in vacuum	ε_0	8.85E-12	8.85E-12	8.85E-12
Zeta potentials of particles	ζ_P	7.00E-02	7.00E-02	7.00E-02
Zeta potentials of collector	ζ_C	5.20E-02	5.20E-02	5.20E-02
Surface potentials of particles	Ψ_P	0.078638	0.078638	0.078638
Surface potentials of collector	Ψ_C	0.058403	0.058403	0.058403
Reynolds number	N_{Re}	1.05E+00	1.05E+00	1.05E+00
Aspect ratio	N_R	2.10E-04	2.10E-04	2.10E-04
Peclet number	N_{pe}	2.41E+06	2.41E+06	2.41E+06
Froude number	N_{Fr}	8.15E-07	8.15E-07	8.15E-07
London number	N_{LO}	6.42E-03	6.42E-03	6.42E-03
First electrokinetic parameter	N_{E1}	2.67E+00	2.67E+00	2.67E+00
Second electrokinetic parameter	N_{E2}	9.57E-01	9.57E-01	9.57E-01
Third electrokinetic parameter	N_{E3}	3.76E+14	3.76E+14	3.76E+14
Double layer force parameter	N_{DL}	2.44E+02	2.44E+02	2.44E+02
Attachment efficiency	α	0.015	0.009	0.0033

Table B-5 Experimental data of attachment efficiency (α) under different ionic strength conditions (IS=0.01M) for a given colloid (dp=1.05μm)

IS=0.01M				
Parameters		Replicate 1	Replicate 2	Replicate 3
Approaching velocity	u	2.00E-04	2.00E-04	2.00E-04
Ionic strength	IS	1.00E-02	1.00E-02	1.00E-02
Particle diameter	d_p	1.05E-06	1.05E-06	1.05E-06
Collector diameter	d_c	5.00E-03	5.00E-03	5.00E-03
Hamaker constant	A	1.00E-20	1.00E-20	1.00E-20
Boltzman's constant	K_B	1.38E-23	1.38E-23	1.38E-23
Absolute temperature	T	2.98E+02	2.98E+02	2.98E+02
Reciprocal of double layer thickness	κ	3.28E+08	3.28E+08	3.28E+08
Avogadro's number	N_A	6.02E+23	6.02E+23	6.02E+23
Elementary charge	e	1.60E-19	1.60E-19	1.60E-19
Density of suspension	ρ	1.05E+03	1.05E+03	1.05E+03
Fluid viscosity	μ	1.00E-03	1.00E-03	1.00E-03
Brownian diffusivity	D	4.16E-13	4.16E-13	4.16E-13
Relative permittivity of fluid media	ε	7.85E+01	7.85E+01	7.85E+01
Permittivity in vacuum	ε_0	8.85E-12	8.85E-12	8.85E-12
Zeta potentials of particles	ζ_P	6.00E-02	6.00E-02	6.00E-02
Zeta potentials of collector	ζ_C	5.00E-02	5.00E-02	5.00E-02
Surface potentials of particles	Ψ_P	0.070725	0.070725	0.070725
Surface potentials of collector	Ψ_C	0.058924	0.058924	0.058924
Reynolds number	N_{Re}	1.05E+00	1.05E+00	1.05E+00
Aspect ratio	N_R	2.10E-04	2.10E-04	2.10E-04
Peclet number	N_{pe}	2.41E+06	2.41E+06	2.41E+06
Froude number	N_{Fr}	8.15E-07	8.15E-07	8.15E-07
London number	N_{LO}	6.42E-03	6.42E-03	6.42E-03
First electrokinetic parameter	N_{E1}	2.14E+00	2.14E+00	2.14E+00
Second electrokinetic parameter	N_{E2}	9.84E-01	9.84E-01	9.84E-01
Third electrokinetic parameter	N_{E3}	7.53E+14	7.53E+14	7.53E+14
Double layer force parameter	N_{DL}	3.45E+02	3.45E+02	3.45E+02
Attachment efficiency	α	0.006	0.019	0.023

Table B-6. Experimental data of attachment efficiency (α) under different ionic strength conditions (IS=0.05M) for a given colloid (dp=1.05μm)

		IS=0.05M		
Parameters		Replicate 1	Replicate 2	Replicate 3
Approaching velocity	u	2.00E-04	2.00E-04	2.00E-04
Ionic strength	IS	5.00E-02	5.00E-02	5.00E-02
Particle diameter	d_p	1.05E-06	1.05E-06	1.05E-06
Collector diameter	d_c	5.00E-03	5.00E-03	5.00E-03
Hamaker constant	A	1.00E-20	1.00E-20	1.00E-20
Boltzman's constant	K_B	1.38E-23	1.38E-23	1.38E-23
Absolute temperature	T	2.98E+02	2.98E+02	2.98E+02
Reciprocal of double layer thickness	κ	7.34E+08	7.34E+08	7.34E+08
Avogadro's number	N_A	6.02E+23	6.02E+23	6.02E+23
Elementary charge	e	1.60E-19	1.60E-19	1.60E-19
Density of suspension	ρ	1.05E+03	1.05E+03	1.05E+03
Fluid viscosity	μ	1.00E-03	1.00E-03	1.00E-03
Brownian diffusivity	D	4.16E-13	4.16E-13	4.16E-13
Relative permittivity of fluid media	ε	7.85E+01	7.85E+01	7.85E+01
Permittivity in vacuum	ε_0	8.85E-12	8.85E-12	8.85E-12
Zeta potentials of particles	ζ_P	4.80E-02	4.80E-02	4.80E-02
Zeta potentials of collector	ζ_C	3.20E-02	3.20E-02	3.20E-02
Surface potentials of particles	Ψ_P	0.069314	0.069314	0.069314
Surface potentials of collector	Ψ_C	0.046198	0.046198	0.046198
Reynolds number	N_{Re}	1.05E+00	1.05E+00	1.05E+00
Aspect ratio	N_R	2.10E-04	2.10E-04	2.10E-04
Peclet number	N_{pe}	2.41E+06	2.41E+06	2.41E+06
Froude number	N_{Fr}	8.15E-07	8.15E-07	8.15E-07
London number	N_{LO}	6.42E-03	6.42E-03	6.42E-03
First electrokinetic parameter	N_{E1}	1.17E+00	1.17E+00	1.17E+00
Second electrokinetic parameter	N_{E2}	9.23E-01	9.23E-01	9.23E-01
Third electrokinetic parameter	N_{E3}	3.76E+15	3.76E+15	3.76E+15
Double layer force parameter	N_{DL}	7.71E+02	7.71E+02	7.71E+02
Attachment efficiency	α	0.091	0.061	0.076

Table B-7. Experimental data of attachment efficiency (α) under different ionic strength conditions (IS=0.1M) for a given colloid (dp=1.05μm)

		IS=0.1M		
Parameters		Replicate 1	Replicate 2	Replicate 3
Approaching velocity	u	2.00E-04	2.00E-04	2.00E-04
Ionic strength	IS	1.00E-01	1.00E-01	1.00E-01
Particle diameter	d_p	1.05E-06	1.05E-06	1.05E-06
Collector diameter	d_c	5.00E-03	5.00E-03	5.00E-03
Hamaker constant	A	1.00E-20	1.00E-20	1.00E-20
Boltzman's constant	K_B	1.38E-23	1.38E-23	1.38E-23
Absolute temperature	T	2.98E+02	2.98E+02	2.98E+02
Reciprocal of double layer thickness	κ	1.04E+09	1.04E+09	1.04E+09
Avogadro's number	N_A	6.02E+23	6.02E+23	6.02E+23
Elementary charge	e	1.60E-19	1.60E-19	1.60E-19
Density of suspension	ρ	1.05E+03	1.05E+03	1.05E+03
Fluid viscosity	μ	1.00E-03	1.00E-03	1.00E-03
Brownian diffusivity	D	4.16E-13	4.16E-13	4.16E-13
Relative permittivity of fluid media	ε	7.85E+01	7.85E+01	7.85E+01
Permittivity in vacuum	ε_0	8.85E-12	8.85E-12	8.85E-12
Zeta potentials of particles	ζ_P	3.80E-02	3.80E-02	3.80E-02
Zeta potentials of collector	ζ_C	1.80E-02	1.80E-02	1.80E-02
Surface potentials of particles	Ψ_P	0.063888	0.063888	0.063888
Surface potentials of collector	Ψ_C	0.030255	0.030255	0.030255
Reynolds number	N_{Re}	1.05E+00	1.05E+00	1.05E+00
Aspect ratio	N_R	2.10E-04	2.10E-04	2.10E-04
Peclet number	N_{pe}	2.41E+06	2.41E+06	2.41E+06
Froude number	N_{Fr}	8.15E-07	8.15E-07	8.15E-07
London number	N_{LO}	6.42E-03	6.42E-03	6.42E-03
First electrokinetic parameter	N_{E1}	6.21E-01	6.21E-01	6.21E-01
Second electrokinetic parameter	N_{E2}	7.74E-01	7.74E-01	7.74E-01
Third electrokinetic parameter	N_{E3}	7.53E+15	7.53E+15	7.53E+15
Double layer force parameter	N_{DL}	1.09E+03	1.09E+03	1.09E+03
Attachment efficiency	α	0.129	0.09	0.12

Table B-8. Experimental data of attachment efficiency (α) under different ionic strength conditions (IS=0.001M) for a given colloid (dp=0.1μm)

		IS=0.001M		
Parameters		Replicate 1	Replicate 2	Replicate 3
Approaching velocity	u	2.00E-04	2.00E-04	2.00E-04
Ionic strength	IS	1.00E-03	1.00E-03	1.00E-03
Particle diameter	d_p	1.00E-07	1.00E-07	1.00E-07
Collector diameter	d_c	5.00E-03	5.00E-03	5.00E-03
Hamaker constant	A	1.00E-20	1.00E-20	1.00E-20
Boltzman's constant	K_B	1.38E-23	1.38E-23	1.38E-23
Absolute temperature	T	2.98E+02	2.98E+02	2.98E+02
Reciprocal of double layer thickness	κ	1.04E+08	1.04E+08	1.04E+08
Avogadro's number	N_A	6.02E+23	6.02E+23	6.02E+23
Elementary charge	e	1.60E-19	1.60E-19	1.60E-19
Density of suspension	ρ	1.05E+03	1.05E+03	1.05E+03
Fluid viscosity	μ	1.00E-03	1.00E-03	1.00E-03
Brownian diffusivity	D	4.37E-12	4.37E-12	4.37E-12
Relative permittivity of fluid media	ε	7.85E+01	7.85E+01	7.85E+01
Permittivity in vacuum	ε_0	8.85E-12	8.85E-12	8.85E-12
Zeta potentials of particles	ζ_P	6.80E-02	6.80E-02	6.80E-02
Zeta potentials of collector	ζ_C	5.70E-02	5.70E-02	5.70E-02
Surface potentials of particles	Ψ_P	0.071804	0.071804	0.071804
Surface potentials of collector	Ψ_C	0.060038	0.060038	0.060038
Reynolds number	N_{Re}	1.05E+00	1.05E+00	1.05E+00
Aspect ratio	N_R	2.00E-05	2.00E-05	2.00E-05
Peclet number	N_{pe}	2.29E+05	2.29E+05	2.29E+05
Froude number	N_{Fr}	8.15E-07	8.15E-07	8.15E-07
London number	N_{LO}	7.08E-01	7.08E-01	7.08E-01
First electrokinetic parameter	N_{E1}	2.90E+01	2.90E+01	2.90E+01
Second electrokinetic parameter	N_{E2}	9.85E-01	9.85E-01	9.85E-01
Third electrokinetic parameter	N_{E3}	7.53E+13	7.53E+13	7.53E+13
Double layer force parameter	N_{DL}	1.04E+01	1.04E+01	1.04E+01
Attachment efficiency	α	0.002	0.0026	0.0033

Table B-9. Experimental data of attachment efficiency (α) under different ionic strength conditions (IS=0.005M) for a given colloid (dp=0.1μm)

		IS=0.005M		
Parameters		Replicate 1	Replicate 2	Replicate 3
Approaching velocity	u	2.00E-04	2.00E-04	2.00E-04
Ionic strength	IS	5.00E-03	5.00E-03	5.00E-03
Particle diameter	d_p	1.00E-07	1.00E-07	1.00E-07
Collector diameter	d_c	5.00E-03	5.00E-03	5.00E-03
Hamaker constant	A	1.00E-20	1.00E-20	1.00E-20
Boltzman's constant	K_B	1.38E-23	1.38E-23	1.38E-23
Absolute temperature	T	2.98E+02	2.98E+02	2.98E+02
Reciprocal of double layer thickness	κ	2.32E+08	2.32E+08	2.32E+08
Avogadro's number	N_A	6.02E+23	6.02E+23	6.02E+23
Elementary charge	e	1.60E-19	1.60E-19	1.60E-19
Density of suspension	ρ	1.05E+03	1.05E+03	1.05E+03
Fluid viscosity	μ	1.00E-03	1.00E-03	1.00E-03
Brownian diffusivity	D	4.37E-12	4.37E-12	4.37E-12
Relative permittivity of fluid media	ε	7.85E+01	7.85E+01	7.85E+01
Permittivity in vacuum	ε_0	8.85E-12	8.85E-12	8.85E-12
Zeta potentials of particles	ζ_P	6.30E-02	6.30E-02	6.30E-02
Zeta potentials of collector	ζ_C	5.20E-02	5.20E-02	5.20E-02
Surface potentials of particles	Ψ_P	0.070934	0.070934	0.070934
Surface potentials of collector	Ψ_C	0.058403	0.058403	0.058403
Reynolds number	N_{Re}	1.05E+00	1.05E+00	1.05E+00
Aspect ratio	N_R	2.00E-05	2.00E-05	2.00E-05
Peclet number	N_{pe}	2.29E+05	2.29E+05	2.29E+05
Froude number	N_{Fr}	8.15E-07	8.15E-07	8.15E-07
London number	N_{LO}	7.08E-01	7.08E-01	7.08E-01
First electrokinetic parameter	N_{E1}	2.46E+01	2.46E+01	2.46E+01
Second electrokinetic parameter	N_{E2}	9.82E-01	9.82E-01	9.82E-01
Third electrokinetic parameter	N_{E3}	3.76E+14	3.76E+14	3.76E+14
Double layer force parameter	N_{DL}	2.32E+01	2.32E+01	2.32E+01
Attachment efficiency	α	0.0048	0.004	0.0035

Table B-10. Experimental data of attachment efficiency (α) under different ionic strength conditions (IS=0.01M) for a given colloid (dp=0.1μm)

		IS=0.01M		
Parameters		Replicate 1	Replicate 2	Replicate 3
Approaching velocity	u	2.00E-04	2.00E-04	2.00E-04
Ionic strength	IS	1.00E-02	1.00E-02	1.00E-02
Particle diameter	d_p	1.00E-07	1.00E-07	1.00E-07
Collector diameter	d_c	5.00E-03	5.00E-03	5.00E-03
Hamaker constant	A	1.00E-20	1.00E-20	1.00E-20
Boltzman's constant	K_B	1.38E-23	1.38E-23	1.38E-23
Absolute temperature	T	2.98E+02	2.98E+02	2.98E+02
Reciprocal of double layer thickness	κ	3.28E+08	3.28E+08	3.28E+08
Avogadro's number	N_A	6.02E+23	6.02E+23	6.02E+23
Elementary charge	e	1.60E-19	1.60E-19	1.60E-19
Density of suspension	ρ	1.05E+03	1.05E+03	1.05E+03
Fluid viscosity	μ	1.00E-03	1.00E-03	1.00E-03
Brownian diffusivity	D	4.37E-12	4.37E-12	4.37E-12
Relative permittivity of fluid media	ε	7.85E+01	7.85E+01	7.85E+01
Permittivity in vacuum	ε_0	8.85E-12	8.85E-12	8.85E-12
Zeta potentials of particles	ζ_P	5.90E-02	5.90E-02	5.90E-02
Zeta potentials of collector	ζ_C	5.00E-02	5.00E-02	5.00E-02
Surface potentials of particles	Ψ_P	0.069704	0.069704	0.069704
Surface potentials of collector	Ψ_C	0.058924	0.058924	0.058924
Reynolds number	N_{Re}	1.05E+00	1.05E+00	1.05E+00
Aspect ratio	N_R	2.00E-05	2.00E-05	2.00E-05
Peclet number	N_{pe}	2.29E+05	2.29E+05	2.29E+05
Froude number	N_{Fr}	8.15E-07	8.15E-07	8.15E-07
London number	N_{LO}	7.08E-01	7.08E-01	7.08E-01
First electrokinetic parameter	N_{E1}	2.21E+01	2.21E+01	2.21E+01
Second electrokinetic parameter	N_{E2}	9.86E-01	9.86E-01	9.86E-01
Third electrokinetic parameter	N_{E3}	7.53E+14	7.53E+14	7.53E+14
Double layer force parameter	N_{DL}	3.28E+01	3.28E+01	3.28E+01
Attachment efficiency	α	0.0092	0.01	0.017

Table B-11. Experimental data of attachment efficiency (α) under different ionic strength conditions (IS=0.05M) for a given colloid (dp=0.1μm)

		IS=0.05M		
Parameters		Replicate 1	Replicate 2	Replicate 3
Approaching velocity	u	2.00E-04	2.00E-04	2.00E-04
Ionic strength	IS	5.00E-02	5.00E-02	5.00E-02
Particle diameter	d_p	1.00E-07	1.00E-07	1.00E-07
Collector diameter	d_c	5.00E-03	5.00E-03	5.00E-03
Hamaker constant	A	1.00E-20	1.00E-20	1.00E-20
Boltzman's constant	K_B	1.38E-23	1.38E-23	1.38E-23
Absolute temperature	T	2.98E+02	2.98E+02	2.98E+02
Reciprocal of double layer thickness	κ	7.34E+08	7.34E+08	7.34E+08
Avogadro's number	N_A	6.02E+23	6.02E+23	6.02E+23
Elementary charge	e	1.60E-19	1.60E-19	1.60E-19
Density of suspension	ρ	1.05E+03	1.05E+03	1.05E+03
Fluid viscosity	μ	1.00E-03	1.00E-03	1.00E-03
Brownian diffusivity	D	4.37E-12	4.37E-12	4.37E-12
Relative permittivity of fluid media	ε	7.85E+01	7.85E+01	7.85E+01
Permittivity in vacuum	ε_0	8.85E-12	8.85E-12	8.85E-12
Zeta potentials of particles	ζ_P	4.00E-02	4.00E-02	4.00E-02
Zeta potentials of collector	ζ_C	3.20E-02	3.20E-02	3.20E-02
Surface potentials of particles	Ψ_P	0.057892	0.057892	0.057892
Surface potentials of collector	Ψ_C	0.046198	0.046198	0.046198
Reynolds number	N_{Re}	1.05E+00	1.05E+00	1.05E+00
Aspect ratio	N_R	2.00E-05	2.00E-05	2.00E-05
Peclet number	N_{pe}	2.29E+05	2.29E+05	2.29E+05
Froude number	N_{Fr}	8.15E-07	8.15E-07	8.15E-07
London number	N_{LO}	7.08E-01	7.08E-01	7.08E-01
First electrokinetic parameter	N_{E1}	9.68E+00	9.68E+00	9.68E+00
Second electrokinetic parameter	N_{E2}	9.76E-01	9.76E-01	9.76E-01
Third electrokinetic parameter	N_{E3}	3.76E+15	3.76E+15	3.76E+15
Double layer force parameter	N_{DL}	7.34E+01	7.34E+01	7.34E+01
Attachment efficiency	α	0.05	0.043	0.059

Table B-12. Experimental data of attachment efficiency (α) under different ionic strength conditions (IS=0.1M) for a given colloid (dp=0.1μm)

		IS=0.1M		
Parameters		Replicate 1	Replicate 2	Replicate 3
Approaching velocity	u	2.00E-04	2.00E-04	2.00E-04
Ionic strength	IS	1.00E-01	1.00E-01	1.00E-01
Particle diameter	d_p	1.00E-07	1.00E-07	1.00E-07
Collector diameter	d_c	5.00E-03	5.00E-03	5.00E-03
Hamaker constant	A	1.00E-20	1.00E-20	1.00E-20
Boltzman's constant	K_B	1.38E-23	1.38E-23	1.38E-23
Absolute temperature	T	2.98E+02	2.98E+02	2.98E+02
Reciprocal of double layer thickness	κ	1.04E+09	1.04E+09	1.04E+09
Avogadro's number	N_A	6.02E+23	6.02E+23	6.02E+23
Elementary charge	e	1.60E-19	1.60E-19	1.60E-19
Density of suspension	ρ	1.05E+03	1.05E+03	1.05E+03
Fluid viscosity	μ	1.00E-03	1.00E-03	1.00E-03
Brownian diffusivity	D	4.37E-12	4.37E-12	4.37E-12
Relative permittivity of fluid media	ε	7.85E+01	7.85E+01	7.85E+01
Permittivity in vacuum	ε_0	8.85E-12	8.85E-12	8.85E-12
Zeta potentials of particles	ζ_P	3.50E-02	3.50E-02	3.50E-02
Zeta potentials of collector	ζ_C	1.80E-02	1.80E-02	1.80E-02
Surface potentials of particles	Ψ_P	0.058977	0.058977	0.058977
Surface potentials of collector	Ψ_C	0.030255	0.030255	0.030255
Reynolds number	N_{Re}	1.05E+00	1.05E+00	1.05E+00
Aspect ratio	N_R	2.00E-05	2.00E-05	2.00E-05
Peclet number	N_{pe}	2.29E+05	2.29E+05	2.29E+05
Froude number	N_{Fr}	8.15E-07	8.15E-07	8.15E-07
London number	N_{LO}	7.08E-01	7.08E-01	7.08E-01
First electrokinetic parameter	N_{E1}	5.71E+00	5.71E+00	5.71E+00
Second electrokinetic parameter	N_{E2}	8.13E-01	8.13E-01	8.13E-01
Third electrokinetic parameter	N_{E3}	7.53E+15	7.53E+15	7.53E+15
Double layer force parameter	N_{DL}	1.04E+02	1.04E+02	1.04E+02
Attachment efficiency	α	0.096	0.136	0.14

Table B-13. Experimental data of attachment efficiency (α) under different flow velocities and ionic strength conditions (u=0.0002cm/s and IS=0.01M) for a given colloid (dp=1.05μm)

U=0.0002cm/s & IS=0.01M				
Parameters		Replicate 1	Replicate 2	Replicate 3
Approaching velocity	u	2.00E-06	2.00E-06	2.00E-06
Ionic strength	IS	1.00E-02	1.00E-02	1.00E-02
Particle diameter	d_p	1.05E-06	1.05E-06	1.05E-06
Collector diameter	d_c	5.00E-03	5.00E-03	5.00E-03
Hamaker constant	A	1.00E-20	1.00E-20	1.00E-20
Boltzman's constant	K_B	1.38E-23	1.38E-23	1.38E-23
Absolute temperature	T	2.98E+02	2.98E+02	2.98E+02
Reciprocal of double layer thickness	κ	3.28E+08	3.28E+08	3.28E+08
Avogadro's number	N_A	6.02E+23	6.02E+23	6.02E+23
Elementary charge	e	1.60E-19	1.60E-19	1.60E-19
Density of suspension	ρ	1.05E+03	1.05E+03	1.05E+03
Fluid viscosity	μ	1.00E-03	1.00E-03	1.00E-03
Brownian diffusivity	D	4.16E-13	4.16E-13	4.16E-13
Relative permittivity of fluid media	ε	7.85E+01	7.85E+01	7.85E+01
Permittivity in vacuum	ε_0	8.85E-12	8.85E-12	8.85E-12
Zeta potentials of particles	ζ_P	6.00E-02	6.00E-02	6.00E-02
Zeta potentials of collector	ζ_C	5.00E-02	5.00E-02	5.00E-02
Surface potentials of particles	Ψ_P	0.070725	0.070725	0.070725
Surface potentials of collector	Ψ_C	0.058924	0.058924	0.058924
Reynolds number	N_{Re}	1.05E-02	1.05E-02	1.05E-02
Aspect ratio	N_R	2.10E-04	2.10E-04	2.10E-04
Peclet number	N_{pe}	2.41E+04	2.41E+04	2.41E+04
Froude number	N_{Fr}	8.15E-11	8.15E-11	8.15E-11
London number	N_{LO}	6.42E-01	6.42E-01	6.42E-01
First electrokinetic parameter	N_{E1}	2.14E+02	2.14E+02	2.14E+02
Second electrokinetic parameter	N_{E2}	9.84E-01	9.84E-01	9.84E-01
Third electrokinetic parameter	N_{E3}	7.53E+14	7.53E+14	7.53E+14
Double layer force parameter	N_{DL}	3.45E+02	3.45E+02	3.45E+02
Attachment efficiency	α	0.025	0.018	0.033

Table B-14. Experimental data of attachment efficiency (α) under different flow velocities and ionic strength conditions (u=0.002cm/s and IS=0.01M) for a given colloid (dp=1.05μm)

U=0.002cm/s & IS=0.01M				
Parameters		Replicate 1	Replicate 2	Replicate 3
Approaching velocity	u	2.00E-05	2.00E-05	2.00E-05
Ionic strength	IS	1.00E-02	1.00E-02	1.00E-02
Particle diameter	d_p	1.05E-06	1.05E-06	1.05E-06
Collector diameter	d_c	5.00E-03	5.00E-03	5.00E-03
Hamaker constant	A	1.00E-20	1.00E-20	1.00E-20
Boltzman's constant	K_B	1.38E-23	1.38E-23	1.38E-23
Absolute temperature	T	2.98E+02	2.98E+02	2.98E+02
Reciprocal of double layer thickness	κ	3.28E+08	3.28E+08	3.28E+08
Avogadro's number	N_A	6.02E+23	6.02E+23	6.02E+23
Elementary charge	e	1.60E-19	1.60E-19	1.60E-19
Density of suspension	ρ	1.05E+03	1.05E+03	1.05E+03
Fluid viscosity	μ	1.00E-03	1.00E-03	1.00E-03
Brownian diffusivity	D	4.16E-13	4.16E-13	4.16E-13
Relative permittivity of fluid media	ε	7.85E+01	7.85E+01	7.85E+01
Permittivity in vacuum	ε_0	8.85E-12	8.85E-12	8.85E-12
Zeta potentials of particles	ζ_P	6.00E-02	6.00E-02	6.00E-02
Zeta potentials of collector	ζ_C	5.00E-02	5.00E-02	5.00E-02
Surface potentials of particles	Ψ_P	0.070725	0.070725	0.070725
Surface potentials of collector	Ψ_C	0.058924	0.058924	0.058924
Reynolds number	N_{Re}	1.05E-01	1.05E-01	1.05E-01
Aspect ratio	N_R	2.10E-04	2.10E-04	2.10E-04
Peclet number	N_{pe}	2.41E+05	2.41E+05	2.41E+05
Froude number	N_{Fr}	8.15E-09	8.15E-09	8.15E-09
London number	N_{LO}	6.42E-02	6.42E-02	6.42E-02
First electrokinetic parameter	N_{E1}	2.14E+01	2.14E+01	2.14E+01
Second electrokinetic parameter	N_{E2}	9.84E-01	9.84E-01	9.84E-01
Third electrokinetic parameter	N_{E3}	7.53E+14	7.53E+14	7.53E+14
Double layer force parameter	N_{DL}	3.45E+02	3.45E+02	3.45E+02
Attachment efficiency	α	0.02	0.012	0.024

Table B-15. Experimental data of attachment efficiency (α) under different flow velocities and ionic strength conditions (u=0.2cm/s and IS=0.01M) for a given colloid (dp=1.05μm)

U=0.2cm/s & IS=0.01M				
Parameters		Replicate 1	Replicate 2	Replicate 3
Approaching velocity	u	2.00E-03	2.00E-03	2.00E-03
Ionic strength	IS	1.00E-02	1.00E-02	1.00E-02
Particle diameter	d_p	1.05E-06	1.05E-06	1.05E-06
Collector diameter	d_c	5.00E-03	5.00E-03	5.00E-03
Hamaker constant	A	1.00E-20	1.00E-20	1.00E-20
Boltzman's constant	K_B	1.38E-23	1.38E-23	1.38E-23
Absolute temperature	T	2.98E+02	2.98E+02	2.98E+02
Reciprocal of double layer thickness	κ	3.28E+08	3.28E+08	3.28E+08
Avogadro's number	N_A	6.02E+23	6.02E+23	6.02E+23
Elementary charge	e	1.60E-19	1.60E-19	1.60E-19
Density of suspension	ρ	1.05E+03	1.05E+03	1.05E+03
Fluid viscosity	μ	1.00E-03	1.00E-03	1.00E-03
Brownian diffusivity	D	4.16E-13	4.16E-13	4.16E-13
Relative permittivity of fluid media	ε	7.85E+01	7.85E+01	7.85E+01
Permittivity in vacuum	ε_0	8.85E-12	8.85E-12	8.85E-12
Zeta potentials of particles	ζ_P	6.00E-02	6.00E-02	6.00E-02
Zeta potentials of collector	ζ_C	5.00E-02	5.00E-02	5.00E-02
Surface potentials of particles	Ψ_P	0.070725	0.070725	0.070725
Surface potentials of collector	Ψ_C	0.058924	0.058924	0.058924
Reynolds number	N_{Re}	1.05E+01	1.05E+01	1.05E+01
Aspect ratio	N_R	2.10E-04	2.10E-04	2.10E-04
Peclet number	N_{pe}	2.41E+07	2.41E+07	2.41E+07
Froude number	N_{Fr}	8.15E-05	8.15E-05	8.15E-05
London number	N_{LO}	6.42E-04	6.42E-04	6.42E-04
First electrokinetic parameter	N_{E1}	2.14E-01	2.14E-01	2.14E-01
Second electrokinetic parameter	N_{E2}	9.84E-01	9.84E-01	9.84E-01
Third electrokinetic parameter	N_{E3}	7.53E+14	7.53E+14	7.53E+14
Double layer force parameter	N_{DL}	3.45E+02	3.45E+02	3.45E+02
Attachment efficiency	α	0.008	0.009	0.0099

Table B-16. Experimental data of attachment efficiency (α) under different flow velocities and ionic strength conditions (u=0.0002cm/s and IS=0.1M) for a given colloid (dp=1.05μm)

U=0.0002cm/s & IS=0.1M				
Parameters		Replicate 1	Replicate 2	Replicate 3
Approaching velocity	u	2.00E-06	2.00E-06	2.00E-06
Ionic strength	IS	1.00E-01	1.00E-01	1.00E-01
Particle diameter	d_p	1.05E-06	1.05E-06	1.05E-06
Collector diameter	d_c	5.00E-03	5.00E-03	5.00E-03
Hamaker constant	A	1.00E-20	1.00E-20	1.00E-20
Boltzman's constant	K_B	1.38E-23	1.38E-23	1.38E-23
Absolute temperature	T	2.98E+02	2.98E+02	2.98E+02
Reciprocal of double layer thickness	κ	1.04E+09	1.04E+09	1.04E+09
Avogadro's number	N_A	6.02E+23	6.02E+23	6.02E+23
Elementary charge	e	1.60E-19	1.60E-19	1.60E-19
Density of suspension	ρ	1.05E+03	1.05E+03	1.05E+03
Fluid viscosity	μ	1.00E-03	1.00E-03	1.00E-03
Brownian diffusivity	D	4.16E-13	4.16E-13	4.16E-13
Relative permittivity of fluid media	ε	7.85E+01	7.85E+01	7.85E+01
Permittivity in vacuum	ε_0	8.85E-12	8.85E-12	8.85E-12
Zeta potentials of particles	ζ_P	3.80E-02	3.80E-02	3.80E-02
Zeta potentials of collector	ζ_C	1.80E-02	1.80E-02	1.80E-02
Surface potentials of particles	Ψ_P	0.063888	0.063888	0.063888
Surface potentials of collector	Ψ_C	0.030255	0.030255	0.030255
Reynolds number	N_{Re}	1.05E-02	1.05E-02	1.05E-02
Aspect ratio	N_R	2.10E-04	2.10E-04	2.10E-04
Peclet number	N_{pe}	2.41E+04	2.41E+04	2.41E+04
Froude number	N_{Fr}	8.15E-11	8.15E-11	8.15E-11
London number	N_{LO}	6.42E-01	6.42E-01	6.42E-01
First electrokinetic parameter	N_{E1}	6.21E+01	6.21E+01	6.21E+01
Second electrokinetic parameter	N_{E2}	7.74E-01	7.74E-01	7.74E-01
Third electrokinetic parameter	N_{E3}	7.53E+15	7.53E+15	7.53E+15
Double layer force parameter	N_{DL}	1.09E+03	1.09E+03	1.09E+03
Attachment efficiency	α	0.23	0.1889	0.237

Table B-17. Experimental data of attachment efficiency (α) under different flow velocities and ionic strength conditions (u=0.002cm/s and IS=0.1M) for a given colloid (dp=1.05μm)

U=0.002cm/s & IS=0.1M				
Parameters		Replicate 1	Replicate 2	Replicate 3
Approaching velocity	u	2.00E-05	2.00E-05	2.00E-05
Ionic strength	IS	1.00E-01	1.00E-01	1.00E-01
Particle diameter	d_p	1.05E-06	1.05E-06	1.05E-06
Collector diameter	d_c	5.00E-03	5.00E-03	5.00E-03
Hamaker constant	A	1.00E-20	1.00E-20	1.00E-20
Boltzman's constant	K_B	1.38E-23	1.38E-23	1.38E-23
Absolute temperature	T	2.98E+02	2.98E+02	2.98E+02
Reciprocal of double layer thickness	κ	1.04E+09	1.04E+09	1.04E+09
Avogadro's number	N_A	6.02E+23	6.02E+23	6.02E+23
Elementary charge	e	1.60E-19	1.60E-19	1.60E-19
Density of suspension	ρ	1.05E+03	1.05E+03	1.05E+03
Fluid viscosity	μ	1.00E-03	1.00E-03	1.00E-03
Brownian diffusivity	D	4.16E-13	4.16E-13	4.16E-13
Relative permittivity of fluid media	ε	7.85E+01	7.85E+01	7.85E+01
Permittivity in vacuum	ε_0	8.85E-12	8.85E-12	8.85E-12
Zeta potentials of particles	ζ_P	3.80E-02	3.80E-02	3.80E-02
Zeta potentials of collector	ζ_C	1.80E-02	1.80E-02	1.80E-02
Surface potentials of particles	Ψ_P	0.063888	0.063888	0.063888
Surface potentials of collector	Ψ_C	0.030255	0.030255	0.030255
Reynolds number	N_{Re}	1.05E-01	1.05E-01	1.05E-01
Aspect ratio	N_R	2.10E-04	2.10E-04	2.10E-04
Peclet number	N_{pe}	2.41E+05	2.41E+05	2.41E+05
Froude number	N_{Fr}	8.15E-09	8.15E-09	8.15E-09
London number	N_{LO}	6.42E-02	6.42E-02	6.42E-02
First electrokinetic parameter	N_{E1}	6.21E+00	6.21E+00	6.21E+00
Second electrokinetic parameter	N_{E2}	7.74E-01	7.74E-01	7.74E-01
Third electrokinetic parameter	N_{E3}	7.53E+15	7.53E+15	7.53E+15
Double layer force parameter	N_{DL}	1.09E+03	1.09E+03	1.09E+03
Attachment efficiency	α	0.164	0.144	0.16

Table B-18. Experimental data of attachment efficiency (α) under different flow velocities and ionic strength conditions (u=0.2cm/s and IS=0.1M) for a given colloid (dp=1.05μm)

U=0.2cm/s & IS=0.1M				
Parameters		Replicate 1	Replicate 2	Replicate 3
Approaching velocity	u	2.00E-03	2.00E-03	2.00E-03
Ionic strength	IS	1.00E-01	1.00E-01	1.00E-01
Particle diameter	d_p	1.05E-06	1.05E-06	1.05E-06
Collector diameter	d_c	5.00E-03	5.00E-03	5.00E-03
Hamaker constant	A	1.00E-20	1.00E-20	1.00E-20
Boltzman's constant	K_B	1.38E-23	1.38E-23	1.38E-23
Absolute temperature	T	2.98E+02	2.98E+02	2.98E+02
Reciprocal of double layer thickness	κ	1.04E+09	1.04E+09	1.04E+09
Avogadro's number	N_A	6.02E+23	6.02E+23	6.02E+23
Elementary charge	e	1.60E-19	1.60E-19	1.60E-19
Density of suspension	ρ	1.05E+03	1.05E+03	1.05E+03
Fluid viscosity	μ	1.00E-03	1.00E-03	1.00E-03
Brownian diffusivity	D	4.16E-13	4.16E-13	4.16E-13
Relative permittivity of fluid media	ε	7.85E+01	7.85E+01	7.85E+01
Permittivity in vacuum	ε_0	8.85E-12	8.85E-12	8.85E-12
Zeta potentials of particles	ζ_P	3.80E-02	3.80E-02	3.80E-02
Zeta potentials of collector	ζ_C	1.80E-02	1.80E-02	1.80E-02
Surface potentials of particles	Ψ_P	0.063888	0.063888	0.063888
Surface potentials of collector	Ψ_C	0.030255	0.030255	0.030255
Reynolds number	N_{Re}	1.05E+01	1.05E+01	1.05E+01
Aspect ratio	N_R	2.10E-04	2.10E-04	2.10E-04
Peclet number	N_{pe}	2.41E+07	2.41E+07	2.41E+07
Froude number	N_{Fr}	8.15E-05	8.15E-05	8.15E-05
London number	N_{LO}	6.42E-04	6.42E-04	6.42E-04
First electrokinetic parameter	N_{E1}	6.21E-02	6.21E-02	6.21E-02
Second electrokinetic parameter	N_{E2}	7.74E-01	7.74E-01	7.74E-01
Third electrokinetic parameter	N_{E3}	7.53E+15	7.53E+15	7.53E+15
Double layer force parameter	N_{DL}	1.09E+03	1.09E+03	1.09E+03
Attachment efficiency	α	0.05	0.043	0.059

Table B-19. Experimental data of attachment efficiency (α) under different flow velocities and ionic strength conditions (u=0.0002cm/s and IS=0.01M) for a given colloid (dp=0.1μm)

U=0.0002cm/s & IS=0.01M				
Parameters		Replicate 1	Replicate 2	Replicate 3
Approaching velocity	u	2.00E-06	2.00E-06	2.00E-06
Ionic strength	IS	1.00E-02	1.00E-02	1.00E-02
Particle diameter	d_p	1.00E-07	1.00E-07	1.00E-07
Collector diameter	d_c	5.00E-03	5.00E-03	5.00E-03
Hamaker constant	A	1.00E-20	1.00E-20	1.00E-20
Boltzman's constant	K_B	1.38E-23	1.38E-23	1.38E-23
Absolute temperature	T	2.98E+02	2.98E+02	2.98E+02
Reciprocal of double layer thickness	κ	3.28E+08	3.28E+08	3.28E+08
Avogadro's number	N_A	6.02E+23	6.02E+23	6.02E+23
Elementary charge	e	1.60E-19	1.60E-19	1.60E-19
Density of suspension	ρ	1.05E+03	1.05E+03	1.05E+03
Fluid viscosity	μ	1.00E-03	1.00E-03	1.00E-03
Brownian diffusivity	D	4.37E-12	4.37E-12	4.37E-12
Relative permittivity of fluid media	ε	7.85E+01	7.85E+01	7.85E+01
Permittivity in vacuum	ε_0	8.85E-12	8.85E-12	8.85E-12
Zeta potentials of particles	ζ_P	5.90E-02	5.90E-02	5.90E-02
Zeta potentials of collector	ζ_C	5.00E-02	5.00E-02	5.00E-02
Surface potentials of particles	Ψ_P	0.069704	0.069704	0.069704
Surface potentials of collector	Ψ_C	0.058924	0.058924	0.058924
Reynolds number	N_{Re}	1.05E-02	1.05E-02	1.05E-02
Aspect ratio	N_R	2.00E-05	2.00E-05	2.00E-05
Peclet number	N_{pe}	2.29E+03	2.29E+03	2.29E+03
Froude number	N_{Fr}	8.15E-11	8.15E-11	8.15E-11
London number	N_{LO}	7.08E+01	7.08E+01	7.08E+01
First electrokinetic parameter	N_{E1}	2.21E+03	2.21E+03	2.21E+03
Second electrokinetic parameter	N_{E2}	9.86E-01	9.86E-01	9.86E-01
Third electrokinetic parameter	N_{E3}	7.53E+14	7.53E+14	7.53E+14
Double layer force parameter	N_{DL}	3.28E+01	3.28E+01	3.28E+01
Attachment efficiency	α	0.03	0.023	0.018

Table B-20. Experimental data of attachment efficiency (α) under different flow velocities and ionic strength conditions (u=0.002cm/s and IS=0.01M) for a given colloid (dp=0.1μm)

U=0.002cm/s & IS=0.01M				
Parameters		Replicate 1	Replicate 2	Replicate 3
Approaching velocity	u	2.00E-05	2.00E-05	2.00E-05
Ionic strength	IS	1.00E-02	1.00E-02	1.00E-02
Particle diameter	d_p	1.00E-07	1.00E-07	1.00E-07
Collector diameter	d_c	5.00E-03	5.00E-03	5.00E-03
Hamaker constant	A	1.00E-20	1.00E-20	1.00E-20
Boltzman's constant	K_B	1.38E-23	1.38E-23	1.38E-23
Absolute temperature	T	2.98E+02	2.98E+02	2.98E+02
Reciprocal of double layer thickness	κ	3.28E+08	3.28E+08	3.28E+08
Avogadro's number	N_A	6.02E+23	6.02E+23	6.02E+23
Elementary charge	e	1.60E-19	1.60E-19	1.60E-19
Density of suspension	ρ	1.05E+03	1.05E+03	1.05E+03
Fluid viscosity	μ	1.00E-03	1.00E-03	1.00E-03
Brownian diffusivity	D	4.37E-12	4.37E-12	4.37E-12
Relative permittivity of fluid media	ε	7.85E+01	7.85E+01	7.85E+01
Permittivity in vacuum	ε_0	8.85E-12	8.85E-12	8.85E-12
Zeta potentials of particles	ζ_P	5.90E-02	5.90E-02	5.90E-02
Zeta potentials of collector	ζ_C	5.00E-02	5.00E-02	5.00E-02
Surface potentials of particles	Ψ_P	0.069704	0.069704	0.069704
Surface potentials of collector	Ψ_C	0.058924	0.058924	0.058924
Reynolds number	N_{Re}	1.05E-01	1.05E-01	1.05E-01
Aspect ratio	N_R	2.00E-05	2.00E-05	2.00E-05
Peclet number	N_{pe}	2.29E+04	2.29E+04	2.29E+04
Froude number	N_{Fr}	8.15E-09	8.15E-09	8.15E-09
London number	N_{LO}	7.08E+00	7.08E+00	7.08E+00
First electrokinetic parameter	N_{E1}	2.21E+02	2.21E+02	2.21E+02
Second electrokinetic parameter	N_{E2}	9.86E-01	9.86E-01	9.86E-01
Third electrokinetic parameter	N_{E3}	7.53E+14	7.53E+14	7.53E+14
Double layer force parameter	N_{DL}	3.28E+01	3.28E+01	3.28E+01
Attachment efficiency	α	0.009	0.015	0.019

Table B-21. Experimental data of attachment efficiency (α) under different flow velocities and ionic strength conditions (u=0.2cm/s and IS=0.01M) for a given colloid (dp=0.1μm)

U=0.2cm/s & IS=0.01M				
Parameters		Replicate 1	Replicate 2	Replicate 3
Approaching velocity	u	2.00E-03	2.00E-03	2.00E-03
Ionic strength	IS	1.00E-02	1.00E-02	1.00E-02
Particle diameter	d_p	1.00E-07	1.00E-07	1.00E-07
Collector diameter	d_c	5.00E-03	5.00E-03	5.00E-03
Hamaker constant	A	1.00E-20	1.00E-20	1.00E-20
Boltzman's constant	K_B	1.38E-23	1.38E-23	1.38E-23
Absolute temperature	T	2.98E+02	2.98E+02	2.98E+02
Reciprocal of double layer thickness	κ	3.28E+08	3.28E+08	3.28E+08
Avogadro's number	N_A	6.02E+23	6.02E+23	6.02E+23
Elementary charge	e	1.60E-19	1.60E-19	1.60E-19
Density of suspension	ρ	1.05E+03	1.05E+03	1.05E+03
Fluid viscosity	μ	1.00E-03	1.00E-03	1.00E-03
Brownian diffusivity	D	4.37E-12	4.37E-12	4.37E-12
Relative permittivity of fluid media	ε	7.85E+01	7.85E+01	7.85E+01
Permittivity in vacuum	ε_0	8.85E-12	8.85E-12	8.85E-12
Zeta potentials of particles	ζ_P	5.90E-02	5.90E-02	5.90E-02
Zeta potentials of collector	ζ_C	5.00E-02	5.00E-02	5.00E-02
Surface potentials of particles	Ψ_P	0.069704	0.069704	0.069704
Surface potentials of collector	Ψ_C	0.058924	0.058924	0.058924
Reynolds number	N_{Re}	1.05E+01	1.05E+01	1.05E+01
Aspect ratio	N_R	2.00E-05	2.00E-05	2.00E-05
Peclet number	N_{pe}	2.29E+06	2.29E+06	2.29E+06
Froude number	N_{Fr}	8.15E-05	8.15E-05	8.15E-05
London number	N_{LO}	7.08E-02	7.08E-02	7.08E-02
First electrokinetic parameter	N_{E1}	2.21E+00	2.21E+00	2.21E+00
Second electrokinetic parameter	N_{E2}	9.86E-01	9.86E-01	9.86E-01
Third electrokinetic parameter	N_{E3}	7.53E+14	7.53E+14	7.53E+14
Double layer force parameter	N_{DL}	3.28E+01	3.28E+01	3.28E+01
Attachment efficiency	α	0.0032	0.002	0.0018

Table B-22. Experimental data of attachment efficiency (α) under different flow velocities and ionic strength conditions (u=0.0002cm/s and IS=0.1M) for a given colloid (dp=0.1μm)

U=0.0002cm/s & IS=0.1M				
Parameters		Replicate 1	Replicate 2	Replicate 3
Approaching velocity	u	2.00E-06	2.00E-06	2.00E-06
Ionic strength	IS	1.00E-01	1.00E-01	1.00E-01
Particle diameter	d_p	1.00E-07	1.00E-07	1.00E-07
Collector diameter	d_c	5.00E-03	5.00E-03	5.00E-03
Hamaker constant	A	1.00E-20	1.00E-20	1.00E-20
Boltzman's constant	K_B	1.38E-23	1.38E-23	1.38E-23
Absolute temperature	T	2.98E+02	2.98E+02	2.98E+02
Reciprocal of double layer thickness	κ	1.04E+09	1.04E+09	1.04E+09
Avogadro's number	N_A	6.02E+23	6.02E+23	6.02E+23
Elementary charge	e	1.60E-19	1.60E-19	1.60E-19
Density of suspension	ρ	1.05E+03	1.05E+03	1.05E+03
Fluid viscosity	μ	1.00E-03	1.00E-03	1.00E-03
Brownian diffusivity	D	4.37E-12	4.37E-12	4.37E-12
Relative permittivity of fluid media	ε	7.85E+01	7.85E+01	7.85E+01
Permittivity in vacuum	ε_0	8.85E-12	8.85E-12	8.85E-12
Zeta potentials of particles	ζ_P	3.50E-02	3.50E-02	3.50E-02
Zeta potentials of collector	ζ_C	1.80E-02	1.80E-02	1.80E-02
Surface potentials of particles	Ψ_P	0.058977	0.058977	0.058977
Surface potentials of collector	Ψ_C	0.030255	0.030255	0.030255
Reynolds number	N_{Re}	1.05E-02	1.05E-02	1.05E-02
Aspect ratio	N_R	2.00E-05	2.00E-05	2.00E-05
Peclet number	N_{pe}	2.29E+03	2.29E+03	2.29E+03
Froude number	N_{Fr}	8.15E-11	8.15E-11	8.15E-11
London number	N_{LO}	7.08E+01	7.08E+01	7.08E+01
First electrokinetic parameter	N_{E1}	5.71E+02	5.71E+02	5.71E+02
Second electrokinetic parameter	N_{E2}	8.13E-01	8.13E-01	8.13E-01
Third electrokinetic parameter	N_{E3}	7.53E+15	7.53E+15	7.53E+15
Double layer force parameter	N_{DL}	1.04E+02	1.04E+02	1.04E+02
Attachment efficiency	α	0.13	0.11	0.18

Table B-23. Experimental data of attachment efficiency (α) under different flow velocities and ionic strength conditions (u=0.002cm/s and IS=0.1M) for a given colloid (dp=0.1μm)

U=0.002cm/s & IS=0.1M				
Parameters		Replicate 1	Replicate 2	Replicate 3
Approaching velocity	u	2.00E-05	2.00E-05	2.00E-05
Ionic strength	IS	1.00E-01	1.00E-01	1.00E-01
Particle diameter	d_p	1.00E-07	1.00E-07	1.00E-07
Collector diameter	d_c	5.00E-03	5.00E-03	5.00E-03
Hamaker constant	A	1.00E-20	1.00E-20	1.00E-20
Boltzman's constant	K_B	1.38E-23	1.38E-23	1.38E-23
Absolute temperature	T	2.98E+02	2.98E+02	2.98E+02
Reciprocal of double layer thickness	κ	1.04E+09	1.04E+09	1.04E+09
Avogadro's number	N_A	6.02E+23	6.02E+23	6.02E+23
Elementary charge	e	1.60E-19	1.60E-19	1.60E-19
Density of suspension	ρ	1.05E+03	1.05E+03	1.05E+03
Fluid viscosity	μ	1.00E-03	1.00E-03	1.00E-03
Brownian diffusivity	D	4.37E-12	4.37E-12	4.37E-12
Relative permittivity of fluid media	ε	7.85E+01	7.85E+01	7.85E+01
Permittivity in vacuum	ε_0	8.85E-12	8.85E-12	8.85E-12
Zeta potentials of particles	ζ_P	3.50E-02	3.50E-02	3.50E-02
Zeta potentials of collector	ζ_C	1.80E-02	1.80E-02	1.80E-02
Surface potentials of particles	Ψ_P	0.058977	0.058977	0.058977
Surface potentials of collector	Ψ_C	0.030255	0.030255	0.030255
Reynolds number	N_{Re}	1.05E-01	1.05E-01	1.05E-01
Aspect ratio	N_R	2.00E-05	2.00E-05	2.00E-05
Peclet number	N_{pe}	2.29E+04	2.29E+04	2.29E+04
Froude number	N_{Fr}	8.15E-09	8.15E-09	8.15E-09
London number	N_{LO}	7.08E+00	7.08E+00	7.08E+00
First electrokinetic parameter	N_{E1}	5.71E+01	5.71E+01	5.71E+01
Second electrokinetic parameter	N_{E2}	8.13E-01	8.13E-01	8.13E-01
Third electrokinetic parameter	N_{E3}	7.53E+15	7.53E+15	7.53E+15
Double layer force parameter	N_{DL}	1.04E+02	1.04E+02	1.04E+02
Attachment efficiency	α	0.08	0.089	0.096

Table B-24. Experimental data of attachment efficiency (α) under different flow velocities and ionic strength conditions (u=0.2cm/s and IS=0.1M) for a given colloid (dp=0.1μm)

U=0.2cm/s & IS=0.1M				
Parameters		Replicate 1	Replicate 2	Replicate 3
Approaching velocity	u	2.00E-03	2.00E-03	2.00E-03
Ionic strength	IS	1.00E-01	1.00E-01	1.00E-01
Particle diameter	d_p	1.00E-07	1.00E-07	1.00E-07
Collector diameter	d_c	5.00E-03	5.00E-03	5.00E-03
Hamaker constant	A	1.00E-20	1.00E-20	1.00E-20
Boltzman's constant	K_B	1.38E-23	1.38E-23	1.38E-23
Absolute temperature	T	2.98E+02	2.98E+02	2.98E+02
Reciprocal of double layer thickness	κ	1.04E+09	1.04E+09	1.04E+09
Avogadro's number	N_A	6.02E+23	6.02E+23	6.02E+23
Elementary charge	e	1.60E-19	1.60E-19	1.60E-19
Density of suspension	ρ	1.05E+03	1.05E+03	1.05E+03
Fluid viscosity	μ	1.00E-03	1.00E-03	1.00E-03
Brownian diffusivity	D	4.37E-12	4.37E-12	4.37E-12
Relative permittivity of fluid media	ε	7.85E+01	7.85E+01	7.85E+01
Permittivity in vacuum	ε_0	8.85E-12	8.85E-12	8.85E-12
Zeta potentials of particles	ζ_P	3.50E-02	3.50E-02	3.50E-02
Zeta potentials of collector	ζ_C	1.80E-02	1.80E-02	1.80E-02
Surface potentials of particles	Ψ_P	0.058977	0.058977	0.058977
Surface potentials of collector	Ψ_C	0.030255	0.030255	0.030255
Reynolds number	N_{Re}	1.05E+01	1.05E+01	1.05E+01
Aspect ratio	N_R	2.00E-05	2.00E-05	2.00E-05
Peclet number	N_{pe}	2.29E+06	2.29E+06	2.29E+06
Froude number	N_{Fr}	8.15E-05	8.15E-05	8.15E-05
London number	N_{LO}	7.08E-02	7.08E-02	7.08E-02
First electrokinetic parameter	N_{E1}	5.71E-01	5.71E-01	5.71E-01
Second electrokinetic parameter	N_{E2}	8.13E-01	8.13E-01	8.13E-01
Third electrokinetic parameter	N_{E3}	7.53E+15	7.53E+15	7.53E+15
Double layer force parameter	N_{DL}	1.04E+02	1.04E+02	1.04E+02
Attachment efficiency	α	0.013	0.0099	0.0087

APPENDIX
SUPPORTING INFORMATION FOR CHAPTER 4

Buckingham-Π approach to develop (N_{STE})

The first step of dimensional analysis using the Buckingham-Π theorem is listing the relevant material parameters, process-related parameters, and universal physical constants. For the case of the interaction between colloid and plant stem surface, relevant parameters are summarized in Table S1.

Table C-1.Relevant parameters and constants for interaction between colloid and plant stem surface

No.	Symbol	Description	Dimension	Type	Phenomena
1	H	Hamaker constant	ML^2T^{-2}	Material parameter	Van der Waals attraction
2	κ	Debye parameter	L^{-1}	Material parameter	Electrostatic double layer repulsion
3	ε_0	Permittivity of vacuum	$T^4I^2M^{-1}L^{-3}$	Material parameter	Electrostatic double layer repulsion
4	ε_τ	Dielectric constant	-	Material parameter	Electrostatic double layer repulsion
5	ζ_P	Surface potential of colloid	$L^2MT^{-3}I$	Material parameter	Electrostatic double layer repulsion
6	ζ_C	Surface potential of collector	$L^2MT^{-3}I$	Material parameter	Electrostatic double layer repulsion
7	d_p	Colloid diameter	L	Material parameter	Multiple-phenomena
8	u/f	Porewater velocity	LT^{-1}	Process parameter	Transport, shear, and detachment
9	μ	Viscosity	$ML^{-1}T^{-1}$	Constant	Multiple-phenomena
10	M_W	Molecular weight of polymer	M/mole	Material parameter	Steric repulsion
11	N_A	Avogadro's number	$Mole^{-1}$	Constant	Steric repulsion
12	L_0	Height of brush layer	L	Material parameter	Steric repulsion
13	σ	Brush density	L^{-2}	Material parameter	Steric repulsion

Based on the traditional DLVO theory, van der Waals attraction and electrostatic double layer repulsion are controlled by parameters 1 to 9. In the previous studies, four

dimensionless numbers such as N_{LO}, N_{E1}, N_{E2} and N_{DL} have been developed to represent these two DLVO interactions. According to grafted polymer brush layer theory, steric repulsion afforded by biopolymer brush layer and decrease of friction due to biopolymer layer are mainly governed by parameters 7 to 13, which are used to develop a new dimensionless number: N_{STE}.

The derivation of this dimensionless number can be found as follows:

	L_0	M_w	u/f	Na	μ	d_p	σ
L	1	0	1	0	-1	1	-2
M	0	1	0	0	1	0	0
T	0	0	-1	0	-1	0	0
Mole	0	-1	0	-1	0	0	0

Core matrix | Residual matrix

After several matrix operations to transform the core matrix to unity matrix, the final matrices are:

	L_0	M_w	u/f	Na	μ	d_p	σ
Z_1=L+T	1	0	0	0	-2	1	-2
Z_2=M	0	1	0	0	1	0	0
Z_3=-T	0	0	1	0	1	0	0
Z_4=M+Mole	0	0	0	-1	1	0	0

Unity matrix | Residual matrix

Therefore,

$$\Pi_1 = \frac{\mu L_0 N_a}{M_W \left(\frac{u}{f}\right)}$$

$$\Pi_2 = \frac{d_p}{L_0}$$

$$\Pi_3 = \sigma L_0^2$$

$$N_{STE} = \Pi_1 \Pi_2 \Pi_3$$

$$N_{STE} = \frac{d_p \mu L_0^3 N_a \sigma}{M_W \left(\frac{u}{f}\right)}$$

Breakthrough curves of both colloid and Br transport with and without plaster

Prior to the runoff experiment, plaster was used to seal the top sand surface to prevent infiltration and to eliminate the filtration of colloids by the soil. Pre-experiment with the flow chambers under the same treatments but without of dense vegetation showed that more than 98% bromide and colloids were recovered from the system, indicating no deposition of colloids on the plaster layer and contribution of infiltration and exchange are insignificant under tested conditions.

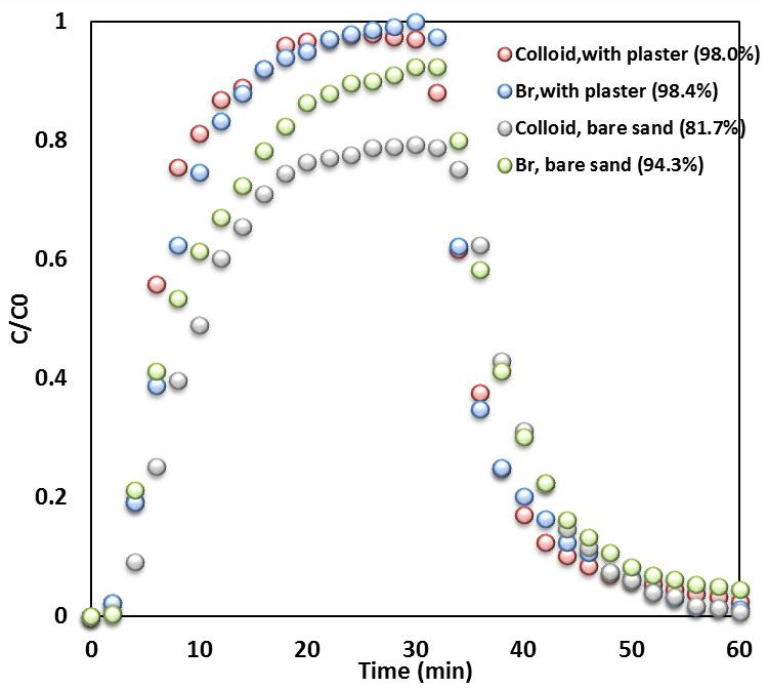

Figure C-1. Breakthrough curves with and without plaster.

Global sensitivity analysis results

To get a qualitative sensitivity analysis of model output, Morris methods was used. According to this method, only parameters separated from the origin of the μ-σ plane are considered important. Figure C-2 showed the graphical representation of the Morris results for model output. The qualitative ranking of factors is as follows: (1) Flow velocity (*u*), (2) vegetation density (1-*f*), (3) ionic strength (*IS*), (4) diameter of collector (d_c), (5) diameter of colloid (d_p), (6) zeta potential of colloid (*ζp*) and collector (*ζc*).

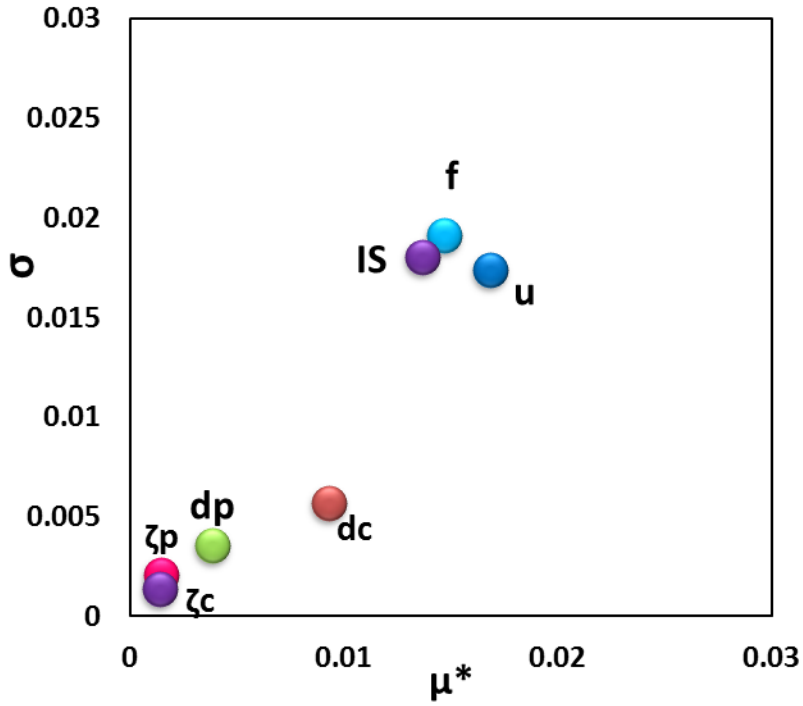

Figure C-2. Morris sensitivity analysis result chart

Flow velocity (*u*), vegetation density (1-*f*) and ionic strength (*IS*) are shown away from both μ and σ axis, which means its influence is not only through first –order effects but also interaction component. The diameter of collector size (d_c) and particle size (d_p) are not far away from the σ axis, which means the influence of these two input factors are mostly through first-order effect with small interaction components. The rest input factors (*ζp* and *ζc*) are very close to origin which indicated they are insensitive to the model output.

To get the quantitative sensitivity analysis of model output, Sobol method was also tested. Base on the qualitative ranking of the input factors, the first five input factors were chosen to test. The first order and total sensitivity indices of the Sobol analysis calculated with 24576 samples were shown in Figure C-3.

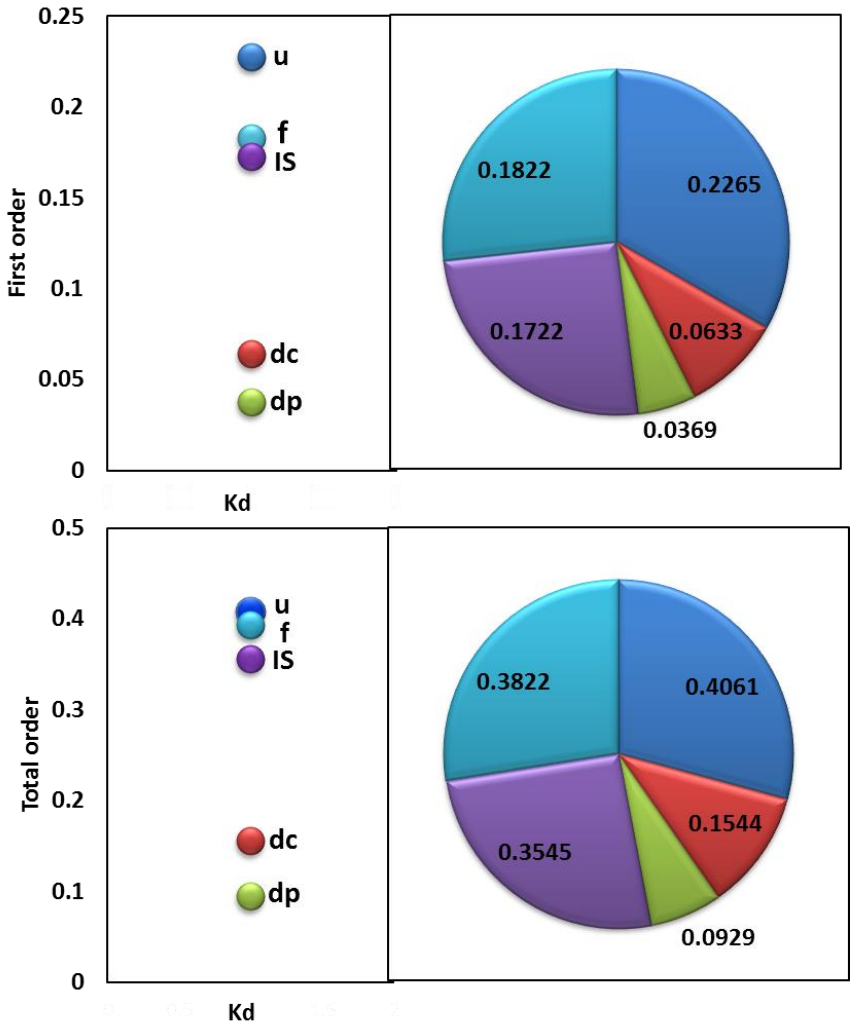

Figure C-3. Sobol sensitivity analysis indices chart

The results of first order indices indicated that flow velocity (the first significant factor) has a larger first order index than the vegetation density (1-*f*) which is the second significant factor. However, the total sensitivity indices of flow velocity and vegetation density are pretty close, which means vegetation density has a large effect by

interactions with other parameters. For example, vegetation density has an important effect on the flow filed around the plant stem which controls on not only physical contact process but also physicochemical attachment process.

It is also noted that the sum of all first order indices (0.6983) is less than 1, which means the model is non-additive, as could be expected. The results showed that all total sensitivity indices are higher than the first order sensitivity indices. This is of course theoretically necessary, since first order indice is a part of the total order indices. For example, the total order indices of the most influential factor –flow velocity (u) (0.4061) included the first order effect (0.2265) and interactions with other factors.

Comparison of experimental deposition rate with predictions of the new dimensionless equation for development dataset

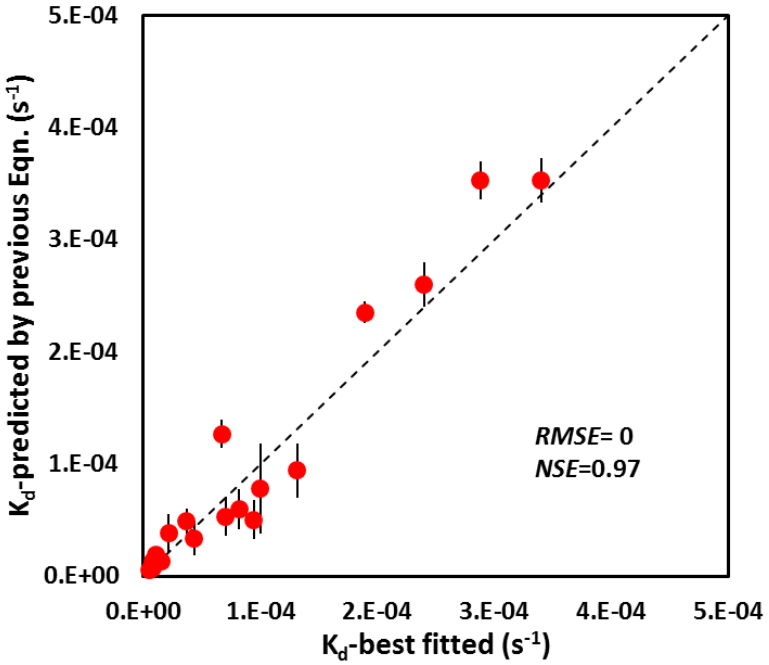

Figure C-4. Comparison of experimental deposition rate with predictions of the new dimensionless equation for development dataset

Table C-2. Experimental data of breakthrough curve under DI water conditions

Time (Minute)	DI water C/C_0 Replicate 1	Replicate 2	Mean
0	0.0277	0.00	0.0163
2	0.01	0.01	0.0092
4	0.1789	0.12	0.1519
6	0.29	0.23	0.2621
8	0.4	0.35	0.3769
10	0.55	0.50	0.5251
12	0.69	0.64	0.6649
14	0.79	0.74	0.7666
16	0.868	0.79	0.8309
18	0.88	0.82	0.8488
20	0.92	0.84	0.8801
22	0.948	0.87	0.9114
24	0.95	0.88	0.9134
26	0.945	0.89	0.916
28	0.947	0.89	0.9197
30	0.944	0.89	0.9156
32	0.947	0.89	0.9161
34	0.942	0.90	0.9187
36	0.862	0.80	0.8292
38	0.68	0.63	0.6552
40	0.42	0.35	0.3836
42	0.263	0.23	0.248
44	0.19	0.12	0.1565
46	0.15	0.09	0.1221
48	0.1	0.06	0.0813
50	0.072	0.05	0.0599
52	0.06	0.03	0.0437
54	0.068	0.02	0.0417
56	0.039	0.02	0.0274
58	0.05	0.00	0.026
60	0.032	0.01	0.0197

Table C-3. Experimental data of breakthrough curve under medium IS conditions (IS=0.01M)

	IS=0.01M		
Time		C/C_0	
(Minute)	Replicate 1	Replicate 2	Mean
0	0.0287	0.00	0.0137
2	0.0321	0.00	0.0116
4	0.078	0.03	0.0537
6	0.254	0.16	0.2058
8	0.43	0.38	0.4048
10	0.66	0.56	0.6123
12	0.74	0.65	0.6947
14	0.77	0.74	0.7547
16	0.82	0.80	0.8084
18	0.86	0.82	0.8421
20	0.9	0.84	0.8713
22	0.899	0.85	0.8744
24	0.91	0.87	0.8918
26	0.91	0.87	0.8915
28	0.92	0.86	0.8913
30	0.92	0.86	0.8923
32	0.92	0.88	0.901
34	0.9	0.88	0.8908
36	0.82	0.78	0.8023
38	0.68	0.64	0.6591
40	0.54	0.45	0.4943
42	0.34	0.27	0.3035
44	0.23	0.17	0.1993
46	0.13	0.10	0.1166
48	0.09	0.06	0.0771
50	0.08	0.05	0.0642
52	0.06	0.02	0.0419
54	0.0487	0.01	0.0297
56	0.045	0.01	0.0253
58	0.042	0.01	0.0261
60	0.032	0.01	0.0195

Table C-4. Experimental data of breakthrough curve under high IS conditions (IS=0.1M)

	IS=0.1M		
Time		C/C_0	
(Minute)	Replicate 1	Replicate 2	Mean
0	0.009	0.01	0.0074
2	0.02	0.00	0.0109
4	0.04	0.01	0.0244
6	0.21	0.15	0.1813
8	0.39	0.37	0.3788
10	0.6	0.55	0.5757
12	0.69	0.66	0.676
14	0.76	0.74	0.7478
16	0.8	0.75	0.7766
18	0.84	0.79	0.8137
20	0.83	0.80	0.8147
22	0.85	0.80	0.8272
24	0.87	0.79	0.8322
26	0.87	0.81	0.8415
28	0.87	0.83	0.852
30	0.9	0.82	0.8597
32	0.89	0.83	0.8591
34	0.87	0.83	0.8491
36	0.84	0.78	0.809
38	0.67	0.64	0.6541
40	0.5	0.46	0.4815
42	0.34	0.29	0.3131
44	0.21	0.17	0.1906
46	0.14	0.10	0.1186
48	0.09	0.07	0.0797
50	0.08	0.03	0.054
52	0.06	0.00	0.0312
54	0.04	0.01	0.0251
56	0.05	0.00	0.0209
58	0.04	0.00	0.0199
60	0.05	0.00	0.0199

Table C-5. Experimental data of breakthrough curve under high IS conditions (IS=0.2M)

IS=0.2M			
Time		C/C_0	
(Minute)	Replicate 1	Replicate 2	Mean
0	0.019	0.00	0.0116
2	0.022	0.01	0.0177
4	0.026	0.01	0.0199
6	0.2	0.13	0.1633
8	0.36	0.30	0.3323
10	0.51	0.47	0.4915
12	0.66	0.60	0.6302
14	0.78	0.73	0.7558
16	0.79	0.75	0.768
18	0.82	0.73	0.7763
20	0.83	0.74	0.7862
22	0.83	0.76	0.7966
24	0.83	0.79	0.8093
26	0.85	0.79	0.8193
28	0.84	0.79	0.8154
30	0.83	0.80	0.8154
32	0.84	0.79	0.8154
34	0.83	0.78	0.8054
36	0.79	0.75	0.77
38	0.62	0.59	0.6032
40	0.46	0.42	0.4388
42	0.28	0.28	0.2782
44	0.24	0.17	0.204
46	0.17	0.13	0.1515
48	0.14	0.08	0.1106
50	0.09	0.05	0.0708
52	0.08	0.05	0.0641
54	0.08	0.03	0.0536
56	0.07	0.02	0.047
58	0.06	0.01	0.0348
60	0.06	0.00	0.0243

Table C-6. Experimental data of breakthrough curve under plant high density conditions (u=0.002 cm/s)

	u=0.002cm/s		
Time		C/C_0	
(Minute)	Replicate 1	Replicate 2	Mean
0	0.0004	0.00	0.0002
2	0.005	0.00	0.003
4	0.0088	0.00	0.0056
6	0.0097	0.00	0.0058
8	0.025	0.00	0.0133
10	0.032	0.00	0.0172
12	0.036	0.00	0.0181
14	0.08	0.00	0.0416
16	0.14	0.05	0.0947
18	0.24	0.13	0.1856
20	0.33	0.24	0.284
22	0.43	0.32	0.3736
24	0.5	0.41	0.4566
26	0.54	0.46	0.499
28	0.57	0.51	0.5394
30	0.64	0.53	0.5873
32	0.64	0.56	0.5999
34	0.65	0.58	0.6139
36	0.68	0.56	0.6185
38	0.66	0.58	0.6208
40	0.67	0.58	0.6232
42	0.68	0.57	0.6255
44	0.67	0.58	0.6229
46	0.66	0.54	0.5999
48	0.57	0.51	0.5385
50	0.51	0.43	0.4694
52	0.42	0.36	0.3899
54	0.36	0.26	0.3089
56	0.31	0.21	0.2615
58	0.26	0.17	0.2135
60	0.23	0.14	0.1873
62	0.2	0.12	0.1582
64	0.18	0.08	0.1319
66	0.14	0.09	0.1161
68	0.15	0.07	0.1112
70	0.12	0.07	0.0928
72	0.11	0.05	0.0805
74	0.09	0.04	0.0649
76	0.09	0.03	0.0598
78	0.08	0.03	0.0547
80	0.08	0.00	0.0491

Table C-7. Experimental data of breakthrough curve under plant high density conditions (u=0.01cm/s)

	u=0.01cm/s		
Time		C/C_0	
(Minute)	Replicate 1	Replicate 2	Mean
0	0.0098	0.00	0.0073
2	0.01	0.01	0.0083
4	0.02	0.02	0.0179
6	0.02	0.02	0.0184
8	0.08	0.03	0.0537
10	0.2	0.17	0.1842
12	0.38	0.33	0.3542
14	0.49	0.45	0.4708
16	0.59	0.55	0.5691
18	0.69	0.61	0.6509
20	0.7	0.66	0.6805
22	0.73	0.68	0.7028
24	0.74	0.70	0.7217
26	0.74	0.72	0.7298
28	0.77	0.72	0.7467
30	0.78	0.73	0.7543
32	0.76	0.75	0.7543
34	0.78	0.73	0.7543
36	0.77	0.74	0.7572
38	0.77	0.71	0.7398
40	0.65	0.59	0.6186
42	0.49	0.43	0.4615
44	0.38	0.30	0.3388
46	0.29	0.22	0.2543
48	0.22	0.14	0.1803
50	0.16	0.11	0.1365
52	0.11	0.08	0.0958
54	0.1	0.05	0.0732
56	0.08	0.03	0.0566
58	0.06	0.03	0.0453
60	0.06	0.02	0.038
62	0.05	0.02	0.0331
64	0.04	0.03	0.0328
66	0.03	0.03	0.0277
68	0.028	0.02	0.025
70	0.03	0.01	0.0218

Table C-8. Experimental data of breakthrough curve under plant high density conditions (u=0.05 cm/s)

	u=0.05cm/s		
Time		C/C_0	
(Minute)	Replicate 1	Replicate 2	Mean
0	0.009	0.01	0.0074
2	0.012	0.01	0.0109
4	0.03	0.02	0.0244
6	0.209	0.15	0.1813
8	0.42	0.34	0.3788
10	0.61	0.54	0.5757
12	0.69	0.66	0.676
14	0.77	0.73	0.7478
16	0.79	0.76	0.7766
18	0.83	0.80	0.8137
20	0.84	0.79	0.8147
22	0.84	0.81	0.8272
24	0.85	0.81	0.8322
26	0.86	0.82	0.8415
28	0.87	0.83	0.852
30	0.88	0.84	0.8597
32	0.87	0.83	0.8491
34	0.84	0.80	0.819
36	0.69	0.62	0.6541
38	0.52	0.44	0.4815
40	0.33	0.30	0.3131
42	0.22	0.16	0.1906
44	0.13	0.11	0.1186
46	0.11	0.05	0.0797
48	0.06	0.05	0.054
50	0.05	0.01	0.0312
52	0.04	0.01	0.0251
54	0.04	0.00	0.0209
56	0.03	0.01	0.0199
58	0.03	0.01	0.0177
60	0.02	0.01	0.013

Table C-9. Experimental data of breakthrough curve under plant high density conditions (u=0.1 cm/s)

	u=0.1cm/s		
Time		C/C_0	
(Minute)	Replicate 1	Replicate 2	Mean
0	0.03	0.02	0.0231
2	0.04	0.01	0.0263
4	0.16	0.10	0.1284
6	0.45	0.36	0.405
8	0.69	0.61	0.6499
10	0.8	0.72	0.7624
12	0.85	0.82	0.8365
14	0.87	0.82	0.8446
16	0.88	0.83	0.857
18	0.9	0.83	0.864
20	0.89	0.83	0.8609
22	0.89	0.84	0.8659
24	0.9	0.85	0.8763
26	0.9	0.86	0.8781
28	0.9	0.85	0.876
30	0.88	0.88	0.8809
32	0.9	0.86	0.8815
34	0.81	0.75	0.7796
36	0.56	0.48	0.5191
38	0.29	0.26	0.2771
40	0.15	0.12	0.1357
42	0.09	0.06	0.0738
44	0.08	0.02	0.0489
46	0.06	0.02	0.038
48	0.05	0.00	0.0265
50	0.04	0.00	0.0216
52	0.03	0.01	0.0198
54	0.03	0.01	0.0179
56	0.02	0.01	0.0169
58	0.02	0.01	0.0169
60	0.0163	0.02	0.0161

Table C-10. Experimental data of breakthrough curve under plant medium density conditions (u=0.002 cm/s)

	u=0.002cm/s		
Time		C/C_0	
(Minute)	Replicate 1	Replicate 2	Mean
0	0.005	0.00	0.0033
2	0.005	0.00	0.004
4	0.009	0.01	0.0081
6	0.01	0.01	0.0086
8	0.02	0.00	0.01
10	0.039	0.01	0.0264
12	0.11	0.08	0.0932
14	0.28	0.24	0.2579
16	0.49	0.44	0.4673
18	0.6	0.56	0.5778
20	0.69	0.63	0.6602
22	0.74	0.68	0.7116
24	0.77	0.70	0.736
26	0.79	0.74	0.766
28	0.8	0.75	0.7738
30	0.82	0.78	0.7995
32	0.83	0.77	0.802
34	0.84	0.78	0.8081
36	0.84	0.76	0.8013
38	0.83	0.77	0.8015
40	0.82	0.77	0.7947
42	0.57	0.50	0.535
44	0.44	0.38	0.4098
46	0.34	0.28	0.3103
48	0.26	0.20	0.23
50	0.183	0.18	0.179
52	0.179	0.13	0.1567
54	0.156	0.12	0.1368
56	0.156	0.08	0.12
58	0.132	0.08	0.1065
60	0.099	0.08	0.0877
62	0.0879	0.07	0.0788
64	0.0865	0.06	0.0711
66	0.089	0.05	0.07
68	0.078	0.06	0.0699
70	0.0773	0.06	0.0678
72	0.0821	0.05	0.0666
74	0.0798	0.05	0.0658
76	0.0787	0.05	0.0643
78	0.0754	0.05	0.0621
80	0.0754	0.04	0.06

Table C-11. Experimental data of breakthrough curve under plant medium density conditions (u=0.01 cm/s)

	u=0.01cm/s		
Time		C/C_0	
(Minute)	Replicate 1	Replicate 2	Mean
0	0.002	0.00	0.0012
2	0.021	0.00	0.0117
4	0.03	0.01	0.0219
6	0.08	0.05	0.0635
8	0.139	0.10	0.1177
10	0.37	0.31	0.3422
12	0.57	0.50	0.5346
14	0.69	0.63	0.6618
16	0.79	0.75	0.7717
18	0.81	0.77	0.7898
20	0.84	0.80	0.8178
22	0.84	0.80	0.8195
24	0.85	0.80	0.8238
26	0.86	0.81	0.8366
28	0.86	0.83	0.8449
30	0.87	0.83	0.8476
32	0.88	0.82	0.8478
34	0.87	0.83	0.8476
36	0.79	0.74	0.765
38	0.55	0.46	0.5049
40	0.328	0.29	0.3075
42	0.19	0.16	0.175
44	0.15	0.07	0.1106
46	0.11	0.05	0.0811
48	0.09	0.03	0.0597
50	0.08	0.03	0.0537
52	0.07	0.01	0.0383
54	0.06	0.01	0.0364
56	0.05	0.02	0.0331
58	0.043	0.00	0.0216
60	0.03	0.01	0.0202
62	0.02	0.00	0.0107
64	0.01	0.00	0.0059
66	0.01	0.00	0.0052
68	0.01	0.00	0.005
70	0.006	0.00	0.0036

Table C-12. Experimental data of breakthrough curve under plant medium density conditions (u=0.05 cm/s)

	u=0.05cm/s		
Time		C/C_0	
(Minute)	Replicate 1	Replicate 2	Mean
0	0.017	0.01	0.0133
2	0.059	0.05	0.056
4	0.17	0.10	0.1374
6	0.51	0.46	0.4869
8	0.72	0.65	0.6861
10	0.84	0.78	0.8121
12	0.89	0.79	0.8419
14	0.9	0.86	0.8822
16	0.93	0.86	0.8943
18	0.94	0.85	0.8971
20	0.94	0.86	0.8994
22	0.95	0.85	0.9022
24	0.95	0.86	0.9061
26	0.95	0.87	0.91
28	0.94	0.88	0.9092
30	0.94	0.88	0.9112
32	0.95	0.85	0.9018
34	0.82	0.74	0.7781
36	0.48	0.42	0.4489
38	0.3	0.21	0.2564
40	0.17	0.08	0.1264
42	0.09	0.04	0.0626
44	0.007	0.06	0.0317
46	0.04	0.01	0.0243
48	0.027	0.00	0.0137
50	0.01	0.01	0.0086
52	0.007	0.00	0.0043
54	0.007	0.00	0.0059
56	0.008	0.00	0.0047
58	0.004	0.00	0.002
60	0.001	0.00	0.0008

Table C-13. Experimental data of breakthrough curve under plant medium density conditions (u=0.1 cm/s)

	u=0.1cm/s		
Time		C/C_0	
(Minute)	Replicate 1	Replicate 2	Mean
0	0.004	0.00	0.0025
2	0.02	0.00	0.0112
4	0.36	0.27	0.3165
6	0.73	0.69	0.7096
8	0.86	0.81	0.8372
10	0.92	0.87	0.8973
12	0.93	0.89	0.9087
14	0.93	0.90	0.9161
16	0.95	0.90	0.927
18	0.96	0.90	0.9277
20	0.94	0.92	0.9295
22	0.95	0.90	0.9267
24	0.96	0.89	0.927
26	0.95	0.90	0.924
28	0.96	0.90	0.9297
30	0.94	0.87	0.9052
32	0.69	0.66	0.6749
34	0.2	0.16	0.178
36	0.09	0.06	0.0774
38	0.07	0.01	0.0411
40	0.08	-0.02	0.032
42	0.04	0.02	0.0294
44	0.03	0.00	0.0155
46	0.04	-0.01	0.0137
48	0.009	0.01	0.0079
50	0.005	0.00	0.0043
52	0.005	0.00	0.0038
54	0.004	0.00	0.0038
56	0.005	0.00	0.0041
58	0.004	0.00	0.0033
60	0.004	0.00	0.0033

Table C-14. Experimental data of breakthrough curve under plant low density conditions (u=0.002 cm/s)

	u=0.002cm/s		
Time		C/C_0	
(Minute)	Replicate 1	Replicate 2	Mean
0	0.005	0.00	0.0034
2	0.009	0.00	0.0062
4	0.016	0.01	0.0122
6	0.019	0.01	0.0156
8	0.019	0.01	0.0159
10	0.0199	0.01	0.0162
12	0.058	0.05	0.0519
14	0.15	0.09	0.1213
16	0.26	0.22	0.2412
18	0.38	0.33	0.3546
20	0.48	0.42	0.4493
22	0.59	0.53	0.5604
24	0.66	0.58	0.6207
26	0.72	0.67	0.6964
28	0.76	0.72	0.7406
30	0.77	0.72	0.7463
32	0.78	0.73	0.7531
34	0.79	0.73	0.7591
36	0.79	0.74	0.7656
38	0.81	0.75	0.7806
40	0.78	0.69	0.7347
42	0.65	0.61	0.6281
44	0.56	0.50	0.5292
46	0.499	0.45	0.4728
48	0.42	0.36	0.3903
50	0.38	0.30	0.3384
52	0.3	0.26	0.28
54	0.25	0.21	0.2316
56	0.21	0.17	0.1908
58	0.2	0.15	0.1755
60	0.17	0.11	0.1414
62	0.15	0.11	0.1295
64	0.14	0.09	0.1165
66	0.13	0.08	0.1037
68	0.1	0.07	0.0856
70	0.09	0.05	0.0697
72	0.09	0.04	0.0663
74	0.08	0.02	0.0507
76	0.06	0.04	0.0508
78	0.07	0.03	0.0502
80	0.05	0.03	0.0414

Table C-15. Experimental data of breakthrough curve under plant low density conditions (u=0.01 cm/s)

	u=0.01cm/s		
Time		C/C_0	
(Minute)	Replicate 1	Replicate 2	Mean
0	0.0098	0.01	0.0083
2	0.019	0.01	0.0169
4	0.058	0.05	0.0534
6	0.083	0.08	0.0794
8	0.15	0.13	0.139
10	0.23	0.17	0.2015
12	0.33	0.28	0.3039
14	0.45	0.39	0.4222
16	0.53	0.50	0.5163
18	0.63	0.59	0.61
20	0.74	0.67	0.7069
22	0.79	0.75	0.7704
24	0.79	0.75	0.7718
26	0.81	0.76	0.7863
28	0.81	0.78	0.7972
30	0.83	0.77	0.8003
32	0.84	0.79	0.8146
34	0.84	0.81	0.8237
36	0.85	0.80	0.826
38	0.83	0.78	0.8029
40	0.73	0.70	0.715
42	0.59	0.53	0.5607
44	0.5	0.46	0.4803
46	0.38	0.31	0.347
48	0.332	0.25	0.293
50	0.25	0.18	0.2165
52	0.21	0.14	0.1745
54	0.17	0.12	0.1452
56	0.14	0.09	0.1149
58	0.12	0.06	0.0902
60	0.08	0.02	0.0485
62	0.06	0.01	0.0371
64	0.05	0.02	0.034
66	0.04	0.02	0.0288
68	0.05	0.00	0.0254
70	0.03	0.01	0.0223

Table C-16. Experimental data of breakthrough curve under plant low density conditions (u=0.05 cm/s)

	u=0.05cm/s		
Time		C/C_0	
(Minute)	Replicate 1	Replicate 2	Mean
0	0.0176	0.01	0.0141
2	0.026	0.02	0.022
4	0.047	0.04	0.0448
6	0.16	0.15	0.1552
8	0.43	0.37	0.3986
10	0.6	0.55	0.5725
12	0.72	0.70	0.7093
14	0.83	0.79	0.8117
16	0.86	0.82	0.8422
18	0.9	0.87	0.8829
20	0.91	0.87	0.8906
22	0.91	0.87	0.8906
24	0.91	0.90	0.9057
26	0.92	0.90	0.9075
28	0.93	0.89	0.9106
30	0.93	0.91	0.9183
32	0.93	0.91	0.9191
34	0.92	0.89	0.9034
36	0.78	0.73	0.7528
38	0.54	0.46	0.5005
40	0.37	0.30	0.3345
42	0.26	0.20	0.2316
44	0.2	0.15	0.1747
46	0.14	0.09	0.116
48	0.1	0.07	0.0873
50	0.09	0.04	0.0674
52	0.08	0.02	0.0517
54	0.06	0.03	0.0443
56	0.06	0.01	0.0341
58	0.05	0.01	0.031
60	0.04	0.01	0.0272

Table C-17. Experimental data of breakthrough curve under plant low density conditions (u=0.1 cm/s)

	u=0.1cm/s		
Time		C/C_0	
(Minute)	Replicate 1	Replicate 2	Mean
0	0.04	0.02	0.0303
2	0.059	0.05	0.0563
4	0.197	0.17	0.1851
6	0.49	0.43	0.4621
8	0.68	0.59	0.6333
10	0.76	0.71	0.7343
12	0.85	0.77	0.8081
14	0.9	0.82	0.8621
16	0.9	0.85	0.8727
18	0.92	0.88	0.8992
20	0.93	0.89	0.9119
22	0.94	0.89	0.9157
24	0.95	0.89	0.9194
26	0.97	0.87	0.9222
28	0.96	0.89	0.927
30	0.97	0.89	0.9313
32	0.96	0.91	0.9343
34	0.89	0.81	0.8475
36	0.57	0.47	0.5199
38	0.35	0.29	0.3207
40	0.23	0.15	0.1924
42	0.15	0.13	0.1394
44	0.11	0.07	0.0907
46	0.06	0.05	0.0525
48	0.05	0.02	0.0341
50	0.03	0.01	0.0189
52	0.02	0.00	0.0111
54	0.02	0.00	0.0101
56	0.016	0.00	0.0088
58	0.01	0.01	0.0083
60	0.02	0.00	0.0109

Table C-18. Experimental data of breakthrough curve under different sizes of colloid conditions (dp=0.1µm)

Time (Minute)	d_p=0.1µm C/C_0 Replicate 1	Replicate 2	Mean
0	0.02	0.003	0.0116
2	0.023	0.012	0.0177
4	0.024	0.016	0.0199
6	0.172	0.155	0.1633
8	0.374	0.291	0.3323
10	0.521	0.462	0.4915
12	0.663	0.597	0.6302
14	0.767	0.745	0.7558
16	0.788	0.748	0.768
18	0.799	0.754	0.7763
20	0.802	0.770	0.7862
22	0.832	0.761	0.7966
24	0.834	0.785	0.8093
26	0.844	0.795	0.8193
28	0.846	0.785	0.8154
30	0.849	0.782	0.8154
32	0.84	0.771	0.8054
34	0.78	0.760	0.77
36	0.621	0.585	0.6032
38	0.453	0.425	0.4388
40	0.287	0.269	0.2782
42	0.243	0.165	0.204
44	0.165	0.138	0.1515
46	0.122	0.099	0.1106
48	0.0876	0.054	0.0708
50	0.076	0.052	0.0641
52	0.067	0.040	0.0536
54	0.054	0.040	0.047
56	0.043	0.027	0.0348
58	0.034	0.015	0.0243
60	0.021	0.017	0.0188

Table C-19. Experimental data of breakthrough curve under different sizes of colloid conditions (dp=1.05µm)

Time (Minute)	d_p=1.05µm C/C_0 Replicate 1	Replicate 2	Mean
0	0.0023	0.002	0.0019
2	0.0044	0.004	0.0042
4	0.0087	0.007	0.0076
6	0.19	0.190	0.1898
8	0.43	0.401	0.4155
10	0.576	0.562	0.5692
12	0.721	0.695	0.7079
14	0.779	0.760	0.7697
16	0.832	0.817	0.8244
18	0.842	0.836	0.8392
20	0.863	0.852	0.8577
22	0.877	0.860	0.8683
24	0.878	0.859	0.8685
26	0.888	0.848	0.8681
28	0.889	0.854	0.8717
30	0.892	0.858	0.8749
32	0.909	0.853	0.8808
34	0.887	0.845	0.866
36	0.679	0.656	0.6677
38	0.467	0.449	0.4579
40	0.338	0.303	0.3205
42	0.221	0.183	0.2021
44	0.134	0.113	0.1236
46	0.098	0.053	0.0757
48	0.065	0.042	0.0537
50	0.045	0.021	0.0331
52	0.034	0.019	0.0265
54	0.033	0.007	0.0202
56	0.021	0.008	0.0146
58	0.017	0.010	0.0134
60	0.013	0.009	0.0112

Table C-20. Experimental data of breakthrough curve under different sizes of colloid conditions (dp=2.0μm)

Time (Minute)	d_p=2.0μm C/C_0 Replicate 1	Replicate 2	Mean
0	0.0098	0.005	0.0074
2	0.0112	0.011	0.0109
4	0.0276	0.021	0.0244
6	0.199	0.164	0.1813
8	0.387	0.371	0.3788
10	0.589	0.562	0.5757
12	0.687	0.665	0.676
14	0.761	0.735	0.7478
16	0.789	0.764	0.7766
18	0.823	0.804	0.8137
20	0.829	0.800	0.8147
22	0.834	0.820	0.8272
24	0.856	0.808	0.8322
26	0.867	0.816	0.8415
28	0.88	0.824	0.852
30	0.887	0.832	0.8597
32	0.888	0.810	0.8491
34	0.88	0.758	0.819
36	0.699	0.609	0.6541
38	0.501	0.462	0.4815
40	0.32	0.306	0.3131
42	0.199	0.182	0.1906
44	0.132	0.105	0.1186
46	0.082	0.077	0.0797
48	0.06	0.048	0.054
50	0.04	0.022	0.0312
52	0.03	0.020	0.0251
54	0.028	0.014	0.0209
56	0.022	0.018	0.0199
58	0.0189	0.017	0.0177
60	0.015	0.011	0.013

APPENDIX D
SUPPORTING INFORMATION FOR CHAPTER 5

D-1 Derivation of Van der Waal Interaction Energy (Eqn.7).

$$\Phi_{VDW}(D) = \int_{S_2} \hat{n}_{S_2} \cdot \hat{k}E(h_2)ds + \int_{S_1} \hat{n}_{S_1} \cdot \hat{k}E(h_1)ds + \int_{S_3} \hat{n}_{S_3} \cdot \hat{k}E(h_3)ds \quad \text{(D-1)}$$

Using Eqn. (2.1), (3.1), (4.2) and (6.1), for outer S_2, we obtain

$$\int_{S_2} \hat{n}_{S_2} \cdot \hat{k}E(h_2)ds = -\frac{Aa\sin\varphi}{12\pi}\int_{-L}^{L}\int_{0}^{\pi}\sin\theta\left[\begin{array}{c}\dfrac{1}{(D - z\cos\varphi - a\sin\varphi\sin\theta)^2} \\ +\dfrac{1}{(D - z\cos\varphi + a\sin\varphi\sin\theta)^2}\end{array}\right]d\theta dz \quad \text{(D-2)}$$

Similarly, from Eqn. (2.2), (3.2), (4.1), (6.1) and Eqn. (2.2), (3.3), (4.3), (6.1), we obtain Eqn. (D-3) and (D-4), respectively,

$$\int_{S_1} \hat{n}_{S_1} \cdot \hat{k}E(h_1)ds = -\frac{A\cos\varphi}{12\pi}\int_{a-R}^{a}\int_{0}^{2\pi}\frac{\rho}{(D - L\cos\varphi - \rho\sin\varphi\sin\theta)^2}d\theta d\rho \quad \text{(D-3)}$$

$$\int_{S_3} \hat{n}_{S_3} \cdot \hat{k}E(h_3)ds = -\frac{A\cos\varphi}{12\pi}\int_{a-R}^{a}\int_{0}^{2\pi}\frac{\rho}{(D + L\cos\varphi - \rho\sin\varphi\sin\theta)^2}d\theta d\rho \quad \text{(D-4)}$$

For Eqn. (D-2), to simplify the notation, we let $D - z\cos\varphi = \alpha$ and $a\sin\varphi = \beta$. Then Eqn. (D-2) can be written as

$$\int_{S_2} \hat{n}_{S_2} \cdot \hat{k}E(h_2)ds = -\frac{Aa\sin\varphi}{12\pi}\int_{-L}^{L}\int_{0}^{\pi}\sin\theta\left[\frac{1}{(\alpha - \beta\sin\theta)^2} + \frac{1}{(\alpha + \beta\sin\theta)^2}\right]d\theta dz \quad \text{(D-5)}$$

To evaluate Eqn. (D-5), we appeal to the following formulas

$$\frac{d}{dt}\int_a^b f(x,t)dx = \int_a^b \frac{\partial f(x,t)}{\partial t}dx \quad \text{(D-6)}$$

$$\frac{d}{dx}\int_{f(x)}^{g(x)} F(t)dt = F(g(x))g'(x) - F(f(x))f'(x) \quad \text{(D-7)}$$

Together with the following integral identity

$$\int_0^{\pi}\left(\frac{1}{\alpha-\beta\sin\theta}-\frac{1}{\alpha+\beta\sin\theta}\right)d\theta=\frac{4}{\sqrt{\alpha^2-\beta^2}}\arctan\left(\frac{\beta}{\sqrt{\alpha^2-\beta^2}}\right) \tag{D-8}$$

The right hand side of Eqn. (D-5) becomes

$$\begin{aligned}
&-\frac{Aa\sin\varphi}{12\pi}\int_{-L}^{L}\int_0^{\pi}\sin\theta\left[\frac{1}{(\alpha-\beta\sin\theta)^2}+\frac{1}{(\alpha+\beta\sin\theta)^2}\right]d\theta dz\\
&=-\frac{Aa\sin\varphi}{12\pi}\frac{\partial}{\partial\beta}\int_{-L}^{L}\int_0^{\pi}\left(\frac{1}{\alpha-\beta\sin\theta}-\frac{1}{\alpha+\beta\sin\theta}\right)d\theta dz \qquad \text{(D-9)}\\
&=-\frac{Aa\sin\varphi}{3\pi}\frac{\partial}{\partial\beta}\int_{-L}^{L}\frac{\arctan\left(\frac{\beta}{\sqrt{\alpha^2-\beta^2}}\right)}{\sqrt{\alpha^2-\beta^2}}dz
\end{aligned}$$

Now, let $\frac{\alpha}{\beta}=t$, $D-L\cos\varphi=\gamma_1$ and $D+L\cos\varphi=\gamma_2$. Then $dz=-\frac{\beta}{\cos\varphi}dt$, and the Eqn. (D-9) becomes

$$-\frac{Aa\sin\varphi}{3\pi}\int_{-L}^{L}\frac{\arctan\left(\frac{\beta}{\sqrt{\alpha^2-\beta^2}}\right)}{\sqrt{\alpha^2-\beta^2}}dz \quad=\frac{Aa\sin\varphi}{3\pi\cos\varphi}\int_{\frac{\gamma_2}{\beta}}^{\frac{\gamma_1}{\beta}}\frac{\arctan\left(\frac{1}{\sqrt{t^2-1}}\right)}{\sqrt{t^2-1}}dt \tag{D-10}$$

By differentiating Eqn. (20) with respect to β and appealing to Eqn. (D-7), we obtain

$$\int_{S_2}\hat{n}_{S_2}\cdot\hat{k}E(h_2)ds=\frac{-A}{3\pi\cos\varphi}\left(\begin{array}{l}\dfrac{\arctan\left(\dfrac{a\sin\varphi}{\sqrt{(D-L\cos\varphi)^2-(a\sin\varphi)^2}}\right)(D-L\cos\varphi)}{\sqrt{(D-L\cos\varphi)^2-(a\sin\varphi)^2}}\\ -\dfrac{\arctan\left(\dfrac{a\sin\varphi}{\sqrt{(D+L\cos\varphi)^2-(a\sin\varphi)^2}}\right)(D+L\cos\varphi)}{\sqrt{(D+L\cos\varphi)^2-(a\sin\varphi)^2}}\end{array}\right) \tag{D-11}$$

Similarly, for inner S_2, we obtain

$$\int_{S_2} \hat{n}_{S_2} \cdot \hat{k}E(h_2)ds = \frac{-A}{3\pi\cos\varphi}\left(\begin{array}{l}\dfrac{\arctan\left(\dfrac{(a-R)\sin\varphi}{\sqrt{(D-L\cos\varphi)^2-((a-R)\sin\varphi)^2}}\right)(D-L\cos\varphi)}{\sqrt{(D-L\cos\varphi)^2-((a-R)\sin\varphi)^2}} \\ -\dfrac{\arctan\left(\dfrac{(a-R)\sin\varphi}{\sqrt{(D+L\cos\varphi)^2-((a-R)\sin\varphi)^2}}\right)(D+L\cos\varphi)}{\sqrt{(D+L\cos\varphi)^2-((a-R)\sin\varphi)^2}}\end{array}\right) \quad \text{(D-12)}$$

For Eqn. (D-3), to simplify the notation, we let $\alpha_1 = D - L\cos\varphi$ and $\beta_1 = -\rho\sin\varphi$. Then Eqn. (D-3) can be written as

$$\int_{S_1} \hat{n}_{S_1} \cdot \hat{k}E(h_1)ds = -\frac{A\cos\varphi}{12\pi}\int_{a-R}^{a}\int_0^{2\pi}\frac{\rho}{(\alpha_1+\beta_1\sin\theta)^2}d\theta d\rho \quad \text{(D-13)}$$

We recall a well-known integral identity

$$\int_0^{2\pi}\frac{1}{\alpha_1+\beta_1\sin\theta}d\theta = \frac{2\pi}{\sqrt{\alpha_1{}^2-\beta_1{}^2}} \quad \text{(D-14)}$$

Eqn. (D-12) can be obtained by differentiating Eqn. (D-14) with respect to α_1 and integrating with respect to ρ, after routine algebraic operation, we obtain

$$\int_{S_1} \hat{n}_{S_1} \cdot \hat{k}E(h_1)ds$$

$$= -\frac{A(D-L\cos\varphi)\cos\varphi}{6\sin^2\varphi}\left[\begin{array}{l}\dfrac{1}{\sqrt{(D-L\cos\varphi)^2-(a\sin\varphi)^2}} \\ -\dfrac{1}{\sqrt{(D-L\cos\varphi)^2-(a-R)^2\sin^2\varphi}}\end{array}\right] \quad \text{(D-15)}$$

Similarly, for Eqn. (D-15), we obtain

$$\int_{S_3} \hat{n}_{S_3} \cdot \hat{k}E(h_3)ds$$

$$= -\frac{A(D+L\cos\varphi)\cos\varphi}{6\sin^2\varphi}\left[\begin{array}{c}\dfrac{1}{\sqrt{(D+L\cos\varphi)^2-(a\sin\varphi)^2}}\\ -\dfrac{1}{\sqrt{(D+L\cos\varphi)^2-(a-R)^2\sin^2\varphi}}\end{array}\right] \quad \text{(D-16)}$$

D-2 Derivation of Electrostatic Double Layer Interaction Energy (Eqn.8)

$$\Phi_{EDL}(D) = \int_{S_2} \hat{n}_{S_2} \cdot \hat{k}E(h_2)ds + \int_{S_1} \hat{n}_{S_1} \cdot \hat{k}E(h_1)ds + \int_{S_3} \hat{n}_{S_3} \cdot \hat{k}E(h_3)ds \quad \text{(D-17)}$$

Using Eqn. (2.1), (3.1), (4.2) and (6.2), we obtain

$$\int_{S_2} \hat{n}_{S_2} \cdot \hat{k}E(h_2)ds = 32a\varepsilon_0\varepsilon_r\gamma_1\gamma_2\kappa\left(\frac{kT}{ve}\right)^2 \sin\varphi\left(\begin{array}{l}\int_{-L}^{L}\int_0^{\pi}\sin\theta e^{-\kappa(D-z\cos\varphi-a\sin\varphi\sin\theta)}dzd\theta\\ +\int_{-L}^{L}\int_0^{\pi}\sin\theta e^{-\kappa(D-z\cos\varphi+a\sin\varphi\sin\theta)}dzd\theta\end{array}\right) \quad \text{(D-18)}$$

Similarly, from Eqn. (2.2), (3.2), (4.1), (6.2) and Eqn. (2.2), (3.3), (4.3), (6.2), we obtain Eqn. (D-19) and (D-20), respectively,

$$\int_{S_1} \hat{n}_{S_1} \cdot \hat{k}E(h_1)ds = 32\varepsilon_0\varepsilon_r\gamma_1\gamma_2\kappa\left(\frac{kT}{ve}\right)^2 \cos\varphi\int_{a-R}^{a}\int_0^{2\pi}\rho e^{-\kappa(D-L\cos\varphi-\rho\sin\varphi\sin\theta)}d\theta d\rho \quad \text{(D-19)}$$

$$\int_{S_3} \hat{n}_{S_3} \cdot \hat{k}E(h_3)ds = 32\varepsilon_0\varepsilon_r\gamma_1\gamma_2\kappa\left(\frac{kT}{ve}\right)^2 \cos\varphi\int_{a-R}^{a}\int_0^{2\pi}\rho e^{-\kappa(D+L\cos\varphi-\rho\sin\varphi\sin\theta)}d\theta d\rho \quad \text{(D-20)}$$

After letting $\alpha = \kappa a\sin\varphi$ and integrating with respect to *z*, Eqn. (D-20) can be written as

$$\int_{-L}^{L}\int_0^{\pi}\sin\theta e^{-\kappa(D-z\cos\varphi-a\sin\varphi\sin\theta)}dzd\theta + \int_{-L}^{L}\int_0^{\pi}\sin\theta e^{-\kappa(D-z\cos\varphi+a\sin\varphi\sin\theta)}dzd\theta$$

$$= \frac{e^{-\kappa D}}{\kappa\cos\varphi}\left(e^{\kappa L\cos\varphi}-e^{-\kappa L\cos\varphi}\right)\int_0^{\pi}\sin\theta\left(e^{\alpha\sin\theta}+e^{-\alpha\sin\theta}\right)d\theta \quad \text{(D-21)}$$

Let $f(\alpha) = \int_0^{\pi}\left(e^{\alpha\sin\theta}-e^{-\alpha\sin\theta}\right)d\theta$ and Eqn. (D-21) can be obtained by differentiation *f (α)* with respect to *α.* Now we recall the integral representation of modified Struve function of order zero *L_0 (z):*

$$L_0(z) = \frac{2}{\pi}\int_0^{\pi/2} \sinh(z\cos\theta)d\theta \tag{D-22}$$

And rewrite *f (α)* in term of $L_0(z)$:

$$f(\alpha) = \int_0^{\pi}\left(e^{\alpha\sin\theta} - e^{-\alpha\sin\theta}\right)d\theta = 4\int_0^{\pi/2}\sinh(\alpha\sin\theta)d\theta = 4\int_0^{\pi/2}\sinh(\alpha\cos\theta)d\theta \tag{D-23}$$

Differentiating *f (α)* with respect to *α*, we obtain

$$\int_0^{\pi}\sin\theta\left(e^{\alpha\sin\theta} + e^{-\alpha\sin\theta}\right)d\theta = 2\pi L_0^{'}(\alpha) \tag{D-24}$$

Based on the recurrence relations of modified Struve functions, we know that

$$L_{-1}(\alpha) + L_1(\alpha) = 2L_0^{'}(\alpha) - \frac{2}{\pi}, \quad L_1(\alpha) = L_0^{'}(\alpha) - \frac{2}{\pi} \tag{D-25}$$

We obtain

$$\int_{S_2}\hat{n}_{S_2}\cdot\hat{k}E(h_2)ds = 64\pi a\sin\varphi\varepsilon_0\varepsilon_r\gamma_1\gamma_2\left(\frac{kT}{ve}\right)^2\frac{e^{-\kappa D}}{\cos\varphi}\left(e^{\kappa L\cos\varphi} - e^{-\kappa L\cos\varphi}\right)L_{-1}(\kappa a\sin\varphi) \tag{D-26}$$

For Eqn. (D-19) and Eqn. (D-20), letting $\mu = \kappa\sin\varphi$, we obtain

$$\begin{aligned}
&\int_{S_1}\hat{n}_{S_1}\cdot\hat{k}E(h_1)ds + \int_{S_3}\hat{n}_{S_3}\cdot\hat{k}E(h_3)ds \\
&= 32\varepsilon_0\varepsilon_r\gamma_1\gamma_2\kappa\left(\frac{kT}{ve}\right)^2\cos\varphi e^{-\kappa D}\left(e^{\kappa L\cos\varphi} + e^{-\kappa L\cos\varphi}\right)\int_{a-R}^{a}\int_0^{2\pi}\rho e^{\mu\rho\sin\theta}d\rho d\theta \\
&= 32\varepsilon_0\varepsilon_r\gamma_1\gamma_2\kappa\left(\frac{kT}{ve}\right)^2\cos\varphi e^{-\kappa D}\left(e^{\kappa L\cos\varphi} + e^{-\kappa L\cos\varphi}\right)\left[\begin{array}{l}\int_0^{a}\int_0^{2\pi}\rho e^{\mu\rho\sin\theta}d\rho d\theta \\ -\int_0^{a-R}\int_0^{2\pi}\rho e^{\mu\rho\sin\theta}d\rho d\theta\end{array}\right]
\end{aligned} \tag{D-27}$$

We now rewrite the integral in the Eqn. (D-27) in term of Bessel function. To do this, first we convert the integral from Polar coordinate to Cartesian coordinate. Let $x = \rho\cos\theta$ and $y = \rho\sin\theta$, we obtain

$$\int_0^{a}\int_0^{2\pi}\rho e^{\mu\rho\sin\theta}d\rho d\theta = 2\int_{-a}^{a}\sqrt{a^2 - y^2}e^{\mu y}dy \tag{D-28}$$

Let $y = at$, Eqn. (D-28) can be also written as

$$\int_0^a \int_0^{2\pi} \rho e^{\mu\rho\sin\theta} d\rho d\theta = 2a^2 \int_{-1}^{1} \frac{1}{\sqrt{1-t^2}} e^{\mu a t} dt - 2a^2 \int_{-1}^{1} \frac{t^2}{\sqrt{1-t^2}} e^{\mu a t} dt \qquad \text{(D-29)}$$

We recall the integral representations of Bessel function of order zero ($J_0(x)$) and modified Bessel function of order zero ($I_0(x)$):

$$J_0(x) = \frac{1}{\pi} \int_{-1}^{1} \frac{e^{ixt}}{\sqrt{1-t^2}} dt \qquad \text{(D-30)}$$

$$I_0(x) = J_0(ix) \qquad \text{(C-31)}$$

Let $x = -i\mu a$ in the Eqn. (D-30), the first integral on the right hand in the Eqn. (D-29) can be written as

$$\int_{-1}^{1} \frac{e^{\mu a t}}{\sqrt{1-t^2}} dt = J_0(-i\mu a)\pi = I_0(\mu a)\pi \qquad \text{(D-32)}$$

Differentiating Eqn. (D-32) with respect to $-i\mu a$, the second integral on the right hand in the Eqn. (D-29) can be written as

$$-\int_{-1}^{1} \frac{t^2 e^{\mu a t}}{\sqrt{1-t^2}} dt = J_0^{''}(-i\mu a)\pi \qquad \text{(D-33)}$$

Based on the recurrence relations of Bessel function, we obtain

$$J_0^{''}(-i\mu a) = \frac{1}{2}\left[J_2(-i\mu a) - J_0(-i\mu a)\right] = \frac{1}{2}\left[I_2(\mu a) - I_0(\mu a)\right] \qquad \text{(D-34)}$$

Inserting Eqn. (D-32) and (D-33) into Eqn. (D-29), we obtain

$$\int_0^a \int_0^{2\pi} \rho e^{\mu\rho\sin\theta} d\rho d\theta = a^2\pi\left[I_0(\kappa \sin\varphi a) + I_2(\kappa \sin\varphi a)\right] \qquad \text{(D-35)}$$

Similarly, we obtain

$$\int_0^{a-R} \int_0^{2\pi} \rho e^{\mu\rho\sin\theta} d\rho d\theta = (a-R)^2\pi\left[I_0(\kappa(a-R)\sin\varphi) + I_2(\kappa(a-R)\sin\varphi)\right] \qquad \text{(D-36)}$$

Inserting Eqn. (D-35) and (D-36) into Eqn. (D-37), we obtain

$$\int_{S_1} \hat{n}_{S_1} \cdot \hat{k}E(h_1)ds + \int_{S_3} \hat{n}_{S_3} \cdot \hat{k}E(h_3)ds$$
$$= 32\varepsilon_0\varepsilon_r\gamma_1\gamma_2\kappa\left(\frac{kT}{ve}\right)^2 \cos\varphi e^{-\kappa D}\begin{pmatrix} e^{\kappa L\cos\varphi} \\ +e^{-\kappa L\cos\varphi}\end{pmatrix}\begin{bmatrix} a^2\pi\left[I_0(\kappa\sin\varphi a)+I_2(\kappa\sin\varphi a)\right]- \\ (a-R)^2\pi\begin{bmatrix} I_0(\kappa(a-R)\sin\varphi) \\ +I_2(\kappa(a-R)\sin\varphi)\end{bmatrix}\end{bmatrix} \quad \text{(D-37)}$$

LIST OF REFERENCES

1. Wiesner, M.R., Lowry, G.V., Alvarez, P., Dionysiou, D., and Biswas, P., Assessing the risks of manufactured nanomaterials. Environmental science & technology, 2006. 40(14): p. 4336-4345.

2. Hotze, E.M., Phenrat, T., and Lowry, G.V., Nanoparticle aggregation: Challenges to understanding transport and reactivity in the environment. Journal of Environmental Quality, 2010. 39(6): p. 1909-1924.

3. Petersen, E.J., Zhang, L., Mattison, N.T., O'Carroll, D.M., Whelton, A.J., Uddin, N., Tinh, N., Huang, Q., Henry, T.B., Holbrook, R.D., and Chen, K.L., Potential release pathways, environmental fate, and ecological risks of carbon nanotubes. Environmental science & technology, 2011. 45(23): p. 9837-9856.

4. McCarthy, J.F. and Zachara, J.M., Subsurface transport of contaminants - mobile colloids in the subsurface environment may alter the transport of contaminants. Environmental science & technology, 1989. 23(5): p. 496-502.

5. Harvey, M., Bourget, E., and Ingram, R.G., Experimental-evidence of passive accumulation of marine bivalve larvae on filamentous epibenthic structures. Limnology And Oceanography, 1995. 40(1): p. 94-104.

6. Elliott, A.H., Settling of fine sediment in a channel with emergent vegetation. Journal of Hydraulic Engineering-Asce, 2000. 126(8): p. 570-577.

7. Saiers, J.E., Harvey, J.W., and Mylon, S.E., Surface-water transport of suspended matter through wetland vegetation of the florida everglades. Geophysical Research Letters, 2003. 30(19).

8. Stumm, W., Chemical interaction in particle separation. Environmental Science & Technology, 1977. 11(2): p. 1066-1070.

9. Kretzschmar, R., Borkovec, M., Grolimund, D., and Elimelech, M., Mobile subsurface colloids and their role in contaminant transport. Advances in Agronomy, Vol 66, 1999. 66: p. 121-193.

10. Chen, G., Flury, M., Harsh, J.B., and Lichtner, P.C., Colloid-facilitated transport of cesium in variably saturated hanford sediments. Environmental science & technology, 2005. 39(10): p. 3435-3442.

11. Grolimund, D. and Borkovec, M., Colloid-facilitated transport of strongly sorbing contaminants in natural porous media: Mathematical modeling and laboratory column experiments. Environmental science & technology, 2005. 39(17): p. 6378-6386.

12. Kim, S.B., Corapcioglu, M.Y., and Kim, D.J., Effect of dissolved organic matter and bacteria on contaminant transport in riverbank filtration. Journal of Contaminant Hydrology, 2003. 66(1-2): p. 1-23.

13. USEPA, National section 303(d) list fact sheet. U.S. Environmental Protection Agency, Office of Water, 2006. http://oaspub.epa.gov/waters/national_rept.control.

14. Gerba, C.P., Rose, J.B., and Haas, C.N., Sensitive populations: Who is at the greatest risk? International Journal Of Food Microbiology, 1996. 30(1-2): p. 113-123.

15. Lenormand, R., Zarcone, C., and Sarr, A., Mechanisms of the displacement of one fluid by another in a network of capillary ducts. Journal of Fluid Mechanics, 1983. 135(OCT): p. 337-353.

16. Loge, F.N., Thompson, D.E., and Call, D.R., Pcr detection of specific pathogens in water: A risk-based analysis. Environmental science & technology, 2002. 36(12): p. 2754-2759.

17. Ryan, J.N. and Elimelech, M., Colloid mobilization and transport in groundwater. Colloids and Surfaces a-Physicochemical and Engineering Aspects, 1996. 107: p. 1-56.

18. Schijven, J.F. and Hassanizadeh, S.M., Removal of viruses by soil passage: Overview of modeling, processes, and parameters. Critical Reviews In Environmental Science And Technology, 2000. 30(1): p. 49-127.

19. Harvey, R.W., Harms, H., and Landkamer, L., Transport of microorganisms in the terrestrial subsurface: In situ and laboratory methods. Manual of environmental microbiology, 3rd ed, ed. Hurst, C.J.C.R.L.G.J.L.L.D.A.M.A.L. and Stetzenbach, L.D.2007. 872-897.

20. Jin, Y. and Flury, M., Fate and transport of viruses in porous media. Advances in Agronomy, Vol 77, 2002. 77: p. 39-+.

21. Ginn, T.R., Wood, B.D., Nelson, K.E., Scheibe, T.D., Murphy, E.M., and Clement, T.P., Processes in microbial transport in the natural subsurface. 25 years of advances in water resources, ed. Miller, C.T.P.M.B.H.S.M.2003. 157-182.

22. de Jonge, L.W., Kjaergaard, C., and Moldrup, P., Colloids and colloid-facilitated transport of contaminants in soils: An introduction. Vadose Zone Journal, 2004. 3(2): p. 321-325.

23. DeNovio, N.M., Saiers, J.E., and Ryan, J.N., Colloid movement in unsaturated porous media: Recent advances and future directions. Vadose Zone Journal, 2004. 3(2): p. 338-351.

24. Rockhold, M.L., Yarwood, R.R., and Selker, J.S., Coupled microbial and transport processes in soils. Vadose Zone Journal, 2004. 3(2): p. 368-383.

25. Sen, T.K. and Khilar, K.C., Review on subsurface colloids and colloid-associated contaminant transport in saturated porous media. Advances in Colloid and Interface Science, 2006. 119(2-3): p. 71-96.

26. Tufenkji, N., Dixon, D.R., Considine, R., and Drummond, C.J., Multi-scale cryptosporidium/sand interactions in water treatment. Water Research, 2006. 40(18): p. 3315-3331.

27. Ryan, J.N., Elimelech, M., Baeseman, J.L., and Magelky, R.D., Silica-coated titania and zirconia colloids for subsurface transport field experiments. Environmental science & technology, 2000. 34(10): p. 2000-2005.

28. El-Farhan, Y.H., Denovio, N.M., Herman, J.S., and Hornberger, G.M., Mobilization and transport of soil particles during infiltration experiments in an agricultural field, shenandoah valley, virginia. Environmental science & technology, 2000. 34(17): p. 3555-3559.

29. Masciopinto, C., La Mantia, R., and Chrysikopoulos, C.V., Fate and transport of pathogens in a fractured aquifer in the salento area, italy. Water Resources Research, 2008. 44(1): p. -.

30. Burkhardt, M., Kasteel, R., Vanderborght, J., and Vereecken, H., Field study on colloid transport using fluorescent microspheres. European Journal of Soil Science, 2008. 59(1): p. 82-93.

31. de Jonge, H., Jacobsen, O.H., de Jonge, L.W., and Moldrup, P., Particle-facilitated transport of prochloraz in undisturbed sandy loam soil columns. Journal Of Environmental Quality, 1998. 27(6): p. 1495-1503.

32. Schelde, K., de Jonge, L.W., Kjaergaard, C., Laegdsmand, M., and Rubaek, G.H., Effects of manure application and plowing on transport of colloids and phosphorus to tile drains. Vadose Zone Journal, 2006. 5(1): p. 445-458.

33. Kjaergaard, C., Poulsen, T.G., Moldrup, P., and de Jonge, L.W., Colloid mobilization and transport in undisturbed soil columns. I. Pore structure characterization and tritium transport. Vadose Zone Journal, 2004. 3(2): p. 413-423.

34. Karathanasis, A.D. and Johnson, D.M.C., Stability and transportability of biosolid colloids through undisturbed soil monoliths. Geoderma, 2006. 130(3-4): p. 334-345.

35. Zhuang, J., Tyner, J.S., and Perfect, E., Colloid transport and remobilization in porous media during infiltration and drainage. Journal of Hydrology, 2009. 377(1-2): p. 112-119.

36. Smith, J., Gao, B., Funabashi, H., Tran, T.N., Luo, D., Ahner, B.A., Steenhuis, T.S., Hay, A.G., and Walter, M.T., Pore-scale quantification of colloid transport in saturated porous media. Environmental science & technology, 2008. 42(2): p. 517-523.

37. Tian, Y.A., Gao, B., Silvera-Batista, C., and Ziegler, K.J., Transport of engineered nanoparticles in saturated porous media. Journal of Nanoparticle Research, 2010. 12(7): p. 2371-2380.

38. Sun, H.M., Gao, B., Tian, Y.A., Yin, X.Q., Yu, C.R., Wang, Y.Q., and Ma, L.N.Q., Kaolinite and lead in saturated porous media: Facilitated and impeded transport. Journal Of Environmental Engineering-asce, 2010. 136(11): p. 1305-1308.

39. Bolster, C.H., Mills, A.L., Hornberger, G.M., and Herman, J.S., Effect of surface coatings, grain size, and ionic strength on the maximum attainable coverage of bacteria on sand surfaces. Journal of Contaminant Hydrology, 2001. 50(3-4): p. 287-305.

40. Zevi, Y., Dathe, A., Gao, B., Zhang, W., Richards, B.K., and Steenhuis, T.S., Transport and retention of colloidal particles in partially saturated porous media: Effect of ionic strength. Water Resources Research, 2009. 45: p. W12403.

41. Morales, V.L., Gao, B., and Steenhuis, T.S., Grain surface-roughness effects on colloidal retention in the vadose zone. Vadose Zone Journal, 2009. 8(1): p. 11-20.

42. Cheng, T. and Saiers, J.E., Colloid-facilitated transport of cesium in vadose-zone sediments: The importance of flow transients. Environmental Science & Technology, 2010. 44(19): p. 7443-7449.

43. Walker, S.L., Redman, J.A., and Elimelech, M., Role of cell surface lipopolysaccharides in escherichia coli k12 adhesion and transport. Langmuir, 2004. 20(18): p. 7736-7746.

44. Steenhuis, T.S., Dathe, A., Zevi, Y., Smith, J.L., Gao, B., Shaw, S.B., DeAlwis, D., Amaro-Garcia, S., Fehrman, R., Cakmak, M.E., Toevs, I.C., Liu, B.M., Beyer, S.M., Crist, J.T., Hay, A.G., Richards, B.K., DiCarlo, D., and McCarthy, J.F., Biocolloid retention in partially saturated soils. Biologia, 2006. 61: p. S229-S233.

45. Shein, E.V. and Devin, B.A., Current problems in the study of colloidal transport in soil. Eurasian Soil Science, 2007. 40(4): p. 399-408.

46. Saiers, J.E. and Ryan, J.N., Introduction to special section on colloid transport in subsurface environments. Water Resources Research, 2006. 42(12).

47. Flury, M. and Qiu, H.X., Modeling colloid-facilitated contaminant transport in the vadose zone. Vadose Zone Journal, 2008. 7(2): p. 682-697.

48. Yu, C., Gao, B., Muñoz-Carpena, R., Tian, Y., Wu, L., and Perez-Ovilla, O., A laboratory study of colloid and solute transport in surface runoff on saturated soil. Journal of Hydrology, 2011. 402(1-2): p. 159-164.

49. Fox, G.A., Matlock, E.M., Guzman, J.A., Sahoo, D., and Stunkel, K.B., Escherichia coli load reduction from runoff by vegetative filter strips: A laboratory-scale study. Journal Of Environmental Quality, 2011(40): p. 980-988.

50. Guber, A.K., Karns, J.S., Pachepsky, Y.A., Sadeghi, A.M., Van Kessel, J.S., and Dao, T.H., Comparison of release and transport of manure-borne escherichia coli and enterococci under grass buffer conditions. Letters In Applied Microbiology, 2007. 44(2): p. 161-167.

51. Leonard, L.A., Controls of sediment transport and deposition in an incised mainland marsh basin, southeastern north carolina. Wetlands, 1997. 17(2): p. 263-274.

52. Yang, S.L., Li, H., Ysebaert, T., Bouma, T.J., Zhang, W.X., Wang, Y., Li, P., Li, M., and Ding, P., Spatial and temporal variations in sediment grain size in tidal wetlands, yangtze delta: On the role of physical and biotic controls. Estuarine Coastal And Shelf Science, 2008. 77(4): p. 657-671.

53. Leonard, L.A., Hine, A.C., and Luther, M.E., Surficial sediment transport and deposition processes in a juncus-roemerianus marsh, west-central florida. Journal of Coastal Research, 1995. 11(2): p. 322-336.

54. Leland, H.V., The influence of water depth and flow regime on phytoplankton biomass and community structure in a shallow, lowland river. Hydrobiologia, 2003. 506(1-3): p. 247-255.

55. Leland, H.V., Brown, L.R., and Mueller, D.K., Distribution of algae in the san joaquin river, california, in relation to nutrient supply, salinity and other environmental factors. Freshwater Biology, 2001. 46(9): p. 1139-1167.

56. Ghisalberti, M. and Nepf, H., Shallow flows over a permeable medium: The hydrodynamics of submerged aquatic canopies. Transport in Porous Media, 2009. 78(3): p. 385-402.

57. Oldham, C.E. and Sturman, J.J., The effect of emergent vegetation on convective flushing in shallow wetlands: Scaling and experiments. Limnology and Oceanography, 2001. 46(6): p. 1486-1493.

58. Pluntke, T. and Kozerski, H.P., Particle trapping on leaves and on the bottom in simulated submerged plant stands. Hydrobiologia, 2003. 506(1-3): p. 575-581.

59. Schulz, M., Kozerski, H.P., Pluntke, T., and Rinke, K., The influence of macrophytes on sedimentation and nutrient retention in the lower river spree (germany). Water Research, 2003. 37(3): p. 569-578.

60. Lightbody, A.F., Nepf, H.M., and Bays, J.S., Modeling the hydraulic effect of transverse deep zones on the performance of short-circuiting constructed treatment wetlands. Ecological Engineering, 2009. 35(5): p. 754-768.

61. Tanino, Y. and Nepf, H.M., Lateral dispersion in random cylinder arrays at high reynolds number. Journal of Fluid Mechanics, 2008. 600: p. 339-371.

62. Tanino, Y. and Nepf, H.M., Laboratory investigation of lateral dispersion within dense arrays of randomly distributed cylinders at transitional reynolds number. Physics of Fluids, 2009. 21(4): p. -.

63. Luhar, M., Rominger, J., and Nepf, H., Interaction between flow, transport and vegetation spatial structure. Environmental Fluid Mechanics, 2008. 8(5-6): p. 423-439.

64. Wilkerson, G.V., Flow through trapezoidal and rectangular channels with rigid cylinders. Journal of Hydraulic Engineering-Asce, 2007. 133(5): p. 521-533.

65. Nepf, H.M., Drag, turbulence, and diffusion in flow through emergent vegetation. Water Resources Research, 1999. 35(2): p. 479-489.

66. Nepf, H.M., Mugnier, C.G., and Zavistoski, R.A., The effects of vegetation on longitudinal dispersion. Estuarine Coastal And Shelf Science, 1997. 44(6): p. 675-684.

67. Nepf, H.M., Sullivan, J.A., and Zavistoski, R.A., A model for diffusion within emergent vegetation. Limnology And Oceanography, 1997. 42(8): p. 1735-1745.

68. Gacia, E., Granata, T.C., and Duarte, C.M., An approach to measurement of particle flux and sediment retention within seagrass (posidonia oceanica) meadows. Aquatic Botany, 1999. 65(1-4): p. 255-268.

69. Huang, Y.H., Saiers, J.E., Harvey, J.W., Noe, G.B., and Mylon, S., Advection, dispersion, and filtration of fine particles within emergent vegetation of the florida everglades. Water Resources Research, 2008. 44(4): p. W04408.

70. Sabbagh, G.J., Fox, G.A., Kamanzi, A., Roepke, B., and J.-Z.Tang, Effectiveness of vegetative filter strips in reducing pesticide loading: Quantifying pesticide trapping efficiency. Journal of Environmental Quality, 2008: p. (in press).

71. Munoz-Carpena, R., Ritter, A., Bosch, D.D., Schaffer, B., and Potter, T.L., Summer cover crop impacts on soil percolation and nitrogen leaching from a winter corn field. Agricultural Water Management, 2008. 95(6): p. 633-644.

72. Munoz-Carpena, R., Parsons, J.E., and Gilliam, J.W., Modeling hydrology and sediment transport in vegetative filter strips. Journal of Hydrology, 1999. 214(1-4): p. 111-129.

73. Yuan, Y.P., Bingner, R.L., and Locke, M.A., A review of effectiveness of vegetative buffers on sediment trapping in agricultural areas. Ecohydrology, 2009. 2(3): p. 321-336.

74. White, M.J. and Arnold, J.G., Development of a simplistic vegetative filter strip model for sediment and nutrient retention at the field scale. Hydrological Processes, 2009. 23(11): p. 1602-1616.

75. Sotomayor-Ramirez, D., Martinez, G.A., Ramirez-Avila, J., and Mas, E., Effectiveness of grass filter strips for runoff nutrient and sediment reduction in dairy sludge-amended pastures. Journal Of Agriculture Of The University Of Puerto Rico, 2008. 92(1-2): p. 1-14.

76. Koelsch, R.K., Lorimor, J.C., and Mankin, K.R., Vegetative treatment systems for management of open lot runoff: Review of literature. Applied Engineering In Agriculture, 2006. 22(1): p. 141-153.

77. Dosskey, M.G., Hoagland, K.D., and Brandle, J.R., Change in filter strip performance over ten years. Journal Of Soil And Water Conservation, 2007. 62(1): p. 21-32.

78. Fox, G.A., Munoz-Carpena, R., and Sabbagh, G.J., Influence of flow concentration on parameter importance and prediction uncertainty of pesticide trapping by vegetative filter strips. Journal of Hydrology, 2010. 384(1-2): p. 164-173.

79. Munoz-Carpena, R., Fox, G.A., and Sabbagh, G.J., Parameter importance and uncertainty in predicting runoff pesticide reduction with filter strips. Journal of Environmental Quality, 2010. 39(2): p. 630-641.

80. Kay, D., Edwards, A.C., Ferrier, R.C., Francis, C., Kay, C., Rushby, L., Watkins, J., McDonald, A.T., Wyer, M., Crowther, J., and Wilkinson, J., Catchment microbial dynamics: The emergence of a research agenda. Progress In Physical Geography, 2007. 31(1): p. 59-76.

81. Oliver, D.M., Heathwaite, A.L., Hodgson, C.J., and Chadwick, D.R., Mitigation and current management attempts to limit pathogen survival and movement within farmed grassland, in Advances in agronomy, vol 932007. p. 95-+.

82. Stout, W.L., Pachepsky, Y.A., Shelton, D.R., Sadeghi, A.M., Saporito, L.S., and Sharpley, A.N., Runoff transport of faecal coliforms and phosphorus released from manure in grass buffer conditions. Letters In Applied Microbiology, 2005. 41(3): p. 230-234.

83. Fajardo, J.J., Bauder, J.W., and Cash, S.D., Managing nitrate and bacteria in runoff from livestock confinement areas with vegetative filter strips. Journal Of Soil And Water Conservation, 2001. 56(3): p. 185-191.

84. Collins, R., Donnison, A., Ross, C., and McLeod, M., Attenuation of effluent-derived faecal microbes in grass buffer strips. New Zealand Journal of Agricultural Research, 2004. 47(4): p. 565-574.

85. Roodsari, R.M., Shelton, D.R., Shirmohammadi, A., Pachepsky, Y.A., Sadeghi, A.M., and Starr, J.L., Fecal coliform transport as affected by surface condition. Transactions Of The Asae, 2005. 48(3): p. 1055-1061.

86. Trask, J.R., Kalita, P.K., Kuhlenschmidt, M.S., Smith, R.D., and Funk, T.L., Overland and near-surface transport of cryptosporidium parvum from vegetated and nonvegetated surfaces. Journal Of Environmental Quality, 2004. 33(3): p. 984-993.

87. Fox, G.A., Matlock, E.M., Guzman, J.A., Sahoo, D., and Stunkel, K.B., Escherichia coli load reduction from runoff by vegetative filter strips: A laboratory-scale study. Journal of Environmental Quality, 2011. 40(3): p. 980-988.

88. Ferguson, C.M., Davies, C.M., Kaucner, C., Krogh, M., Rodehutskors, J., Deere, D.A., and Ashbolt, N.J., Field scale quantification of microbial transport from bovine faeces under simulated rainfall events. Journal of Water and Health, 2007. 5(1): p. 83-95.

89. Duchemin, M. and Hogue, R., Reduction in agricultural non-point source pollution in the first year following establishment of an integrated grass/tree filter strip system in southern quebec(canada). Agriculture Ecosystems & Environment, 2009. 131(1-2): p. 85-97.

90. Dosskey, M.G., Helmers, M.J., and Eisenhauer, D.E., A design aid for determining width of filter strips. Journal Of Soil And Water Conservation, 2008. 63(4): p. 232-241.

91. Liu, X.M., Mang, X.Y., and Zhang, M.H., Major factors influencing the efficacy of vegetated buffers on sediment trapping: A review and analysis. Journal Of Environmental Quality, 2008. 37(5): p. 1667-1674.

92. Munoz-Carpena, R. and Parsons, J.E., A design procedure for vegetative filter strips using vfsmod-w. Transactions Of The Asae, 2004. 47(6): p. 1933-1941.

93. Turner, A.K. and Chanmeesri, N., Shallow flow of water through non-submerged vegetation. Agricultural Water Management, 1984. 8(4): p. 375-385.

94. James, C.S., Birkhead, A.L., Jordanova, A.A., and O'Sullivan, J.J., Flow resistance of emergent vegetation. Journal Of Hydraulic Research, 2004. 42(4): p. 390-398.

95. Ghadiri, H., Rose, C.W., and Hogarth, W.L., The influence of grass and porous barrier strips on runoff hydrology and sediment transport. Transactions Of The Asae, 2001. 44(2): p. 259-268.

96. Hofmann, T. and von der Kammer, F., Estimating the relevance of engineered carbonaceous nanoparticle facilitated transport of hydrophobic organic contaminants in porous media. Environmental Pollution, 2009. 157(4): p. 1117-1126.

97. Perez, S., Farre, M., and Barcelo, D., Analysis, behavior and ecotoxicity of carbon-based nanomaterials in the aquatic environment. Trac-Trends in Analytical Chemistry, 2009. 28(6): p. 820-832.

98. Petersen, E.J., Pinto, R.A., Landrum, P.F., and Weber, W.J., Influence of carbon nanotubes on pyrene bioaccumulation from contaminated soils by earthworms. Environmental Science & Technology, 2009. 43(11): p. 4181-4187.

99. Peralta-Videa, J.R., Zhao, L.J., Lopez-Moreno, M.L., de la Rosa, G., Hong, J., and Gardea-Torresdey, J.L., Nanomaterials and the environment: A review for the biennium 2008-2010. Journal Of Hazardous Materials, 2011. 186(1): p. 1-15.

100. Hardman, R., A toxicologic review of quantum dots: Toxicity depends on physicochemical and environmental factors. Environmental Health Perspectives, 2006. 114(2): p. 165-172.

101. Crespy, A., Boleve, A., and Revil, A., Influence of the dukhin and reynolds numbers on the apparent zeta potential of granular porous media. Journal Of Colloid And Interface Science, 2007. 305(1): p. 188-194.

102. Oberdorster, G., Oberdorster, E., and Oberdorster, J., Nanotoxicology: An emerging discipline evolving from studies of ultrafine particles. Environmental Health Perspectives, 2005. 113(7): p. 823-839.

103. Zhang, W.X., Nanoscale iron particles for environmental remediation: An overview. Journal of Nanoparticle Research, 2003. 5(3-4): p. 323-332.

104. Chen, K.L., Smith, B.A., Ball, W.P., and Fairbrother, D.H., Assessing the colloidal properties of engineered nanoparticles in water: Case studies from fullerene c-60 nanoparticles and carbon nanotubes. Environmental Chemistry, 2009. 7(1): p. 10-27.

105. Klaine, S.J., Alvarez, P.J.J., Batley, G.E., Fernandes, T.F., Handy, R.D., Lyon, D.Y., Mahendra, S., McLaughlin, M.J., and Lead, J.R., Nanomaterials in the environment: Behavior, fate, bioavailability, and effects. Environmental Toxicology and Chemistry, 2008. 27(9): p. 1825-1851.

106. Nel, A., Xia, T., Madler, L., and Li, N., Toxic potential of materials at the nanolevel. Science, 2006. 311(5761): p. 622-627.

107. Zheng, L.X., O'Connell, M.J., Doorn, S.K., Liao, X.Z., Zhao, Y.H., Akhadov, E.A., Hoffbauer, M.A., Roop, B.J., Jia, Q.X., Dye, R.C., Peterson, D.E., Huang, S.M., Liu, J., and Zhu, Y.T., Ultralong single-wall carbon nanotubes. Nature Materials, 2004. 3(10): p. 673-676.

108. Pan, B. and Xing, B., Adsorption mechanisms of organic chemicals on carbon nanotubes. Environmental Science & Technology, 2008. 42(24): p. 9005-9013.

109. Nowack, B. and Bucheli, T.D., Occurrence, behavior and effects of nanoparticles in the environment. Environmental Pollution, 2007. 150(1): p. 5-22.

110. Lam, C.W., James, J.T., McCluskey, R., Arepalli, S., and Hunter, R.L., A review of carbon nanotube toxicity and assessment of potential occupational and environmental health risks. Critical Reviews in Toxicology, 2006. 36(3): p. 189-217.

111. Mauter, M.S. and Elimelech, M., Environmental applications of carbon-based nanomaterials. Environmental Science & Technology, 2008. 42(16): p. 5843-5859.

112. Avouris, P., Freitag, M., and Perebeinos, V., Carbon-nanotube photonics and optoelectronics. Nature Photonics, 2008. 2(6): p. 341-350.

113. Takagi, S., Eguchi, M., Tryk, D.A., and Inoue, H., Porphyrin photochemistry in inorganic/organic hybrid materials: Clays, layered semiconductors, nanotubes, and mesoporous materials. Journal of Photochemistry and Photobiology C-Photochemistry Reviews, 2006. 7(2-3): p. 104-126.

114. Gruner, G., Carbon nanotube transistors for biosensing applications. Analytical and Bioanalytical Chemistry, 2006. 384(2): p. 322-335.

115. Lecoanet, H.F., Bottero, J.Y., and Wiesner, M.R., Laboratory assessment of the mobility of nanomaterials in porous media. Environmental science & technology, 2004. 38(19): p. 5164-5169.

116. Thomas, K. and Sayre, P., Research strategies for safety evaluation of nanomaterials, part i: Evaluating the human health implications of exposure to nanoscale materials. Toxicological Sciences, 2005. 87(2): p. 316-321.

117. Petosa, A.R., Jaisi, D.P., Quevedo, I.R., Elimelech, M., and Tufenkji, N., Aggregation and deposition of engineered nanomaterials in aquatic environments: Role of physicochemical interactions. Environmental science & technology, 2010. 44(17): p. 6532-6549.

118. Jaisi, D.P. and Elimelech, M., Single-walled carbon nanotubes exhibit limited transport in soil columns. Environmental science & technology, 2009. 43(24): p. 9161-9166.

119. Jaisi, D.P., Saleh, N.B., Blake, R.E., and Elimelech, M., Transport of single-walled carbon nanotubes in porous media: Filtration mechanisms and reversibility. Environmental science & technology, 2008. 42(22): p. 8317-8323.

120. Tian, Y., Gao, B., Silvera-Batista, C., and Ziegler, K.J., Transport of engineered nanoparticles in saturated porous media. Journal of Nanoparticle Research, 2010. 12(7): p. 2371-2380.

121. Tian, Y., Gao, B., Wang, Y., Morales, V.L., Carpena, R.M., Huang, Q., and Yang, L., Deposition and transport of functionalized carbon nanotubes in water-saturated sand columns. Journal of hazardous materials, 2012. 213: p. 265-272.

122. Tian, Y., Gao, B., Wu, L., Munoz-Carpena, R., and Huang, Q., Effect of solution chemistry on multi-walled carbon nanotube deposition and mobilization in clean porous media. Journal of hazardous materials, 2012. 231-232: p. 79-87.

123. Tian, Y., Gao, B., and Ziegler, K.J., High mobility of sdbs-dispersed single-walled carbon nanotubes in saturated and unsaturated porous media. Journal of hazardous materials, 2011. 186(2-3): p. 1766-1772.

124. Bhattacharjee, S. and Elimelech, M., Surface element integration: A novel technique for evaluation of dlvo interaction between a particle and a flat plate. Journal of Colloid and Interface Science, 1997. 193(2): p. 273-285.

125. Bhattacharjee, S., Chen, J.Y., and Elimelech, M., Dlvo interaction energy between spheroidal particles and a fiat surface. Colloids and Surfaces a-Physicochemical and Engineering Aspects, 2000. 165(1-3): p. 143-156.

126. Bhattacharjee, S., Elimelech, M., and Borkovec, M., Dlvo interaction between colloidal particles: Beyond derjaguin's approximation. Croatica Chemica Acta, 1998. 71(4): p. 883-903.

127. Stolarczyk, J.K., Sainsbury, T., and Fitzmaurice, D., Evaluation of interactions between functionalised multi-walled carbon nanotubes and ligand-stabilised gold nanoparticles using surface element integration. Journal Of Computer-aided Materials Design, 2007. 14(1): p. 151-165.

128. Cavalcanti, G.G. and Lockaby, B.G., Effects of sediment deposition on aboveground net primary productivity, vegetation composition, and structure in riparian forests. Wetlands, 2006. 26(2): p. 400-409.

129. Yao, K.M., Habibian, M.M., and Omelia, C.R., Water and waste water filtration - concepts and applications. Environmental science & technology, 1971. 5(11): p. 1105-&.

130. Rajagopalan, R. and Tien, C., Trajectory analysis of deep-bed filtration with sphere-in-cell porous-media model. Aiche Journal, 1976. 22(3): p. 523-533.

131. Palmer, M.R., Nepf, H.M., and Pettersson, T.J.R., Observations of particle capture on a cylindrical collector: Implications for particle accumulation and removal in aquatic systems. Limnology and Oceanography, 2004. 49(1): p. 76-85.

132. Rajagopalan, R. and Tien, C., Experimental-analysis of particle deposition on single collectors. Canadian Journal of Chemical Engineering, 1977. 55(3): p. 256-264.

133. Tufenkji, N. and Elimelech, M., Correlation equation for predicting single-collector efficiency in physicochemical filtration in saturated porous media. Environmental science & technology, 2004. 38(2): p. 529-536.

134. Langmuir, I., Filtration of aerosols and the devlopment of filter materials. Office of Scientific Rsearch, 1942. Report No. 865.

135. Natanson, G.L., Diffusive deposition of aerosols on a cylinder in a flow in the case of small capture coefficients. Doklady Akademii Nauk Sssr, 1957. 112(1): p. 100-103.

136. Elimelech, M., Particle deposition on ideal collectors from dilute flowing suspensions: Mathematical formulation, numerical solutions, and simulations. Separations Technol., 1994. 4: p. 186– 212.

137. Kretzschmar, R., Barmettler, K., Grolimund, D., Yan, Y.D., Borkovec, M., and Sticher, H., Experimental determination of colloid deposition rates and collision efficiencies in natural porous media. Water Resources Research, 1997. 33(5): p. 1129-1137.

138. Camesano, T.A. and Logan, B.E., Influence of fluid velocity and cell concentration on the transport of motile and nonmotile bacteria in porous media. Environmental science & technology, 1998. 32(11): p. 1699-1708.

139. Compere, F., Porel, G., and Delay, F., Transport and retention of clay particles in saturated porous media. Influence of ionic strength and pore velocity. Journal of Contaminant Hydrology, 2001. 49(1-2): p. 1-21.

140. Elimelech, M., Effect of particle-size on the kinetics of particle deposition under attractive double-layer interactions. Journal of Colloid and Interface Science, 1994. 164(1): p. 190-199.

141. Zhuang, J., Qi, J., and Jin, Y., Retention and transport of amphiphilic colloids under unsaturated flow conditions: Effect of particle size and surface property. Environmental science & technology, 2005. 39(20): p. 7853-7859.

142. Elimelech, M. and Omelia, C.R., Effect of particle-size on collision efficiency in the deposition of brownian particles with electrostatic energy barriers. Langmuir, 1990. 6(6): p. 1153-1163.

143. Harvey, J.W., Saiers, J.E., and Newlin, J.T., Solute transport and storage mechanisms in wetlands of the everglades, south florida. Water Resources Research, 2005. 41(5).

144. Lightbody, A.F. and Nepf, H.M., Prediction of velocity profiles and longitudinal dispersion in emergent salt marsh vegetation. Limnology And Oceanography, 2006. 51(1): p. 218-228.

145. Elimelech, M. and Omelia, C.R., Kinetics of deposition of colloidal particles in porous-media. Environmental science & technology, 1990. 24(10): p. 1528-1536.

146. Hahn, M.W. and O'Melia, C.R., Deposition and reentrainment of brownian particles in porous media under unfavorable chemical conditions: Some concepts and applications. Environmental science & technology, 2004. 38(1): p. 210-220.

147. Shen, C., Huang, Y., Li, B., and Jin, Y., Predicting attachment efficiency of colloid deposition under unfavorable attachment conditions. Water Resources Research, 2010. 46: p. W11526, doi:10.1029/2010WR009218.

148. Kouznetsov, M.Y., Roodsari, R., Pachepsky, Y.A., Sheltonc, D.R., Sadeghi, A.M., Shirmohammadi, A., and Starr, J.L., Modeling manure-borne bromide and fecal coliform transport with runoff and infiltration at a hillslope. Journal Of Environmental Management, 2007. 84(3): p. 336-346.

149. Saiers, J.E., Harvey, J.W., and Mylon, S.E., Surface-water transport of suspended matter through wetland vegetation of the florida everglades. Geophysical Research Letters, 2003. 30(19): p. doi:10.1029/2003gl018132.

150. Harvey, J.W., Noe, G.B., Larsen, L.G., Nowacki, D.J., and McPhillips, L.E., Field flume reveals aquatic vegetation's role in sediment and particulate phosphorus transport in a shallow aquatic ecosystem. Geomorphology, 2011. 126(3-4): p. 297-313.

151. Sabbagh, G.J., Fox, G.A., Kamanzi, A., Roepke, B., and Tang, J.Z., Effectiveness of vegetative filter strips in reducing pesticide loading: Quantifying pesticide trapping efficiency. Journal of Environmental Quality, 2009. 38(2): p. 762-771.

152. Harvey, J.W., Saiers, J.E., and Newlin, J.T., Solute transport and storage mechanisms in wetlands of the everglades, south florida. Water Resources Research, 2005. 41(5): p. doi:10.1029/2004wr003507.

153. Yu, C.R., Gao, B., and Muñoz-Carpena, R., Effect of dense vegetation on colloid transport and removal in surface runoff. Journal of Hydrology, 2012: p. doi: 10.1016/j.jhydrol.2012.02.042.

154. Huang, Y.H., Saiers, J.E., Harvey, J.W., Noe, G.B., and Mylon, S., Advection, dispersion, and filtration of fine particles within emergent vegetation of the florida everglades. Water Resources Research, 2008. 44(4): p. W04408 Doi 10.1029/2007wr006290.

155. Wu, L., Gao, B., and Munoz-Carpena, R., Experimental analysis of colloid capture by a cylindrical collector in laminar overland flow. Environmental Science & Technology, 2011. 45(18): p. 7777-7784.

156. Elimelech, M., Predicting collision efficiencies of colloidal particles in porous-media. Water Research, 1992. 26(1): p. 1-8.

157. Davis, J.A., Adsorption of natural dissolved organic-matter at the oxide water interface. Geochimica Et Cosmochimica Acta, 1982. 46(11): p. 2381-2393.

158. Tipping, E. and Cooke, D., The effects of adsorbed humic substances on the surface-charge of goethite (alpha-feooh) in fresh-waters. Geochimica Et Cosmochimica Acta, 1982. 46(1): p. 75-80.

159. Harvey, J.W., Krupa, S.L., Gefvert, C., Mooney, R.H., Choi, J., King, S.A., and Giddings, J.B., Interactions between surface water and ground water and effects on mercury transport in the north-central everglades. Water Resource Investigations Report, 2002(02-4050): p. 02-4050.

160. Tufenkji, N. and Elimelech, M., Breakdown of colloid filtration theory: Role of the secondary energy minimum and surface charge heterogeneities. Langmuir, 2005. 21(3): p. 841-852.

161. Hahn, M.W., Abadzic, D., and O'Melia, C.R., Aquasols: On the role of secondary minima. Environmental science & technology, 2004. 38(22): p. 5915-5924.

162. Johnson, P.R. and Elimelech, M., Dynamics of colloid deposition in porous-media - blocking based on random sequential adsorption. Langmuir, 1995. 11(3): p. 801-812.

163. Bolster, C.H., Mills, A.L., Hornberger, G.M., and Herman, J.S., Spatial distribution of deposited bacteria following miscible displacement experiments in intact cores. Water Resources Research, 1999. 35(6): p. 1797-1807.

164. Johnson, W.P., Ma, H.L., and Pazmino, E., Straining credibility: A general comment regarding common arguments used to infer straining as the mechanism of colloid retention in porous media. Environmental science & technology, 2011. 45(9): p. 3831-3832.

165. Johnson, W.P. and Tong, M., Observed and simulated fluid drag effects on colloid deposition in the presence of an energy barrier in an impinging jet system. Environmental science & technology, 2006. 40(16): p. 5015-5021.

166. Li, X.Q., Zhang, P.F., Lin, C.L., and Johnson, W.P., Role of hydrodynamic drag on microsphere deposition and re-entrainment in porous media under unfavorable conditions. Environmental science & technology, 2005. 39(11): p. 4012-4020.

167. Shellenberger, K. and Logan, B.E., Effect of molecular scale roughness of glass beads on colloidal and bacterial deposition. Environmental science & technology, 2002. 36(2): p. 184-189.

168. Xu, S.P., Gao, B., and Saiers, J.E., Straining of colloidal particles in saturated porous media. Water Resources Research, 2006. 42(12): p. W12S16, doi:10.1029/2006WR004948.

169. Bradford, S.A., Simunek, J., Bettahar, M., Van Genuchten, M.T., and Yates, S.R., Modeling colloid attachment, straining, and exclusion in saturated porous media. Environmental science & technology, 2003. 37(10): p. 2242-2250.

170. Johnson, W.P., Li, X.Q., and Yal, G., Colloid retention in porous media: Mechanistic confirmation of wedging and retention in zones of flow stagnation. Environmental science & technology, 2007. 41(4): p. 1279-1287.

171. Gao, B., Saiers, J.E., and Ryan, J., Pore-scale mechanisms of colloid deposition and mobilization during steady and transient flow through unsaturated granular media. Water Resources Research, 2006. 42 (1): p. W01410, doi:10.1029/2005WR004233.

172. Rose, C.W., Yu, B., Hogarth, W.L., Okom, A.E.A., and Ghadiri, H., Sediment deposition from flow at low gradients into a buffer strip - a critical test of re-entrainment theory. Journal of Hydrology, 2003. 280(1-4): p. 33-51.

173. Shen, C.Y., Li, B.G., Huang, Y.F., and Jin, Y., Kinetics of coupled primary- and secondary-minimum deposition of colloids under unfavorable chemical conditions. Environmental science & technology, 2007. 41(20): p. 6976-6982.

174. Li, X.Q. and Johnson, W.P., Nonmonotonic variations in deposition rate coefficients of microspheres in porous media under unfavorable deposition conditions. Environmental science & technology, 2005. 39(6): p. 1658-1665.

175. Kuznar, Z.A. and Elimelech, M., Direct microscopic observation of particle deposition in porous media: Role of the secondary energy minimum. Colloids and Surfaces a-Physicochemical and Engineering Aspects, 2007. 294(1-3): p. 156-162.

176. Bergendahl, J. and Grasso, D., Prediction of colloid detachment in a model porous media: Hydrodynamics. Chemical Engineering Science, 2000. 55(9): p. 1523-1532.

177. Torkzaban, S., Bradford, S.A., and Walker, S.L., Resolving the coupled effects of hydrodynamics and dlvo forces on colloid attachment in porous media. Langmuir, 2007. 23(19): p. 9652-9660.

178. Shen, C.Y., Huang, Y.F., Li, B.G., and Jin, Y., Predicting attachment efficiency of colloid deposition under unfavorable attachment conditions. Water Resources Research, 2010. 46: p. W11526, doi:10.1029/2010WR009218.

179. Bai, R.B. and Tien, C., A new correlation for the initial filter coefficient under unfavorable surface interactions. Journal of Colloid and Interface Science, 1996. 179(2): p. 631-634.

180. Bai, R.B. and Tien, C., Particle deposition under unfavorable surface interactions. Journal of Colloid and Interface Science, 1999. 218(2): p. 488-499.

181. Chang, Y.-I. and Chan, H.-C., Correlation equation for predicting filter coefficient under unfavorable deposition conditions. Aiche Journal, 2008. 54(5): p. 1235-1253.

182. Chang, Y.-I., Cheng, W.-Y., and Chan, H.-C., A proposed correlation equation for predicting filter coefficient under unfavorable deposition conditions. Separation And Purification Technology, 2009. 65(3): p. 248-250.

183. Johnson, P.R., Sun, N., and Elimelech, M., Colloid transport in geochemically heterogeneous porous media: Modeling and measurements. Environmental science & technology, 1996. 30(11): p. 3284-3293.

184. Pelley, A.J. and Tufenkji, N., Effect of particle size and natural organic matter on the migration of nano- and microscale latex particles in saturated porous media. Journal of Colloid and Interface Science, 2008. 321(1): p. 74-83.

185. Litton, G.M. and Olson, T.M., Particle size effects on colloid deposition kinetics: Evidence of secondary minimum deposition. Colloids and Surfaces a-Physicochemical and Engineering Aspects, 1996. 107: p. 273-283.

186. Semmler, M., Ricka, J., and Borkovec, M., Diffusional deposition of colloidal particles: Electrostatic interaction and size polydispersity effects. Colloids and Surfaces a-Physicochemical and Engineering Aspects, 2000. 165(1-3): p. 79-93.

187. Harvey, R.W., Kinner, N.E., Macdonald, D., Metge, D.W., and Bunn, A., Role of physical heterogeneity in the interpretation of small-scale laboratory and field observations of bacteria, microbial-sized microsphere, and bromide transport through aquifer sediments. Water Resources Research, 1993. 29(8): p. 2713-2721.

188. Liu, D.L., Johnson, P.R., and Elimelech, M., Colloid deposition dynamics in flow-through porous-media - role of electrolyte concentration. Environmental science & technology, 1995. 29(12): p. 2963-2973.

189. Tong, M. and Johnson, W.P., Excess colloid retention in porous media as a function of colloid size, fluid velocity, and grain angularity. Environmental science & technology, 2006. 40(24): p. 7725-7731.

190. Yang, C., Dabros, T., Li, D.Q., Czarnecki, J., and Masliyah, J.H., Kinetics of particle transport to a solid surface from an impinging jet under surface and external force fields. Journal of Colloid and Interface Science, 1998. 208(1): p. 226-240.

191. Shen, C., Li, B., Huang, Y., and Jin, Y., Kinetics of coupled primary- and secondary-minimum deposition of colloids under unfavorable chemical conditions. Environmental science & technology, 2007. 41(20): p. 6976-6982.

192. Raviv, U. and Klein, J., Fluidity of bound hydration layers. Science, 2002. 297(5586): p. 1540-1543.

193. Bradford, S.A., Simunek, J., Bettahar, M., van Genuchten, M.T., and Yates, S.R., Significance of straining in colloid deposition: Evidence and implications. Water Resources Research, 2006. 42(12): p. W12s15,doi:10.1029/2005wr004791.

194. Nelson, K.E. and Ginn, T.R., New collector efficiency equation for colloid filtration in both natural and engineered flow conditions. Water Resources Research, 2011. 47: p. W05543,doi:Doi 10.1029/2010wr009587.

195. Saiers, J.E. and Lenhart, J.J., Colloid mobilization and transport within unsaturated porous media under transient-flow conditions. Water Resources Research, 2003. 39(1): p. doi:10.1029/2002WR001370.

196. Huang, Y.H., Saiers, J.E., Harvey, J.W., Noe, G.B., and Mylon, S., Advection, dispersion, and filtration of fine particles within emergent vegetation of the florida everglades. Water Resources Research, 2008. 44(4).

197. Wu, L., Gao, B., Munoz-Carpena, R., and Pachepsky, Y.A., Single collector attachment efficiency of colloid capture by a cylindrical collector in laminar overland flow. Environmental science & technology, 2012. 46(16): p. 8878-86.

198. Pachepsky, Y.A., Sadeghi, A.M., Bradford, S.A., Shelton, D.R., Guber, A.K., and Dao, T., Transport and fate of manure-borne pathogens: Modeling perspective. Agricultural Water Management, 2006. 86(1-2): p. 81-92.

199. Yu, C., Gao, B., Munoz-Carpena, R., Tian, Y., Wu, L., and Perez-Ovilla, O., A laboratory study of colloid and solute transport in surface runoff on saturated soil. Journal of Hydrology, 2011. 402(1-2): p. 159-164.

200. Yu, C., Gao, B., and Munoz-Carpena, R., Effect of dense vegetation on colloid transport and removal in surface runoff. Journal of Hydrology, 2012. 434: p. 1-6.

201. Koch, K., Bhushan, B., and Barthlott, W., Multifunctional surface structures of plants: An inspiration for biomimetics. Progress in Materials Science, 2009. 54(2): p. 137-178.

202. Koch, K., Bhushan, B., and Barthlott, W., Diversity of structure, morphology and wetting of plant surfaces. Soft Matter, 2008. 4(10): p. 1943-1963.

203. Valkama, E., Salminen, J.P., Koricheva, J., and Pihlaja, K., Comparative analysis of leaf trichome structure and composition of epicuticular flaivonoids in finnish birch species. Annals of Botany, 2003. 91(6): p. 643-655.

204. Gorb, E., Haas, K., Henrich, A., Enders, S., Barbakadze, N., and Gorb, S., Composite structure of the crystalline epicuticular wax layer of the slippery zone in the pitchers of the carnivorous plant nepenthes alata and its effect on insect attachment. Journal of Experimental Biology, 2005. 208(24): p. 4651-4662.

205. Kerstiens, G. and Society for Experimental, B. Plant cuticles : An integrated functional approach. Oxford, UK; Herndon, VA: BIOS Scientific Publishers.

206. Levin, D.A., The role of trichomes in plant defense. The Quarterly Review of Biology, 1973. 48(1): p. 3-15.

207. Phenrat, T., Song, J.E., Cisneros, C.M., Schoenfelder, D.P., Tilton, R.D., and Lowry, G.V., Estimating attachment of nano- and submicrometer-particles coated with organic macromolecules in porous media: Development of an empirical model. Environmental science & technology, 2010. 44(12): p. 4531-4538.

208. Louie, S.M., Phenrat, T., Small, M.J., Tilton, R.D., and Lowry, G.V., Parameter identifiability in application of soft particle electrokinetic theory to determine polymer and polyelectrolyte coating thicknesses on colloids. Langmuir, 2012. 28(28): p. 10334-10347.

209. Morales, V.L., Sang, W., Fuka, D.R., Lion, L.W., Gao, B., and Steenhuis, T.S., Correlation equation for predicting attachment efficiency (alpha) of organic matter-colloid complexes in unsaturated porous media. Environmental science & technology, 2011. 45(23): p. 10096-101.

210. Morales, V.L., Zhang, W., Gao, B., Lion, L.W., Bisogni, J.J., Jr., McDonough, B.A., and Steenhuis, T.S., Impact of dissolved organic matter on colloid transport in the vadose zone: Deterministic approximation of transport deposition coefficients from polymeric coating characteristics. Water Research, 2011. 45(4): p. 1691-1701.

211. Lin, S., Cheng, Y., Liu, J., and Wiesner, M.R., Polymeric coatings on silver nanoparticles hinder autoaggregation but enhance attachment to uncoated surfaces. Langmuir, 2012. 28(9): p. 4178-4186.

212. Lin, S. and Wiesner, M.R., Theoretical investigation on the steric interaction in colloidal deposition. Langmuir, 2012. 28(43): p. 15233-15245.

213. de Kerchove, A.J. and Elimelech, M., Impact of alginate conditioning film on deposition kinetics of motile and nonmotile pseudomonas aeruginosa strains. Applied and Environmental Microbiology, 2007. 73(16): p. 5227-5234.

214. Biggs, S., Steric and bridging forces between surfaces fearing adsorbed polymer - an atomic-force microscopy study. Langmuir, 1995. 11(1): p. 156-162.

215. Cisneros, L., Dombrowski, C., Goldstein, R.E., and Kessler, J.O., Reversal of bacterial locomotion at an obstacle. Physical Review E, 2006. 73(3).

216. Halperin, A., Polymer brushes that resist adsorption of model proteins: Design parameters. Langmuir, 1999. 15(7): p. 2525-2533.

217. Kim, J.U. and Matsen, M.W., Repulsion exerted on a spherical particle by a polymer brush. Macromolecules, 2008. 41(1): p. 246-252.

218. Franchi, A. and O'Melia, C.R., Effects of natural organic matter and solution chemistry on the deposition and reentrainment of colloids in porous media. Environmental science & technology, 2003. 37(6): p. 1122-1129.

219. Phenrat, T., Kim, H.-J., Fagerlund, F., Illangasekare, T., Tilton, R.D., and Lowry, G.V., Particle size distribution, concentration, and magnetic attraction affect transport of polymer-modified fe-0 nanoparticles in sand columns. Environmental science & technology, 2009. 43(13): p. 5079-5085.

220. Milner, S.T., Witten, T.A., and Cates, M.E., Theory of the grafted polymer brush. Macromolecules, 1988. 21(8): p. 2610-2619.

221. Milner, S.T., Polymer brushes. Science, 1991. 251(4996): p. 905-914.

222. Heredia, A., Biophysical and biochemical characteristics of cutin, a plant barrier biopolymer. Biochimica Et Biophysica Acta-General Subjects, 2003. 1620(1-3): p. 1-7.

223. Gumel, A.M., Annuar, M.S.M., and Heidelberg, T., Biosynthesis and characterization of polyhydroxyalkanoates copolymers produced by pseudomonas putida bet001 isolated from palm oil mill effluent. Plos One, 2012. 7(9).

224. Liebergesell, M., Sonomoto, K., Madkour, M., Mayer, F., and Steinbuchel, A., Purification and characterization of the poly(hydroxyalkanoic acid) synthase from chromatium-vinosum and localization of the enzyme at the surface of poly(hydroxyalkanoic acid) granules. European Journal of Biochemistry, 1994. 226(1): p. 71-80.

225. Tian, D., Tooker, J., Peiffer, M., Chung, S.H., and Felton, G.W., Role of trichomes in defense against herbivores: Comparison of herbivore response to woolly and hairless trichome mutants in tomato (solanum lycopersicum). Planta, 2012. 236(4): p. 1053-1066.

226. Abu-Lail, N.I. and Camesano, T.A., Role of ionic strength on the relationship of biopolymer conformation, dlvo contributions, and steric interactions to bioadhesion of pseudomonas putida kt2442. Biomacromolecules, 2003. 4(4): p. 1000-1012.

227. Adebooye, O.C., Hunsche, M., Noga, G., and Lankes, C., Morphology and density of trichomes and stomata of trichosanthes cucumerina (cucurbitaceae) as affected by leaf age and salinity. Turkish Journal of Botany, 2012. 36(4): p. 328-335.

228. Hariharan, R., Biver, C., and Russel, W.B., Ionic strength effects in polyelectrolyte brushes: The counterion correction. Macromolecules, 1998. 31(21): p. 7514-7518.

229. Vangenuchten, M.T. and Wierenga, P.J., Mass-transfer studies in sorbing porous-media .1. Analytical solutions. Soil Science Society of America Journal, 1976. 40(4): p. 473-480.

230. Tong, M.P. and Johnson, W.P., Excess colloid retention in porous media as a function of colloid size, fluid velocity, and grain angularity. Environmental science & technology, 2006. 40(24): p. 7725-7731.

231. Ivkov, R., Butler, P.D., Satija, S.K., and Fetters, L.J., Effect of solvent flow on a polymer brush: A neutron reflectivity study of the brush height and chain density profile. Langmuir, 2001. 17(10): p. 2999-3005.

232. Deng, M., Li, X., Liang, H., Caswell, B., and Karniadakis, G.E., Simulation and modelling of slip flow over surfaces grafted with polymer brushes and glycocalyx fibres. Journal of Fluid Mechanics, 2012. 711: p. 192-211.

233. Klein, J., Shear, friction, and lubrication forces between polymer-bearing surfaces. Annual Review of Materials Science, 1996. 26: p. 581-612.

234. Klein, J., Kumacheva, E., Mahalu, D., Perahia, D., and Fetters, L.J., Reduction of frictional forces between solid-surfaces bearing polymer brushes. Nature, 1994. 370(6491): p. 634-636.

235. Klein, J., Perahia, D., and Warburg, S., Forces between polymer-bearing surfaces undergoing shear. Nature, 1991. 352(6331): p. 143-145.

236. Ritter, A. and Muñoz-Carpena, R., Performance evaluation of hydrological models: Statistical significance for reducing subjectivity in goodness-of-fit assessments. Journal of Hydrology, 2013. 480(0): p. 33-45.

237. Currie, E.P.K., Norde, W., and Stuart, M.A.C., Tethered polymer chains: Surface chemistry and their impact on colloidal and surface properties. Advances in Colloid and Interface Science, 2003. 100: p. 205-265.

238. Crist, J.T., Zevi, Y., McCarthy, J.F., Throop, J.A., and Steenhuis, T.S., Transport and retention mechanisms of colloids in partially saturated porous media. Vadose Zone Journal, 2005. 4(1): p. 184-195.

239. Wan, J.M. and Tokunaga, T.K., Film straining of colloids in unsaturated porous media: Conceptual model and experimental testing. Environmental science & technology, 1997. 31(8): p. 2413-2420.

240. Gao, B., Saiers, J.E., and Ryan, J., Pore-scale mechanisms of colloid deposition and mobilization during steady and transient flow through unsaturated granular media. Water Resources Research, 2006. 42(1).

241. Wan, J.M. and Wilson, J.L., Visualization of the role of the gas-water interface on the fate and transport of colloids in porous-media. Water Resources Research, 1994. 30(1): p. 11-23.

242. Tans, S.J., Devoret, M.H., Dai, H.J., Thess, A., Smalley, R.E., Geerligs, L.J., and Dekker, C., Individual single-wall carbon nanotubes as quantum wires. Nature, 1997. 386(6624): p. 474-477.

243. Wong, S.S., Harper, J.D., Lansbury, P.T., and Lieber, C.M., Carbon nanotube tips: High-resolution probes for imaging biological systems. Journal of the American Chemical Society, 1998. 120(3): p. 603-604.

244. Tans, S.J., Verschueren, A.R.M., and Dekker, C., Room-temperature transistor based on a single carbon nanotube. Nature, 1998. 393(6680): p. 49-52.

245. Fan, S.S., Chapline, M.G., Franklin, N.R., Tombler, T.W., Cassell, A.M., and Dai, H.J., Self-oriented regular arrays of carbon nanotubes and their field emission properties. Science, 1999. 283(5401): p. 512-514.

246. Kong, J., Franklin, N.R., Zhou, C.W., Chapline, M.G., Peng, S., Cho, K.J., and Dai, H.J., Nanotube molecular wires as chemical sensors. Science, 2000. 287(5453): p. 622-625.

247. Collins, P.G., Bradley, K., Ishigami, M., and Zettl, A., Extreme oxygen sensitivity of electronic properties of carbon nanotubes. Science, 2000. 287(5459): p. 1801-1804.

248. Haggenmueller, R., Gommans, H.H., Rinzler, A.G., Fischer, J.E., and Winey, K.I., Aligned single-wall carbon nanotubes in composites by melt processing methods. Chemical Physics Letters, 2000. 330(3-4): p. 219-225.

249. Liu, Z., Tabakman, S., Welsher, K., and Dai, H., Carbon nanotubes in biology and medicine: In vitro and in vivo detection, imaging and drug delivery. Nano Research, 2009. 2(2): p. 85-120.

250. Hobbie, E.K., Ihle, T., Harris, J.M., and Semler, M.R., Empirical evaluation of attractive van der waals potentials for type-purified single-walled carbon nanotubes. Physical Review B, 2012. 85(24).

251. Tulevski, G.S., Hannon, J., Afzali, A., Chen, Z., Avouris, P., and Kagan, C.R., Chemically assisted directed assembly of carbon nanotubes for the fabrication of large-scale device arrays. Journal of the American Chemical Society, 2007. 129(39): p. 11964-11968.

252. Vijayaraghavan, A., Blatt, S., Weissenberger, D., Oron-Carl, M., Hennrich, F., Gerthsen, D., Hahn, H., and Krupke, R., Ultra-large-scale directed assembly of single-walled carbon nanotube devices. Nano Letters, 2007. 7(6): p. 1556-1560.

253. Rajter, R.F., Podgornik, R., Parsegian, V.A., French, R.H., and Ching, W.Y., Van der waals-london dispersion interactions for optically anisotropic cylinders: Metallic and semiconducting single-wall carbon nanotubes. Physical Review B, 2007. 76(4).

254. Girifalco, L.A., Hodak, M., and Lee, R.S., Carbon nanotubes, buckyballs, ropes, and a universal graphitic potential. Physical Review B, 2000. 62(19): p. 13104-13110.

255. Zhbanov, A.I., Pogorelov, E.G., and Chang, Y.-C., Van der waals interaction between two crossed carbon nanotubes. Acs Nano, 2010. 4(10): p. 5937-5945.

256. Shvartzman-Cohen, R., Nativ-Roth, E., Baskaran, E., Levi-Kalisman, Y., Szleifer, I., and Yerushalmi-Rozen, R., Selective dispersion of single-walled carbon nanotubes in the presence of polymers: The role of molecular and colloidal length scales. Journal of the American Chemical Society, 2004. 126(45): p. 14850-14857.

257. Volkov, A.N. and Zhigilei, L.V., Mesoscopic interaction potential for carbon nanotubes of arbitrary length and orientation. Journal of Physical Chemistry C, 2010. 114(12): p. 5513-5531.

258. Nap, R. and Szleifer, I., Control of carbon nanotube-surface interactions: The role of grafted polymers. Langmuir, 2005. 21(26): p. 12072-12075.

259. French, R.H., Parsegian, V.A., Podgornik, R., Rajter, R.F., Jagota, A., Luo, J., Asthagiri, D., Chaudhury, M.K., Chiang, Y.-m., Granick, S., Kalinin, S., Kardar, M., Kjellander, R., Langreth, D.C., Lewis, J., Lustig, S., Wesolowski, D., Wettlaufer, J.S., Ching, W.-Y., Finnis, M., Houlihan, F., von Lilienfeld, O.A., van Oss, C.J., and Zemb, T., Long range interactions in nanoscale science. Reviews of Modern Physics, 2010. 82(2): p. 1887-1944.

260. Chen, J., Hamon, M.A., Hu, H., Chen, Y.S., Rao, A.M., Eklund, P.C., and Haddon, R.C., Solution properties of single-walled carbon nanotubes. Science, 1998. 282(5386): p. 95-98.

261. Vigolo, B., Penicaud, A., Coulon, C., Sauder, C., Pailler, R., Journet, C., Bernier, P., and Poulin, P., Macroscopic fibers and ribbons of oriented carbon nanotubes. Science, 2000. 290(5495): p. 1331-1334.

262. Balasubramanian, K. and Burghard, M., Chemically functionalized carbon nanotubes. Small, 2005. 1(2): p. 180-192.

263. Krupke, R., Hennrich, F., Kappes, M.M., and Lohneysen, H.V., Surface conductance induced dielectrophoresis of semiconducting single-walled carbon nanotubes. Nano Letters, 2004. 4(8): p. 1395-1399.

264. White, B., Banerjee, S., O'Brien, S., Turro, N.J., and Herman, I.P., Zeta-potential measurements of surfactant-wrapped individual single-walled carbon nanotubes. Journal of Physical Chemistry C, 2007. 111(37): p. 13684-13690.

265. Mamedov, A.A., Kotov, N.A., Prato, M., Guldi, D.M., Wicksted, J.P., and Hirsch, A., Molecular design of strong single-wall carbon nanotube/polyelectrolyte multilayer composites. Nature Materials, 2002. 1(3): p. 190-194.

266. Chapot, D., Bocquet, L., and Trizac, E., Interaction between charged anisotropic macromolecules: Application to rod-like polyelectrolytes. Journal of Chemical Physics, 2004. 120(8): p. 3969-3982.

267. Lowen, H., Charged rodlike colloidal suspensions - an ab-initio approach. Journal of Chemical Physics, 1994. 100(9): p. 6738-6749.

268. Elimelech, M., Particle deposition and aggregation : Measurement, modelling and simulation2010, Woburn, Mass.: Butterworth-Heinemann.

269. Heister, E., Lamprecht, C., Neves, V., Tilmaciu, C., Datas, L., Flahaut, E., Soula, B., Hinterdorfer, P., Coley, H.M., Silva, S.R.P., and McFadden, J., Higher dispersion efficacy of functionalized carbon nanotubes in chemical and biological environments. Acs Nano, 2010. 4(5): p. 2615-2626.

270. Smith, B., Wepasnick, K., Schrote, K.E., Bertele, A.H., Ball, W.P., O'Melia, C., and Fairbrother, D.H., Colloidal properties of aqueous suspensions of acid-treated, multi-walled carbon nanotubes. Environmental science & technology, 2009. 43(3): p. 819-825.

271. Wang, P., Shi, Q., Liang, H., Steuerman, D.W., Stucky, G.D., and Keller, A.A., Enhanced environmental mobility of carbon nanotubes in the presence of humic acid and their removal from aqueous solution. Small, 2008. 4(12): p. 2166-2170.

272. Yi, P. and Chen, K.L., Influence of surface oxidation on the aggregation and deposition kinetics of multiwalled carbon nanotubes in monovalent and divalent electrolytes. Langmuir, 2011. 27(7): p. 3588-3599.

273. Liu, J., Rinzler, A.G., Dai, H.J., Hafner, J.H., Bradley, R.K., Boul, P.J., Lu, A., Iverson, T., Shelimov, K., Huffman, C.B., Rodriguez-Macias, F., Shon, Y.S., Lee, T.R., Colbert, D.T., and Smalley, R.E., Fullerene pipes. Science, 1998. 280(5367): p. 1253-1256.

274. Parsegian, V.A., Van der waals forces : A handbook for biologists, chemists, engineers, and physicists2006, New York: Cambridge University Press.

275. Israelachvili, J.N., Intermolecular and surface forces2011, San Diego, Calif.: Elsevier Science Publ.

276. Hamaker, H.C., The london - van der waals attraction between spherical particles. Physica, 1937. 4: p. 1058-1072.

277. Gregory, J., Interaction of unequal double-layers at constant charge. Journal of Colloid and Interface Science, 1975. 51(1): p. 44-51.

278. de Kerchove, A.J. and Elimelech, M., Relevance of electrokinetic theory for "soft" particles to bacterial cells: Implications for bacterial adhesion. Langmuir, 2005. 21(14): p. 6462-6472.

279. Hoek, E.M.V., Bhattacharjee, S., and Elimelech, M., Effect of membrane surface roughness on colloid-membrane dlvo interactions. Langmuir, 2003. 19(11): p. 4836-4847.

280. Bradford, S.A., Torkzaban, S., and Walker, S.L., Coupling of physical and chemical mechanisms of colloid straining in saturated porous media. Water Research, 2007. 41(13): p. 3012-3024.

281. Bhardwaj, R., Fang, X., Somasundaran, P., and Attinger, D., Self-assembly of colloidal particles from evaporating droplets: Role of dlvo interactions and proposition of a phase diagram. Langmuir, 2010. 26(11): p. 7833-7842.

282. Eichmann, S.L., Smith, B., Meric, G., Fairbrother, D.H., and Bevan, M.A., Imaging carbon nanotube interactions, diffusion, and stability in nanopores. Acs Nano, 2011. 5(7): p. 5909-5919.

283. Paillet, M., Poncharal, P., and Zahab, A., Electrostatics of individual single-walled carbon nanotubes investigated by electrostatic force microscopy. Physical Review Letters, 2005. 94(18).

284. Li, X.H., Niu, J.L., Zhang, J., Li, H.L., and Liu, Z.F., Labeling the defects of single-walled carbon nanotubes using titanium dioxide nanoparticles. Journal Of Physical Chemistry B, 2003. 107(11): p. 2453-2458.

285. Peralta-Inga, Z., Lane, P., Murray, J.S., Body, S., Grice, M.E., O'Connor, C.J., and Politzer, P., Characterization of surface electrostatic potentials of some (5,5) and (n,1) carbon and boron/nitrogen model nanotubes. Nano Letters, 2003. 3(1): p. 21-28.

286. Wang, Z., Zdrojek, M., Melin, T., and Devel, M., Electric charge enhancements in carbon nanotubes: Theory and experiments. Physical Review B, 2008. 78(8).

287. Solomentsev, Y. and Anderson, J.L., Electrophoresis of slender particles. Journal of Fluid Mechanics, 1994. 279: p. 197-215.

288. Ohshima, H., Henry's function for electrophoresis of a cylindrical colloidal particle. Journal of Colloid and Interface Science, 1996. 180(1): p. 299-301.

289. O'Brien, R.W. and Ward, D.N., The electrophoresis of a spheroid with a thin double layer. Journal of Colloid and Interface Science, 1988. 121(2): p. 402-413.

290. Sun, C.H., Lu, G.Q., and Cheng, H.M., Simple approach to estimating the van der waals interaction between carbon nanotubes. Physical Review B, 2006. 73(19).

291. Zdrojek, M., Heim, T., Brunel, D., Mayer, A., and Melin, T., Inner-shell charging of multiwalled carbon nanotubes. Physical Review B, 2008. 77(3).

292. Sun, C.H., Yin, L.C., Li, F., Lu, G.Q., and Cheng, H.M., Van der waals interactions between two parallel infinitely long single-walled nanotubes. Chemical Physics Letters, 2005. 403(4-6): p. 343-346.

293. Pogoreloy, E.G., Zhbanov, A.I., Chang, Y.-C., and Yang, S., Universal curves for the van der waals interaction between single-walled carbon nanotubes. Langmuir, 2012. 28(2): p. 1276-1282.

294. Derjaguin, B. and Landau, L., Theory of the stability of strongly charged lyophobic sols and of the adhesion of strongly charged-particles in solutions of electrolytes. Progress In Surface Science, 1993. 43(1-4): p. 30-59.

295. Verwey, E.J.W., Theory of the stability of lyophobic colloids. Journal of Physical and Colloid Chemistry, 1947. 51(3): p. 631-636.

296. Elimelech, M., Gregory, J., Jia, X., and Williams, R.A., Particle deposition and aggregtion: Measurement, modeling and simulation, 1995, Butterworth-Heinemann Ltd.

297. van Oss, C.J., Giese, R.F., and Costanzo, P.M., Dlvo and non-dlvo interactions in hectorite. Clays And Clay Minerals, 1990. 38(2): p. 151-159.

298. Shen, C.Y., Huang, Y.F., Li, B.G., and Jin, Y., Predicting attachment efficiency of colloid deposition under unfavorable attachment conditions. Water Resources Research, 2010. 46.

299. Duffadar, R.D. and Davis, J.M., Dynamic adhesion behavior of micrometer-scale particles flowing over patchy surfaces with nanoscale electrostatic heterogeneity. Journal of Colloid and Interface Science, 2008. 326(1): p. 18-27.

300. Bradford, S.A., Torkzaban, S., and Wiegmann, A., Pore-scale simulations to determine the applied hydrodynamic torque and colloid immobilization. Vadose Zone Journal, 2011. 10(1): p. 252-261.

BIOGRAPHICAL SKETCH

Lei Wu was born in Shandong province, China. She received her bachelor's degree in environmental engineering from School of Environmental Science and Engineering, Qingdao University, China in 2004. After three year study and research in Peking University graduate school, she got a master's degree in environmental science in 2007. She then started her doctoral research in Department of Agricultural and Biological Engineering, University of Florida, Gainesville, FL under the supervisory of Dr. Rafael Muñoz Carpena and Dr. Bin Gao.